UNIVERSIDAD AUTÓNOMA DE MADRID

PROGRAMA DE DOCTORADO EN BIOCIENCIAS MOLECULARES

The anti-inflammatory effect of mesenchymal stromal cells in urate crystal-induced arthritis and its mechanism of action

TESIS DOCTORAL

JUAN PABLO MEDINA GIMÉNEZ

MADRID 2020

DEPARTAMENTO DE BIOQUÍMICA
FACULTAD DE MEDICINA

UNIVERSIDAD AUTÓNOMA DE MADRID

The anti-inflammatory effect of mesenchymal stromal cells in urate crystal-induced arthritis and its mechanism of action

Memoria de Investigación presentada por **Juan Pablo Medina Giménez**,
Graduado en Biotecnología, para optar al título de Doctor por la
Universidad Autónoma de Madrid

Trabajo dirigido por la Dra. Raquel Largo y el Dr. Gabriel Herrero-Beaumont

Madrid, 2020

Este trabajo ha sido realizado bajo la supervisión de la Dra. Raquel Largo y el Dr. Gabriel Herrero-Beaumont en el Laboratorio de Reumatología y Metabolismo Óseo del Instituto de Investigación Sanitaria Fundación Jiménez Díaz (IIS-FJD) UAM, Madrid (España). Juan Pablo Medina ha sido financiado por un contrato asociado al Proyecto Integrado de Excelencia (PIE15/00048) del Instituto de Salud Carlos III (ISCIII), cofinanciado con el Fondo Europeo de Desarrollo Regional (FEDER) entre septiembre de 2016 y junio 2020.

Doña Raquel Largo Carazo, Doctora en Ciencias Químicas por la Universidad Autónoma de Madrid y Don Gabriel Herrero-Beaumont Cuenca, Doctor en Medicina y Profesor Titular de Medicina en la Universidad Autónoma de Madrid,

CERTIFICAN:

Que Don Juan Pablo Medina Giménez, Graduado en Biotecnología por la Universidad Francisco de Vitoria, ha realizado en el Laboratorio de Reumatología y Metabolismo Óseo del Instituto de Investigación Sanitaria Fundación Jiménez Díaz (IIS-FJD), bajo nuestra dirección, la presente Tesis Doctoral.

Madrid, a 20 de diciembre de 2020

Dra. Raquel Largo Carazo **Dr. Gabriel Herrero-Beaumont**

Doctorando: Juan Pablo Medina Giménez

IIS-Fundación Jiménez Díaz, Avenida de los Reyes Católicos 2, 28040, Madrid

A mis padres

A Belén

A mis abuelos

AGRADECIMIENTOS

Embarcarse en la realización de una tesis doctoral no es una decisión sencilla y que pueda tomarse a la ligera. Para llevarla a cabo se necesita poseer un espíritu vocacional, siendo consciente de que la mayor satisfacción se logra al profundizar en el conocimiento de la naturaleza, en indagar en el porqué de las cosas y en saber que esa dedicación está dirigida a intentar aportar un granito de arena al conocimiento científico y al beneficio de la sociedad. Cuando empiezas, eres sabedor de que te esperan años de mucho trabajo y esfuerzo, en donde normalmente la frustración y la incertidumbre están presentes durante todo el proceso y pueden minar el entusiasmo y la motivación con la que la afrontas al principio. Por ello, redactar un epígrafe de agradecimientos no es una mera cuestión formal, sino un reconocimiento sincero a la gente con la que te has rodeado esos años y te han facilitado la consecución de tus objetivos.

En primer lugar, me gustaría trasmitir mis más sinceros agradecimientos a mis directores de tesis, al Dr. Gabriel Herrero-Beaumont y a la Dra. Raquel Largo, por toda lo confianza que han depositado en mí a lo largo de estos años, por su implicación, sus consejos y enseñanzas, y por haber tenido en todo momento las puertas de sus despachos abiertas ante cualquier problema que me surgía. Su visión traslacional de la investigación es un ejemplo a seguir. Sin duda, su trabajo y esfuerzo han guiado esta tesis doctoral hasta su buen término y han contribuido enormemente a mi formación profesional.

Por supuesto, expreso mi gratitud al Instituto de Salud Carlos III, que ha aportado los fondos económicos para la ejecución de este proyecto.

A la gente de todos los grupos de laboratorio que han participado en el Proyecto Integrado del que nace este trabajo, su espíritu crítico y esfuerzo han permitido su desarrollo. Gracias especialmente al Dr. Damián García Olmo y al Dr. Mariano García Arranz, al Servicio de Genética y por supuesto a los miembros del CIEMAT implicados en el proyecto, especialmente a Rosa y María que siempre han estado dispuestas a ayudar en todo lo que se les pedía.

El ambiente de trabajo en el laboratorio es fundamental para encarar los desafíos que se presentan en el día a día con optimismo y energía. No me iba a imaginar que los compañeros que me he encontrado en “Reuma” durante estos años me harían sentir como en casa. No me puedo olvidar de Sergio, a quien a pesar del breve tiempo que compartimos en el “labo”, agradezco enormemente su ayuda y consejo cuando empecé y que me sirvió para sentirme más seguro con el trabajo experimental. A Pedro Esbrit y Arancha Ortega agradezco sus aportaciones a nuestro trabajo durante las sesiones de grupo. También a Iván, por los consejos que me has estado dando desde que entré por primera vez al laboratorio y que de tanto me han servido.

Por supuesto y qué menos que dedicar una referencia especial a las increíbles personas que han estado al “pie del cañón” compartiendo poyata conmigo durante estos años. Muchas gracias a Patri por aportar alegría y vida al laboratorio. Arancha, eres una gran jefa y un ejemplo de eficacia en el trabajo, te agradezco la ayuda que me has prestado cuando te he necesitado. Por supuesto Sandra, que has sido como una hermana mayor y has estado desde el primer día corrigiéndome, ayudándome y dándome buenos consejos; eres un gran ejemplo tanto a nivel profesional como personal. Paula, eres una gran persona y una amiga extraordinaria en la que se puede confiar sin dudar. También Ana, gracias por tu paciencia al enseñarme y por tu bondad infinita. Fran, mi otro “pack” en el laboratorio y en la cancha; nunca olvidaré los buenos momentos que hemos pasado juntos. Y cómo no, a la última gran incorporación a nuestra pequeña familia, Isma, estoy seguro de que aprendo más de ti de lo que aprendes tú de mí, me has enriquecido tanto a nivel profesional como personal, y no solo has demostrado ser una persona maravillosa, sino tener todos los ingredientes para llegar a ser un gran científico. Por último, Gloria, te agradezco todo lo que me has enseñado estos meses; aunque hemos compartido poco tiempo en el laboratorio, has demostrado tener una curiosidad por las cosas difícil de encontrar. Estoy seguro que todos vosotros vais a tener muchísimo éxito en todo lo que os venga, os lo merecéis.

También me acuerdo de los estudiantes que han pasado por el laboratorio, todos me han ayudado demostrando interés y empeño; cuestionando lo que hacíamos me han ayudado a mejorar como investigador. Gracias a Víctor, María, Elisa y Sara.

Dos personas que han pasado por el hospital y me han marcado de algún modo han sido Alberto y Marlid. De Alberto he aprendido lo que no está escrito y no solo a nivel científico. Su afán de superación, de querer mejorar continuamente y los consejos que me ha estado dando desde que lo conocí son un tesoro precioso. La humanidad y bondad de Marlid también son un ejemplo indudable a seguir.

Agradezco también a todo el servicio clínico de Reumatología de la FJD: a Javier, Juan Antonio, Fredi, Sara, Silvia, Pablo, Rafa, Sheila, Otto, Lina… especialmente a la Dra. Olga, por sus acertadas aportaciones y a la Dra. Esperanza, que ha contribuido especialmente a esta tesis doctoral y de la que tanto se aprende. Ha sido muy enriquecedor compartir estos años con ellos, facilitando el tener siempre un punto de vista traslacional.

También y de forma muy especial, a todos los compañeros del IIS con los que he compartido tantos momentos tanto dentro como fuera de la FJD. A Álvaro, Dani, Melani, Ruth, Olaya, Rocío, por vuestra ayuda en el trabajo y por todas las risas que nos hemos echado desde que entré en la Fundación. Por supuesto a Lara, tu amistad y tu apoyo en todo momento son de las cosas más grandes que me llevo de aquí. También me alegro enormemente de haber podido disfrutar de gente tan maravillosa con las que tantas “cerves”, desayunos e incluso “pachangas”, que sí, no todo es beber y comer, hemos compartido. A Patri en especial por su cariño y apoyo en momentos difíciles, a Susana, Nacho, Gema, Luna, Lucas, las tres Lauras, Lucía, Tamara, Morgui, Raúl, Leti, Fonti, Gina y Zaza. Me habéis ayudado mucho y vuestra simpatía ha hecho que haya disfrutado de momentos increíbles. Tampoco olvidaré, como no puede ser de otra forma, a Emilio, a Antonio, y también a Sergio, tres grandísimas personas con los que no he parado de reír. Nuestras discusiones sobre tantos temas “trascendentales” han hecho más llevadero estos “años de ciencia”.

Al final tanto tiempo pasado en el animalario se ha hecho más llevadero gracias a las personas que trabajan allí. Marta, Juani, Victor, Diego, Irene y los Carlos me han ayudado mucho con los animales y eso se agradece enormemente. También a nuestras auxiliares favoritas, Amelia y sobre todo Julia, por su cariño y ayuda en todo momento, siempre es una alegría verte entrar al laboratorio.

Desde hace muchos años y durante todo este tiempo he contado con la increíble amistad de grandes amigos. A mis queridos biotecnólogos y algún escorialense, Miguel, David, Rubén, Manu, Alberto, Diego, Juanma, Adri, Edu, Paco, Antonio y nuestro capi Rodri. Hemos vivido experiencias increíbles, y vuestro apoyo y comprensión han sido fundamentales para mí.

Y qué más decir de la gente con las que prácticamente he crecido desde pequeño y con quienes tantas cosas he vivido. Victor, Germán, Borjita, Marcos, Carlos, Irene, Sara, Maite, David, Javier, Alberto, Jorge, Ale, Yago, Ana, Elena, Bruno, Guille y todos los demás…que me han estado aguantando estos meses y se han estado preocupando por mí todo este tiempo.

A mi pequeña familia de Selvas, en especial a Alexia y Mar, que tanto me ha enseñado sobre el sacrificio y la entrega a los demás. Del mismo modo, a las otras personas con las que he cruzado caminos y que también intentan ayudar a construir un mundo más justo, especialmente Víctor, Toni y Miguel. La dedicación y esfuerzo de todos ellos es admirable. No tengo palabras para agradecerles el haberme dado la oportunidad de vivir experiencias inolvidables y a crecer a nivel personal. Son todo un ejemplo y modelos a seguir.

También tengo que agradecer mucho a Bea. Me has ayudado muchísimo estos últimos meses, a pesar de las circunstancias, haciendo que este proceso me haya resultado más fácil. La motivación que me trasmites, tus incansables palabras de ánimo y el enorme apoyo y cariño que me has mostrado todo este tiempo no tiene precio. Haces que quiera mejorar cada día.

A toda mi familia por su apoyo, en especial a Tete y también a Conrado, a quien no solo admiro por su encomiable labor en la Fundación Madrina, sino también porque me regaló el primer microscopio con el que alentó mi entusiasmo por la biología.

De forma muy especial me acuerdo de mis abuelos, me hubiera gustado que me hubierais visto acabar la tesis, aunque presiento que siempre estaréis conmigo como ángeles que guían mis pasos.

A Belén, mi hermana, que siempre serás para mí mi pequeña sin importar los años que tengas. Te admiro y te quiero muchísimo y quiero que sepas lo orgulloso que estoy de ti.

Y, por último, a mis padres por su amor incondicional desde el principio, mi madre por su ternura, mi padre por su sacrificio. Los valores que me habéis inculcado y vuestro apoyo en todos los sentidos valen más que cualquier cosa que me puede ofrecer este mundo.

De todo corazón os doy las gracias a todos.

ABSTRACT

“Of course much remains to know, but we know how to learn: through scientific research”.

- *Mario Bunge*

ABSTRACT

Mesenchymal stromal cells (MSC) have been considered a promising therapeutic tool for the treatment of many autoimmune and inflammatory diseases. However, its efficacy has not been confirmed in most large-scale clinical trials. Up-to-date, most studies have focused on chronic diseases, in which the adaptive and the innate immune responses are integrated, coexisting a complex network of interactions that makes the mechanisms of action involved in the improvement of these conditions difficult to dissect. Thus, in order investigate whether MSC can act specifically on inflammatory response mechanisms, it is necessary to resort to models of acute, self-limited inflammation, only mediated by innate immunity. In this thesis we studied the effect of human adipose tissue-derived MSC administration in an acute auto-limited gouty arthritis model, which is the paradigm of acute joint disease. The flare-up was induced in rabbit knee joints through monosodium urate (MSU) crystals injection.

In order to assess the evolution of acute synovitis, firstly we validated B-mode and power Doppler musculoskeletal ultrasound imaging in our experimental model. Subsequently, we analyzed the effect of MSC therapy in the acute gouty arthritic rabbits. We observed that a single dose of systemically delivered MSC through the auricular artery significantly decreased inflammation shortly after their administration, while no effects were observed after intra-articular MSC injection. We also tested the effect of the systemic infusion of MSC through the right femoral artery, to investigate whether bypassing MSC vascular distribution through the organism could improve its effects in the right arthritic knee. Our results indicated that MSC exerted the same benefit in both limbs. On the other hand, we also tested whether a unique MSC administration was able to modify the inflammatory response of rabbits that underwent an acute gouty relapse induced by the administration of a second injection of MSU crystals into the knee joints. We did not observe a significant improvement in MSC-treated rabbits after the re-aggression. Finally, our results revealed that intra-femoral infusion of MSC in the acute arthritis model reduced the activity of nuclear factor-κB (NF-κB), and decreased the NLR family pyrin domain containing 3 (NLRP3) inflammasome components synthesis and pro-inflammatory cytokine presence in

rabbit synovial membranes. Concurrently, MSC induced the synthesis of anti-inflammatory cytokines and promoted M2 macrophage phenotype polarization in damaged synovium. *In vitro* studies showed that MSC inhibited the expression of different cytokines and NLRP3 inflammasome components in MSU crystal-stimulated THP-1 macrophages.

Altogether, we have demonstrated that systemic administration of a single dose of human MSC relieves a severe acute arthritis flare in rabbit knees, and we have shed some light on the mechanisms involved. Additionally, our findings suggest that MSC could be considered a novel therapeutic alternative for the treatment of acute gouty flares in patients in whom the use of traditional drugs could cause adverse effects.

RESUMEN

Las células estromales mesenquimales (CEM) han sido consideradas una herramienta terapéutica prometedora para el tratamiento de muchas enfermedades autoinmunes e inflamatorias. Sin embargo, su eficacia no se ha podido confirmar en la mayoría de los ensayos clínicos a gran escala. Hasta la fecha, la mayoría de los estudios se han centrado en enfermedades crónicas, en las que la respuesta inmunitaria adaptativa e innata están integradas, coexistiendo una compleja red de interacciones que dificulta el estudio de los mecanismos de acción implicados en la mejoría de estas condiciones. Por lo tanto, para investigar si las CEM pueden actuar específicamente sobre los mecanismos de respuesta inflamatoria, es necesario recurrir a modelos de inflamación aguda autolimitada, mediada únicamente por la inmunidad innata. En esta tesis investigamos el efecto de la administración de CEM derivadas de tejido adiposo humano en un modelo de artritis gotosa aguda autolimitada, que es el paradigma de la enfermedad articular aguda. El brote de artritis gotosa se indujo en ambas rodillas de conejo mediante la inyección de cristales de urato monosódico (UMS).

Para evaluar la evolución de la sinovitis aguda, en primer lugar validamos la ecografía musculo-esquelética en modo B y Doppler de potencia en conejos con artritis gotosa aguda. Posteriormente, analizamos el efecto de la terapia con CEM en este modelo. A diferencia de las CEM inyectadas localmente, una dosis única de CEM administrada sistémicamente a través de la arteria auricular disminuyó la inflamación poco después de su administración. También probamos el efecto de la infusión de CEM a través de la arteria femoral derecha, con el fin de investigar si evitando su distribución vascular a través del organismo podría mejorar su efecto en la rodilla artrítica derecha. Nuestros resultados indicaron que las CEM ejercieron el mismo efecto en ambas rodillas. Por otro lado, estudiamos si una dosis única de CEM fue capaz de modificar la respuesta inflamatoria de los conejos que sufrieron un rebrote de gota aguda inducida por la administración de una segunda inyección de cristales de UMS en las rodillas. No observamos una mejora significativa en los conejos tratados con CEM después de la re-agresión. Finalmente, desde un punto de vista mecanicista, nuestros resultados revelaron que la infusión intrafemoral de CEM en el modelo de

artritis aguda redujo la actividad del factor nuclear-κB y disminuyó la presencia de los componentes del inflamasoma NLRP3 (de sus siglas en inglés NOD-, LRR- and pyrin domain-containing protein 3) y de citoquinas proinflamatorias en las membranas sinoviales artríticas. Por el contrario, las CEM indujeron la síntesis de citoquinas antiinflamatorias y promovieron el fenotipo de macrófagos M2 en la membrana sinovial dañada. Estudios in vitro mostraron que las CEM inhibieron la expresión de diferentes citoquinas y componentes del inflamasoma NLRP3 en macrófagos THP-1 estimulados por cristales de UMS.

En conjunto, hemos demostrado que la administración sistémica de una dosis única de CEM humana alivia un brote de artritis aguda en rodillas de conejo, y hemos arrojado algo de luz sobre los mecanismos implicados. Además, nuestros hallazgos sugieren que la CEM podría considerarse una alternativa terapéutica novedosa para el tratamiento de brotes de gota aguda en pacientes en los que el uso de fármacos tradicionales podría provocarles efectos adversos.

INDEX

INDEX OF FIGURES

INTRODUCTION

METHODS

RESULTS

INDEX OF TABLES

INTRODUCTION

METHODS

RESULTS

LIST OF ABBREVIATIONS

ACR	American College of Rheumatology
Ad	Adipose tissue-derived
AG	Aggregates
Apo	Apolipoproteins
ARDS	Acute respiratory distress syndrome
Arg-1	Arginase-1
ARRIVE	Animal Research Reporting of In Vivo Experiments
ASC	Adaptor apoptosis-associated speck-like proteins containing a CARD
ATP	Adenosine triphosphate
AUR	Auricular artery
BF	Bright foci
C+	Positive control
Ca	Calcium
CARD	Caspase activation and recruitment domain
CCL	C-C motif ligand
CCR	C-C chemokine receptor type
CEM	Células estromales mesenquimales
CIS	Cytokine-inducible SH2-containing protein
CLP	Cecal ligation and puncture
CO_2	Carbon dioxide
Con A	Concanavalin A
CRP	C-reactive protein
CXCL	C-X-C motif chemokine ligand
CXCR	C-X-C motif chemokine receptor
DAMPs	Damage-associated molecular patterns
DSS	Dextran sodium sulfate
DTT	Ditiotreitol
EDTA	Ethylenediaminetetraacetic Acid

ELISA	Enzyme-linked immunosorbent assay
ESC	Embryonic stem cells
EULAR	European League Against Rheumatism
FBS	Fetal bovine serum
FEM	Femoral artery
FFA	Free fatty acids
Freq	Frequency
GD	GD global distension
GSDMD	Gasdermin D
GvHD	Graft-versus-host disease
hAd	Human adipose tissue derived
hBM	human bone marrow
HEPES	4-(2-hydroxyethyl)-1-piperazineethanesulfonic acid
h	hours
HPRT	Hypoxanthine-guanine phosphoribosyltransferase
hUC	Human umbilical cord
IA	Intra-articular
IC	Immune-complex
IDO	Indoleamine 2,3-dioxygenase
IFN	Interferon
IL	Interleukin
IL-1R1	Interleukin-1 receptor type 1
IL-1RA	Interleukin-1 receptor antagonist
IRI	Ischemia-reperfusion injury
IV	Intra-venous
JNK	Jun N-terminal kinase
K	Potassium
L	Left
Lfc	Lateral femoral condyle
LPS	Lipopolysaccharide
mBM	Mouse bone marrow

miRNA	MicroRNA
MN	Mononuclear
MPO	Myeloperoxidase
MSC	Mesenchymal stromal cells
MSK-US	Musculoskeletal ultrasound
MSU	Monosodium urate
MT-CYB	Mitochondrial cytochrome b
Na_2MoO_4	Sodium molybdate
Na3VO4	Sodium orthovanadate
NaCl	Sodium chloride
NADPH	Nicotinamide adenine dinucleotide phosphate
NaF	Sodium fluoride
NaOH	Sodium hydroxide
NE	Neutrophil elastase
Nek-7	NIMA-related kinases
NETs	Neutrophil extracellular traps
NF-κB	Nuclear factor kappa-light-chain-enhancer of activated B cells
NIMA	Never in mitosis gene A
NLR	Nucleotide-binding oligomerization domain and leucine-rich repeat
NLRP3	NLR family pyrin domain containing 3
NO	Nitric oxide
NP-40	Nonyl phenoxypolyethoxylethanol-40
NSAIDs	Non-steroidal anti-inflammatory drugs
NSP	Neutrophil serine proteases
NT	Non-treated
OA	Osteoarthritis
OD	Optical density
OMERACT	Outcome Measures in Rheumatology
PBS	Phosphate buffer
PCR	Polymerase chain reaction

PD	Power Doppler
PGE2	Prostaglandin E2
PMA	Phorbol 12-myristate 13-acetate
PMN	Polymorphonuclear
PMSF	Phenylmethanesulfonylfluoride
PRR	Pattern recognition receptor
PS	Phosphatidylserine
R	Right
RA	Rheumatoid arthritis
rAd	Rat adipose tissue-derived
RNA	Ribonucleic acid
ROS	Reactive oxygen species
RT	Room temperature
RT-PCR	Reverse transcription polymerase chain reaction
SC	Stem cell
SD	Standard deviation
SEM	Standard error of the mean
SF	Synovial fluid
SM	Synovial membrane
SLM	Sand-like material
SNP	Single-nucleotide polymorphism
SOCS	Suppressors of cytokine signaling
SOD	Superoxide dismutase
STAT	Signal transducer and activator of transcription
STh	Synovial thickening
TGF	Tumor growth factor
Th	T helper
TLR	Toll like receptor
TNF	Tumor necrosis factor
TSG	TNF-stimulated gene
UMS	Urato monosódico

US	Ultrasound
USA	United States of America
V	Vehicle

PREFACE

Most of this thesis work has led to the writing of an original paper in preparation: Medina, JP. et al. 2021. *Parenteral Injection Of Human Adipose-Derived Mesenchymal stromal cells Shortens An Experimental Acute Gouty Arthritis Inactivating NLRP3 Inflamasome*; and to an original publication: Naredo, E. et al. 2018. *Validation of Musculoskeletal Ultrasound in the Assessment of Experimental Gout Synovitis*. Ultrasound Med Biol. 44(7):1516–24. In those studies, I participated in experimental design, sample and data collection, analysis and interpretation of results and manuscript drafting.

INTRODUCTION

“It is not knowing, but the love of learning, that characterizes the scientific man”.

- *Charles Sanders Peirce*

INTRODUCTION

Mesenchymal stromal cells

Mesenchymal stromal cells (MSC), also commonly referred to as mesenchymal stem cells, are a multipotent stem cell (SC) population that is present in multiple adult tissues. A SC is a progenitor cell type capable of renewing itself through proliferative symmetrical division, and of differentiating into other cell types with specialized functions through asymmetrical division (1). According to their capacity to differentiate into other cell types, SCs can be classified in three groups. Pluripotent embryonic SCs are able to divide into any cell lineage derived from the three embryo germ layers. Unipotent cells have the potency of differentiating into only one cell type. Multipotent SCs can differentiate into a defined number of cells in a specific tissue or organ (Figure 1 A). Among the latter ones, MSC have achieved a growing clinical significance (2).

MSC were first identified in the bone marrow of guinea pigs in the 1960s, as fibroblast-like clonogenic cells (3). Further work from 1980 demonstrated that these cells had a multi-lineage differentiation potential and could support hematopoiesis creating an appropriate niche *in vivo* (4). Thus, these cells began to be considered as part of a stromal system, supporting parenchymal cells in organs and tissues (5). At the beginning of the 90s, Caplan proposed the term “mesenchymal stem cells” to describe a progenitor cell population with multipotential and proliferative capabilities that could lead to tissue formation and turnover (6).

MSC derived from bone marrow were the first to be used in cell therapy studies, and since then have been extensively employed. However, other authors described many different possible sources to obtain MSC from an adult body. MSC arrange in niches at perivascular locations in a wide variety of organs and tissues: adipose tissues, including synovial membrane, dental pulp, Wharton’s jelly, hair follicles or umbilical cord blood are among the most common MSC sources (7).

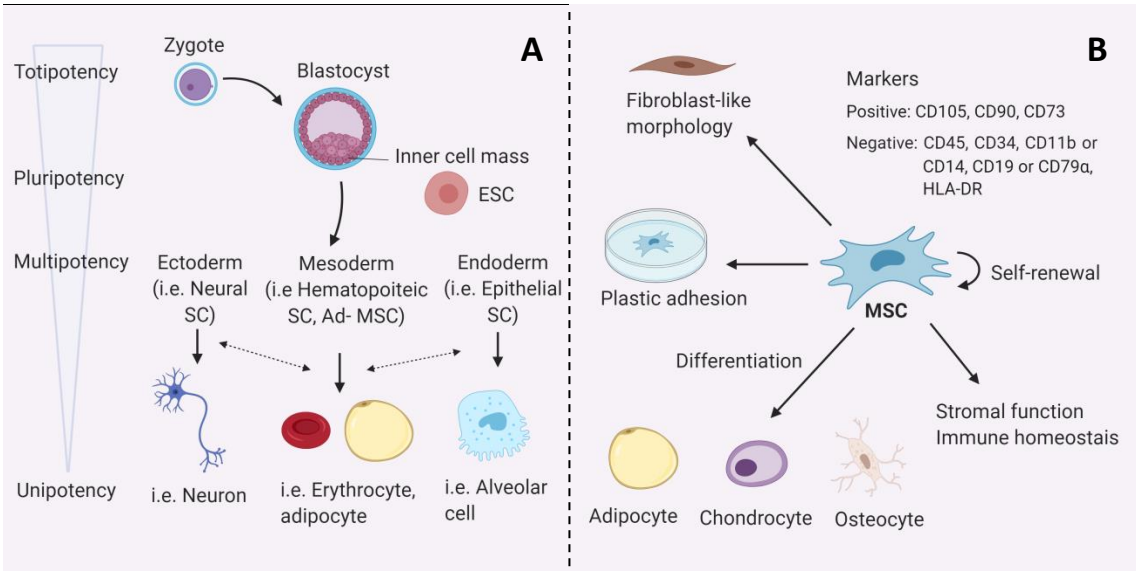

FIGURE 1. Schematic illustration of the developmental origin of SCs (A) and principal features of MSC (B). Ad: adipose tissue-derived; ESC: embryonic stem cells; MSC: mesenchymal stromal cells; SC: stem cell.

In order to unify different criteria, in 2005, the International Society for Cellular Therapy proposed the term "multipotent Mesenchymal Stromal Cell" (8). Hence, MSC were defined as undifferentiated, self-renewing cells characterized by plastic adherence in standard culture, fibroblast-like appearance and expression of specific cell markers such as CD105, CD90, CD73, and lack of CD45, CD34, CD14, CD19, CD79a, CD11b and MHCII, and low levels of MHCI, with the capacity of differentiating into chondrocytes, adipocytes and osteocytes *in vitro* (Figure 1 B) (9).

Physiology of regeneration

Eukaryotic organisms are able to reconstitute at some degree their integrity in response to injury. Superior species of metazoans, as mammalians, have the capacity to repair their tissue; this is a form of healing which implies a process of recognition of cell damage, inflammation and fibrosis that restores tissue homeostasis in an unspecific way. Some metazoans such as planarians or salamanders have the capacity to recover the initial tissue structure, substituting injured organs and tissues by new completely functional ones. This ability of regeneration is also characteristic of early fetal development, in which a low inflammatory response combined with a high expression of morphogenetic factors differs from tissue repair of adult organisms (10).

In fact, regenerating limbs in amphibians resembles the process of embryonic development (11). Humans, as other superior metazoans, retain molecular mechanisms involved in regeneration, although their capacity remains limited probably due to a fast fibrotic response and scar formation. In this context, endogenous SCs present in adult tissues appear to be hindered to display a complete regenerating response despite their potential to differentiate into multiple cell types.

MSC as cell replacement tool in regenerative medicine

Caplan was one of the first investigators to suggest the possibility of employing their differentiation potential as a therapeutic opportunity, with the hypothesis that these cells would engraft in damaged tissue and replace impaired cells (6). Since then, several experiments in preclinical models and clinical trials have tested the capacity of MSC to replace injured tissue.

Regeneration in preclinical models

Many of the earlier experiments with MSC were tested in musculoskeletal diseases (12). Some reports have described that autologous or allogenic transplantation of MSC fostered in scaffold matrix promotes bone and cartilage repair in different animal models (13,14). The observation that MSC were able to differentiate into other adult cell types at certain culture conditions encouraged their application on neurodegenerative, cardiac, and skin diseases among others. It has been even reported that MSC are capable of differentiating into renal tubular epithelial-like cells *in vivo* improving the outcome of acute renal failure in a rat model (15).

Regeneration in clinical trials

At the end of the 90s, assumption of the regenerative properties of MSC led to the design of many clinical trials. Therefore, the firsts clinical studies using bone marrow (BM) MSC as a therapeutic agent were performed in 1995 (16), proving to be a potential safe treatment when administered intravenously. Subsequent transplantation of MSC into a reduced number of patients demonstrated their efficacy

to treat children with acquired or congenital disorders such as osteogenesis imperfecta (17), or to improve advanced breast cancer outcome after chemotherapy (18) favoring hematopoietic restoration. However, most of these clinical trials were designed with a poor knowledge of the cell mechanisms responsible for MSC response, and this has led to little success in translating MSC therapeutics into large groups of patients. As an example, different animal models of osteoarthritis (OA) support the notion that MSC improves meniscal regeneration (19), but its translation to the clinic has not achieved clear positive outcomes (20). Due to the modest results obtained up-to-date in the field of regenerative medicine, many investigators have studied the role of these cells as immunomodulatory agents, rather than a cell replacement source.

MSC and immunomodulation

During the 90's, studies of autoimmune disorders in preclinical models showed that transplantation of bone marrow cells improved mice survival, preventing graft failure and suggested that these cells could interact with B and T cells (21). Subsequent investigations demonstrated the ability of these cells to regulate T lymphocyte differentiation and proliferation *in vitro*. Shortly after, MSC use was patented in 1998 for the control of the immune response in organ transplant (22,23). Further *in vitro* experiments have proved that MSC inhibit proliferation and activity of T-cytotoxic (CD8+) cells (24), and the development of (CD4+) into T helper (Th) cells Th1 and Th17 (25). MSC also affect antibodies production, proliferation and differentiation of B lymphocytes (26). On the other hand, MSC promote differentiation and activity of regulatory T cells (27). Different studies have also described that MSC are able to inactivate dendritic and natural killer cells (28), impeding cross-talk between innate and adaptive immune systems, which is highly important in controlling the development of chronic diseases. Increasing interest has turned to the study of the inter-relation of innate immune system and MSC. For example, the capacity of MSC to induce macrophage anti-inflammatory functions have been widely described (29).

Immunomodulation in preclinical models

These findings seem to indicate that improvement of tissue lesions after MSC treatment could not be based on their potency to differentiate into specific parenchymal cells, but rather to the prevention of damage due to their immune-regulatory capacities. This was supported by evidence of short MSC life after administration, poor engraftment and limited differentiation capacity (30–32). Additionally, some experimental models have been successfully treated with MSC-derived sectretome obtained after their stimulation (33,34).

MSC immunomodulatory function has been tested in a wide variety of disease models, proving that MSC restore immunological homeostasis and favor tissue repair. Most of these models have assessed the effect of MSC on chronic diseases, focusing on adaptive or innate immune response. For instance, it has been observed in a collagen-induced arthritis model that MSC are able to modulate T cells populations towards an anti-inflammatory balance (35). The same group also demonstrated that MSC attenuated arthritis progression by modulating peripheral monocytes differentiation towards interleukin (IL)-10 secreting macrophages (36).

Immunomodulation in clinical trials

Relatively great success in preclinical studies has encouraged the launch of a growing number of clinical trials, especially those focused on the treatment of systemic autoimmune diseases, organ transplantation and chronic inflammatory diseases (7). Le Blanc performed one of the first successful applications using allogeneic MSC in 2004. Her team treated a child suffering from acute lymphoblastic leukemia who developed treatment-resistant GvHD. Despite achieving positive therapeutic results in a phase II study in patients with severe steroid-refractory GvHD (37), in 2009 a phase III trial failed. Nevertheless, a deeper analysis suggested that children with GvHD positively responded to the treatment, and the first MSC pharmacological products obtained marketing approval. But with some exceptions, its use has remained restricted to clinical trials. In 2008, Alofisel (darvadstrocel), the first MSC product was approved in Europe to treat patients with complex perianal enterocutaneous fistulas associated to

Crohn's disease. However, an overwhelming number of clinical trials performed up-to-date have not reached the latter phases of clinical trials. To give an example, 15 clinical trials employing MSC for the treatment of Rheumatoid Arthritis (RA) have been launched, but only short term benefits have been observed with moderate therapeutic outcomes (38,39).

Currently, prediction of MSC response in certain disease conditions is limited. The precise mechanisms through which the interaction between MSC and immune cells drives into a therapeutic outcome remain elusive. That is probably the main reason why most of the efforts trying to transfer MSC therapy from "bench" to "bedside" have failed. In most diseases, both the adaptive and innate immune responses are integrated during chronic inflammation, and therefore, the processes of induction and resolution of the phenomena associated with the chronic condition coexist. This complex network of interactions makes it difficult to dissect the closing mechanisms displayed during the chronic inflammatory response. However, the study of acute, "pure" inflammatory diseases could bring about an opportunity to much better understand the role of MSC on the active resolution of acute inflammation.

Physiology of inflammation

Exogenous threats, such as traumatic lesions, microorganisms and environmental agents; or endogenous dangers, such particulates formation, auto-inflammatory disorders and any kind of cellular-stress associated condition can produce tissue injury. This damage is sensed by local parenchymal and immune system cells, which triggers a functional response to eliminate harmful stimulus, repair damage and restore tissue homeostasis (40).

Acute inflammation has a rapid onset and brief evolution, and it is characterized by fluid and plasma exudation and leukocyte migration to the injury site. Soluble mediators secreted in a dynamic spatiotemporal fashion actively regulate this process. Most of them act at injured location, but some systemic effects may take place triggering a metabolic and endocrine response. Immediately after insult, local vascular dilatation increases blood flow and permeability after a short period of

vasoconstriction. This produces redness, heat and swelling signs of inflammation. Dilated vessels slow down the blood flow favoring immune cells attraction to the vessel wall. Endothelial cells, that form vessels walls, undergo phenotypic changes, expressing selectins, integrins and intercellular adhesion molecules, which allow permeability and extravasation of immune cells. Subsequent leukocyte extravasation allows migration to the insult localization following a chemotactic gradient (41).

Circulating neutrophils are the first line of defense against pathogens and other aggressive agents. Neutrophils release bactericide peptides, undergo oxidative stress responses and produce extracellular traps (NETs) to eliminate the aggressor agent (42). Monocytes are then recruited into the inflammation site, differentiating into macrophage or dendritic cell populations. Macrophages are able to display distinct phenotypes, presenting variations in marker expression and secretion of specific mediators. Commonly, macrophages have been clustered into the M1 pro-inflammatory, and the M2 anti-inflammatory polarization phenotypes (43). Recruited monocytes may differentiate towards one of the macrophages subsets depending on the signals present in the inflammatory microenvironment, promoting either inflammation or wound repair (44). While M1 macrophages are characterized by expression of pro-inflammatory molecules such as IL-1β, tumor necrosis factor (TNF)-α, interferon (IFN)-γ and nitric oxide (NO), alternative activated macrophages produce high levels of IL-10 and usually express higher levels of surface markers such as CD206 and CD163 (45,46).

Therefore, neutrophils and macrophages deploy a molecular arsenal of degradative proteins and soluble mediators that enhances the inflammatory response, but also contributes to its resolution. These molecules, together with their phagocytic capacity, remove the aggressor agent and clear death cells and debris. Macrophages and other antigen presenting cells are able to migrate to lymph node through lymphatic vessels triggering the specific adaptive immune response.

Sometimes the harmful agent is intense and cannot be easily removed. Consequently, the inflammatory reaction can be excessive, causing severe tissue injury (40,41). If the source of damage persists during long time, inflammation and repair

processes become integrated in a self-persisting loop where tissue suffers further damage. This unresolved inflammation leads to the chronification of the process, where the innate and adaptive immune systems are integrated coexisting stages of high inflammatory onset activity and resolution processes (40,47).

MSC in the inflammatory microenvironment

It has been suggested that endogenous MSC may help to orchestrate and regulate the immune response during inflammation, promoting tissue repair (48). Hence, administration of exogenous MSC could favor the healing process of an inflammatory disease. When inflammation arises in a damaged tissue, systemically administered MSC have the potential to mobilize and temporarily home into the injury site. However, most MSC accumulate in the lung microvasculature, interacting with circulating and resident phagocytes (30). MSC that reach inflammatory site are attracted by different chemokines such as C-X-C motif chemokine ligand 12 (CXCL12) or C-C motif ligand 2 (CCL2) released by host cells, which are recognized by MSC C-X-C motif chemokine receptor 4 (CXCR4) and C-C chemokine receptor type 2 (CCR2) respectively (49,50). At inflammation site, MSC induce host cells, such as leukocytes, fibroblasts, endothelial and tissue progenitor cells, to restore homeostasis through several mechanisms, including the secretion of growth and immunosuppressive factors (51) (Figure 2). In 2008 it was discovered that immunosuppressive capacity of MSC was enhanced by high concentration of pro-inflammatory chemokines such as IFN-γ, TNF-α or IL-1β present in the inflammatory milieu (52). Additionally, other environmental factors as low oxygen concentration in the inflammatory environment may promote anti-inflammatory MSC phenotype (53). However, MSC can also exert a pro-inflammatory action if the dynamic immune fluctuations during disease course alter their regulatory status. Different stimuli can be detected by MSC through different TLRs types, switching on different signaling pathways which determine their regulatory response (54). Therefore, cross-talk between MSC and a strong inflammatory milieu is essential to achieve a favorable immune modulation.

MSC therapy in acute inflammation

The employment of exogenous MSC as a therapeutic tool for the treatment acute inflammatory diseases has been partially investigated (55,56). It has been recently described in different preclinical models, including myocardial infarction (57), acute liver injury (58) or renal failure (59) among others, that MSC exert a prompt therapeutic action on injured organs. Furthermore, several clinical trials are underway, although data is still limited (55,60).

Different microbial or sterile etiologic agents could induce acute organ injury. For instance, ischemia-reperfusion injury (IRI) can lead to a severe sterile inflammatory response producing organ failure. Sterile inflammation, which is similar to microbial triggered inflammation, is characterized by damage-associated molecular patterns (DAMPs) release and recruitment of neutrophils and macrophages, and sometimes it implies the activation of adaptive immune response (61). Sterile inflammation is also observed in other acute conditions such as trauma, toxin exposure or crystal-induced arthritis. MSC therapy has been proposed to be an effective therapy to address acute sterile inflammation (62). Outstanding results have been achieved in preclinical models of acute myocardial infarction treated with MSC (63) and some clinical studies have even reached industry-sponsored phase III clinical trials (64,65). Clearly, it is essential to understand the interplaying of MSC with innate immune cells in order to delve into the mechanisms through which MSC modulate the inflammatory response in these acute disease models.

The interaction between MSC and innate immune cells has been widely studied *in vitro* and *in vivo* and several mechanism of action have been described (66). Both neutrophils and macrophages are essential players during inflammatory diseases. In the table below, some mechanisms through which MSC interact with both cell populations are described (Table 1). On the other hand, a wide number of studies have focused on the capacity of MSC to actively interact with monocytes and macrophages in different tissue locations favoring their anti-inflammatory functions (67). Additionally, passive effects on macrophage regulation have also been proposed (Figure 2). Macrophages are able to react to MSC presence even when MSC are not

metabolically fit and non-functional. For example, apoptotic MSC entrapped in the lung microvasculature are phagocyted by macrophages through a process termed "efferocytosis" favoring the release of anti-inflammatory mediators (68).

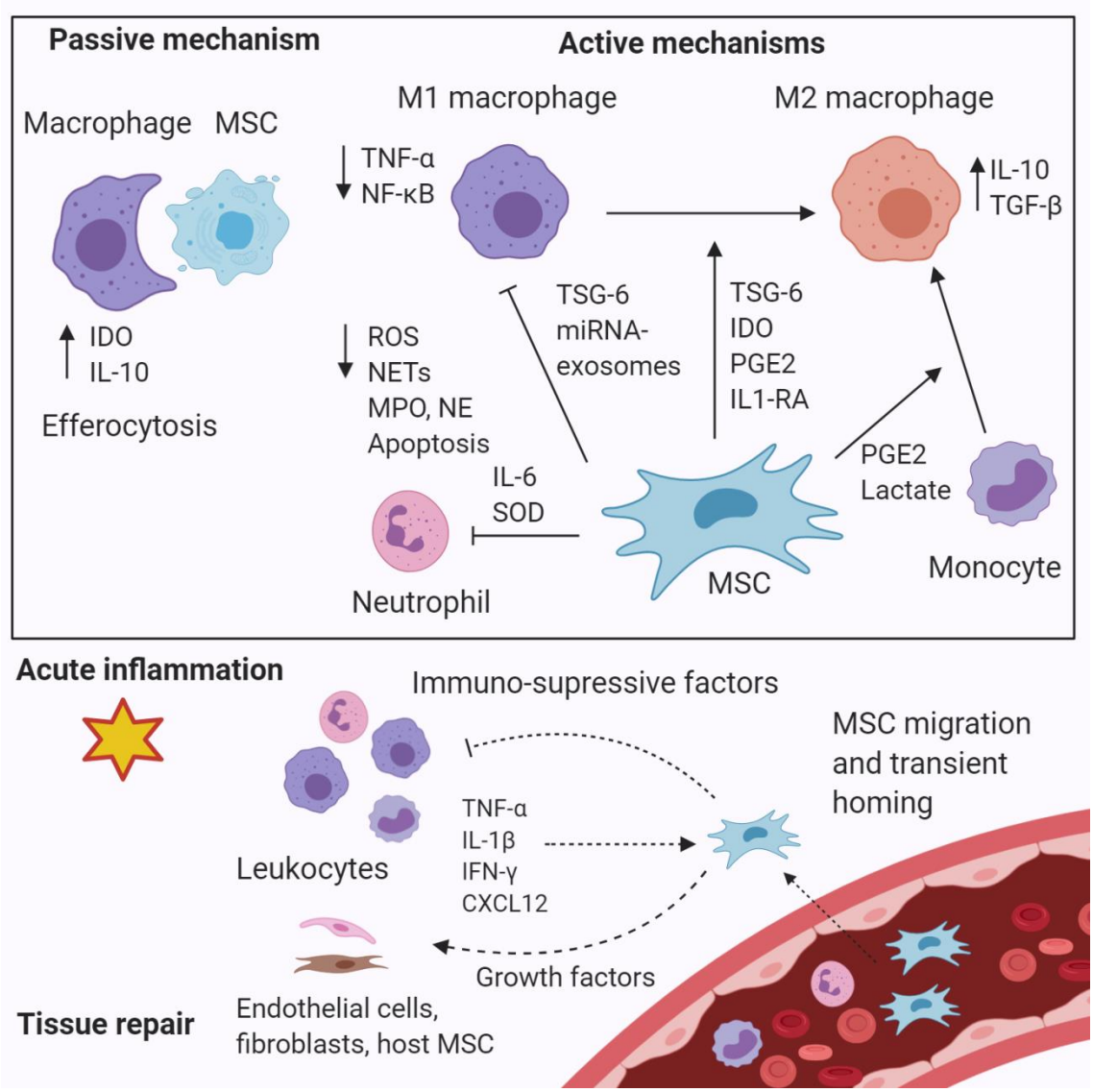

FIGURE 2. Schematic illustration of MSC mode of action in the acute inflammation site and their effects on mononuclear phagocytes and neutrophils. When MSC are administered systemically, a small MSC fraction is able to migrate into the injury site attracted by chemokines and home transiently before being cleared by host phagocytes. A severe inflammatory microenvironment is essential to trigger an active MSC immunosuppressive reaction. Immunosuppression and modulation of host cells by the release of growth factors can promote tissue repair, promoting the recovery of tissue homeostasis. CXCL-12: C-X-C motif chemokine 12; IDO: indoleamine 2,3-dioxygenase; IFN-γ: interferon-γ; IL: interleukin; IL-1RA: interleukin-1 receptor antagonist; miRNA: microRNA; MSC: mesenchymal stromal cells; MPO: myeloperoxidase; NE: neutrophil elastase; NETs: neutrophil extracellular traps; NF-κB: nuclear factor-κB; PGE2: prostaglandin E2; ROS: reactive oxygen species; SOD: superoxide dismutase; TGF-β: tumor growth factor-β; TNF-α: tumor necrosis factorα; TSG-6: TNF-stimulated gene-6.

However, it is difficult to attribute the improvement observed in acute disorders to the modulation of innate leukocytes alone, as adaptive immunity is usually induced as well. In fact, several works describe how MSC are able to suppress adaptive immunity indirectly through regulating mononuclear phagocytes (69). Few works have been focused on the study of the specific action of MSC on innate immunity *in vivo*, avoiding the involvement of an adaptive response. Some examples include corneal wound healing (70), acute pancreatitis (71), severe burned wound (72), or zymosan-induced peritonitis models (73). In order to understand how MSC exert their anti-inflammatory activity *in vivo*, it is necessary to resort to models of acute, self-limited inflammation, in which the mechanisms whereby MSC modulate the inflammatory response associated to the activation of the innate immunity can be studied. In the joint, the therapeutic effect of MSC on acute arthritis has never been assessed before. Gouty arthritis is the paradigm of an auto-limited articular inflammatory disease, being a perfect tool to study the effect of MSC on an acute inflammatory disease mediated by innate immune system.

Gouty arthritis

Gouty arthritis is an inflammatory joint disease characterized by recurrent acute flares of articular and periarticular inflammation which usually affects a single joint and can progress to a chronic state with progressive tissue destruction (74). Gouty flares affect patients under hyperuricaemic state, when serum urate levels exceed 6.8 mg/l (420 µmol/l) leading to the formation and deposition of monosodium urate (MSU) crystals in the joints. Needle shaped MSU crystals are negatively birefringent under polarized light and usually size from 2 to 22 µm (75).

Uric acid (UA) is the final metabolite of purine metabolism in humans and other primates, being principally produced in the liver. Supersaturation can be commonly reached from high cell turnover disorders, from excessive production during metabolism, and by dietary intake (76,77). The crystallization process depends on the presence of specific proteins, chondroitin sulfate, phosphatidylcholine, mechanical injury, high calcium concentration, and low pH and temperature (76).

Target cells	Source MSC	Mechanism of action of MSC	Effect of MSC	Disease model/assay
Neutrophil	hBM-MSC	IL-6	Inhibition apoptosis.	*In vitro* assay (78).
	hAd-MSC	SOD	Inhibition NET formation and respiratory burst.	IC-mediated vasculitis in mice (79).
	mBM-MSC	Cell–cell contact interaction	Reduces oxidative metabolism and respiratory burst.	Corneal injury model in mice (80).
Mononuclear phagocytes	hUC-MSC hBM-MSC	Lactate PGE2	Differentiation of monocytes into macrophages (M2) and up-regulation of CD163, CD14, MHCII and CD16.	*In vitro* assay (81,82).
	mBM-MSC hAd-MSC	PGE2	Increase macrophage production of IL-10. NLRP3 inflammasome inhibition. Macrophages polarization from M1 to M2 phenotype.	CLP-induced sepsis in mice (83). DSS-induced colitis in mice (84).
	hAd-MSC hBM-MSC	TSG-6	Macrophages polarization from M1 to M2 phenotype. Suppress macrophage function, inhibiting NF-κB signaling.	DSS-induced colitis in mice (85). Zymosan-induced peritonitis in mice (73).
	hBM-MSC	Stanniocalcin-2	Macrophages polarization from M1 to M2 phenotype.	LPS-induced acute lung injury in mice (86).
	hBM-MSC	Mitochondrial transfer	Enhance macrophage bioenergetics and phagocytosis.	ARDS in mice (87).
	rAd-MSC	Enhance efferocytosis of neutrophils	Macrophages polarization from M1 to M2 phenotype.	Myocardial IRI model in mice (63).
	mBM-MSC	IL-1RA	Macrophages polarization from M1 to M2 phenotype.	Con A-induced hepatic injury in mice (88).
	hBM-MSC	Apoptotic MSC	Macrophage production of IDO.	Acute GvHD in mice (89).
	hAd-MSC	Heat-inactivated MSC	Suppress monocyte function.	LPS-induced sepsis model in mice (90).

TABLE 1. Mechanisms of action of MSC from different origins on neutrophils and mononuclear phagocytes in inflammatory model systems. ARDS: acute respiratory distress syndrome; CLP: cecal ligation and puncture; Con A: concanavalin A; IDO: indoleamine 2,3-dioxygenase; DSS: dextran sodium sulfate; GvHD: graft-versus-host disease; hAd: human adipose tissue derived; hBM: human bone marrow; hUC: human umbilical cord; IC: immune-complex; IL-1RA: interleukin-1 receptor antagonist; IL: interleukin; IRI: ischemia-reperfusion injury; LPS: lipopolysaccharide; mBM: mouse bone marrow; miRNA: microRNA; MPO: myeloperoxidase; NE: neutrophil elastase; NLRP3: NLR family pyrin domain containing 3; NETs: neutrophil extracellular traps; NFκB: nuclear factor κB; PGE2: prostaglandine E2; rAd: rat adipose tissue derived; SOD: superoxide dismutase; TSG-6: TNFα-stimulated gene-6.

Clinical presentation

Common clinical manifestations are given in patients under hyperuricaemic state who suffer recurrent episodes of acute flares involving one joint at a time. Among the affected joints, ankles, knees, and fingers are the most common ones. In patients, the first metatarsophalangeal joint is usually affected, condition which is termed *podagra*. An acute flare has a rapid onset, usually from 12 to 24 hours, and reaching the peak of pain and swelling 6 to 12 hours later. Intermittent acute episodes occur regularly between asymptomatic periods. Usually, acute attacks spontaneously auto-resolve within 7 to 10 days (91). Local periarthritis, bursitis or tendinitis might develop, while systemic fatigue and fever may also occur. It is common that other attacks reappear over 6 months to 2 years after the initial attacks, leading to chronification of the process, if UA is not reduced. Chronic gout may develop after few years of recurrent acute gout attacks and is characterized by a continuous mild granulomatous inflammation and progressive tissue destruction (92).

Epidemiology and risk factors

Nowadays, gout is one of the most common inflammatory joint diseases in adults, and worldwide data point out an increase in incidence and prevalence in both developed and developing countries. Currently, incidence is estimated to reach almost 0.1% with a prevalence of 0.54% of worldwide population. However, prevalence estimation comprises about 2.5 - 6.5% population in Western countries, and the risk of suffering gout increases with age (93).

Genetic, metabolic, and environmental factors are involved in the development of gout. The diet and lifestyle of Western countries clearly influence the onset of this disease, as it is directly related to hyperuricemia and the use of certain medications that affect UA excretion. On the other hand, genetic factors are also implicated. In native populations of Taiwan and Pacific Polynesia prevalence arises up to 8% of adults, and this can be associated with the presence of specific SNPs in urate transporter genes. Additionally, men are four times more susceptible to suffer an acute gout attack than women (94).

Pathophysiology

Gout is considered one of the oldest metazoans diseases. Bone erosions characteristic of gout were identified in the tyrannosaurus fossil Sue's at Denver Museum of Natural History. This is probably related to the conserved first defense mechanisms of metazoan, the innate immune system (95). Acute gout flares are considered to be the prototypical joint inflammatory disease where innate immune system activation plays a pivotal role (96). Given the fact that the aggressor agent derives from the organism itself, it has even been considered an auto-inflammatory disease, although it is not directly a hereditary disorder (77).

Onset phase

When high UA concentration in synovial fluid precipitates, the resulting MSU crystals deposit in the joint tissues. MSU crystals are considered a danger agent by host primary defenses known as DAMPs. DAMPs are endogenous signals released when cells are in a dangerous or stressful situation. After their precipitation in the synovium, resident macrophages recognize them, triggering the inflammatory response. During this process, IL-1β released by inflammasome action plays a crucial role, leading to vasodilatation and immediate recruitment of neutrophils and monocytes into the crystal deposition location, amplifying the acute inflammatory process (97).

DAMPs are recognized by sensor proteins, also referred to as cytosolic pattern recognition receptors (PRR). One of the best described cytosolic PRR is the nucleotide-binding oligomerization domain and leucine-rich repeat (NLR) family pyrin domain containing 3 (NLRP3) inflammasome (98). Inflammasomes are large cytosolic multiproteic complexes mainly present in myeloid-lineage derived leukocytes, but have also been described in other cell types such as endothelial fibroblasts or chondrocytes. Different inflammasome families and domains have been described. All of them are composed by a sensor, an adapter and an effector protein, but they are activated by different mechanisms (99). When NLRP3 senses the danger signal, the assembly and oligomerization of the components is triggered, leading to the

recruitment of the adaptor apoptosis-associated speck-like proteins containing a CARD (ASC); and subsequent recruitment of the effector component caspase-1. This process of auto-assembly into large oligomers is known as 'prion-like' polymerization (100). After oligomerization is completed, caspase-1 auto-cleaves into its active form, leading to the inflammasome activation. Caspase-1 is then able to process the pro-inflammatory cytokines pro-IL-1β and pro-IL-18 into their mature active forms IL-1β and IL-18, triggering the inflammatory response (98,101). It has also been described that caspase-1 is able to perform proteolysis of the protein gasdermin D, which polymerizes forming cytotoxic pores in cytoplasmic membrane, leading to pyroptosis (102). Pyroptosis is an inflammatory form of programmed cell death involved in gout pathogenesis. Pore formation allows the release of pro-inflammatory molecules and danger signals associated to stress of the cell (Figure 3). These processes form part of a protection mechanism orchestrated by innate immunity to restore tissue homeostasis. However, persistent or un-cleared danger signals leads to a continual inflammasome activity which can result in severe tissue damage (103).

Given the wide variety of signals derived from homeostatic alterations in the microenvironment, different stimuli do not interact directly with inflammasome, but meet in a common molecular event which induces its oligomerization and subsequent activation (99). In gout, it has been described that MSU crystals themselves are not able to induce a complete inflammasome engagement, but other signals are necessary. At least two steps are required to induce inflammasome action: priming and an activation signal. This increases the specificity of the response to the aggressor agent (104).

The first signal induces the expression of all inflammasome protein components necessary for the assembly and formation of the complex, including the caspase substrates. This priming signal is not specific, depends on the inflammatory microenvironment and engages innate immune receptors on the cell surface. Toll-like receptors (TLR) are the most common ones, being TLR2 and TLR4 involved in gouty inflammation. There are different mechanisms through which TLRs from phagocytes can be activated. It has been suggested that MSU crystals are able to interact directly

with TLRs given their electrostatic nature (105). On the other hand, detection of certain molecules by such as ATP derived from necrotic cells, long-chain free fatty acids (FFAs) and proteins such as S100A8 and S100A9 are recognized by different TLRs in gout triggering downstream NF-kB signaling (106,107) (Figure 3). Additionally, the complement protein C5a induces inflammasome components transcription (108).

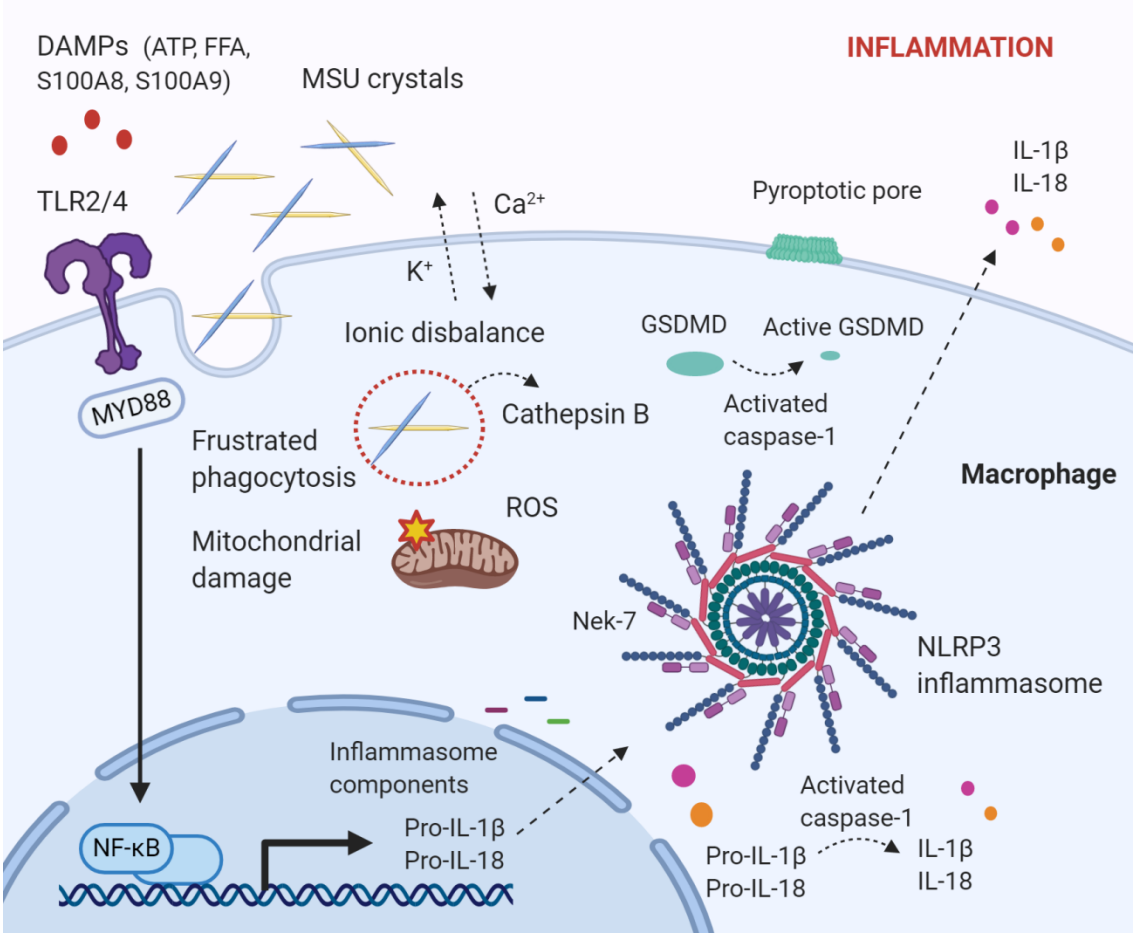

FIGURE 3. NLRP3 inflammasome activation triggers the inflammatory response in gouty arthritis. MSU crystals are recognized by synovial resident macrophages. MSU crystals and other DAMPs present in the microenvironment bind to TLR receptors leading to the up-regulation of inflammasome components and of pro-IL-1β and pro-IL-18 cytokines through NF-κB activity. Impaired MSU crystal phagocytosis by phagosomes leads to ionic cytoplasmic imbalance due to excessive K^+ efflux, Ca^{2+} influx, and to cathepsin B release and mitochondrial dysfunction, which induce elevated ROS production. These signals induce the recruitment of inflammasome components and the consequent release of mature pro-inflammatory IL-1β, IL-18 cytokines and pyroptotic GSDMD through caspase-1 activity. DAMP: danger-associated molecular patterns; FFA: free fatty acids; GSDMD: gasdermin D; IL: interleukin; Nek-7: NIMA-related kinases; NF-κB: nuclear factor-κB; NLRP3: NLR family pyrin domain containing 3; ROS: reactive oxygen species; TLR: toll like receptor.

The second signal activates aggregation and assembly of the previously synthetized components. This signal is more specific than the first step pre-requisite and allows

inflammasome activity (104). In gouty arthritis, it is suggested that frustrated phagocytosis of MSU crystals leads to misbalance of intracellular ionic equilibrium, producing potassium (K^+) efflux and calcium (Ca^{2+}) influx (109). This ionic dysregulation sparks mitochondrial dysfunction triggering the generation of reactive oxygen species (ROS) and oxidative stress (110). ROS production may catalyze Nek-7, a NIMA-related serine/threonine kinase, direct binding to inflammasome, acting as an activating ligand (111). Cytoplasmic acidification and cathepsin B released as a consequence lysosomal disruption has also been suggested to play a role in NLRP3 inflammasome activation, although the exact mechanism through which engages inflammasome is unknown (112) (Figure 3).

Upon NLRP3 inflammasome activation in phagocytes, IL-1β is released promoting the inflammatory response (113). IL-1β acts on IL-1 receptor type 1 (IL-1R1) present in many cell types, including endothelial cell and synoviocytes. IL-1 β and other mediators produce vasodilatation and induce synthesis of selectins and integrins on endothelial cells surface, which leads to further recruitment of neutrophils followed by monocytes into the synovium. Activation of IL 1-R1 activates a downstream signaling pathway of transcription factors such as NF-κB and p38-Jun N-terminal kinase (JNK). These transcription factors turn on the expression of cytokines, chemokines and other pro-inflammatory mediators such as IL-6 or IL-8 that amplify the inflammatory response. IL-8, principally secreted by macrophage and neutrophils, activates neutrophil response.

Neutrophils can also process the precursor of IL-1β by neutrophil serine proteases (NSP), such as myeloblastin, elastase and cathepsin G. At inflammatory site high neutrophil concentrations favor the extracellular release of their chromatin with a range of granular enzymes, myeloperoxidase and other NSP. This forms a complex net-like structure of cellular aggregates and NETs debris. This process results in a form of necroptotic neutrophil death, termed as NETosis. NETosis amplify the immune system response, as NETs components are detected as DAMPs, driving the release of inflammatory cytokines (96) (Figure 4).

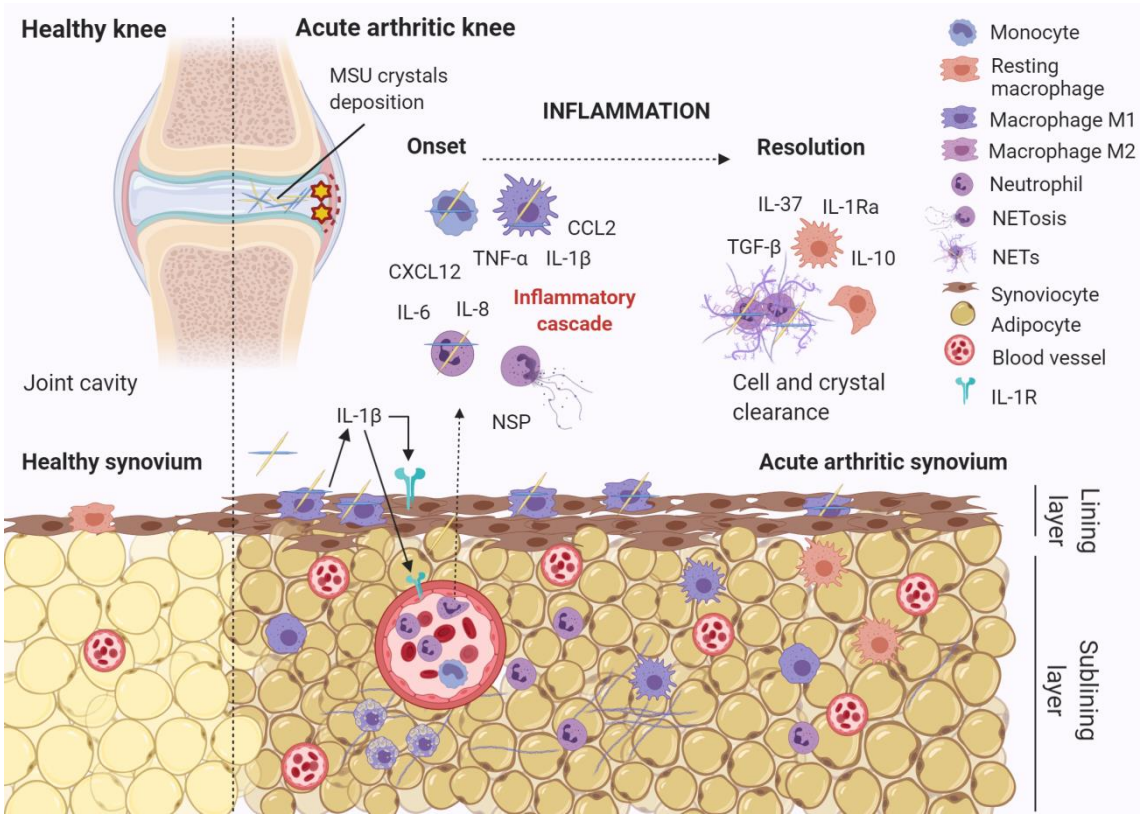

FIGURE 4. The inflammatory process in the self-limited acute gouty flare. MSU crystals are deposited in the joint cavity, stimulating synovial resident macrophages that release IL-1β. This cytokine is recognized by IL-1R on synoviocytes and vessel endothelial cells, which express chemotactic and adhesion factors. Neutrophils are then recruited, boosting the inflammatory response. Monocytes also infiltrate into the injury site, exacerbating tissue damage. MSU crystals clearance and negative regulators of inflammation promote the resolution of the inflammatory process. CCL2: C-C motif ligand 2; CXCL-12: C-X-C motif chemokine 12; IL: interleukin; IL-1R: interleukin-1 receptor; IL-1RA: interleukin-1 receptor antagonist; miRNA: microRNA; MPO: myeloperoxidase; NETs: neutrophil extracellular traps; NSP: neutrophil serine proteases; TGF-β: tumor growth factor-β, TNF-α: tumor necrosis factor α.

Resolution phase

Acute gouty flares are characterized by its spontaneous self-limiting nature. Innate immunity plays a pivotal role exerting a negative counter-regulation of the inflammatory process. The launch of different anti-inflammatory mechanisms is time dependent and the dynamic interaction between them is essential to exert an effective limitation of the inflammatory response (74) (Figure 4).

MSU crystals themselves are involved in the resolution process. MSU crystals may solubilize if UA concentration in the synovium diminishes, and consequently does the inflammatory input. Also it has been proposed that lipoproteins ApoB and ApoE are able to coat crystals by electrostatic forces, concealing the crystals to immune cells

(114). But also MSU crystals can actively drive the resolution phase. Detection of the microcrystals by specific surface receptors of different innate immune cells can also induce the turn-down of the inflammatory response, for instance, activating inhibitory C-type lectin receptors (115,116). Direct down-regulation of inflammasome activity is also an important auto-limiting procedure. While some negative regulators of TLR signaling prevent the first priming signal of inflammasome activation (117), many intracellular mechanisms can affect inflammasome activation. For example, mitochondrial autophagy and the consequent ROS clearance can counterbalance inflammasome activity (118).

Moreover, anti-inflammatory cytokines released by leukocytes, such as IL-10, TGF-β1 and IL-1Ra are critical regulators of inflammation. IL-1Ra is an antagonist of the IL-1 receptor being a potent competitive inhibitor of IL-1β pathway (119). IL-1Ra production, mainly from macrophages and neutrophils, can be promoted by expression of TGF-β (120). TGF-β can also induce the synthesis of IL-37 in monocytes, which attenuates pro-inflammatory cytokines levels (121). It has been observed that IL-10 can mediate down-regulation of pro-inflammatory cytokines, such as TNF-α produced by macrophages. Intracellular signal transducer and activator of transcription (STAT), cytokine-inducible SH2-containing protein (CIS), and suppressors of cytokine signaling (SOCS) are outstanding mediators in the resolution phase of inflammation. In acute arthritic flares, CIS and SOCS3 expression prevents IL-1β and TNF-α production and induces STAT-3-mediated transcription of TGF-β in macrophages (119,122). The clearance of apoptotic cells and debris by macrophages also limits the inflammatory response. As it has been described before, enhanced phagocytic capacity is attributed to M2 macrophage subsets (123).

Neutrophils can mediate resolution of inflammation through different mechanisms. Phosphatidylserine from neutrophils inhibits macrophage NLRP3 inflammasome activity and enhances TGF-β production. On the other hand, aggregation of NETs sequestrates MSU crystals and drives the proteolysis and degradation of pro-inflammatory mediators by the neutrophil proteases present among this fibrotic network (96,124).

Current treatments and future perspectives

The American College of Rheumatology (ACR) in 2012, and the European League Against Rheumatism (EULAR) in 2016 have established four general reference approaches to treat gout patients. It is important to take into account that gout management should be individualized based on lifestyle habits, associated comorbidity, the use of other medications, the state of the disease and the age of the patient (125).

The first principle recommends the use of drugs to address inflammation after a gout flare, such as non-steroidal anti-inflammatory drugs (NSAIDs), corticosteroids, colchicine or IL-1 inhibitors. The second principle implies the use of urate serum lowering therapies. This approach is necessary to control long-term symptomatology, when gout has been diagnosed and the patient suffer at least frequent flares, tophi deposition, past urolithiasis or mild chronic kidney disease. The third principle of gout management consists on the application of anti-inflammatory prophylaxis with urate-lowering therapy, as dissolution of tophi can induce short-term painful arthritic flares. Lastly, comorbid disorders such as cardiovascular diseases, type 2 diabetes mellitus, chronic kidney disease or obesity associated to metabolic syndrome must be taken into account. These disorders have been associated with increased death risk, and so the medication must be carefully managed (126).

A large percentage of gout patients are elderly, being considered a risk group with greater comorbidity and usually poly-medicated, which further limit the use of the previously described drugs. Gout is a really painful, incapacitating disease that has a deep impact in the quality of life. For this reason it is essential to investigate alternatives to the usual pharmacological arsenal, which in many cases does not offer therapeutic options.

Principles of gout management	Indications	Risks/ side effects/ disadvantages
1. Treatment of acute gouty flare	NSAIDs, corticosteroids or colchicine	Gastrointestinal, cardiovascular and renal side effects. Contraindicated in patients with chronic renal disease and receiving anti-coagulants. Not recommended in polymedicated and comorbid patients, especially in the elderly (127).
	Corticosteroids	Systemic risk due to their effects on the endocrine system. Weight gain, hypertension and glycemic alterations (127).
	Colchicine	Gastric alterations: vomiting, diarrhea, and gastrointestinal colic. Not recommended in patients with renal dysfunction (127).
	Biological therapies: i.e. IL-1β antagonist: anakinra or canakinumab	High cost limits their use. Lack of evidence of safety in elder patients and side effects (126). May involve susceptibility to infections (128).
2. Urate serum lowering therapies	Xanthine oxidase inhibitors: allopurinol or febuxostat	Allopurinol: contraindicated in patients with kidney disease, may cause allopurinol hypersensitivity syndrome. Febuxostat: contraindicated in patients with cardiovascular diseases (127).
	Uricosuric drugs: Benzbromarone Or Lesinurad	Benzbromarone: May imply hepatic damage Lesinurad: might promote kidney toxicity (74).
	Recombinant pegylateduricase	Restricted to patients with severe gout and whom other options are not possible. Extremely high cost. Infusion reactions and loss of efficacy related to the production of host antibodies (74).
3. Anti-inflammatory prophylaxis with urate-lowering therapy	Low-dose NSAIDS, colchicines, corticosteroids	Similar to the first and second principle. IL-inhibitors are not approved (74).
4. Comorbid disorders	Depending on the patient comorbidity	Usually polymedicated patients (74).

TABLE 2. Summary of drawbacks of current treatments indicated in the general principles of gout management. IL-1β: interleukin-1β; NSAID: Non-steroidal anti-inflammatory drugs.

OBJECTIVES

“We need a dream-world in order to discover the features of the real world we think we inhabit.”

- *Paul Karl Feyerabend*

OBJECTIVES

Global conceptual objective

We aimed to study the anti-inflammatory effect of human adipose tissue-derived MSC in acute joint inflammation employing a model of MSU crystal-induced arthritis in rabbits, and to investigate the mechanisms of action involved.

Therefore, this thesis has been structured in the following specific objectives:

1. To validate musculoskeletal ultrasound (MSK-US) imaging for the sequential evaluation of acute synovitis in MSU crystal-induced arthritis in rabbit knees.

2. To study whether the administration of MSC has an anti-inflammatory effect on the acute MSU crystal-induced arthritis model.

3. To analyze different doses and routes of administration, and the distribution of MSC in the MSU-induced arthritis model.

    a. To compare the efficacy of different doses of intra-articularly administered MSC into the arthritic knee joint versus the systemic intra-arterial delivery of MSC through the auricular artery.

    b. To determine the therapeutic outcome of the systemic administration of MSC through the right femoral artery in both knees, in order to compare the effect of a direct arrival of MSC to the inflamed synovium (in the right knee) versus MSC reaching the inflamed synovium after the circulatory cycle (in the left knee), when the majority of them could be trapped in different organs.

    c. To evaluate the biodistribution of MSC after their infusion through the right femoral artery in different rabbit organs and tissues.

4. To investigate whether MSC sustain a protective effect upon an acute arthritis relapse in the MSU-induced arthritis model.

5. To explore the cellular and molecular mechanisms associated to the effect of MSC administration on synovial inflammation, both in the acute arthritis model in rabbits and conducting *in vitro* experiments.

METHODS

“Good tests kill flawed theories; we remain alive to guess again”

- Karl Raimund Popper

In vivo studies

All experimental procedures employing animal models were performed in accordance with the Spanish regulation and the Guidelines for the Care and Use of Laboratory Animals, drawn up by the National Institutes of Health (Bethesda, MS, USA) and complied with the animal care protocols established in the Animal Research Reporting of In Vivo Experiments (ARRIVE) guidelines (129). Experimental protocols were approved by the Institutional Ethics and Welfare Committee of Jiménez Díaz Foundation University and Research Institute (Ref. 2013/10).

Three-month old New Zealand white male rabbits weighting between 2.5-3.0 kg (Granja San Bernardo, Spain) were housed in individual cages (0.50 m of cage height and 0.6 m^2 of floor space), were fed with an *ad libitum* diet of commercial chow (Panlab, Barcelona, Spain) had free access to water and were exposed to a 12-hour light/dark cycle. Body weight was measured weekly along the study. After 2 weeks of adaptation to the hospital animal facilities, rabbits were randomly distributed into different groups according to the experimental study, as will be explained later.

Induction of acute arthritic flare

In order to produce an acute gouty attack, MSU crystals were injected into both rabbit knee joints as formerly reported (130). MSU crystals were synthetized in our laboratory as previously described, with some modifications.

Briefly, 0.03 M NaOH was heated to 80-90ºC on a magnetic stirrer. UA (Sigma-Aldrich, St Louis, Missouri, USA) was added at 5 mg/ml and immediately was allowed to cool overnight under agitation at RT. The resulting solution was filtered, dried and sterilized through UV light exposure. MSU crystals were observed under polarized light to check needle shape (filiform), birefringent properties and size, that ranged between 2-20 µm long (131).

The final product was resuspended in sterile phosphate buffer (PBS 1X) at 50 mg/ml, and 1 ml of the solution was injected into each rabbit knee for the arthritis induction (Figure 5). Healthy control animals received an equal volume of vehicle (PBS) into both knees instead of the MSU crystals.

For the relapse arthritis model, the same dose of MSU crystals or vehicle (PBS) was re-injected in each knee 15 days after the first one (Figure 5).

The procedure was carried out with rabbits under general anesthesia, induced by 5 ml of intra-muscular injection of 20 mg/ml xylazine (Rompun, Bayer, Kiel, Germany) and 50 mg/ml ketamine (Ketolar, Pfizer, Hameln, Germany) in a 2:1 ratio, under aseptic conditions in an operating room.

MSK-US evaluation

Both rabbit knee joints were blindly assessed by B-mode and power Doppler (PD) US at 24 and 72 hours after MSU injection by Dr. Naredo, who is a rheumatology specialist in US imaging. The examinations were performed using a real-time scanner (LOGIQ e R7, GE Medical Systems, Jiangsu, China) provided with a 22-MHz linear transducer. Equipment settings were standardized with B-mode gain of 47 dB, dynamic range of 72 dB, Doppler frequency of 14.3 MHz, Doppler gain of 28 dB, low-wall filters and pulse repetition frequency of 700 Hz.

For the experimental procedure, rabbits were anesthetized and accommodated in supine position with knees flexed in a 10º to 20º angle. Both longitudinal and transverse evaluations of the lateral recesses of the right and left knees were performed and blindly scored by the same specialist. The parameters evaluated were based on definitions stated on the Outcome Measures in Rheumatology (OMERACT) (132) US for synovitis components with some modifications: B-mode global distension (GD), synovial fluid (SF), synovial thickening (STh) and intra-synovial PD signal (PD). SF described hypo- or anechoic elements within the synovial recess subjected to displacement by the compression with the US probe. STh refers to anomalous hypo-echoic tissue within the synovial recess that is not displaceable and poorly compressible with the US probe. GD refers to global distension of the joint recess and

includes both SF and STh components. PD mode detects blood flow signal within the synovial thickening. Images were saved for subsequent scoring. The parameters were semi-quantitatively scored on a scale of 0 to 3 (0 = absence, 1 = mild, 2 = moderate; 3 = marked) as previously described (133). A score ≥ 2 for GD and SF and a score ≥ 1 were considered pathologic for STh and PD. Other features characteristic of acute gouty flares that can be considered material of MSU crystals deposition present in synovial fluid were considered (134), as iso-echoic sand-like material (SLM); and hyper-echoic aggregates (AG) and bright foci (BF) within the sand-like material. These parameters were scored as present = 1 and no presence = 0.

MSC generation and characterization

MSC were isolated from human healthy donor's lipoaspirates. Informed consent was obtained according to institutional guidelines for the site of sample procurement (Hospital Fundación Jiménez Díaz, Madrid). Human adipose aspirates were processed and MSC were isolated, expanded and characterized at Centro de Investigaciones Energéticas, Medioambientales y Tecnológicas (CIEMAT) cleanroom facilities by Dr. Yáñez and Dr. Fernández-García, from the Hematopoietic Innovative Therapies Division from CIEMAT, headed by Dr. Bueren, as already described (135).

MSC administration

In order to obtain MSC for rabbit injections, MSC were cultured for a week at 37°C and 5% CO_2 in α-MEM supplemented with GlutaMAX™ (Thermo Fisher Scientific), 50 units/ml penicillin-streptomycin and 5% human platelet lysate (Cook Regentec, USA) at a density of 4 x 10^3 cells/cm^2. Then, cells at passage 3 were harvested, counted and resuspended in cooled PBS for immediate injection.

Route of administration and doses:

MSC were always administered 1 hour after the injection of MSU crystals in aseptic conditions, in an operating room and with animals under general anesthesia (Figure 5). Different routes and cell doses were administered:

- **Intra-articular (IA) application:** Rabbits in supine position were injected with a single dose of one of the following doses in each knee:
    - 1 x 10^6 MSC/kg in 200 µl of cooled PBS (MSC IA-HIGH).
    - 2.5 x 10^5 MSC/kg in 200 µl of cooled PBS (MSC IA-LOW).

  The same volume of PBS was intra-articularly injected as vehicle in selected animals.

- **Infusion through the auricular artery (AUR):** Rabbits were placed in prone position and 2 x 10^6 MSC/kg re-suspended in 2 ml of cooled PBS was infused in a single dose (MSC AUR). Control rabbits received PBS as vehicle following the same procedure.

- **Administration through the femoral artery (FEM)**: Animals were placed in supine position and a vertical incision was performed over the right femoral artery extending above inguinal ligament level to approximately 3 cm below. Then, a deeper incision was carried out through the Scarpa's facia in a vertical approach to the artery and a sling was slide under the artery avoiding the femoral vein and nerve. Finally, the sling was lift up; exposing the femoral artery and a small dissection was performed along the artery. Subsequently, the artery was cannulated with a 24 G gauge needle (Abbocath, Venisystems, Spain). Rabbits were administered with a single dose of 2 x 10^6 MSC/kg resuspended in 2 ml of cooled PBS through the cannula (MSU+MSC FEM group). On the other side, control injured rabbits received an equal volume of cooled vehicle. This administration route allows the evaluation of the effect of the treatment in the right knee, which receive the cells directly after its vascular administration, compared to the contralateral joint, which receive the cells after its biodistribution throughout the organism.

Joint swelling assessment

For the acute arthritis model, a tape measure was used to determine the perimeter of knee joints at different consecutive time points: before IA injection (time 0), and 6, 18, 24, 48 and 72 hours after MSU crystals administration. For the relapse model (Figure 5), the perimeter was additionally measured at days 15, 16, 17, 18 after the first MSU crystal injection.

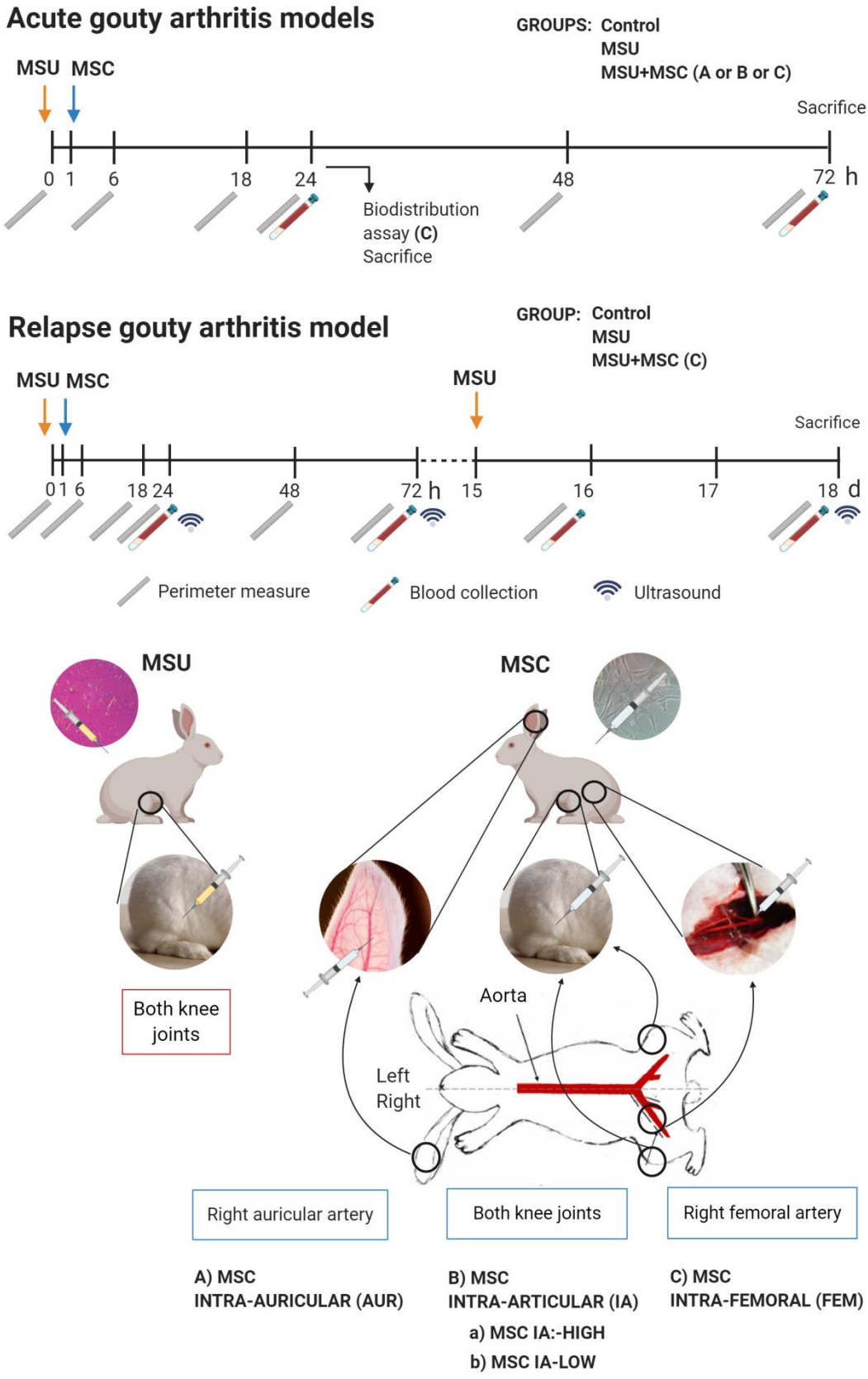

FIGURE 5. Experimental design for the studies carried out with MSC *in vivo*. AUR: auricular artery; d: days; h: hours; FEM: femoral artery; MSC: mesenchymal stromal cells; MSU: monosodium urate.

All rabbit limbs were shaved before measurement. To obtain the knee perimeter measures without anesthesia, animals were completely immobilized in supine position and limbs were completely stretched, in a 180º angle to the body. At each time point, joint perimeter measurements were taken twice by the same observer after animal reposition, to avoid biases. The final measure for each time point was the mean of the two measures.

Blood sample collection

Serum for cytokine analyses was extracted from 10 ml total blood collected from the central auricular artery 24 and 72 hours after MSU crystals administration. Additionally, blood was collected at days 16 and 18 from animals belonging to the relapse model (Figure 5). Rabbits were immobilized without anesthesia using a special cage, and the central auricular artery was cannulated for blood extraction. After blood clotting, tubes were centrifuged at 4ºC 2500 rpm for 30 minutes. Serum was stored at -80ºC for further studies.

Tissue sample collection

Animals were euthanatized, after overnight fasting, 72 hours (acute model) or 18 days (relapse model) after MSU crystal injection through intra-cardiac injection of Tiobarbital (tiopental, Braun Medical SA, Barcelona, Spain). Immediately after euthanasia, the different samples were collected for further studies (Figure 5). Synovial fluid was extracted after knee cavity lavages with 1 ml of saline (0.9% NaCl, Braun Medical, Barcelona, Spain) IA injection. The knee joints were massaged before incision with a surgical blade to collect the synovial fluid. A sample of synovial fluid was employed for total cell count, while a small drop was smeared on a microscopic slide for differential cell count, as explained later.

Subsequently, both synovial membranes were collected. Using a surgical blade, the capsule was ripped out uncovering the synovial membrane. The upper part of the tissue was immersed in formalin 10% for 24 hours, and then embedded in paraffin for

histological studies. The inferior section was immediately frozen in liquid nitrogen for molecular biology studies.

A small group of arthritic rabbits were euthanatized 24 hours after MSU crystal injection for the assessment of MSC distribution in the organism after its systemic administration through the femoral artery. Lung, liver and spleen samples and both the right and the left synovial membranes were harvested for human DNA detection. Additionally, synovial fluid was collected for cell count studies.

Histological evaluation

Inflammation of the synovium was evaluated in 3 µm thick paraffin sections stained with hematoxylin-eosin. Then, tissues were microscopically evaluated by three blinded observers who were unaware of the group of the study the sample belonged to. Histological damage was scored by consensus employing the Krenn score (136) with minor modifications to adapt the evaluation to acute arthritis damage. Briefly, a semi-quantitative subscale graded from 0 to 3 points was used to independently assess tissue lining hyperplasia, leukocyte infiltration in the synovium and sublining layer alterations. The final score was calculated summing the grades up to a maximum of 9 points (Table 3). Samples without a defined lining were not evaluated.

Synovial fluid cell count

Total cell count

Firstly, total number of leukocytes present in the synovial fluid of each joint were stained with Türk's solution (Sigma-Aldrich, St Louis, Missouri, USA) and counted by LUNA-II™ Automated Cell Counter (Logos Biosystems, Gyeonggi-do, South Korea). Hemorrhagic samples were discarded to avoid biases in cell count.

Differential cell count

Secondly, leukocyte differential count was performed for each synovial fluid sample. Smears were fixed in methanol at RT and subsequently stained with May-Grünwald-Giemsa (Sigma-Aldrich, St Louis, Missouri, USA) staining. Ten different

pictures in each sample were obtained with a Leica DM 6000 LED instrument (Leica, Microsystems, Inc. Buffalo Grove, IL, USA) to calculate the percentage of polymorphonuclear (PMN) and mononuclear (MN) cells present in each joint.

Morphological feature	Score
A. Hyperplasia of synovial lining cell layer	
• Absent.	**0**
• Slight enlargement (one to two cell layers).	**1**
• Moderate enlargement (three to four cell layers).	**2**
• Strong enlargement (more than four cell layers).	**3**
B. Inflammatory infiltration	
• Absent	**0**
• Slight inflammatory infiltration (diffusely located single cells and small perivascular aggregates of MC and PMN leukocytes).	**1**
• Moderate inflammatory infiltration (perivascular and superficial diffused aggregates of MC and PMN leukocytes).	**2**
• Strong inflammatory infiltration (confluent aggregates of MC and PMN leukocytes).	**3**
C. Activation of synovial stroma	
• Absent.	**0**
• Slight synovial stroma activation (low cellularity with slight edema, slight fibrosis).	**1**
• Moderate synovial stroma activation (moderate cellularity with a moderate density of fibroblasts, vascularity and apoptotic adipocytes).	**2**
• Strong synovial stroma activation (high cellularity with important fibrosis, vascularity, and apoptotic adipocytes.	**3**
Maximum possible score for grading	**9**

TABLE 3. **Morphological features of the Krenn score adjusted to acute arthritis (Adapted from Krenn et al. 2006).** MC: mononuclear; PMN: polymorphonuclear.

Serum C-reactive protein (CRP) measurement

Rabbit serum CRP levels were determined at 24 and 72 hours after MSU crystal injections using a commercial Enzyme-Linked Immunosorbent Assay (ELISA kit) (ab157726, Abcam, Cambridge, UK) as described in manufacturer's instruction manual.

Immunohistochemistry

Three µm sections of synovial tissue embedded in paraffin blocks were rehydrated in ethanol series after deparaffination. Absolute methanol and 3% H_2O_2 at 1:1 ratio was used to inhibit endogenous peroxidase after 30 minutes incubation at RT. Macrophage populations were identified employing specific antibodies against RAM11 (rabbit macrophage protein), CD163 and arginase-1 antigens, while vascularization in the synovium was marked through endothelial CD31 antigen. The procedures followed to test these antibodies are detailed below.

Macrophage population

RAM11, CD163 and arginase-1 antigen retrieval was performed employing citrate buffer (10 mM, pH 6, 85ºC for 30 minutes). Slides were incubated with blocking solution (PBS 6% sheep serum, 4% BSA) 30 minutes at RT. Synovial membrane macrophages were marked using monoclonal anti-rabbit macrophage RAM11 antibody (Dako, Glostrup, Denmark; 1/100 dilution) (137), the monoclonal anti-human CD163 antibody (Serotec, Raleigh, NC, USA; clone EDhu-1, 1/500 dilution) (138) and a goat polyclonal anti-Liver Arginase (Abcam, Cambridge, UK; 1/500 dilution) antibody (139). Tissue sections were incubated with primary antibodies in blocking solution (PBS 6% sheep serum, 4% BSA), overnight at 4ºC. As secondary antibody, biotinylated goat anti-mouse IgG (Amersham, Arlington Heights, IL, USA; 1/800 dilution) was used, followed by incubation with horseradish peroxidase ABComplex (Dako, Golstrup, Denmark) and 3,3 diaminobenzidine tetra-hydrochloride as chromogen (Dako, Golstrup, Denmark) to visualize the antigen expression. Tissue specimens were counterstained with hematoxylin staining, dehydrated in a series of ethanol and mounted with DPX medium (VWR International, Leuven, Belgium).

Five random microphotographs along lining area were taken at 40X magnification for RAM11 and CD163 analysis, while 20X images were applied for arginase-1 study. Pictures were obtained with a Leica DM 6000 LED instrument (Leica, Microsystems, Inc. Buffalo Grove, IL, USA). Every image was analyzed using the Color Deconvolution plugin of ImageJ software (NIH, Bethesda, MD, USA) so as to calculate the percentage

of positive staining relative to the total tissue area. In order to obtain the value of positive staining for each sample, the mean of the different pictures of each sample was calculated for each synovial membrane (140,141).

Vascularization

CD31 was exposed through proteinase-K (0.1%) in TE buffer (50 mM Tris Base, 1 mM EDTA, 0,5% Triton-X-100, pH 8, 37ºC for 30 minutes). Slides were incubated with blocking solution (PBS 3% sheep serum, 4% BSA) 30 minutes at RT. Synovial vessels were evaluated using monoclonal anti-CD31 antibody (Abcam, Cambridge, UK; clone JC/70A; 1/20 dilution). Samples were incubated with primary antibodies in blocking solution (PBS 3% sheep serum, 4% BSA), overnight at 4ºC. As secondary antibody, biotinylated goat anti-mouse IgG (Amersham, Arlington Heights, IL, USA; 1/800 dilution) was used, followed by incubation with horseradish peroxidase ABComplex (Dako, Golstrup, Denmark) and 3,3 diaminobenzidine tetra-hydrochloride as chromogen (Dako, Golstrup, Denmark) to visualize the antigen expression. Tissue samples were counterstained with hematoxylin staining, dehydrated in ethanol series and mounted with DPX medium (VWR International, Leuven, Belgium).

Finally, pictures were taken in 10 randomly selected areas of synovial membrane per slide to perform CD31+ staining analysis (20X magnification). Pictures were obtained with a Leica DM 6000 LED instrument (Leica, Microsystems, Inc. Buffalo Grove, IL, USA). Each image was analyzed using the Color Deconvolution plugin of ImageJ software (NIH, Bethesda, MD, USA) to calculate the percentage of positive staining relative to the total tissue area. The value of positive staining for each sample was obtained calculating the mean of the different pictures for each synovial membrane (140,141).

NF-κB activation assay

An ELISA-based TransAM NF-κB p65 kit (Active Motif, CA, USA) was used to study activation of NF-κB, in accordance to manufacturer's protocol. Firstly, total nuclear proteins were isolated from cell protein extracts and incubated with NF-κB consensus

segments attached to the plate. Then, hybridization was detected by a colorimetric reaction, and quantified by absorbance measurement.

Detection of Human DNA in rabbit tissues

The right and the left knee synovial membranes, as well as the lung, liver and spleen of rabbits were obtained for DNA analysis. Following the manufacturer's instructions, DNA was extracted by an automated DNA extractor (BioRobotEZ1; QIAGEN, Hilden, Germany).

PCR were performed to detect presence of human DNA in Rabbit tissue samples. In order to analyze human DNA, a primer pair (forward: TATTGCAGCCCTAGCAGCACTCCA and reverse: AGAATGAGGAGGTCTGCGGC) specific for human mitochondrial cytochrome b (MT-CYB) gene (ENST00000361789.2) (142), was used to amplify a 441-bp amplicon. To check reliability of the test, rabbit mitochondrial DNA was analyzed using rabbit 12S rRNA (ENSOCUT00000033107.1) primer pairs, which amplify a 771-bp DNA sequence. A touch-down PCR strategy was followed to amplify 200 ng of DNA samples in 25 µL of PCR mix. DNA isolated from cultured MSC was used as positive control. Amplicons were checked in a 2% agarose gel and a semi-quantitative analysis of the PCR bands was performed using the Fragment Analyzer Auto Capillary Electrophoresis System (Advanced Analytical Technologies, Inc. Ankeny, IA, USA).

Preparation of protein extracts

Preparation of total extracts from tissue

Frozen tissues samples were pulverized in liquid nitrogen, and 50 mg were homogenized for protein extraction in 15 mM HEPES, 10% glycerol, 0.5% NP-40, 250 mM NaCl, 1 mM EDTA, 1 mM PMSF, 1 mMNaF, 1 mM β-glycerophosphate, 1 mM Na3VO4 and protease-inhibitor cocktail (Sigma-Aldrich, St. Louis, Missouri, USA). Resulting extracts were centrifuged (16.000 x g at 4°C for 15 minutes) and supernatants were stored at -80ºC. Protein concentration was determined with the BCA Protein Assay Kit (Pierce, Rockford, Illinois, USA).

Preparation of nuclear extracts from tissue

Frozen, minced synovial membranes were pulverized in liquid nitrogen. Nuclear extracts were isolated from 50 mg of each sample, after homogenization in 20 mM HEPES, 5 nM NaF, 10µM Na_2MoO_4, 0.1 mM EDTA, 0.01% NP-40, 1 M DTT and a phosphatase- and protease-inhibitor cocktail (Sigma-Aldrich, St. Louis, Missouri, USA). The resulting extracts were centrifuged 850 x g at 4ºC for 10 minutes. Pellets were subsequently incubated in hypotonic buffer for 15 minutes at 4ºC, and centrifuged (4°C, 21900 x g, 30 seconds). Finally, the resulting nuclear pellets were suspended in 50 µl of Complete Lysis Buffer (Active Motif, La Hulpe, Belgium), incubated for 30 minutes on ice on a rocking platform and centrifuged at 4°C, 219,00 x g for 10 minutes). Protein concentration present in the supernatant was evaluated by the Bradford's method (Biorad, Madrid, Spain).

Western-blotting

Extraction of total proteins for each synovial membrane was performed (141), and 30 µg were ran on SDS-PAGE gels. Proteins were transferred to nitrocellulose membranes in a semi-dry Trans-Blot device (Bio-Rad, Madrid, Spain) for 40 minutes at 25 V. Membranes were subsequently incubated in blocking solution (5% skimmed milk) for 1 hour at RT.

The primary antibodies listed in the table below were applied by incubating at 4°C overnight (Table 4). For detection of antibody binding, membranes were incubated for 1 hour at RT with peroxidase-linked species-specific secondary antibodies: anti-guinea pig (Abcam, Cambridge, UK; 1:1000) or anti-goat (Merck Millipore, Darmstadt, Germany; 1:5000), or anti-mouse (GE Healthcare Life Sciences Piscataway, New Jersey, USA). Control of total proteins transferred to the membranes was performed staining gels with EZ Blue reagent (Sigma-Aldrich, St Louis, Missouri, USA) (143).

Target	Concentration of use (µg/ml)	Supplier	Product reference
Caspase-1	0.5 µg/ml	Thermo Fisher Scientific, IL, USA	14F468
COX-2	0.4 µg/ml	Santa Cruz Biotechnology, Dallas TX, USA	sc-1745
IL-10	2 µg/ml	Cloud-Clone Corp, Houston TX, USA	PAA056Rb51
IL-18	0.1 µg/ml	Cloud-Clone Corp, Houston TX, USA	PAA064Rb51
IL-1β	1.3 µg/ml	Cloud-Clone Corp, Houston TX, USA	PAA563Rb51
IL-6	1 µg/ml	Cloud-Clone Corp, Houston TX, USA	PAA079Rb51
NLRP3	1 µg/ml	AdipoGen, Liestal, Switzerland	AG-20B-0014
TGF-β	1.3 µg/ml	Cloud-Clone Corp, Houston TX, USA	PAA124Rb51
TNF-α	1 µg/ml	Cloud-Clone Corp, Houston TX, USA	PAA133Rb51

TABLE 4. Primary antibodies employed in western blot studies. COX-2: ciclooxygenase-2; IL: interleukin; NLRP3: NLR family pyrin domain containing 3; TGF-β: tumor growth factor-β, TNF-α: tumor necrosis factor-α.

In vitro experiments

Culture of THP-1 cells

THP-1 monocyte cells (passage 6 to 11) (ATCC, Manassas, Virginia, USA) were grown at 37°C and 5% CO_2 in RPMI 1640 (Gibco BRL, Grand Island, NY) supplemented with 10% heat-inactivated fetal bovine serum (FBS), 50 units/ml penicillin-streptomycin and 2 mM L-Glutamine (Gibco BRL, Grand Island, NY). THP-1 monocytes were differentiated into macrophages in the presence of 0.5 µM Phorbol 12-myristate 13-acetate (PMA, Sigma-Aldrich, St Louis, Missouri, USA) for 3 hours. Cells were centrifuged at 350 x g, washed in PBS and 1 x 10^6 Thp-1 cells per well were plated in 6 well plates. Cells were incubated overnight at 37°C and 5% CO_2 in RPMI 1640, 2% FBS, 50 units/ml penicillin-streptomycin and 2 mM L-Glutamine.

MSC culture

MSC were cultured at 37°C and 5% CO_2 in α-MEM supplemented with GlutaMAX™ (Thermo Fisher Scientific), 50 units/ml penicillin-streptomycin and 5% human platelet lysate (Cook Regentec, USA) at a density of 4 x 10^3 cells/cm^2 and were grown, reaching

80-90% of confluence. Then, cells between passages 3 to 4 were employed for subsequent experiments.

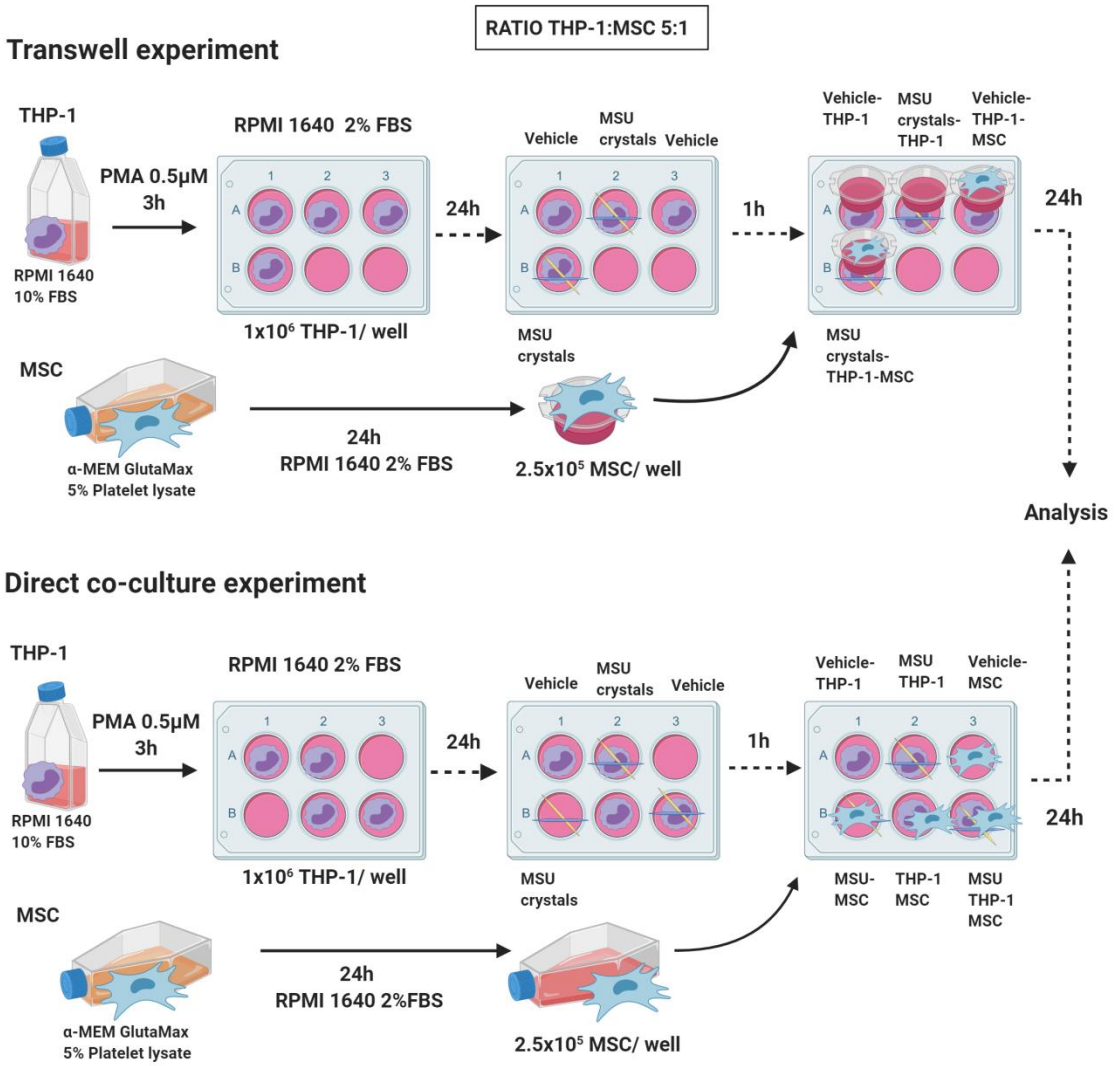

FIGURE 6. Schematic illustration of *in vitro* experimental designs. MSU: monosodium urate crystals; MSC: mesenchymal stromal cells; PMA: phorbol 12-myristate 13-acetate.

Transwell experiments

For Transwell experiments, 2.5 x 10^5 MSC were seeded into polycarbonate Transwell inserts of 24 mm and 0.4 µm membrane pore size (Corning, New York, USA) and cultured overnight at 37°C and 5% CO_2 in RPMI 1640, 2% FBS, 50 units/ml penicillin-streptomycin and 2 mM L-Glutamine. PMA-differentiated THP-1 macrophages were stimulated with 300 µg MSU crystals (Invivogen, San Diego, USA) or

vehicle for 24 hours. One hour after stimuli, empty or MSC-Transwell inserts were placed over THP-1 cells, as explained in Figure 6.

Direct co-culture experiments

MSC were incubated overnight in RPMI 1640, 2% FBS, 50 units/ml penicillin-streptomycin and 2 mM L-Glutamine. PMA-differentiated THP-1 macrophages were stimulated with 300 µg MSU crystals (Invivogen, San Diego, USA) or vehicle (PBS) for 24 hours. One hour after the addition of the stimuli, MSC were harvested and 2.5 x 10^5 cells were seeded into 6 well plates, as explained in Figure 6.

RNA isolation and RT-PCR

RNA was isolated from *in vitro* experiments using TRIzol reagent (Roche Diagnostics, Barcelona, Spain) following manufacturer's instructions and dissolved in nuclease-free water and quantified with a NanoDrop ND1000 spectrophotometer (Thermo Fisher Scientific, Waltham, Massachusetts, USA).

Gene	Reference sequence	Product reference	Amplicon length
Caspase-1	NM_001223.4	Hs00354836_m1	76
COX-2	NM_000963.3	Hs00153133_m1	75
HPRT	NM_000194.2	Hs99999909_m1	100
IDO	NM_002164.5	Hs00984148_m1	66
IL-10	NM_000572.2	Hs00961622_m1	74
IL-1β	NM_000576.2	Hs00174097_m1	94
NLRP3	NM_001079821.2	HS00918082_m1	84
TGF-β	NM_000660.5	Hs00998133_m1	57
TNF-α	NM_000594.3	Hs00174128_m1	80
TSG-6	NM_007115.3	Hs00200180_m1	60

TABLE 5. Commercial TaqMan® gene expression assays used for quantitative PCR studies. Reference sequence refers to nucleotide GenBank ID code (NIH, USA). Product reference alludes to item number in Applied Biosystems assay library. COX-2: ciclooxygenase-2; HPRT: hypoxanthine-guanine phosphoribosyl transferase; IDO: indoleamine 2,3-dioxygenase; IL: interleukin; NLRP3: NLR family pyrin domain containing 3; TGF-β: tumor growth factor-β, TNF-α: tumor necrosis factor-α; TSG-6: TNFα-stimulated gene-6.

A High Capacity cDNA Reverse Transcription Kit (Applied Biosystems, San Francisco, California, USA) was used to reverse-transcript a total of 0.8 µg RNA. RNA expression was determined by single-reporter real-time PCR using the Step One Plus Detection system (Applied Biosystems, Foster City, CA). Commercial TaqMan® primers and probes were used to analyze expression of the genes listed in the table above (Table 5). RNA expression levels were quantified with the ΔΔCt method using the housekeeping gene hypoxanthine-guanine phosphoribosyltransferase (HPRT) as endogenous control.

Statistics

Sample size for each experiment was calculated based on reported recommendations in animal research guidelines (129). Shapiro-Wilks test for sample size inferior to 50 demonstrated non-normal data distribution. Graphpad Prism package (Version 5.0 for Windows) and the SPSS package (Version 11.0 for Windows) were used for statistical analyses. Quantitative data are shown as the mean ± standard deviation (SD) for descriptive statistics; or as the mean ± standard error of the mean (SEM), while categorical variables are shown as absolute frequencies and percentages.

US clinical parameters were correlated with joint swelling and histopathological scores using Spearman's correlation coefficient. Fisher's exact test was applied to assess differences for categorical variables.

Intra-observer reliability was checked with weighted Cohen's κ for GD, STh and PD scoring results and unweighted Cohen's κ for deposit features. 0–0.20 κ values were considered poor, > 0.20– 0.40 fair, > 0.40–0.60 moderate, > 0.60–0.80 good and > 0.80–1 excellent.

When indicated, the right and the left knee joints were analyzed separately to compare direct vs. indirect effect of the treatment administration. To evaluate differences between quantitative variables, multiple comparisons analysis for more than three groups was performed using Kruskal-Wallis non-parametric test with *post-hoc* Dunn test. Mann-Whitney U test was used for the comparison of pairwise groups. The evolution of joint edema between the different groups was compared using two-

way analysis of variance ANOVA (two-way ANOVA), followed by Bonferroni *post hoc* correction for each group. *P* values <0.05 were considered to indicate significance.

RESULTS

“Our empirical criterion for a series of theories is that it should produce new facts. The idea of growth and the concept of empirical character are soldered into one”

- Imre Lakatos

Performance and validity of MSK-US for the assessment of synovial inflammation in rabbit acute gouty arthritis

Firstly, we tested whether MSK-US was a reliable technique for the evaluation of the inflammatory course of the knee synovium of rabbits with acute MSU crystal-induced arthritis, in view of using this approach for the evaluation of the effect of MSC treatment in future experiments.

Measure of joint perimeter

After IA injections of MSU crystals or PBS in both rabbit knees, joint inflammation was followed up by measuring the knee swelling as it is described in the Methods section. We decided to study perimeter increment of each knee at two time points: 24 and 72 hours post injury induction. Arthritic animals displayed greater swelling compared to controls at both time points; 24 h: 1.04 ± 0.71 vs. 0.35 ± 0.48 cm, p=0.011; 72 h: 1.02 ± 0.60 vs. 0.44 ± 0.34, p=0.048).

MSK-US features

MSK-US features of synovitis and crystal-related findings were evaluated at two time points of the study, 24 and 72 hours after MSU or PBS injections. As shown in Table 6, clear differences can be distinguished in both the frequency and the semi-quantitative score mean of MSK-US inflammation components between healthy and arthritic knee joints at both time points. Only PD score was not statistically significant between MSU and control at 72 hours (Table 6). Representative US images (Figure 7 A-C, 7 E-F) of the lateral recess of the knee joint show characteristic phenomena associated to MSU crystal-induced inflammation and crystal deposition. The lateral recess of a healthy knee joint is also represented (Figure 7 D). Both STh and PD signals, which were mostly present in arthritic joints compared to healthy knees (Table 6),

were principally located in the outer border of the joint cavities (Figure 7 A-F). However, discrimination of crystal-related features (Figure 7 A-C) was only possible at 24 hours (Table 6) after injections.

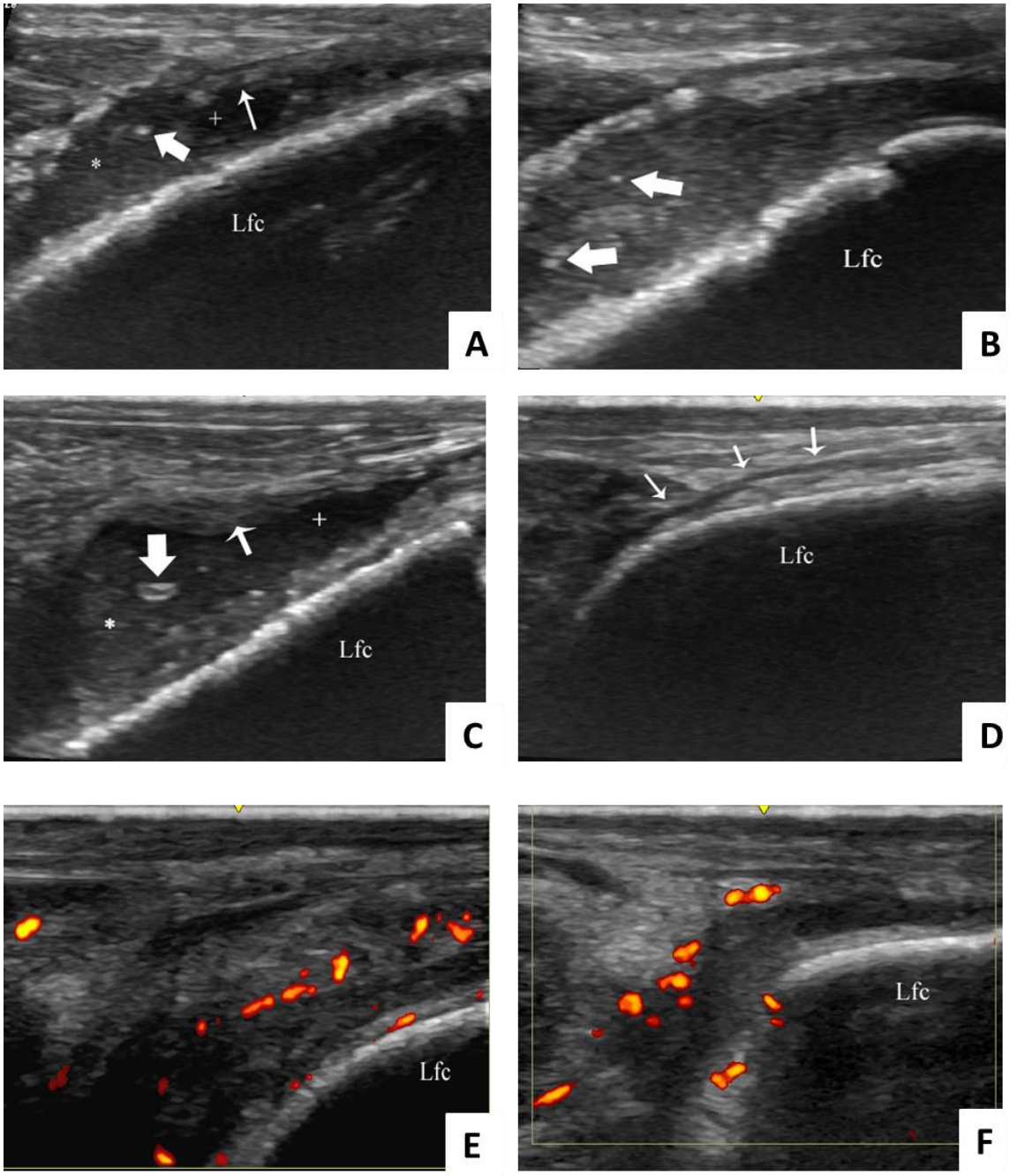

FIGURE 7. Ultrasound images of the lateral recess of rabbit knee joints. (A-C) Monosodium urate crystal-injected rabbit knees **(A)** Increased synovial fluid (+), synovial thickening (thin arrow), sand-like material (*) and a bright focus (thick arrow). **(B)** Bright foci (thick arrows) inside sand-like material. **(C)** Increased synovial fluid (+), synovial thickening (thin arrow), sand-like material (*) and a hyperechoic aggregate (thick arrow). **(D)** Lateral recess of a healthy control rabbit knee (arrows). **(E, F)** Power Doppler-flow signal of an arthritic synovial tissue. Lfc = lateral femoral condyle.

As shown in Table 6, 15 out of 20 MSU-injected knees exhibited different crystal related findings such as SLM, BF or AG at 24 hours, while only 8 of 20 showed those features at 72 hours in the MSU group.

		MSU Freq. n (%)	Control Freq. n (%)	MSU Mean ± SD	Control Mean ± SD
MSK-US features 24 h	**GD**	19 (95)*	0 (0)	2.5 ± 0.6*	1 ± 0
	SF	19 (95)*	0 (0)	2.4 ± 0.6*	1 ± 0
	STH	14 (70)*	0 (0)	1 ± 0.8*	0 ± 0
	PD	11 (55)*	0 (0)	1.2 ± 1.3*	0 ± 0
	SM	11 (55)*	0 (0)		
	AG	7 (35)*	0 (0)		
	BF	11 (55)*	0 (0)		
	SLM	15 (75)*	0 (0)		
MSK-US features 72 h	**GD**	19 (95)*	1 (16.67)	2.0 ± 0.7*	1.2 ± 0.4
	SF	15 (75)*	1 (16.67)	2.0 ± 0.7*	1.2 ± 0.4
	STh	12 (60)*	0 (0)	1.1 ± 0.8*	0 ± 0
	PD	9 (45)*	0 (0)	1.0 ± 1.1	0 ± 0
	SM	8 (40)	0 (0)		
	AG	1 (5)	0 (0)		
	BF	2 (10)	0 (0)		
	SLM	8 (40)*	0 (0)		

TABLE 6. Prevalence and scores of MSK-US pathologic findings in MSU crystal-injected knees and control knees 24 and 72 hours after MSU injection. Values are expressed as the number (and the percentage, %) or as the mean ± SD (n = 6 for control, n = 20 for MSU knees). Fisher's exact test, *p<0.05 vs. Control group. AG: hyperechoic aggregates; BF: bright foci; Freq.: frequency; GD: global distension; MSK-US: musculoskeletal ultrasound; MSU: monosodium urate; PD: synovial power Doppler signal; SF: synovial fluid; SLM: sand-like material; STh: synovial thickening.

An important clearance of crystals-related presence was observed from 24 to 72 hours. No crystal-related findings were detected in healthy animals at any time point (Table 6). Additionally, in contrast to healthy knees, it was possible to observe an

important decrease of inflammatory GD and SF scores from 24 to 72 hours in arthritic knees, while STh and PD did not show a significant variation (Table 7).

Intra-observer reliability (κ value) of US assessment was excellent for most findings. At 24 hours, κ values were 0.82 for GD, 0.81 for SF, 0.82 for STh, 0.84 for PD, 0.92 for SLM, 1 for AG and 0.92 for BF. At 72 hours, κ values were 0.62 for GD, 0.62 for SF, 1 for STh, 0.96 for PD, 1 for SLM and 1 for AG. It was not possible to calculate the κ value for BF at 72 hours because this measure was considered constant for both readings.

		24 h Score, mean ± SD	72 h Score, mean ± SD
MSK-US features MSU	GD	2.5 ± 0.6*	2.0 ± 0.7
	SF	2.4 ± 0.6*	2.0 ± 0.7
	STh	1.0 ± 0.8	1.0 ± 0.8
	PD	1.2 ± 1.3	1.0 ± 1.1
MSK-US features Control	DS	1 ± 0	1.2 ± 0.4
	SF	1 ± 0	1.2 ± 0.4
	STh	0 ± 0	0 ± 0
	PD	0 ± 0	0 ± 0

TABLE 7. Comparison of MSK-US scores of the inflammation findings between 24 and 72 h in the MSU crystal-injected and control groups. Values are expressed as mean ± SD (n = 6 for control, n = 20 for MSU knees). Fisher's exact test, *p<0.05 vs. 72 h. MSK-US: musculoskeletal ultrasound; GD: global distension; h: hours; MSU: monosodium urate; PD: synovial power Doppler signal; SF: synovial fluid; STh: synovial thickening.

Association between MSK-US features and knee joint swelling

We then studied the correlation of the increase observed in the knee perimeter with the GD score measured by MSK-US at both 24 and 72 hours for each rabbit. A statistically significant association was observed with the data obtained 24 hours after MSU crystal injection (Spearman's correlation coefficient r=0.60, p=0.002) (Figure 8 A). However, at 72 hours the measures did not significantly correlated (Spearman's correlation coefficient r=0.03, p=0.9) (Figure 8 B).

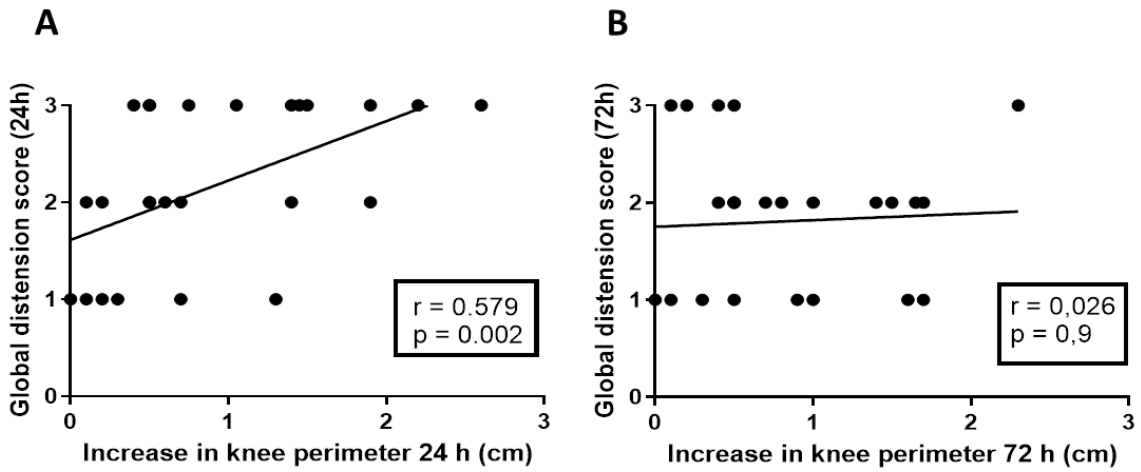

FIGURE 8. Spearman correlation between increase in knee perimeter and GD measurement by MSK-US at 24 h (A) and 72 h (B) after intra-articular injections of MSU crystals. GD: global distension; h: hours; MSK-US: musculoskeletal ultrasound; MSU: monosodium urate.

Association of MSK-US features with synovial histopathology

Rabbits that received MSU crystal injections were sacrificed 72 hours after this aggression, and synovial membranes were then isolated to analyze the histological injury in paraffin embedded sections. In these tissues, we observed significant histological lesions, consisting in lining hyperplasia, stromal activation characterized by altered adipocyte structure and viability, increased vascularization and fibrosis, together with wide spread leukocyte infiltration. The measurement of synovitis using the Krenn score (Figure 9 C) showed a 4-fold increase in this parameter in MSU injected rabbits, in comparison to healthy controls (p<0.001) (Figure 9 A, B). STh score measured by MSK-US at 72 hours was significantly associated with global histopathological score (Spearman's correlation coefficient r=0.47, p=0.019) (Figure 9 D).

Association of US-PD signal with synovial vascularization

The presence of vessels was studied by the immunohistochemical localization of CD31 antigens in the synovial membrane as described in the Methods section. Arthritic animals displayed twice higher vascularization nearby the hyperplasic lining and sub-lining than the healthy synovium (p<0.001) (Figure 10 A, B).

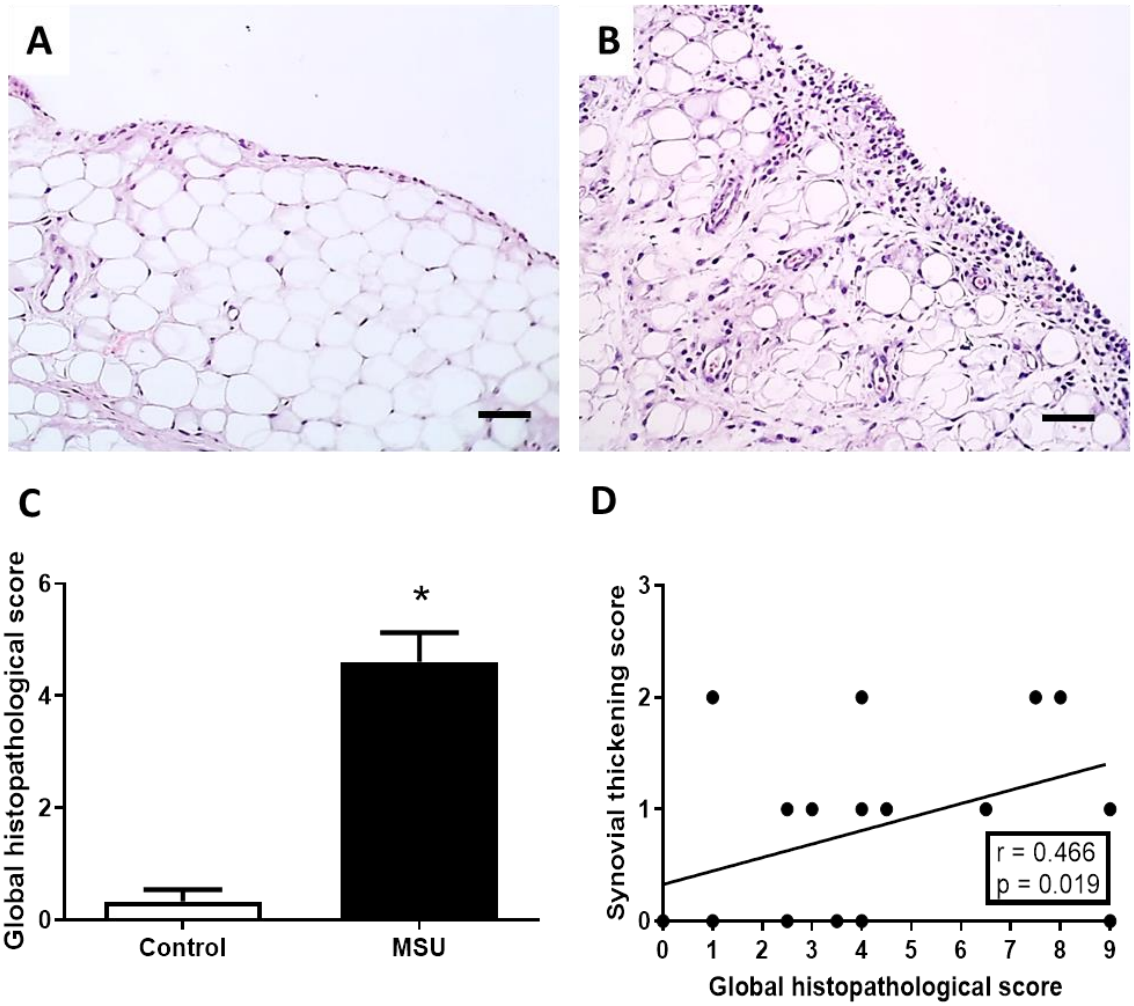

FIGURE 9. **Histopathological evaluation of rabbit synovial membranes. (A, B)** Representative images of healthy control **(A)** and MSU injected **(B)** rabbit synovium stained with hematoxylin and eosin, 72 h after the intra-articular injection. Bars = 50 µm. **(C)** Bars show histopathological scores for control and MSU-injected joints and expressed as the mean and SEM (n = 6 for control, n = 20 for MSU knees). Mann-Whitney test, **p*<0.05 vs. MSU group. **(D)** Spearman correlation between musculoskeletal synovial thickening and the global histopathological score. h: hours; MSU: monosodium urate.

Increased vascularization in MSU injected knees was demonstrated quantifying the percentage of CD31 positive staining, in comparison to that measured in healthy control animals (Figure 10 C). Furthermore, a statistically significant association was observed between the intensity of intra-synovial PD signal and CD31-positive staining, both measured 72 hours after MSU injection (*r*=0.46, *p*=0.017) (Figure 10 D).

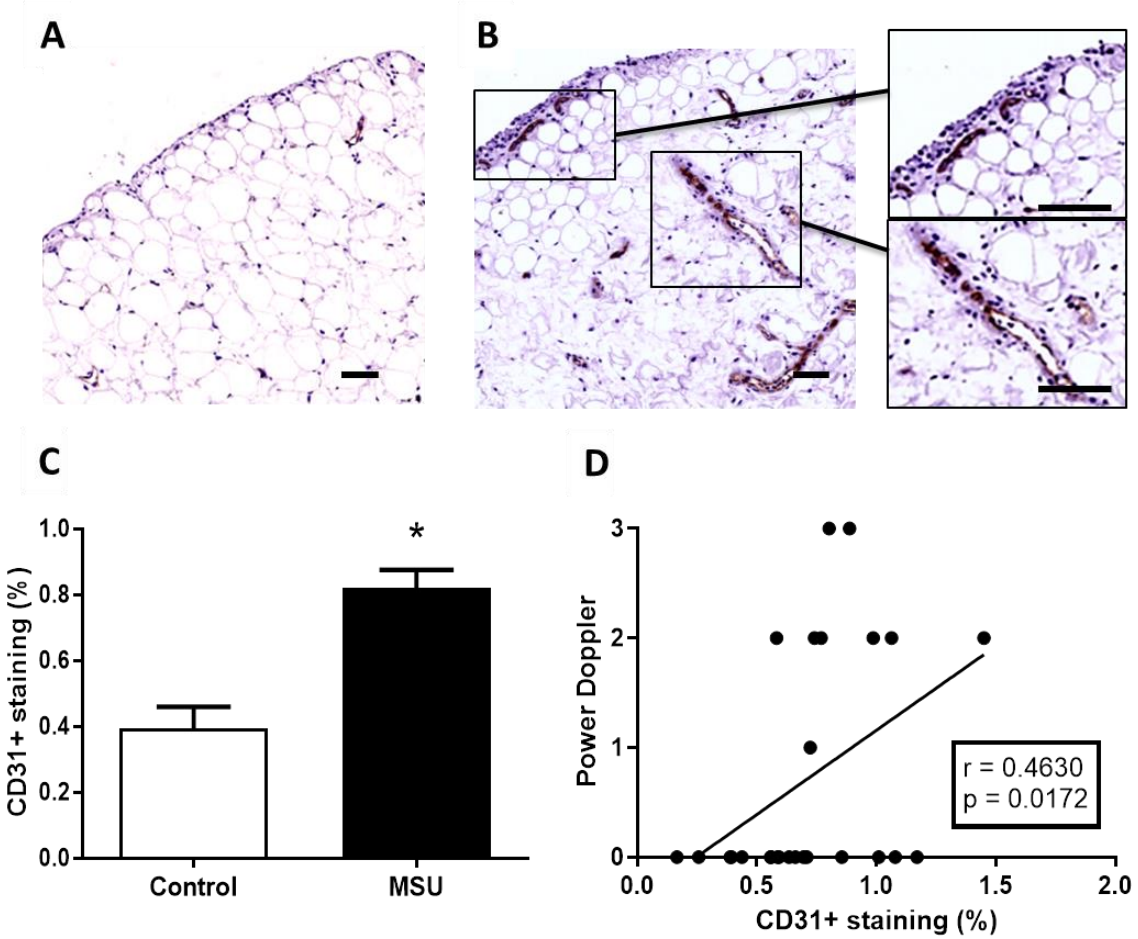

FIGURE 10. Analysis of rabbit synovial vascularization. (A, B) Representative pictures of CD31 immunohistochemical staining in the synovial membrane of control **(A)** and arthritic **(B)** knee joints. Bar = 50 µm. (**C)** Semi-quantitative analysis of CD31-positive vascularization in the synovium of animals in each group. Bars represent the mean and SEM (n = 6 for control, n = 20 for MSU knees). Mann-Whitney test, **p*<0.05 vs. MSU group. **(D)** Spearman correlation between the percentage of CD31-positive staining and power Doppler score in the synovium of rabbits 72 h after the intra-articular MSU crystal injections. h: hours; MSU: monosodium urate.

Association of MSK-US features with IL-1β concentration at synovial membranes

Western blot analysis showed that the level of the pro-inflammatory cytokine IL-1β was increased in the synovial tissue of the MSU group compared to healthy samples (Figure 11 A). GD score, measured by MSK-US 72 hours after MSU injections, was significantly associated with the concentration of pro-IL-1β (r=0.52, p=0.007) in the rabbits' synovium (Figure 11 B).

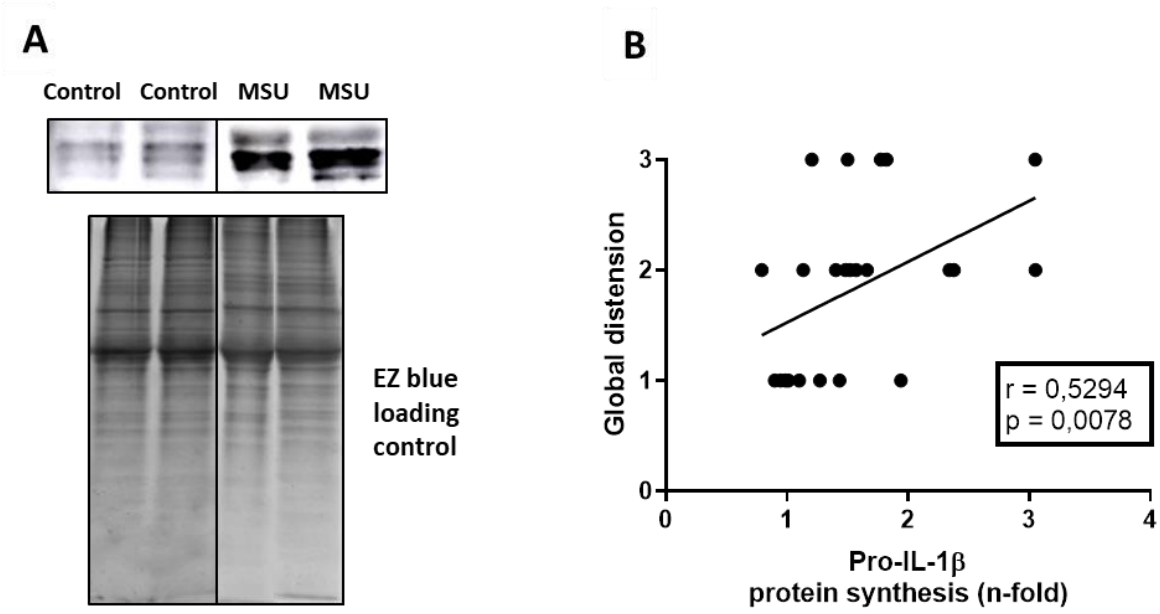

FIGURE 11. Evaluation of IL-1β synthesis in rabbit synovial membranes. (A) Representative Western blot of IL-1β protein levels in the knee synovium of each group. EZ blue staining was employed as protein loading control. **(B)** Spearman correlation between global distension score and pro-IL-1β protein synthesis in the synovial membrane. IL-1β: interleukin-1β; MSU: monosodium urate.

Study of the anti-inflammatory effects and pharmacokinetics of MSC in experimental acute gouty arthritis

Comparison of the therapeutic outcome between local administration and systemic infusion of MSC in acute arthritic rabbits

In order to explore whether MSC administration produced any improvement of inflammation after the MSU crystal injection, and to select the most effective administration route, we firstly evaluated the effect of a systemic infusion through the auricular artery and a local IA application into both rabbit knees, using the same total dose per animal (2.5 x 10^6 MSC/kg). As expected, IA injections of MSU crystals boosted an inflammatory response in a few hours, as it is reflected in the increment of knee perimeter (p<0.001 vs. Control, Figure 12 A), which reached a 1 cm peak on the day after injury. Additionally, serum CRP levels, a measurement of systemic inflammation, (p<0.001 vs. Control), increased up to 750 µg/ml in serum of MSU group (Figure 12 B) 24 hours after MSU injection.

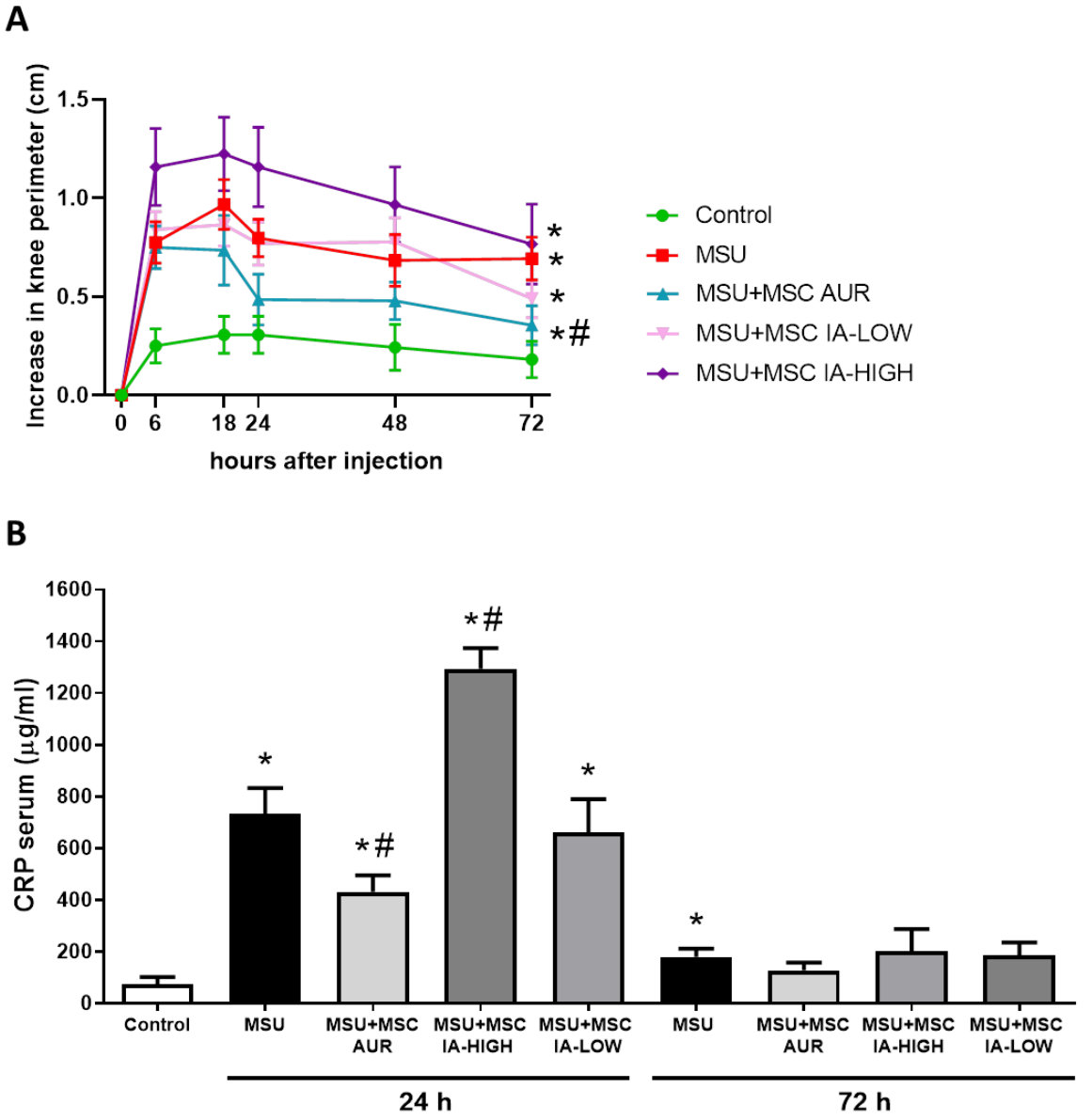

FIGURE 12. Systemic administration of MSC through the right auricular artery, but not local injection into the arthritic knee attenuates knee synovitis. A, joint swelling evolution of each limb during 72 h after MSU crystal injection, comparing different administration routes and doses. Bars show the mean and SEM (n = 10 for control, n = 22 for MSU, n = 18 for MSU+MSC AUR group, n = 6 for MSU+MSC IA-HIGH group, n = 16 for MSU+MSC IA-LOW group). Two-way ANOVA for the comparison between groups, **p*<0.05 vs. Control, #*p*<0.05 vs. MSU. **B,** serum CRP concentration levels of each rabbit at 24 h and 72 h of study. Bars show the mean and SEM (n = 5 for control, n = 10 for MSU, n = 9 for MSU+MSC AUR group, n = 3 for MSU+MSC IA-HIGH group, n = 8 for MSU+MSC IA-LOW group). Mann-Whitney test, **p*<0.05 vs. Control, #*p*<0.05 vs. MSU. AUR: auricular artery; CRP: C-reactive protein; h: hours; IA: intra-articular; MSC: mesenchymal stromal cells; MSU: monosodium urate.

Arthritic animals treated with MSC through systemic administration (MSU+MSC AUR) showed a significantly milder inflammatory response compared to MSU rabbits. The time course of joint swelling was significantly different in MSU+MSC AUR rabbits in

comparison to MSU animals (p=0.026). However, local administration of MSC did not seem to induce any significant change in the joint swelling during this acute phase of the disease. As it can be observed in Figure 12 A, the administration of the same total dose of MSC to that systemically inoculated, did not significantly modify joint perimeter in MSU+MSC IA-HIGH group, in comparison to MSU group measurements (*p*=0.065).

Since local administration of MSC has been proposed as a method to reduce the number of MSC to be administered in order to reach a significant improvement in tissue inflammation, we also tested the effect of a lower dose: 5 x 10^5 MSC/kg. MSU+MSC IA LOW knees showed a similar joint swelling evolution to that observed in the MSU vehicle group (*p*=0.9 vs. MSU) (Figure 12 A).

Additionally, 24 hours after the MSU crystal injection, concentration of serum CRP levels in the MSU+MSC AUR group were significantly lower than those measured in the MSU (*p*=0.02), as shown in Figure 12 B. Local administration of the same total dose evoked an increase in CRP serum levels, almost reaching 1300 µg/ml (*p*=0.028, MSU+MSC IA-HIGH vs. MSU). On the other hand, a lower dose of locally injected MSC (MSC IA-LOW) produced a similar increment of systemic CRP levels to that observed in the MSU group (*p*=0.76) 24 hours after injury (Figure 12 B). The increase in circulating CRP persisted 72 hours after MSU injection in the MSU group, in comparison to control (*p*=0.02), while none of the MSC-treated groups showed significant differences in these levels neither vs. MSU group, nor vs. Control animals (Figure 12 B).

Effect of systemic administration of MSC through the right femoral artery

After we demonstrated that local injection of the therapy resulted in no better outcome than infusing MSC through the auricular artery, we proceeded to further study the anti-inflammatory effects of a systemic administration of these cells. Hence, we decided to test the intra-femoral delivery of MSC instead of intra-auricular route, to test whether MSC reaching the arthritic synovium directly from the blood stream exerted an improved therapeutic effect compared to MSC that reached the inflamed

tissue through distant infusion. Subsequently, MSC were infused along the right femoral artery 1 cm below the aortic bifurcation. According to this approach, the right synovial membrane received the cells directly through the right femoral artery, while the left synovial membrane received the cells after its vascular distribution through the organism.

So, firstly we aimed to compare the effect of MSC infusion through the right femoral artery between both the right and left knee joints. Likewise, as previously observed, MSU crystals triggered a substantial increase in the knee perimeter after injections (p<0.001 vs. Control). Additionally, the therapeutic effect achieved injecting MSC through the femoral route was comparable to the auricular one. The increase of knee perimeter in the right knee of MSC-treated animals was not significantly different to that observed in the untreated MSU group (p=0.29). Similar results were observed in the left knee of MSU+MSC FEM animals when compared to the untreated group (p=0.16) (Figure 13 A). However, it is important to note that both the right and left limbs of the MSC-treated group were independently analyzed, and the sample sizes of these groups were probably lower than those needed to obtain statistically significant results. Nevertheless, the main goal of this study was to compare the right vs. the left knee of MSU+MSC FEM rabbits. As it can be observed in Figure 13 A, no differences were found in the increase of knee joint swelling between both limbs that received MSC (p>0.99). Synovial membranes from MSU+MSC FEM rabbits had reduced pathological features, such as softer stromal activation, less number of infiltrating cells and a slightly thinner lining layer, in contrast with non-treated arthritic synovium, in both the right (p=0.047 vs. MSU) and left (p=0.021 vs. MSU) knees. Histopathological score also showed that right and left synovial membranes were likewise damaged at 72 hours after MSU injection *(*p=0.48, Figure 13 B-F).

In order to better describe the effect of MSC on the pathological features of the arthritic synovium, we studied tissue vascularization, analyzing the percentage of endothelial $CD31^+$ antigens marked by immunohistochemistry, as explained in the Methods section (Figure 14 A-D).

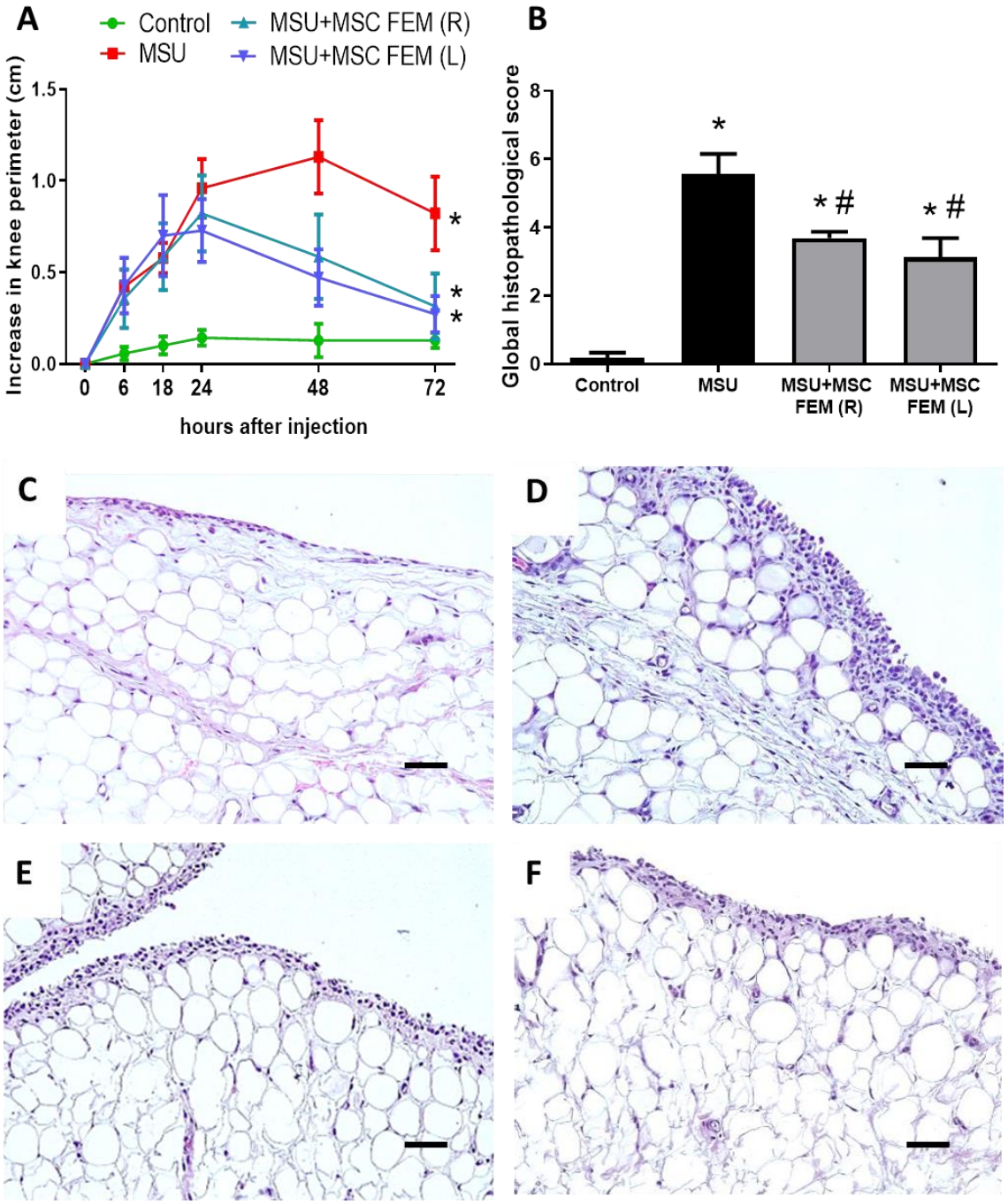

FIGURE 13. Systemic administration of MSC through the right femoral artery produces the same effect in rabbit knees injected with MSU crystals. A-B, joint swelling evolution of each limb during 72 h after MSU crystal injection. Bars show the mean and SEM (n = 7 for controls, n = 16 for MSU, n = 7 for MSU+MSC FEM (R) group and n = 7 for MSU+MSC FEM (L) group). Two-way ANOVA for the comparison between groups, *p<0.05 vs. Control, #p<0.05 vs. MSU. **C-D,** global histopathology score according to Krenn scale; C, Bars show the mean and SEM (n = 7 for controls, n = 16 for MSU, n = 7 for MSU+MSC FEM (R) group and n = 7 for MSU+MSC FEM (L) group); **E-H**, Representative sections of hematoxylin and eosin staining of the synovium. Control **(E),** MSU **(F)**, MSU+MSC FEM (R) **(G)**, MSU+MSC FEM (L) **(H).** Scale bar = 50 µm. Mann-Whitney test, *p<0.05 vs. Control, #p<0.05 vs. MSU. FEM: femoral artery; h: hours; L: left; MSC: mesenchymal stromal cells; MSU: monosodium urate; R: right.

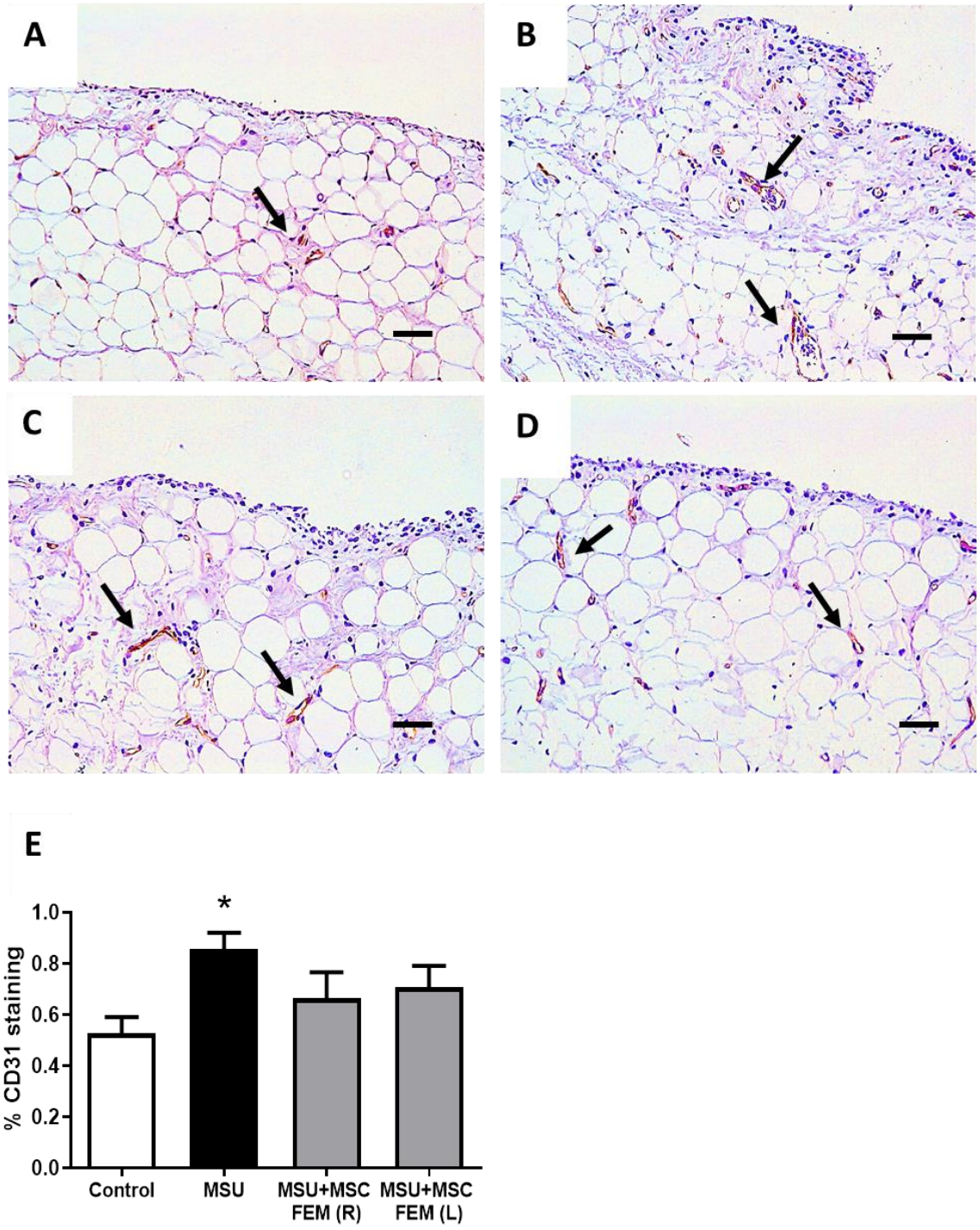

FIGURE 14. Systemic infusion of MSC through the right femoral artery produces the same effect in both right and left arthritic synovial membranes. (A-D) Representative images of CD31 immunostaining in the synovial membranes of control **(A)**, MSU **(B)**, MSU+MSC FEM (R) **(C)** and MSU+MSC FEM (L) **(D)** groups at 72 h, scale bar = 50 µm. Arrows point out some blood vessels**. E**, densitometric assessment of the percentage of CD31+ cells in the synovial membrane of each group of animals. Bars show the mean and SEM (n = 7 for controls, n = 16 for MSU, n = 7 for MSU+MSC FEM (R) and n = 7 for MSU+MSC FEM (L). Mann-Whitney test, *p<0.05 vs. Control, # p<0.05 vs. MSU. FEM: femoral artery; h: hours; MSC: mesenchymal stromal cells; MSU: monosodium urate.

Synovial membranes from the MSU group presented an intensified CD31 staining (*p*=0.0016) in comparison to control animals. However, there was a non-statistically significant reduction of synovial blood vessels in the right (*p*=0.077 vs. MSU) and left (*p*=0.12 vs. MSU) knee joints. Remarkably, no differences were found between MSC-treated arthritic right and left paws (p>0.99) (Figure 14).

Biodistribution of human MSC in rabbit tissues after systemic administration

We then proceed to investigate whether the intra-femoral administration of MSC resulted in a different distribution into both the right and left arthritic synovial membranes, and whether these cells were entrapped in different rabbit tissues. Thus, we harvested different organs 24 hours after injury. We studied the presence of human xenogeneic DNA analyzing human mitochondrial cytochrome C gene in rabbit synovial membranes, lung, liver and spleen tissues.

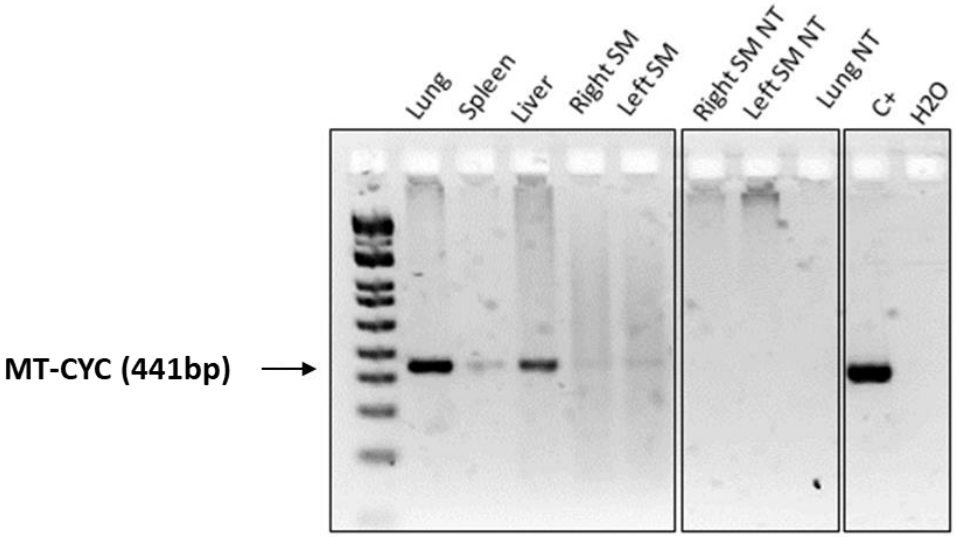

FIGURE 15. Biodistribution of MSC in different arthritic rabbit tissues. Representative touch-down PCR of human cytochrome C (441bp) in different arthritic rabbit tissues 24 hours after human MSC systemic administration. Left panel: Tissue from rabbits that received human MSC through the femoral artery; Middle panel: Tissue from rabbits that no received human MSC. NT: non-treated rabbits; MT-CYC: mitochondrial cytochrome C gene; SM: synovial membrane; C+: positive control.

In contrast to non-treated animals, PCR amplicons of human genetic material were detected on arthritic animals that received FEM administration of MSC (Figure 15). Human mitochondrial DNA was detected in every lung and liver (4 out of 4), and in the

75% of spleens (3 out of 4) of the MSC-treated rabbits assayed (Table 8). Human DNA material was also found in the arthritic synovium of the treated rabbits, although in a much lesser quantity than those observed in the rabbit lung, liver or spleen tissues accordingly to band intensity. In fact, we were able to detect human DNA in 38% (37.5%) of the synovial tissues in the treated animals (Table 8). According to our data, the percentage of synovial membranes where we were able to detect human DNA was similar between the left and right synovial membranes (p=0.5).

	MSU+MSC FEM					MSU		
Tissue	**Lung**	**Spleen**	**Liver**	**Right SM**	**Left SM**	**Lung**	**Right SM**	**Left SM**
FREQUENCY	4/4 100%	3/4 100%	4/4 100%	2/8 25%	4/8 50%	0%	0%	0%
				6/16 37,5%				

TABLE 8. Biodistribution frequencies of MSC in rabbit tissues of treated (MSU+MSC FEM) and non-treated (MSU) arthritic animals. FEM: femoral artery; MSC: mesenchymal stromal cells; MSU: monosodium urate; SM: synovial membrane.

Study of the therapeutic outcome of MSC on rabbits after an acute arthritis relapse

We then decided to investigate whether, besides its effect on acute inflammation 72 hours after MSU administration, MSC were able to exert a protective effect after the induction of a second arthritic flare. For this purpose, we employed a group of rabbits in which MSU crystals were re-injected into both injured knees 15 days after the first insult (Figure 16).

As expected, MSU and MSU+MSC FEM rabbits showed a significant joint swelling after the first MSU crystal injection (p<0.001 vs. Control respectively). This was clearly diminished by MSC systemic administration (p=0.021 vs. MSU, Figure 16 A).

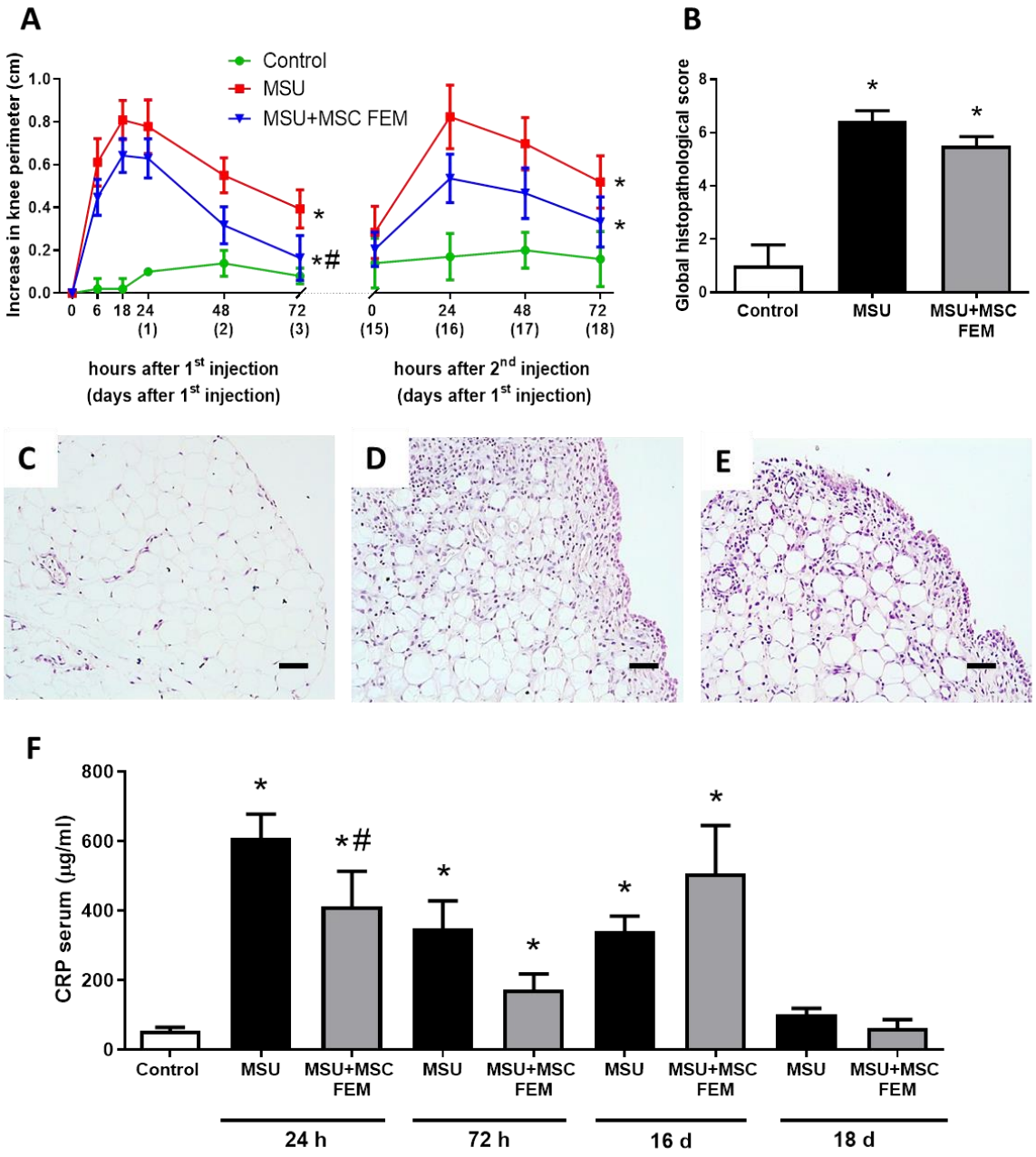

FIGURE 16. Systemic administration of MSC through the right femoral artery does not protect against a second arthritic flare. A, joint swelling evolution of each limb during 72 h after MSU crystal injection and during 72 h after the second MSU crystal injection. Bars show the mean and SEM. (n = 6 for controls, n = 22 for MSU, n = 24 for MSU+MSC FEM group). Two-way ANOVA for the comparison between groups, **p*<0.05 vs. Control, #*p*<0.05 vs. MSU. **B,** global histopathology score according to Krenn scale; (n = 6 for controls, n = 20 for MSU, n = 22 for MSU+MSC FEM group). **C-E**, Representative sections of synovium. Control **(C),** MSU **(D)**, MSU+MSC FEM **(E).** Scale bar = 50 µm. **F,** serum C-Reactive protein concentration levels. Bars show the mean and SEM (n = 6 rabbits for controls, n = 10 for MSU and n = 12 for MSU+MSC FEM group at 24 and 72 h of study; n = 4 for both MSU and MSU+MSC FEM groups at day 16 and 18 of study). Mann-Whitney test, **p*<0.05 vs. Control, #*p*<0.05 vs. MSU. FEM: femoral artery; h: hours; MSC: mesenchymal stromal cells; MSU: monosodium urate.

After a second injection of MSU crystals was administered 15 days apart into the same joints, MSU and MSU+MSC FEM groups developed an increase in joint perimeter comparable to that observed after the first MSU administration (p<0.001, and p=0.014 vs. Control, respectively). However, there were no statistically significant differences in the joint swelling between arthritic MSC-treated and non-treated groups (p=0.074, Figure 16 A).

Serum CRP levels in MSU group were very much alike to those observed previously 24 hours after the first MSU crystals-induced flare, increasing up to 650 µg/ml (p<0.001) (Figure 16 F). Consistently with previous findings, MSC therapy was able to accelerate the reduction of CRP levels (p=0.027 vs. MSU). At 72 hours, differences between MSU and MSU+MSC FEM group were not so evident (p=0.09) (Figure 16 F).

On the other hand, 1 day after the re-aggression, CRP concentration levels reached 350 µg/ml in MSU group (p<0.001 vs. Control). Nevertheless, in this case, no differences were found between MSU and MSU+MSC animals (p=0.68 24 hours after the second injury). Three days day following the second crystal injection, circulating CRP levels of arthritic animals were normalized (p=0.053 MSU vs. Control). As expected, at this time point CRP concentration of treated and non-treated animals was similar (p=0.2) (Figure 16 F).

We also evaluated joint inflammation by MSK-US evaluation in the animals studied 24 and 72 hours after the second MUS administration. US inflammatory features GD (p<0.001 at 24 h, p=0.006 at 72 h), STh (p=0.003 at 24 h, p=0.002 at 72 h), and PD (p=0.003 at 24 h), were able to discriminate between the healthy controls and the MSU group. PD at 72 hours approached significance (p=0.056 vs. Control). However, no differences were found between the MSU and MSU+MSC FEM groups, either at 24 or at 72 hours after the first MSU injections (GD p=0.5 at 24 h, p=0.6 at 72 h; STh p=0.9 at 24 h, p=0.98 at 72 h; PD p=0.9 at 24 h, p=0.39 at 72 h, Figure 17).

Three days after the MSU crystals re-aggression, MSK-US was capable to differentiate GD, STh and PD of MSU from Control synovial membranes (p=0.016, p=0.008, p=0.015 respectively). In line with the above described, this technique did not reveal meaningful differences between the MSU and MSU+MSC FEM animals 3 days

after the induction of the second arthritic flare (GD p=0.49; STh p=0.65; PD p=0.56, vs. MSU, Figure 17).

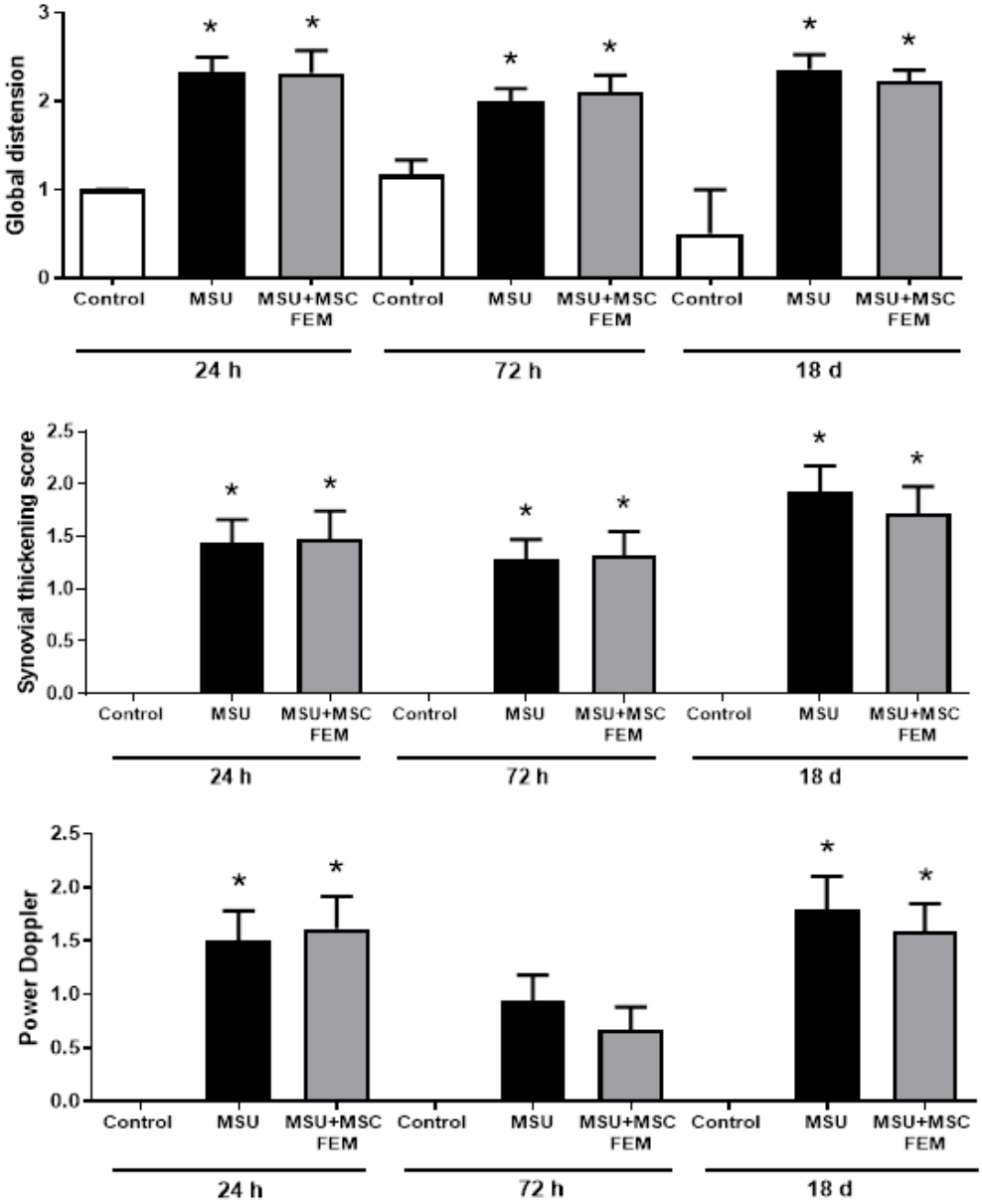

FIGURE 17. MSK-US inflammatory features 24 h, 72 h and 18 days after the first MSU crystal flare. Bars show the mean and SEM (n = 6 for controls, n = 18 – 14 for MSU, n = 19 – 18 for MSU+MSC FEM group). Mann-Whitney test, *p<0.05 vs. Control, #p<0.05 vs. MSU. FEM: femoral artery; h: hours; MSC: mesenchymal stromal cells; MSU: monosodium urate.

Interestingly enough, histopathological evaluation revealed that 72 hours after the second MSU administration, synovial membranes presented severe pathological features likewise to those observed 72 hours after the first MSU injection, depicted in Figure 16 B. However, a unique dose of MSC administered 1 hour after the first MSU

injection was not capable of significantly attenuating the histopathological score 3 days after the second MSU-induced injury (p=0.08 MSU+MSC FEM vs. MSU) (Figure 16 B), although a downward tendency was observed.

Study of MSC effects on inflammatory mechanisms in the acute arthritis model after their intra-femoral administration

We previously observed that not only MSC exerted the same beneficial effect in both the right and left limbs, but also they distributed equally into both synovial membranes. We then decided to go deeper into the molecular mechanisms triggered by MSC on the MSU crystal-induced synovitis. In order to diminish the number of animals employed for this purpose, we considered that both the right and the left synovial membranes of MSU arthritic rabbits that systemically received MSC through their right femoral arteries were independent samples. Hence, data from both membranes were gathered for the subsequent analyses, allowing decreasing the number of animals employed for these studies.

Resulting data indicated that MSC clearly ameliorated joint swelling (p=0.042 vs. MSU), which was noticeable from 24 to 72 hours after MSU injections (Figure 18 A). Additionally, MSC-treated synovial membranes presented milder pathological findings 72 hours after injury, as mentioned before (Figure 18 C-E); being evidenced in the histopathological score (p=0.009 vs. MSU, Figure 18 F). In line with these data, MSC-treated animals exhibited less new forming vessels (p=0.03 vs. MSU, Figure 19).

Regarding the systemic effects, the injection of MSU crystals into the joints induced a time-dependent increase in rabbit serum CRP levels (p<0.001 vs. Control) similarly to preceding results. Also in this case, MSC had a marked effect on systemic inflammation evoked by MSU injection, especially 24 hours after injury (p=0.004, Figure 18 B), while at 72 hours this difference was not so pronounced.

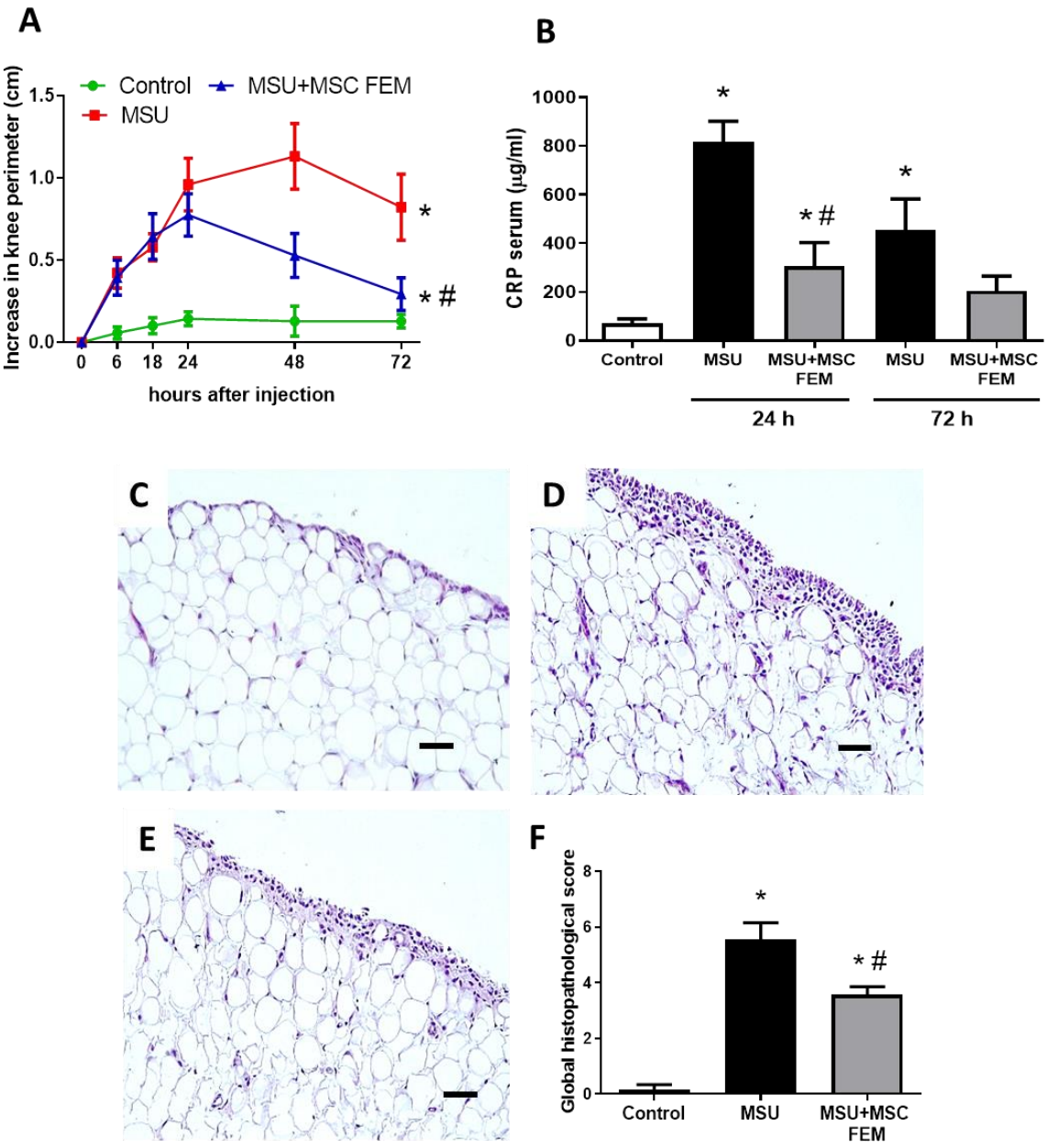

FIGURE 18. Systemic administration of MSC through the right femoral artery attenuates synovitis in both rabbit knees injected with MSU crystals. A, joint swelling evolution of each limb during 72 h after MSU crystal injection. Bars show the mean and SEM. **A** (n = 7 for controls, n = 16 for MSU and n = 14 for MSU+MSC FEM group). Two-way ANOVA for the comparison between groups, **p*<0.05 vs. Control, #*p*<0.05 vs. MSU. **B,** serum CRP concentration levels at 24 h and 72 h of study. Bars show the mean and SEM (n = 4 for controls, n = 8 for MSU and n = 7 for MSU+MSC FEM group). Representative sections of synovium hematoxylin and eosin staining. Control **(C)**, MSU **(D)**, MSU+MSC FEM **(E)**. Scale bar = 50 µm. **F,** global histopathology score according to Krenn scale. Bars show the mean and SEM (n = 7 for controls, n = 15 for MSU and n = 12 for MSU+MSC FEM group). Mann-Whitney test, **p*<0.05 vs. Control, #*p*<0.05 vs. MSU. CRP: C-reactive protein; FEM: femoral artery; h: hours; MSC: mesenchymal stromal cells; MSU: monosodium urate.

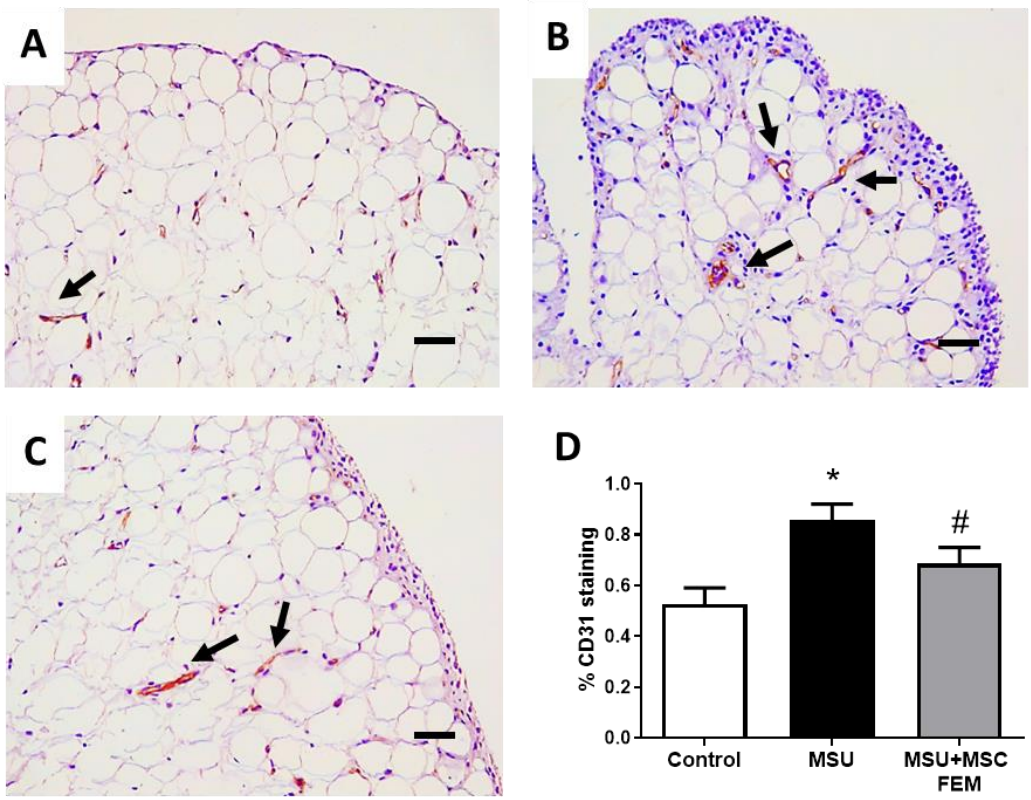

FIGURE 19, Systemic administration of MSC through the right femoral artery reduces vascularization of rabbit-arthritic synovium. (A-C) Representative sections of immunohistochemical staining of CD31 in the synovium of control **(A)**, MSU and **(B)** and MSU+MSC FEM **(C)** groups at 72 h, scale bar = 50 µm. Arrows point out blood vessels. **D**, shows densitometric analysis of CD31 staining percentage in the synovial membrane of each group of animals. Bars show the mean and SEM (n = 7 for controls, n = 16 for MSU and n = 14 for MSU+MSC FEM). Mann-Whitney test, *p<0.05 vs. Control, # p<0.05 vs. MSU. FEM: femoral artery; MSC: mesenchymal stromal cells; MSU: monosodium urate.

Leukocyte presence in synovial fluid of rabbit knees

We next performed a sequential study of leukocyte infiltrate in the synovial fluid of each rabbit knee at 24 and 72 hours after MSU crystal injections. Total leukocyte number was dramatically increased in the synovial fluid of MSU and MSU+MSC FEM animals compared to controls (p<0.001 vs. Control) 24 hours after injury. No significant differences were found between both groups at this time point (p=0.29, Figure 20 A). Interestingly, a 10-fold drop of cellularity from 24 to 72 hours was observed (Figure 20 A). At 72 hours, arthritic animals also showed a marked increment of total leukocyte number in comparison to controls (p<0.001 MSU vs. Control). Meaningfully, at this time point MSC administration decreased the number of inflammatory cells in the

synovial fluid of inflamed knees, compared with untreated ones (p=0.018, Figure 20 A), reducing the mean of total leukocyte number from 5 x 10^6 to 2 x 10^6 leukocytes/ml.

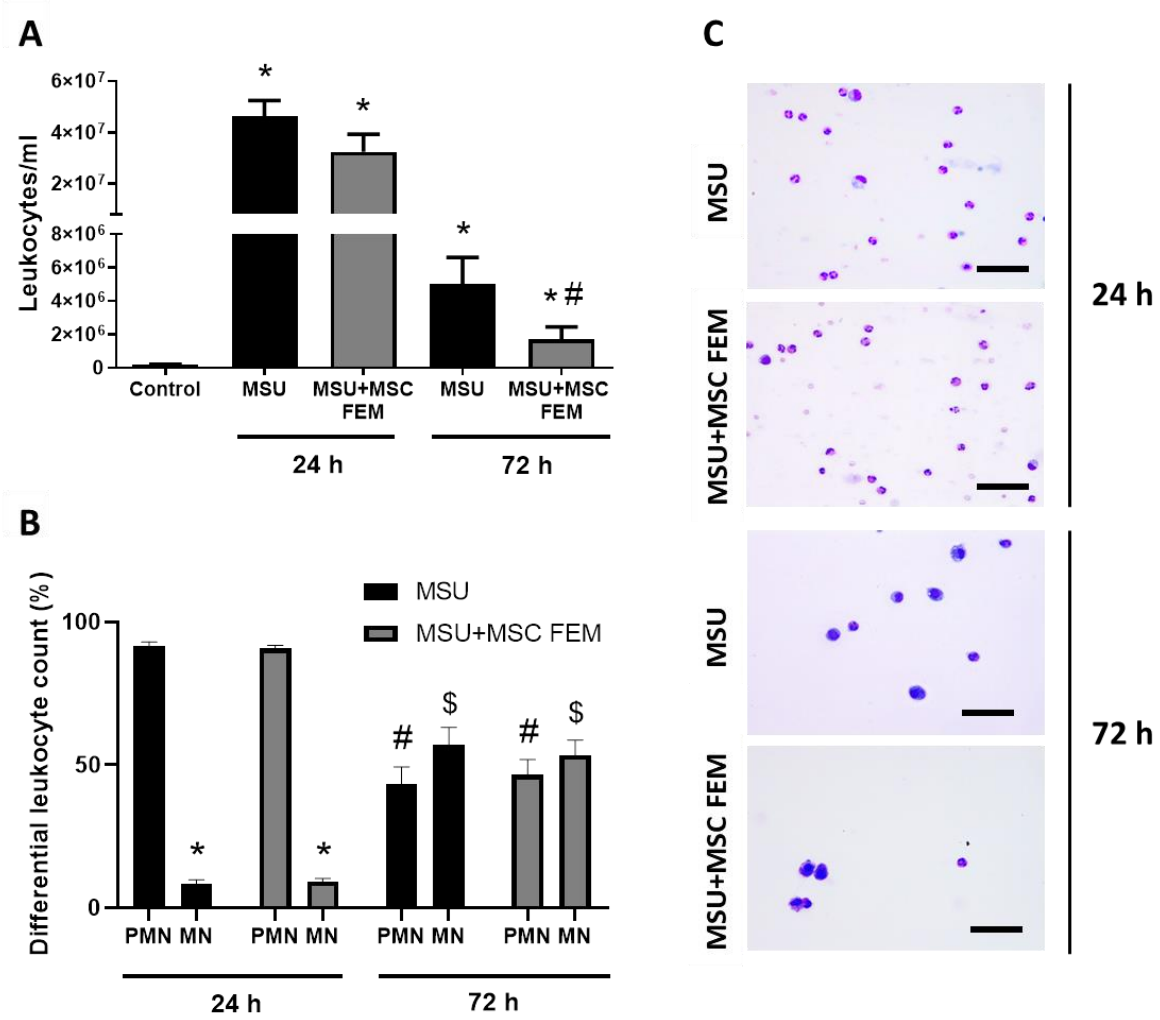

FIGURE 20. Systemic administration of MSC through the right femoral artery reduces total leukocyte population at 72 h but do not alter percentage of PMN-MN cells. A, leukocyte count in synovial fluid at 24 h and 72 h. Mann-Whitney test, * p<0.05 vs. Control, # p<0.05 vs. MSU at their respective time. **B,** differential leukocyte count at 24 h and 72 h. Mann-Whitney test, * p<0.05 vs. PMN at 24 h, # p<0.05 vs. PMN at 24 h, $ p<0.05 vs. MN at 24 h. Bars show the mean and SEM (n = 7 for controls, n = 8 for MSU and n = 8 for MSU+MSC FEM group at 24 h; n = 15 for MSU and n = 12 for MSU+MSC FEM group at 72 h). **C**, representative images of synovial fluid samples of MSU and MSU+MSC FEM groups stained with May-Grünwald Giemsa at 24 h and 72 h**.** Scale bar = 50 µm. FEM: femoral artery; h: hours; MN: mononuclear; MSC: mesenchymal stromal cells; MSU: monosodium urate; PMN: polymorphonuclear.

Concerning the percentage of PMN and MN cells present in each sample 24 hours after MSU-induced arthritis, the synovial fluid from both MSU and MSU+MSC FEM animals was essentially infiltrated by PMN, reaching approximately 90% of the total leukocyte population (p<0.001 MN vs. PMN). No meaningful differences in the

distribution of leukocyte types, PMN (p=0.54) and MN (p=0.54) cells percentage, were found between MSU and MSU+MSC FEM groups (Figure 20 B).

Differential cell count results showed that, 72 hours after MSU crystal injury, the distribution of leukocyte types changed, in comparison to the distribution observed at 24 hours. Interestingly enough, PMN presence drastically diminished from 24 to 72 hours in both arthritic groups (p<0.001), while MN cells were highly increased (p<0.001, Figure 20 B). At 72 hours, synovial fluid was populated by a similar percentage of PMN and MN cells in both MSU (43% and 57% respectively); and MSU+MSC FEM knees (47% and 53%, respectively). Alike to that occurring at 24 hours, no important differences of PMN (p=0.58) and MN (p=0.58) percentage were found between these animals (Figure 20 B). Differential staining of leukocyte population in synovial fluid of both MSC-treated and non-treated arthritic animals at both time points studied after the injection of MSU crystals into the joints can be observed in Figure 20 C.

Study of MSC treatment on total macrophage synovial infiltration, and M1 and M2 macrophage polarization

Extensive macrophage infiltration is characteristic of MSU crystal-induced arthritis. We evaluated whether the treatment with MSC was able to alter the balance of different macrophage subsets towards an anti-inflammatory phenotype in the arthritic synovial membrane. In order to study the presence and disposition of rabbit macrophages, we immune-stained synovial samples with both a RAM11 antibody, which detects rabbit macrophages in all their different phenotypes; and an anti-CD163, a cell marker of monocyte and macrophage lineage that has been reported to be overexpressed in anti-inflammatory M2a macrophages (46,144).

Our results indicated that RAM11 positive cells were mostly distributed along the synovial lining cell layer of synovial membranes (Figure 21 A-C). Additionally, in some joints injected with MSU crystals, macrophages aggregations were observed surrounding adipocytes arranging in “crown-like” structures nearby sub-lining vessels.

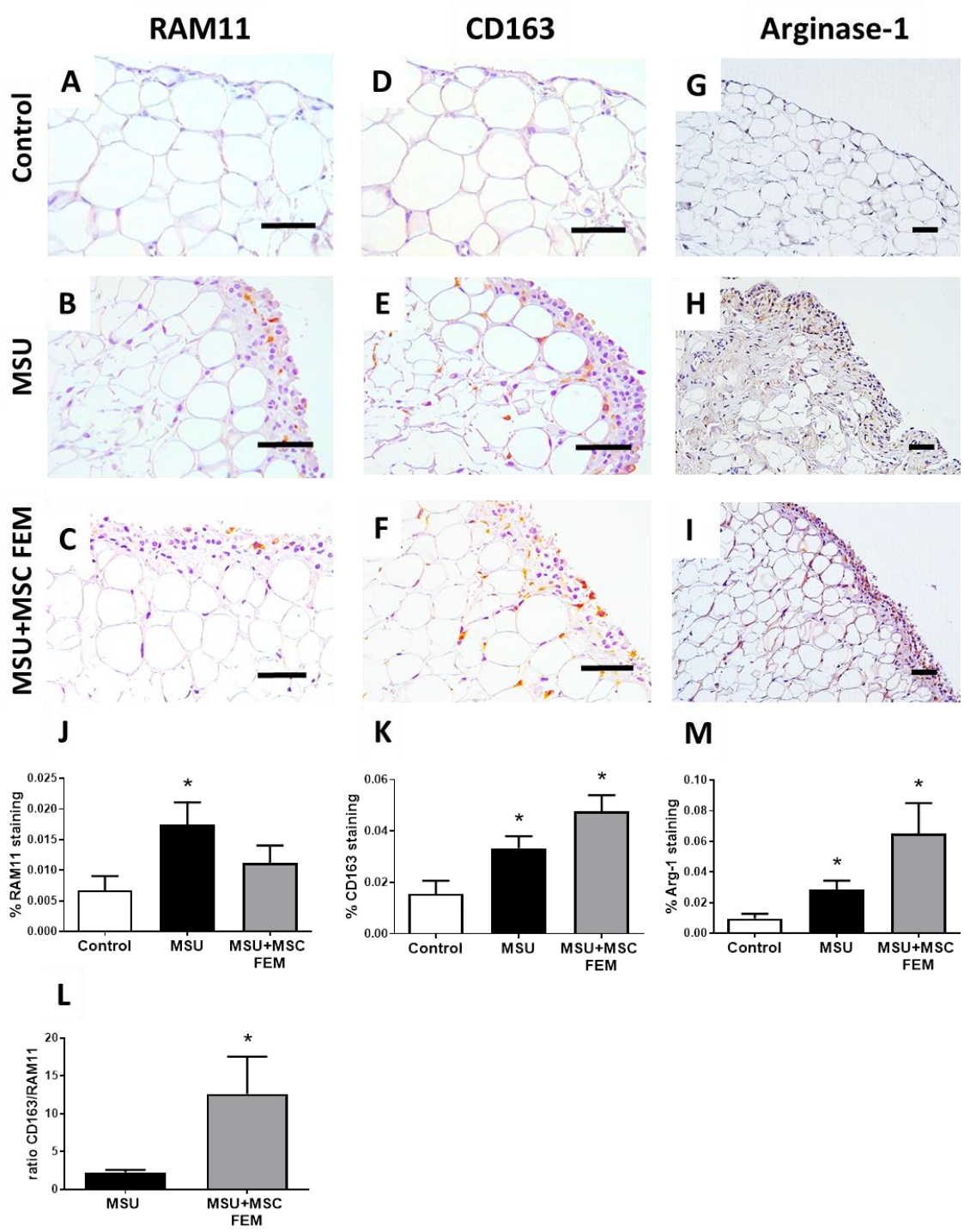

FIGURE 21. Immunohistochemical analysis of macrophage population within synovial membranes at 72 hours after insult. Representative sections of RAM11 antigen staining **(A-C)** in the synovium of control **(A)**, MSU and **(B)** and MSU+MSC FEM **(C)** groups; CD163 staining **(D-F)** in control **(D)**, MSU and **(E)** and MSU+MSC FEM **(F)** groups; and arginase-1 staining **(G-I)** in control **(G)**, MSU and **(H)** and MSU+MSC FEM **(I)** groups, scale bars = 50 µm. Densitometric analysis of RAM11 **(J)**, CD163 **(K)**, Arginase-1 **(M)** staining percentage in the synovium of each group. **L**, ratio of CD163 to RAM11 positive staining. Bars show the mean and SEM (n = 7 – 8 for controls, n = 14 for MSU and n = 9 – 12 for MSU+MSC FEM group). Mann-Whitney test, *p<0.05 vs. Control, #p<0.05 vs. MSU. Arg-1: arginase-1; FEM: femoral artery; MSC: mesenchymal stromal cells; MSU: monosodium urate.

RAM11 positive cell number was significantly incremented in MSU rabbits compared to healthy animals (p=0.027 vs. Control, Figure 21 J). In MSU+MSC FEM treated group, no statistically significant decrease was observed in RAM11 positive staining compared to the MSU group (p=0.14).

We also examined CD163 along the synovial lining layer, where RAM11 staining predominates (Figure 21 D-F). In this case, $CD163^+$ cells were statistically significantly increased in both MSU treated (p=0.003) and MSU+MSC FEM groups (p=0.03) when compared to healthy samples. However, no significant differences were found between these two groups (p=0.1, Figure 21 K). Notwithstanding, to evaluate a putative change in the polarization of the infiltrated macrophages population between the arthritic groups, we analyzed the ratio of the anti-inflammatory M2 marker presence (CD163+ macrophages) and the total macrophage presence (RAM11+ macrophages) for each synovial membrane sample (145). Noteworthy, this CD163/RAM11 ratio showed a clear increase in the MSU+MSC FEM group in comparison to MSU animals (p=0.037 vs. MSU), as shown in Figure 21 L.

Thereafter, in order to support this result, we performed the analysis of arginase-1, which has been employed as a marker of M2 polarization (146). We observed an increased amount of arginase-1 along the lining layer of MSU injected groups, where most of macrophages were distributed (Figure 21 G-I). Positive staining quantification revealed that MSU+MSC FEM rabbits showed an increased presence of arginase-1 in comparison to untreated rabbits, that was very close to reach statistical significance (p=0.063 vs. MSU, Figure 21 M).

The effect of MSC on the synthesis of different pro- and anti-inflammatory mediators in arthritic rabbit synovium

As expected, MSU rabbits showed increased levels of pro-inflammatory cytokines in the synovial membrane 72 hours after MSU crystal injections. COX-2 (p=0.012) and TNF-α (p=0.031) synthesis were increased in MSU rabbits when compared to healthy synovial membranes, while no differences were observed in IL-6 levels (p=0.4) (Figure 22 A-C). However, the systemic infusion of MSC induced a substantial reduction in the

synthesis of COX-2 (p=0.040 vs. MSU) and TNF-α (p=0.014 vs. MSU) in the arthritic synovial membranes of MSU+MSC FEM rabbits (Figure 22 A-B).

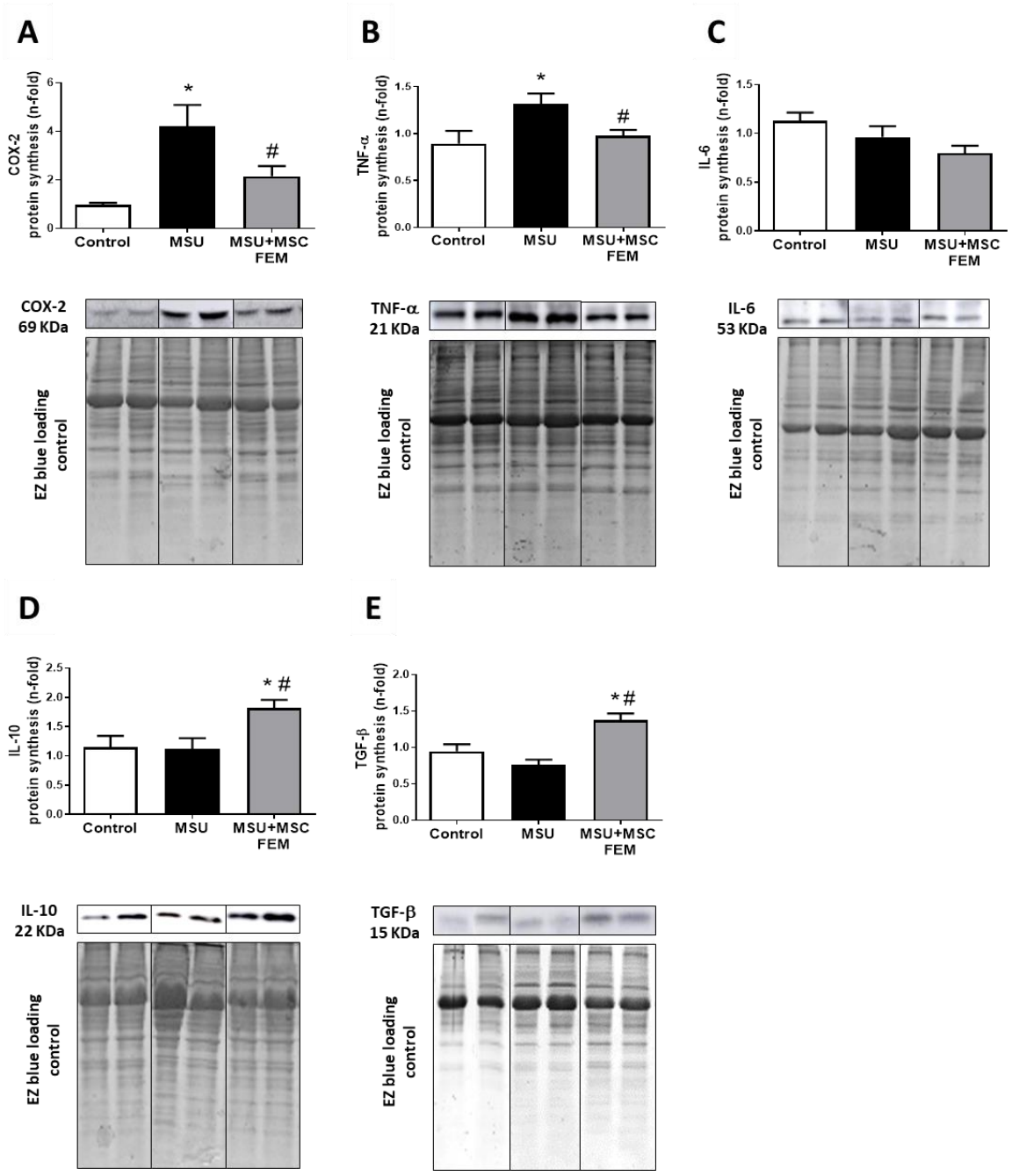

FIGURE 22. MSC modulates pro- and anti-inflammatory cytokine profile in synovial membranes of arthritic rabbits. Western blot analysis and representative cropped blots of COX-2 (**A**), TNF-α (**B**), IL-6 (**C**) IL-10 (**D**), and TGF-β (**E**) protein levels in rabbit synovial membranes. EZ blue staining was used as protein loading control and to normalize the results, which are expressed as a fold-change of the control group. Bars show the mean and SEM (n =7 for controls, n = 16 for MSU and n = 14 for MSU+MSC FEM group). Mann-Whitney test, *p<0.05 vs. Control, #p<0.05 vs. MSU. COX-2: ciclooxygenase-2; FEM: femoral artery; IL: interleukin; MSC: mesenchymal stromal cells; MSU: monosodium urate; TGF-β: tumor growth factor-β, TNF-α: tumor necrosis factor α.

IL-10 and TGF-β are considered important mediators in the resolution of acute inflammation resolution. No differences were observed in the presence of these mediators between healthy controls and MSU group (for IL-10, p=0.5; for TGF-β, p=0.070) at the time of study (Figure 22 D, E). Nonetheless, a statistically significant increment in the anti-inflammatory cytokines IL-10 (p=0.004 vs. MSU) and TGF-β (p=0.001 vs. MSU) protein levels was detected in the synovial membranes of MSU+MSC FEM animals compared to MSU ones (Figure 22 D, E).

Protein expression of inflammasome components in the synovial membranes of arthritic rabbits treated with MSC

NLRP3 inflammasome activation is essential in gouty arthritis pathogenesis. In order to determine whether the treatment with MSC was able to decrease inflammasome activation in MSU crystal-injected rabbit synovium, we analyzed the levels of different protein components and mediators associated to the activation of this system in the synovial membrane.

Our results showed that local synthesis of inflammasome components NLRP3 (p=0.015 vs. Control), pro-caspase-1 (p=0.004 vs. Control), and pro-IL-1β (p=0.004 vs. Control) proteins were significantly increased in the arthritic synovial rabbits, especially in the MSU group. However, IL-18 synthesis levels did not vary compared to healthy animals (Figure 23 A-D). Our results indicated that the arterial administration of MSC halved the synthesis levels of NLRP3 (p=0.049), caspase-1 (p=0.009), and produced an important inhibition of the master inflammatory cytokine pro-IL-1β (p=0.05), compared to the un-treated arthritic group (Figure 23 A-D).

Furthermore, the nuclear transcription factor NF-κB, which is a downstream effector of the inflammasome pathway, was also active in the MSU crystal-injected synovial membranes of rabbits (p=0.001 vs. Control), while a reduction of 33% of activity was observed in arthritic animals treated with MSC (p=0.006 vs. MSU, Figure 23 E).

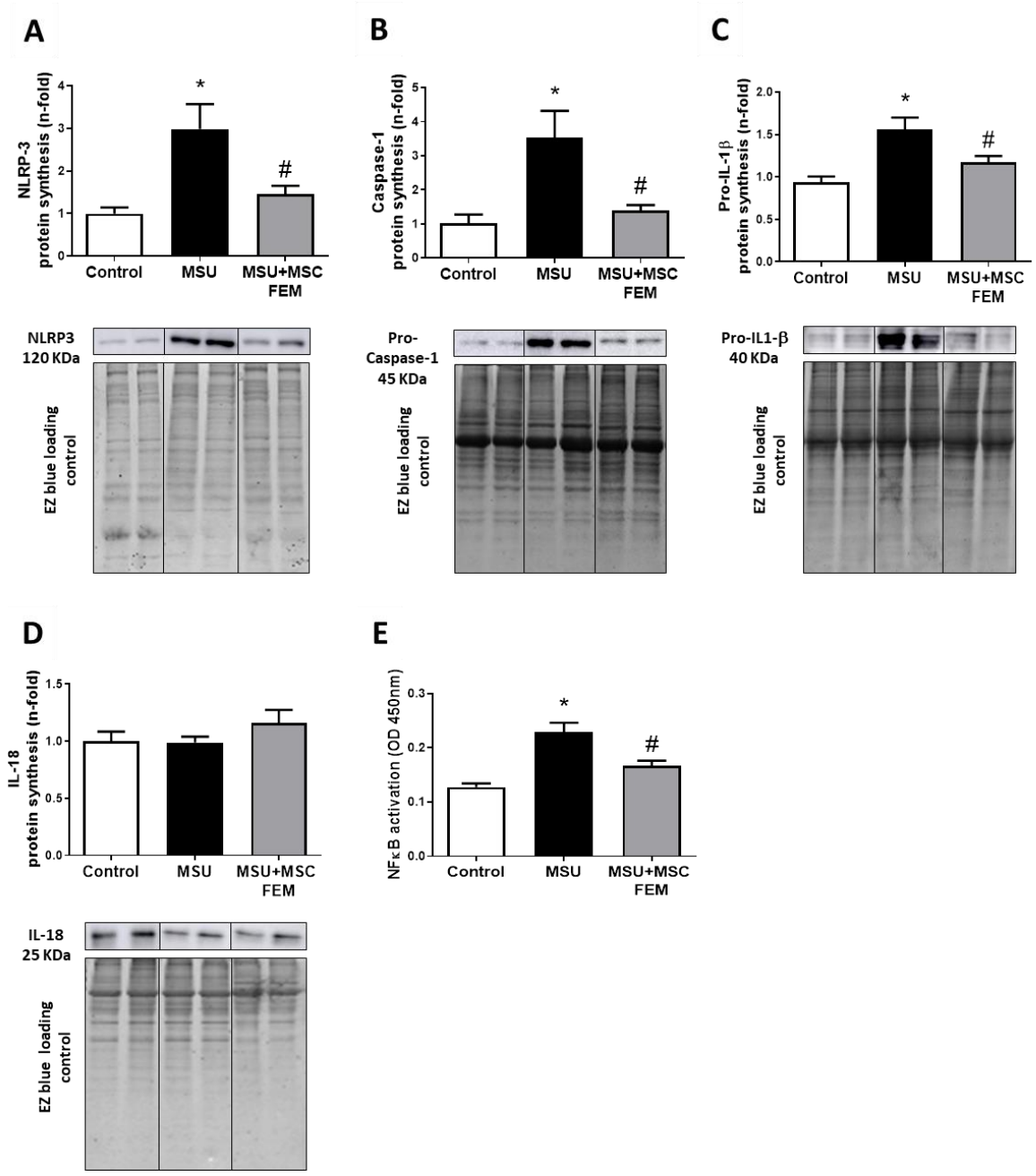

FIGURE 23. Inflammasome components are modulated in arthritic rabbits treated with MSC. Protein levels of NLRP3 (**A**), pro-caspase-1 (**B**), IL-1β (**C**), and IL-18 (**D**) were assessed by western blot. EZ blue staining was used as protein loading control. Results are normalized by EZ blue staining and expressed as a fold-change of the control group. Representative cropped blots of each group are shown. **E,** NF-kB p65 was analyzed by TransAM kit assay**.** Results are expressed in optical density (OD) units. Bars show the mean and SEM (n =7 for controls, n = 16 for MSU and n = 14 for MSU+MSC FEM group). Mann-Whitney test, **p*<0.05 vs. Control, #*p*<0.05 vs. MSU. FEM: femoral artery; IL: interleukin; NLRP3: NLR family pyrin domain containing 3; MSU: monosodium urate; MSC: mesenchymal stromal cells.

Analysis of the interaction between MSC and THP-1 cells in presence of MSU crystals in different in vitro systems

Our previous results showed that MSC induced changes in synovial macrophage population of rabbits with acute arthritis. Therefore, we next researched on the mechanisms by which MSC are able to modulate the inflammatory activity of macrophages stimulated by MSU crystals in different *in vitro* assays.

On the one hand, we tested MSC ability to regulate the inflammatory profile of macrophages releasing paracrine mediators through Transwell co-culture system. In this design, macrophages and MSC are cultured in the same culture media, although a direct cell to cell contact is not allowed. Thus, cells interact only through the release of different mediators to the shared culture media. According to this design, the analysis of the response of the two different cells can be analyzed separately. THP-1 differentiated macrophages were stimulated with MSU crystals, triggering a robust inflammatory response, as observed in NLRP3 (p=0.029), caspase-1 (p=0.029), IL-1β (p=0.029), TNF-α (p=0.029) and COX-2 (p=0.029) gene expression increase, when compared to vehicle expression 24 hours post-stimuli. IL-10 and TGF-β were also over-expressed (p=0.029) at this time point. In order to reproduce the *in vivo* settings in our experimental model, MSC were transferred into THP-1 wells 1 hour after MSU stimulation. It was interesting to note, as observed in Figure 24 A, the increase on the levels of cytokines expressed by MSU crystals-activated THP-1 co-cultured with MSC, in comparison to vehicle-stimulated cells. However, the presence of MSC (p=0.029) significantly inhibited the gene expression of these mediators in comparison to MSU crystals stimulated cells (p=0.029 MSU+MSU+MSC vs. MSU). Notably, NLRP3 (p=0.029) but not caspase-1 (p=0.34) expression was also inhibited in MSU+MSC-treated macrophages stimulated with MSU crystal (Figure 24 A).

We also investigated different mediators synthesized by MSC that could modulate THP-1 macrophage activation. We observed that COX-2, TSG-6 and IDO (p=0.029 vs. THP-1+Vehicle respectively) were up-regulated in MSC 24 hours after the stimulation of macrophages with MSU crystals (Figure 24 B).

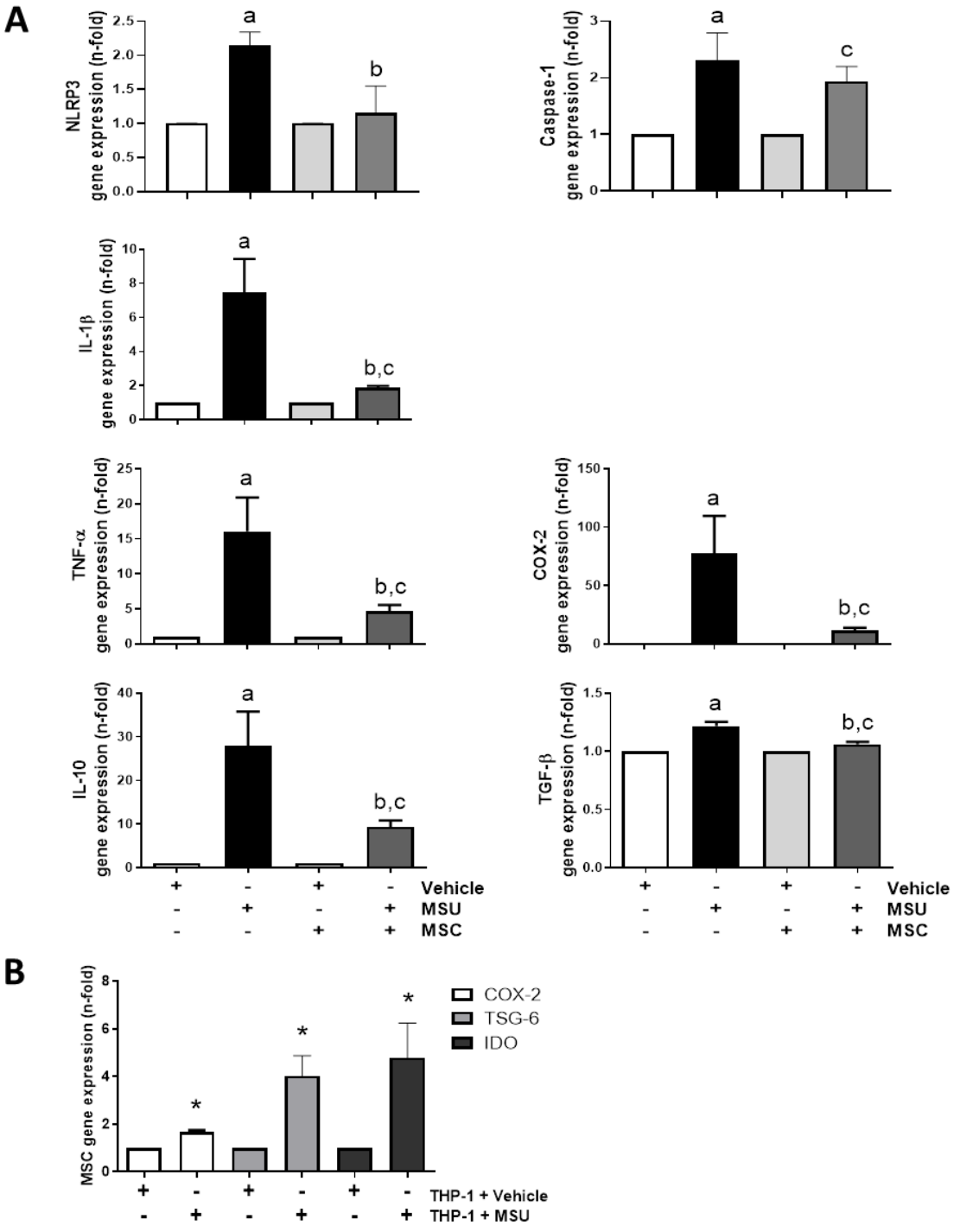

FIGURE 24. MSC block MSU crystal-stimulated THP-1 cells activity in Transwell co-culture system. Gene expression of NLRP3, caspase-1, IL-1β, TNF-α, COX-2, IL-10 and TGF-β in THP-1 macrophages **(A)**, and of COX-2, IDO and TSG-6 in MSC **(B),** 24 hours after THP-1 stimulation with MSU crystals. Gene expression of each gene is normalized to endogenous control. Each MSU-induced gene is expressed as fold change relative to its respective control. Bars show the mean and SEM (n = 4 independent experiments). Mann-Whitney test, a: $p<0.05$ vs. V alone, b: $p<0.05$ vs. MSU alone, c: $p<0.05$ vs. V+MSC **(A),** and *$p<0.05$ vs. THP-1 + V group. COX-2: ciclooxygenase-2; IDO: indoleamine 2,3-dioxygenase; IL: interleukin; MSC: mesenchymal stromal cells; MSU: monosodium urate; NLRP3: NLR family pyrin domain containing 3; TGF-β: tumor growth factor-β; TNF-α: tumor necrosis factor α; TSG-6: TNFα-stimulated gene-6; V: vehicle.

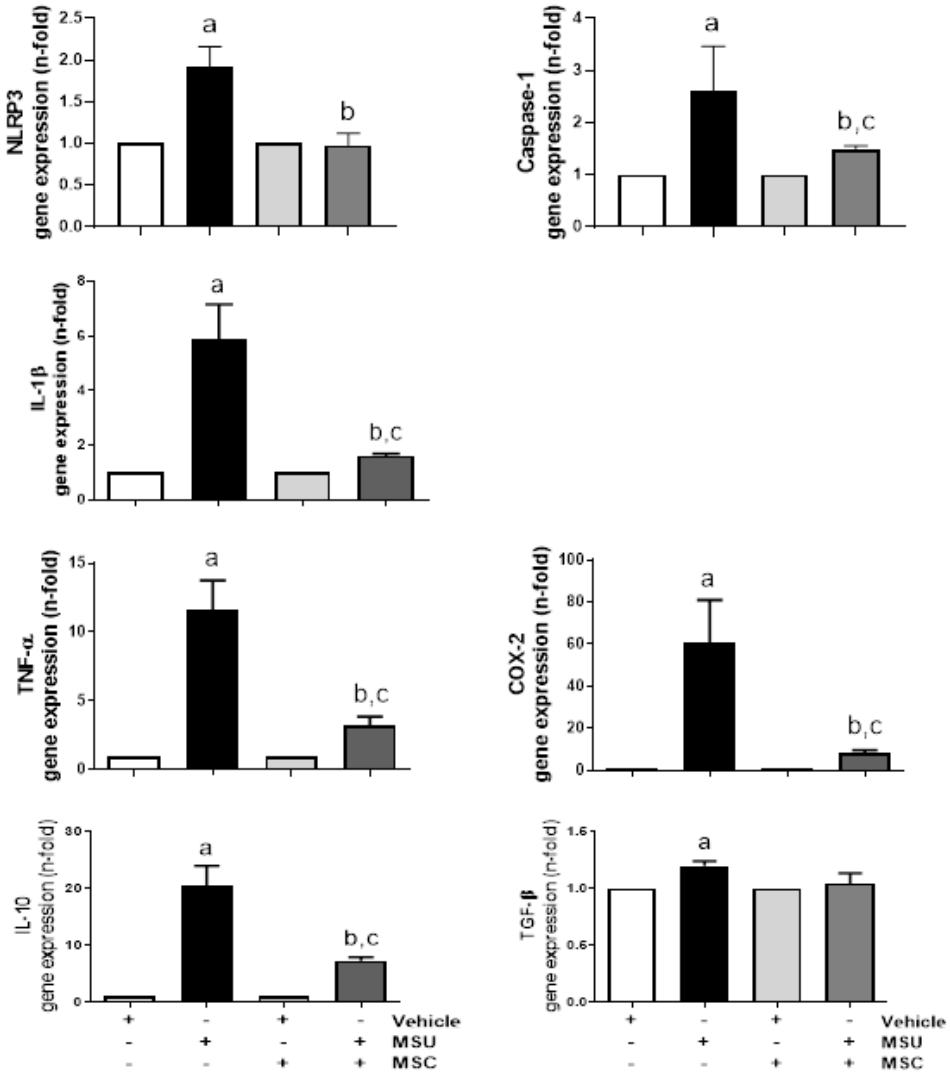

FIGURE 25. MSC block MSU crystal-stimulated THP-1 cells activity in direct co-culture systems. Gene expression of NLRP3, caspase-1, IL-1β, TNF-α, COX-2, IL-10 and TGF-β in THP-1 cells 24 hours after stimuli. Gene expression of each gene is normalized to endogenous control. Each MSU-induced gene is expressed as fold change relative to its respective control. Bars show the mean and SEM (n = 4 independent experiments). Mann-Whitney test, a: $p<0.05$ vs. V alone, b: $p<0.05$ vs. MSU alone, c: $p<0.05$ vs. V+MSC. COX-2: ciclooxygenase-2; IL: interleukin; NLRP3: NLR family pyrin domain containing 3; MSC: mesenchymal stromal cells; MSU: monosodium urate; TGF-β: tumor growth factor-β; TNF-α: tumor necrosis factor α; V: vehicle.

On the other hand, direct co-culture system allowed us to study the direct interaction between MSC and THP-1-derived macrophages, both being in contact with MSU crystals. Similarly to the Transwell co-culture system design, MSC were added into the THP-1 wells 1 hour after stimuli. MSC prevented the increase in the gene expression of different mediators, in a similar extent to those experiments in Transwell experiments. A curious difference between these two designs was observed regarding

TGF-β expression levels: while in direct contact, MSU+MSC condition was not significantly different to MSU condition, the Transwell design resulted in a significant decrease in the TGF-β gene expression in MSU+MSC vs. MSU condition. Concerning inflammasome components, both NLRP3 (p=0.029) and caspase-1 (p=0.029) gene expression were significantly attenuated after MSC addition vs. MSU condition (Figure 25).

DISCUSSION

“In science novelty emerges only with difficulty, manifested by resistance, against a background provided by expectation”

- *Thomas Samuel Kuhn*

DISCUSSION

During this thesis work, we have been delving deeper into the mechanisms by which MSC could regulate inflammatory pathways associated to the activation of the innate immune response. Despite initial promising preclinical results in the treatment of autoimmune diseases with MSC, and in the early phases of clinical trials in different human diseases, its success has not yet been further confirmed in most high standard, large-scale clinical trials. This could indicate that experimental models likely do not accurately reproduce human diseases; or that the beneficial effect of MSC is a consequence of the inhibition of pathways that are not well represented in these models. Up-to-date, most studies have focused on chronic diseases, in which the adaptive and the innate immune responses are integrated, coexisting a continuum of induction and resolution processes occurring during the chronic condition. This complex network of interactions makes it difficult to detect the mechanisms of action involved in the improvement of these chronic conditions. Therefore, in order to find out whether MSC can act specifically on the innate immune mechanisms, it is necessary to resort to models of acute, self-limited inflammation, where the innate immunity plays the unique role.

MSC therapy has been successfully applied in different models of acute sterile inflammation. In a rhabdomyolysis-induced acute kidney injury model, MSC improved tubular injury and renal function shortly after their administration (147). Likewise, in rats with acute corneal injury, systemic administered human MSC diminished the corneal opacity and ameliorated leukocyte infiltration 72 hours after insult (148). NaT-induced acute pancreatitis was promptly alleviated after intra-venous (IV) application of human MSC, improving histological alterations (71). However, some harming etiologic agents that induce the acute lesion in these models do not entirely reproduce human clinical processes. On the other hand, the injured tissues in some of those models are difficult to be sequentially and directly assessed. This complexity hinders the study of MSC effect in specific acute conditions and its translation into the clinic.

Besides, these models reproduce infrequent acute conditions given in the general population making the translation of MSC results from pre-clinical to clinical studies difficult. Accordingly, we developed an acute auto-limited gouty arthritis model, which is the paradigm of acute joint disease mediated by innate immune system without any contribution of adaptive response.

In Western countries, prevalence of gout increases up to 9% in adults over 60 years of age in the USA (93). Older adults are susceptible of suffering comorbidities, so the use of traditional drugs for the treatment of gout flares could cause adverse effects. Currently, the use of NSAIDs and colchicine are the most common treatments in the first 24 hours after flare, but they can produce severe gastrointestinal adverse effects or dyspepsia. Urate-lowering strategies may also imply serious contraindications effects (127). IL-1β inhibitors such as anakinra and canakinumab are a high cost therapy and their use is not recommended for patients with high infection risk (126,128). Therefore, the development of alternative therapies is urgently required

In light of this thesis work, we have provided original data about the therapeutic outcome that MSC produce in a self-limited inflammatory flare in the rabbit joint, employing different methodological approaches. First, we proceeded to validate the US technique as a promising tool for the assessment of acute synovitis in rabbits' knees. Then, we went into investigating the anti-inflammatory effects of MSC on acute arthritis flare. To accomplish this, we tested different routes of MSC administration. Once we had selected the systemic one, which resulted in a better therapeutic outcome, we assessed whether systemically-administered MSC arriving into the arthritic joint directly from the blood stream exerted a better therapeutic effect compared to the contralateral inflamed synovium, which received MSC after its vascular distribution through the organism. As MSC alleviated inflammation evenly in both the right and left knee joints, we next studied whether MSC kept a protective effect after an acute arthritis relapse. Finally, we examined the molecular mechanisms underlying the therapeutic outcome both *in vivo* and *in vitro*.

Different experimental models have been employed to reproduce a human gouty arthritis break out. MSU crystal injection into the joint cavity is the most commonly

used method (124), as it directly triggers joint inflammation and swelling. Therefore, several models of MSU injection in mice and rat joints have been developed (149–154). However, given the challenging injection into small rodent joints and the difficulties that entails collecting synovial fluid, MSU crystals are usually applied in extra-articular locations (97,155–162). These models are characterized by the production of large volumes of inflammatory exudates. However, these experimental gout models cannot exactly reproduce the intricate relationship between the hyperuricaemic metabolic status and inflammation given in gout patients. Hence, different approaches have been used to evoke hyperuricemia in some of these models (151,163–165). In our case, we just aimed to focus on the inflammatory response triggered by MSU crystals, so we avoided the induction of the hyperuricaemic status. Previous works point out that MSU crystals induce a pronounced inflammatory response in the rabbit joint (130,166,167). Not only does this model faithfully reproduces the pathophysiology of human knee response to an acute arthritic flare, but also, compared to other pure inflammation models, the knee joint size and the amount of exudate produced facilitate its follow-up through a direct observational measurement of joint swelling (130,131,166). In addition, this model allows performing diagnostic investigations similarly applied in patients, such as visualization of MSU crystals in synovial fluid, the use of imaging techniques as CT and ultrasonography (76), and the possibility to perform synovial biopsies with sequential histological and molecular studies. What is more, our model can be easily reproduced, displaying a homogeneous clinical outcome. Therefore, MSU crystal-induced acute arthritis in rabbit is a reliable model to study the pathophysiology of acute inflammatory processes *in vivo*, as well as the efficacy and mechanisms of action of novel therapeutic options.

Performance and validity of MSK-US for the assessment of synovial inflammation in rabbit acute gouty arthritis

Our first aim was to assess that US was a reliable technique for the evaluation of inflammation in the knee of rabbits in the acute gouty arthritis model. In patients,

MSK-US is being used as a diagnosis tool for detection of MSU crystal deposits and different inflammatory features (168,169). In our study, we demonstrated that by using commercial US equipment we were able to differentiate MSU crystal features and inflammatory signs between healthy and arthritic knees during the inflammatory course of a rabbit gouty flare. Additionally, both GD and SF inflammatory scores, and MSU crystal-related features improved within days, in accordance to the self-limiting nature of a gouty flare. Finally, we were able to correlate inflammatory findings with joint swelling, synovial histopathology, vascularization and the presence of IL-1β, a key pro-inflammatory mediator, in this disease. This new data supports previous studies in which MSK-US has been employed to evaluate gout features in experimental models and in patients (130,168).

Among the different inflammatory findings, GD correlated with knee perimeter increase 24 hours after injury induction. This increment of joint edema is similar to that occurring in patients, in whom the inflammatory peak occurs between 24-48 hours from the onset (170). Nevertheless, at 72 hours after MSU injection, when the inflammation in the rabbit knee is considerably lower, the correlation is lost. One possible explanation is that comparison of a sensitive continuous variable with a semi-quantitative measure cannot discriminate small alterations in the same degree. Additionally, it is important to take into account that joint swelling is measured by calculating the increment of the knee joint perimeter. Thus, it reflects not only intra-articular variations, but also peri-articular changes that occur during the inflammatory course. It is possible that the swelling in the peri-articular tissue fades while inflammation in the joint cavity is still active.

The evaluation of histological synovitis is the gold standard method to evaluate tissue inflammation during arthritis (171). This Krenn score was adapted to grade acute synovitis, where tissue damage is not as severe as other joint diseases such as RA. Based on the Krenn's evaluation, we took into account the enlargement of the lining cell layer, inflammatory infiltrate and synovial stroma alterations such as density of resident cells, fibrosis and vascularization. Additionally, alterations in synovial adipocyte size and morphology have been previously correlated with inflammatory

status (141). Thus, we also considered sub-lining adipocyte tissue structure as a feature of stromal activation. Remarkably, global histopathological damage correlated with MSK-US STh at time of sacrifice. In RA models, it has already been reported that US scores correlate with analogous histopathological scores (172,173). In our acute arthritis model, STh evaluation reflects the grade of damage and inflammatory characteristics of synovitis, such as hyperplasia and other pathologic structural alterations. It is important to note that Krenn score also evaluates cell proliferation in the lining and stroma, infiltrating cells and fibrotic events during arthritis. So, MSK-US assessment of acute synovitis can be a valid technique to evaluate the degree of inflammation in the rabbit model. Of note, the synovial region examined by MSK-US and the one evaluated under histopathologic study do not coincide, which indicates that inflammation is evenly spread throughout the synovial membrane.

Vasodilation, increased vascular permeability, and angiogenesis are promoted by the inflammatory microenvironment (174). Therefore, vascular density reflects the inflammatory status of the tissue. CD31 is a well-known marker of endothelial cells forming blood vessel wall, being involved in leukocyte transmigration (175). Accordingly, this antigen has been considered a marker of disease activity (176–178). On the other hand, US PD detects blood flow signals, and its quantification in synovial tissue correlated with vascularity and expression of angiogenic factors in early RA patients (179). In our model, synovial vessels were located in tissue sections employing an anti-CD31 antibody. Interestingly enough, vascularity within the synovial membrane correlated with PD mode 72 hours after MSU injection. Thus, MSK-US allows the study of vascularity related to the inflammatory state in an experimental acute gouty arthritis.

In gouty arthritis, IL-1β is considered a key inflammatory cytokine that promotes a strong inflammatory storm (180). Thus, concentration of IL-1β present in arthritic synovial membranes can reflect the severity of the inflammatory response. Circulating IL-1β levels have been directly related with disease severity in RA patients (181). US GD was associated with synthesis levels of pro-IL-1β, which suggest that GD could be a reliable parameter to measure inflammatory status.

A major weakness of this study is the small sample size employed, which did not allow us to explore histopathology, vascularization and molecular biology at 24 hours. Furthermore, despite MSK-US was able to discriminate between healthy and arthritic conditions, we have not empirically demonstrated its ability to evaluate a therapeutic outcome. Our results showed that 72 hours after the injection, when there is a lower degree of inflammation, the association of GD with joint swelling was lost, while significant differences of some inflammatory findings between 24 and 72 hours were lost as well. This could indicate that the discriminatory power of this technique decreases at 72 hours, suggesting that MSK-US could not be sensitive enough to detect variations in low degree synovial inflammation. Its application for the evaluation of MSC therapeutic effect is discussed below. Overall, MSK-US is a promising effective diagnosis tool, although further studies are needed.

Study of the anti-inflammatory effects and pharmacokinetics of MSC in experimental acute gouty arthritis

In this study, we demonstrated for the first time that a single dose of systemically administered xenogeneic MSC was able to shorten the intensity and duration of severe acute arthritis induced by injection of MSU crystals in the rabbit knee.

In order to obtain an effective therapeutic result with MSC, different treatment aspects shall be taken into account, such as the immune compatibility, source, dose and route of administration (65). We employed human MSC in an animal model. Xenogeneic models have been widely used to test the immunosuppressive potential of human MSC (182). Indeed, some comparative studies, such as those performed in an acute cerebral infarct in rat, have shown that MSC from different sources displayed similar efficacy and safety profiles (183). Additionally, it seems relevant to employ MSC from human origin to understand the mechanisms underlying their potential functional outcome in patients. Recently, MSC have been considered “immune-evasive” rather than “immune-privileged” (184): despite MSC express few constitutive MHCI molecules, some inflammatory cytokines can induce MHCII expression, being recognized by the host adaptive immune system, which may frustrate MSC action

(185). Thus, it should be considered taking advantage of MSC fast action in diseases where a rapid, short term effect is critical for the therapeutic outcome, such as is the case of acute injuries (65).

On the other side, we employed MSC derived from adipose tissue (Ad-MSC), which can entail certain advantages over other common tissue sources. To give an example, some published studies explain that Ad-MSC are easily isolated without invasive surgery, and exhibit comparable immunomodulatory capacities to BM-MSC from the same donor (135). By contrast, other works have revealed that Ad-MSC are metabolically more active than BM-MSC, which could imply proliferative and immunomodulatory advantages over BM-MSC (186,187).

Dosing is also a questionable issue, as MSC concentration depends on application route and animal species. Therefore, we decided to assess the anti-inflammatory effect of MSC comparing local injection into the knee joint vs. systemic infusion through the auricular artery. Both procedures have been tested in chronic inflammatory diseases, such as systemic lupus erythematosus, RA or OA (188,189). Although there still is a lack of direct comparative studies between both routes, suggestive results have been described for both local or systemic transfusion through both vascular and extravascular locations in acute models of inflammation (148,190).

For most clinical trials, the amount of cells injected through IV administration ranges from 1-2 x 10^6 MSC/kg (100-150 x 10^6 total MSC) (191). Accordingly, we proposed to adjust MSC dosage to body weight comparable to a clinical situation. Additionally, rabbits have been given systemic doses ranging between 2- 4 x 10^6 MSC/kg in different disease models showing good results (192–194). By contrast, the IA injection dose of MSC in clinical studies usually approximates 50 × 10^6 cells, which is substantially a lower dose compared to IV one (189), probably indicating that local administration could allow a lower cell dose.

Therefore, for the IA administration route, we decided to test two different doses. On the one hand, we applied the same dose employed per animal in the systemic

approach: 10^6 MSC/kg (2.5 x 10^6 MSC each knee). On the other hand, we also tested a lower dose consisting in 2.5 x 10^5 MSC/kg (6.5 x 10^5 each knee).

In order to test the effect of local vs. systemic MSC administration, we assessed both articular, through the measurement of knee swelling, and systemic inflammation, by the measurement of serum CRP levels, as previously described (131,166). Remarkably, our results showed that systemically administered MSC substantially improved knee swelling during the MSU crystals-induced arthritis, and normalized serum CRP concentration in a short interval of time. On the contrary, IA MSC administration did not significantly alter these parameters in comparison to untreated animals. Systemic infusion of MSC halved joint swelling 72 hours after aggression, and reduced CRP levels 24 hours after injury. The pronounced drop of CRP levels at 72 hours could be a consequence of the steady binding of serum CRP to MSU crystals (195). By contrast, a plausible unfavorable effect was observed when a higher dose of MSC was applied locally into the joint, as reflected in an increase in joint perimeter and in CRP levels over the ones observed in the MSU group. Although MSC are considered clinically safe and few side effects have been reported, many adverse effects occurring in preclinical models are probably poorly described (20). It is important to take into account that MSC can exert pro-inflammatory actions given their immune-regulatory plasticity. In this scenario, a previous work reported negative outcomes after MSC transplant into a corneal allograft in rabbits (196). Interestingly enough, this possible negative effect was not observed with a lower IA dose, but no beneficial effect was accomplished either. All these data indicate that local injection of MSC into the arthritic joint does not improve inflammatory condition in the acute MSU-induced arthritis in rabbit knees. However, MSC infused into the vascular system alleviate inflammation in this model, suggesting that the MSC administration route has to be carefully assessed in other human rheumatic diseases.

Thus, in the subsequent study we decided to employ the intra-femoral delivery of MSC instead of an intra-auricular route. It is well-known that MSC are easily trapped in the lung capillaries after their intravascular administration, and it seems plausible that it can undermine MSC action (30,197). So, it has been suggested that infusing the cells

through the artery that irrigate the injured tissue would favor their arrival to the target tissue and that the beneficial effects could be enhanced, avoiding cell entrapment in distant organs (198). Previous findings in rabbits have demonstrated that infusion of 5×10^6 MSC through the superior mesenteric artery promoted MSC retention in the targeted digestive organ, in contrast to IV administration, as it bypassed pulmonary circulation (199). Therefore, we tested the effect of MSC administration through the femoral artery to study whether MSC reaching the arthritic synovium directly from the femoral artery produced an improved anti-inflammatory action compared to the contra-lateral synovium, which received the cells after its vascular distribution throughout the organism. Our results revealed that the administration of MSC through the right femoral artery was able to decrease joint swelling and the histopathological alterations observed in the synovial tissue. No significant differences were observed when we compared the effects observed in the right vs. the left synovial membrane. According to this data, we decided to test whether MSC homing into both synovial membranes was different when the cells were applied through the right femoral artery.

In our model, MSC effect was already evident 24 hours after the inflammatory boost, so we explored their fate and distribution in different rabbit organs and tissues at that time point. Different strategies have been employed to track MSC in different species, as the amplification of xenogeneic DNA sequences one of the most common procedures (200). In line with published reports (198), all MSC injected rabbits showed evident accumulation of human DNA in lungs, spleen and liver. However, we were unable to detect human genomic DNA in every right synovial membrane. Furthermore, we detect human DNA in a similar percentage of the left synovial membranes of the treated rabbits. Therefore, this detection method did not allowed us to accurately measure the presence of human MSC in the rabbits' synovial membranes at the time point studied (24 hours after administration). This method was not sensitive enough to compare whether a different amount of MSC reached each membrane. Similar limitations have previously been described in different animals (201,202). It should be considered that at this time point, MSC that reached the synovial membranes had

already been cleared by host immune cells in most of animals. It is known that MSC are short-lived after infusion (32), and in fact, their actions have been referred to as a "hit and run" effect, to explain a rapid and short-term interaction with host cells. This could imply a low rate of engraftment but a long-term benefit (30).

Our data has shown that femoral administration of MSC elicited similar effects in both rabbit membranes. These results contrast with the observations of Arnberg et al. (199), probably because at this time point of study arthritic synovial membranes are not as irrigated as other tissues are, and the cell entrapment in this target tissue is less efficient. Alternatively, it is possible that the therapeutic effect would be more dependent on the intensity of the inflammation present in the tissue, rather than in the availability of cells in the nearby bloodstream. Although it has been reported that MSC survival and number of cells that migrate into the knee in RA and OA mouse models is independent of the presence or intensity of inflammation, it is also possible that the number of cells these mice received was too high to discriminate between different degrees of inflammation (202).

Study of the therapeutic outcome of MSC on rabbit after an acute arthritis relapse

As we formerly evinced that MSC were able to accelerate the recovery of rabbits from an acute MSU crystal-induced aggression, and recurrent acute flares characterize gouty arthritis, we then inquired whether MSC were able to keep a protective effect after a second flare-up. In gouty arthritis, recurrent flares are common, becoming even a chronic state in most cases (74). For this reason, the recurrent gouty outbreak model has previously been developed in rabbits (203).

The resolution of acute inflammation brings a second influx of monocytes-derived macrophages and dendritic cells, and myeloid derived suppressor cells into the damaged tissue. This post-resolution phase produces an optimum tissue microenvironment for the induction of adaptive immunity (204). On the other hand, MSC are rapidly cleared from the organism. ^{111}In-oxine-labeled human decidual SC rapidly drop 30 hours after systemic administration into rabbits (199). Therefore,

assuming that MSC were likewise removed in our model, we hypothesized that MSC signature left in damaged tissue would protect against recurrent arthritis flares. However, our data indicates that a unique MSC injection was not able to prevent a relapse occurring 15 days after the first aggression.

In this study, we included MSK-US examination at different time points to evaluate inflammatory status of synovial membranes. Differences between healthy controls and MSU rabbits were evident, showing that the relapse model was able to induce a significant inflammation in the knees that received two injections of MSU 15 days apart. Furthermore, it seems to be a trend of improvement in the MSC-treated group, in comparison to MSU rabbits. Disappointingly, remission of inflammation in the MSC-treated group was not statistically significant in any of the US evaluated features. This design would probably require a bigger sample size so as to adequately assess the effect of MSC in the relapse model. Although we did not explore it, the role that adaptive immunity in this experimental model of joint damage would be probably more pronounced than in the acute model.

Study of MSC effects on inflammatory mechanisms in the acute arthritis model after their intra-femoral administration

Finally, our objective was to gain insight into the anti-inflammatory mechanisms displayed by MSC in the acute arthritis model. As no differences between the right and left MSC-treated arthritic synovial membranes were observed in the rabbits that received the cells through the femoral artery, we employed both synovial membranes from these animals, without further discrimination, so as to determine the cellular mechanisms modulated by the treatment.

We observed that a single dose of xenogeneic MSC was able to ameliorate a severe acute arthritis induced by a MSU crystal injection in the rabbit knee. Molecular studies showed that MSC inhibited synthesis of NLRP3 inflammasome components, reducing NF-κB activation and pro-IL-1β secretion in synovial tissue. Likely, these mechanisms could be responsible, at least partially, of an increase in synovial macrophage

polarization towards M2 phenotype observed in the MSC-treated rabbits, along with an increased expression of anti-inflammatory cytokines.

Histological studies confirmed that synovial membranes from MSC-treated animals presented less pathological features compared to the MSU group. The synovium of the former group showed a thinner lining layer and less altered stromal structure, which included less apoptotic adipocytes, reduced fibrosis, and diminished synovial vascularization (205). The reduction of vascular network in treated synovial membranes could be a result of an improved inflammatory condition. Synovial fluid examination revealed that total leukocyte number per ml was similar between treated and non-treated groups 24 hours after injury, while two days later, treated joints showed 65% less cellularity than non-treated joints. At the former time point, PMN cells covered 90% of total population, whereas at 72 hours, the number of mononuclear phagocytes rose, comprising almost 55-60% of total leukocytes, in both groups. Thus, MSC promoted total cell clearance from 24 to 72 hours. Accordingly, these data suggest that MSC do not exert a direct or specific effect on PMN clearance in our model. The modification of the ratio PMN/mononuclear cells during the evolution of the inflammatory response agrees with other acute inflammation models. In a mouse peritonitis model, the total number of infiltrated cells decreased a few hours after the human MSC peritoneal application, and monocyte number rose followed by PMN clearance (73). In our model, MSC reduced about 65% of joint swelling 72 hours after injury. Noteworthy, although caution should be taken when comparing treatment efficacy, the size effect achieved by MSC was similar to that observed when using COX-2 inhibitors. Both salidroside and celecoxib halved ankle swelling, cell count and histologic scores 24 hours after MSU induced injury in rat and rabbit models (206). On the other hand, IL-1 blockade slightly limited ankle swelling for 4 days in MSU arthritic mice (207). In a randomized, double-blind clinical trial using anakinra in gout patients, joint swelling score diminished about 50% in three days. Additionally, the short half-life (46 hours) of this drug requires daily administration. All these data indicate that a single dose of MSC in our model display at least comparable

effects to those observed after the administration of IL-1 inhibitor in different MSU models and in a clinical trial.

NF-κB, which is responsible for the up-regulation of the synthesis of inflammasome components and other pro-inflammatory proteins (208–210), was active in arthritic animals 72 hours post crystals injection. In line with previously published findings, MSC diminished NF-κB activation (71,73,211); and NLRP3, caspase-1 and IL-1β levels were decreased in treated arthritic synovial membranes. Inhibition of NLRP3 inflammasome by MSC in sterile acute inflammatory disease models has been scarcely investigated *in vivo*. In a Na-T induced severe acute pancreatitis in mice (71), NLRP3 inflammasome activity and NF-κB activation was down-regulated in acinar cells after MSC treatment. Secretome from perivascular SC (precursors of MSC) was also able to attenuate MSU crystal-induced peritonitis in mice, inhibiting expression of NLRP3 inflammasome proteins in cultured macrophages (212). Although pro-IL-1β and pro-caspase-1 proteins were detected, the signal of their mature forms was faded, perhaps due to a rapid degradation in the tissue. On the other side, IL-18 remained invariable among healthy and arthritic groups probably because at this time course of the pathogenic process, this cytokine is not induced. In a MSU air-pouch model in mice, there was no increase of exudate IL-18 levels (213). Similarly, IL-6 levels were not importantly modulated. This fact could be in contradiction with a study of the inflammatory profile in gouty patients, in which both cytokines correlated with inflammatory activity (214). Notwithstanding, this study was performed in peripheral blood leukocytes, and in patients who were already diagnosed with gout, exhibiting a chronic condition. What is more, the evolution of inflammatory profile in a peritoneal model of MSU induced-arthritis indicates that different cytokines may be overexpressed while others could have returned to normal levels, given the self-limiting nature of gouty arthritis (157). In agreement with previous data, COX-2 and TNF-α levels, which were increased in MSU synovial membranes, were reduced in the synovium of MSC-treated animals.

In vitro studies were designed to shed some light into the specific effect of MSC on macrophages in the control of MSU crystal-induced inflammation. MSC presence abrogated macrophage activation, inhibiting NLRP3 and cytokine expression 24 hours

after MSU stimulation in both Transwell and direct co-culture systems. Pro-caspase-1 expression was suppressed in direct but not in the Transwell system. This difference might be explained because in direct co-culture experiments the gene expression of both cell populations was analyzed, while in the Transwell system, only THP-1 cells were targeted. Probably, a larger sample size would be required to find out bigger differences between MSC-treated and non-treated THP-1 macrophages.

Our results suggest that the effect of MSC could be both mediated by the release of paracrine and juxtacrine/cell-cell factors. We found that COX-2, TSG-6 and IDO were up-regulated in MSC sharing the same culture media with THP-1-derived macrophages stimulated with MSU crystals. Previous data describe that NLRP3, COX-2 and pro-IL-1β synthesis was triggered in THP-1 cells by MSC, while IL-1β and IL-18 secretion was inhibited. This process was mediated by PGE2 and induced macrophage skewing towards M2 phenotype (84). On the other hand, expression of IDO by stimulated MSC catabolizes tryptophan to kynurenic acid, which binds to the aryl hydrocarbon receptor (AhR), activating TSG-6 synthesis (215). The immunosuppressive role of MSC-derived TSG-6 in macrophages has also been described *in vitro* (216). Therefore, these molecules could be interesting candidates involved in the mediation of the accelerated resolution of inflammation in our model. Additionally, previous data showed that MSC are able to secrete the anti-apoptotic protein stanniocalcin-1 in response to activated macrophages *in vitro*, suppressing the production of ROS and subsequently inhibiting NLRP3 inflammasome action (217). MSC were also able to prevent pyroptotic cell death dependent of NLRP3 inflammasome activity in macrophages triggered by endocytosis of MSU crystals (218). These mechanisms will be further investigated in order to find out the molecular pathways through which MSC inhibit the activity of THP-1-derived macrophages.

It has been established that the spontaneous shutdown of the gouty inflammation process is curtailed by several mechanisms, which includes clearance of apoptotic cells and induction of anti-inflammatory cytokines, such as TGF-β and IL-10, by M2 macrophages (122,157,160). Although the assessment of the macrophage population within tissues is a controverted issue due to their wide phenotypic plasticity (219), it

has been widely described that in the M2 subset, expression of NLRP3 inflammasome components is suppressed (220), while both TGF-β and IL-10 cytokines are up-regulated (221). Interestingly, CD163 expression was also triggered in macrophages isolated from synovial fluid of gouty patients, and this was related to enhanced anti-inflammatory activity (222). Additionally, both CD163 and arginase-1 were up-regulated in M2 macrophage phenotype in different animal models, including rabbits (223–227). In fact, in our case we observed a higher number of M2 macrophage together with an increase of TGF-β and IL-10 proteins in MSC-treated synovium. These results would support the enhanced clearance of the total leukocyte population in synovial fluid of MSC-treated animals. It has already been described that MSC can favor its polarization toward an alternative M2 macrophage phenotype. MSC tested in an asthma model in mice induced the expression of TGF-β and IL-10 in lung macrophages (228). It has also been depicted in different models of acute colitis and corneal injury that MSC could hinder frequency of total infiltrated macrophages and induce their anti-inflammatory phenotype (84,85,229). Furthermore, it has been described that MSC enhance macrophage accumulation into damaged tissue favoring their differentiation into M2 subsets (70,83,147,190). Conventional anti-inflammatory treatments in gout can produce similar results. As an example, it has been reported that colchicine can promote macrophage M2 polarization (230), inhibit activation of NLRP3 inflammasome and increase the level of TGF-β (231).

We observed that, in our model, most MSC accumulated in peripheral organs, implying that leukocyte modulation could be produced from distant sites by the release of soluble factors. Nevertheless, we cannot exclude that the small fraction of MSC localized at damaged synovium could take part in the therapeutic process (232). MSC could be directly promoting monocyte polarization towards the M2 subset, favoring their presence in arthritic synovial membranes. It is known that MSC-derived TSG-6 promote macrophage phenotype switch from the M1 to the anti-inflammatory M2 (85). Some studies specify that during the polarization of macrophages towards M2 phenotype, NLRP3 expression is suppressed, and so is IL-1β secretion (220). This process could be mediated through a diminished NF-kB activity (233). On the other

hand, several MSC-derived soluble factors have been described to inhibit NLRP3 activity (84,217,234). Hence, suppression of NLRP3 activity could alter macrophage phenotype into the M2 subset, limiting the inflammatory response. Up-regulation of COX-2 in MSC directly inhibited NLRP3 inflammasome activity in macrophages through PGE2 synthesis, in response to IL-1β (235,236). Furthermore, MSC-derived PGE2 induced IL-10 production in macrophages (83,237). Lastly, it has also been reported that MSC-derived TSG-6 inhibited TLR2-mediated nuclear translocation of NF-kB, suppressing the transcription of pro-inflammatory cytokines (73). Additionally, TSG-6 was proposed to inhibit NF-kB activity and synthesis of NLRP3 inflammasome components (71). Thus, MSC targeting NF-kB activity could lead to inhibition of pro-inflammatory cytokines and NLRP3 inflammasome components, favoring the M2 macrophage phenotype.

Altogether, we have demonstrated that MSC are able to diminish the intensity and the duration of the inflammatory flare in an acute model of gouty arthritis in rabbits. This model has allowed us to create an active inflammatory environment, where MSC administration regulates the innate immune response, accelerating the restoration of tissue homeostasis. Thus, this thesis work provides a robust background in order to study the mechanisms of closure of inflammation, which could involve specialized pro-resolving mediators, peptides or other molecules. Conspicuously, this study promotes the design of studies with gouty patients using MSC as a therapeutic option to alleviate acute gout flares, especially in older adults, poly-medicated or poly-morbid patients, in which the use of conventional treatments could cause adverse effects in them. In our model, MSC reduced joint inflammation without completely inhibiting IL-1β synthesis. Therefore, MSC therapy could emerge as a potential, save alternative to the use IL-1β inhibitors such as anakinra or canakinumab.

CONCLUSIONS

“Science is not a heartless pursuit of objective information. It is a creative human activity, its geniuses acting more as artists than as information processors”.

- *Stephen Jay Gould*

CONCLUSIONS

Validation of MSK-US for the sequential assessment of synovial inflammation in rabbit acute gouty arthritis

1. MSK-US is able to discriminate between healthy and inflamed knees, but is not sensitive enough to detect low degree variations in synovial inflammation. However, as it correlates with pathological and molecular features, it can be considered a reliable technique for the sequential evaluation of acute synovitis in rabbit knees.

Study of the anti-inflammatory effects of MSC in acute gouty arthritis

2. Systemic administration of human adipose tissue-derived MSC is able to decrease joint swelling and serum CRP concentration, substantially decreasing the duration and intensity of the acute flare in MSU crystal-induced arthritis in rabbit.

Pharmacokinetics of different routes of administration, doses and distribution of MSC in MSU-induced arthritis model

3. The anti-inflammatory effect of the systemic administration of MSC through the auricular artery is not reproduced after their intra-articular injection, indicating that the local MSC administration has to be carefully evaluated in other human joint diseases.
4. The application of MSC through the right femoral artery produces similar effects on inflammation to those observed after auricular artery infusion, decreasing inflammation 72 hours after insult. Furthermore, MSC do not display an improved anti-inflammatory effect on the right arthritic knee compared to its contralateral knee, despite the direct arrival of MSC from the femoral artery to the right synovium.

5. Systemically delivered MSC principally accumulate in the lungs, liver and spleen, while a small fraction could reach inflamed synovial membranes.

Study of the therapeutic outcome of MSC on rabbit after an acute arthritis relapse

6. A single, systemic administration of MSC is not able to maintain the anti-inflammatory effect after a second MSU crystal-induced injury in rabbit knees.

Study of MSC effects on inflammatory mechanisms in the MSU-induced acute arthritis model

7. MSC reduce the synthesis of NLRP3 inflammasome components in arthritic joints, simultaneously inhibiting the NF-κB pathway.
8. MSC down-regulate the expression of pro-inflammatory cytokines in the arthritic synovium, and induce the synthesis of anti-inflammatory cytokines earlier than that observed in the non-treated joints. In addition, MSC promotes the presence of M2 macrophages in the arthritic synovium.
9. *In vitro* studies confirm that MSC block the expression of NLRP3 inflammasome components and the expression of different cytokines in THP-1-derived macrophages stimulated by MSU crystals, probably through the release of anti-inflammatory soluble factors.
10. Altogether, we have demonstrated that MSC are capable of reducing joint inflammation of an acute arthritis flare-up induced with MSU crystals in rabbits.
    a. MSC could be considered a novel therapy for treating acute gouty flares in patients, in which the use of traditional drugs is contraindicated.
    b. Additionally, this experimental model provides an excellent model to study the mechanisms of resolution of innate immune-mediated inflammation.

CONCLUSIONES

Validación de la ecografía musculo-esquelética para la evaluación de la inflamación sinovial en la artritis gotosa aguda en conejo

1. La ecografía musculo-esquelética puede discriminar entre rodillas sanas e inflamadas, pero no es lo suficientemente sensible para detectar pequeñas variaciones en la inflamación sinovial. Sin embargo, dado que se correlaciona con características patológicas y moleculares, puede considerarse una técnica fiable para la evaluación secuencial de la sinovitis aguda en las rodillas de conejo.

Estudio de los efectos anti-inflamatorios de la CEM en la artritis gotosa aguda

2. Las administración sistémica de CEM derivadas de tejido adiposo humano es capaz de disminuir la hinchazón articular y la concentración en suero de proteína C-reactiva, disminuyendo sustancialmente la duración y la intensidad del brote agudo de artritis inducido por cristales de UMS en conejo.

Farmacocinética de diferentes vías de administración, dosis y distribución de CEM en el modelo de artritis inducida por UMS.

3. El efecto antiinflamatorio de la administración sistémica de CEM a través de la arteria auricular no se reproduce cuando la inyección es intraarticular, lo que indica que la administración local de CEM debe de ser evaluada cuidadosamente en otras enfermedades articulares humanas.
4. La aplicación de CEM a través de la arteria femoral derecha produce efectos similares a los observados después de la administración por la arteria auricular, disminuyendo la inflamación 72 horas después de la agresión. Además, las CEM no muestran un mejor efecto antiinflamatorio en la rodilla artrítica derecha en comparación con su contralateral, a pesar de la llegada directa de CEM desde la arteria femoral a la sinovial derecha.

5. Las CEM administradas sistémicamente se acumulan principalmente en los pulmones, el hígado y el bazo, mientras que una pequeña fracción podría llegar a las membranas sinoviales inflamadas.

Estudio del resultado terapéutico de la administración de CEM en conejo después de una recidiva de artritis aguda

6. Una sola administración sistémica de CEM no mantiene el efecto antiinflamatorio después de una segunda agresión inducida por cristales UMS en las rodillas de conejo.

Estudio de los efectos de las CEM sobre los mecanismos inflamatorios en el modelo de artritis aguda

7. Las CEM reducen la síntesis de los componentes del inflamasoma NLRP3 en las articulaciones artríticas, inhibiendo simultáneamente la vía NF-κB.
8. Las CEM disminuyen la expresión de citoquinas proinflamatorias en la sinovial artrítica, e inducen la síntesis de citoquinas antiinflamatorias de forma precoz, en comparación con la observada en las articulaciones no tratadas. Además, las CEM promueven la presencia de macrófagos M2 en la sinovial artrítica.
9. Los estudios *in vitro* confirman que las CEM bloquean la expresión de los componentes del inflamasoma NLRP3 y la expresión de diferentes citoquinas en macrófagos derivados de THP-1 estimulados por cristales de UMS, probablemente a través de la liberación de factores solubles antiinflamatorios.
10. En conjunto, hemos demostrado que las CEM son capaces de disminuir la inflamación articular en un brote de artritis aguda inducida por cristales de MSU en conejos.
    a. Las CEM podrían considerarse una terapia novedosa para tratar los brotes de gota aguda en pacientes en los que está contraindicado el uso de fármacos tradicionales.
    b. Además, este modelo experimental proporciona un modelo excelente para estudiar los mecanismos de resolución de la inflamación mediada por la inmunidad innata.

REFERENCES

REFERENCES

1. Zakrzewski W, Dobrzyński M, Szymonowicz M, Rybak Z. Stem cells: past, present, and future. Stem Cell Res Ther. 2019;10(1):68.

2. Berdasco M, Esteller M. DNA methylation in stem cell renewal and multipotency. Stem Cell Res Ther. 2011;2(5):42.

3. Friedenstein AJ, Chailakhjan RK, Lalykina KS. The development of fibroblast colonies in monolayer cultures of guinea-pig bone marrow and spleen cells. Cell Tissue Kinet. 1970;3(4):393–403.

4. Prockop DJ. Marrow stromal cells as stem cells for nonhematopoietic tissues. Science. 1997;276(5309):71–4.

5. Owen M. Marrow stromal stem cells. J Cell Sci. 1988;(SSUPL. 10):63–76.

6. Caplan AI. Mesenchymal stem cells. J Orthop Res. 1991;9(5):641–50.

7. Wang L-T, Ting C-H, Yen M-L, Liu K-J, Sytwu H-K, Wu KK, et al. Human mesenchymal stem cells (MSCs) for treatment towards immune- and inflammation-mediated diseases: review of current clinical trials. J Biomed Sci. 2016;23(1):76.

8. Horwitz EM, Le Blanc K, Dominici M, Mueller I, Slaper-Cortenbach I, Marini FC, et al. Clarification of the nomenclature for MSC: The International Society for Cellular Therapy position statement. Cytotherapy. 2005;7(5):393–5.

9. Dominici M, Le Blanc K, Mueller I, Slaper-Cortenbach I, Marini F, Krause D, et al. Minimal criteria for defining multipotent mesenchymal stromal cells. The International Society for Cellular Therapy position statement. Cytotherapy. 2006;8(4):315–7.

10. Reinke JM, Sorg H. Wound repair and regeneration. Eur Surg Res. 2012;49(1):35-

43.

11. Gurtner GC, Werner S, Barrandon Y, Longaker MT. Wound repair and regeneration. Nature. 2008;453(7193):314-21.

12. Caterson EJ, Nesti LJ, Albert T, Danielson K, Tuan R. Application of mesenchymal stem cells in the regeneration of musculoskeletal tissues. MedGenMed. 2001;E1.

13. Bruder SP, Kraus KH, Goldberg VM, Kadiyala S. The effect of implants loaded with autologous mesenchymal stem cells on the healing of canine segmental bone defects. J Bone Jt Surg - Ser A. 1998;80(7):985–96.

14. Richardson SM, Curran JM, Chen R, Vaughan-Thomas A, Hunt JA, Freemont AJ, et al. The differentiation of bone marrow mesenchymal stem cells into chondrocyte-like cells on poly-l-lactic acid (PLLA) scaffolds. Biomaterials. 2006;27(22):4069–78.

15. Qian H, Yang H, Xu W, Yan Y, Chen Q, Zhu W, et al. Bone marrow mesenchymal stem cells ameliorate rat acute renal failure by differentiation into renal tubular epithelial-like cells. Int J Mol Med. 2008;22(3):325–32.

16. Lazarus HM, Haynesworth SE, Gerson SL, Rosenthal NS, Caplan AI. Ex vivo expansion and subsequent infusion of human bone marrow-derived stromal progenitor cells (mesenchymal progenitor cells): Implications for therapeutic use. Bone Marrow Transplant. 1995;16(4):557–64.

17. Horwitz EM, Prockop DJ, Fitzpatrick LA, Koo WWK, Gordon PL, Neel M, et al. Transplantability and therapeutic effects of bone marrow-derived mesenchymal cells in children with osteogenesis imperfecta. Nat Med. 1999;5(3):309–13.

18. Koç ON, Gerson SL, Cooper BW, Dyhouse SM, Haynesworth SE, Caplan AI, et al. Rapid Hematopoietic Recovery After Coinfusion of Autologous-Blood Stem Cells and Culture-Expanded Marrow Mesenchymal Stem Cells in Advanced Breast Cancer Patients Receiving High-Dose Chemotherapy. J Clin Oncol. 2000;18(2):307–307.

19. Hatsushika D, Muneta T, Horie M, Koga H, Tsuji K, Sekiya I. Intraarticular injection of synovial stem cells promotes meniscal regeneration in a rabbit massive meniscal defect model. J Orthop Res. 2013;31(9):1354–9.

20. Lukomska B, Stanaszek L, Zuba-Surma E, Legosz P, Sarzynska S, Drela K. Challenges and Controversies in Human Mesenchymal Stem Cell Therapy. Stem Cells Int. 2019;2019:9628536.

21. Ishida T, Inaba M, Hisha H, Sugiura K, Adachi Y, Nagata N, et al. Requirement of donor-derived stromal cells in the bone marrow for successful allogeneic bone marrow transplantation. Complete prevention of recurrence of autoimmune diseases in MRL/MP-Ipr/Ipr mice by transplantation of bone marrow plus bones (stromal cells) from the same donor. J Immunol. 1994;152(6):3119–27.

22. Deans RJ, Moseley AB. Mesenchymal stem cells: biology and potential clinical uses. Exp Hematol. 2000;28(8):875-84.

23. Kevin JD., Mcintosh R KE. Mesenchymal stem cells for prevention and treatment of immune responses in transplantation. US patent; WO1999047163, 1998.

24. Xue Q, Luan XY, Gu YZ, Wu HY, Zhang GB, Yu GH, et al. The negative co-signaling molecule B7-H4 is expressed by human bone marrow-derived mesenchymal stem cells and mediates its T-cell modulatory activity. Stem Cells Dev. 2010;19(1):27–37.

25. Luz-Crawford P, Kurte M, Bravo-Alegría J, Contreras R, Nova-Lamperti E, Tejedor G, et al. Mesenchymal stem cells generate a CD4+CD25+Foxp3 + regulatory T cell population during the differentiation process of Th1 and Th17 cells. Stem Cell Res Ther. 2013;4(3):65.

26. Corcione A, Benvenuto F, Ferretti E, Giunti D, Cappiello V, Cazzanti F, et al. Human mesenchymal stem cells modulate B-cell functions. Blood. 2006;107(1):367–72.

27. Aggarwal S, Pittenger MF. Human mesenchymal stem cells modulate allogeneic immune cell responses. Blood. 2005;105(4):1815–22.

28. Gao F, Chiu SM, Motan DAL, Zhang Z, Chen L, Ji H-L, et al. Mesenchymal stem cells and immunomodulation: current status and future prospects. Cell Death Dis. 2016;7(1):e2062.

29. Kim J, Hematti P. Mesenchymal stem cell-educated macrophages: A novel type of alternatively activated macrophages. Exp Hematol. 2009;37(12):1445–53.

30. von Bahr L, Batsis I, Moll G, Hägg M, Szakos A, Sundberg B, et al. Analysis of tissues following mesenchymal stromal cell therapy in humans indicates limited long-term engraftment and no ectopic tissue formation. Stem Cells. 2012;30(7):1575–8.

31. Mizukami A, Swiech K. Mesenchymal Stromal Cells: From Discovery to Manufacturing and Commercialization. Stem Cells Int. 2018;2018:4083921.

32. Eggenhofer E, Benseler V, Kroemer A, Popp FC, Geissler EK, Schlitt HJ, et al. Mesenchymal stem cells are short-lived and do not migrate beyond the lungs after intravenous infusion. Front Immunol. 2012;3(SEP):297.

33. Spees JL, Lee RH, Gregory CA. Mechanisms of mesenchymal stem/stromal cell function. Stem Cell Res Ther. 2016;7(1):125.

34. Abbasi-Malati Z, Roushandeh AM, Kuwahara Y, Roudkenar MH. Mesenchymal Stem Cells on Horizon: A New Arsenal of Therapeutic Agents. Stem Cell Rev. 2018;14(4):484–99.

35. Lopez-Santalla M, Mancheño-Corvo P, Menta R, Lopez-Belmonte J, DelaRosa O, Bueren JA, et al. Human Adipose-Derived Mesenchymal Stem Cells Modulate Experimental Autoimmune Arthritis by Modifying Early Adaptive T Cell Responses. Stem Cells. 2015;33(12):3493–503.

36. Lopez-Santalla M, Menta R, Mancheño-Corvo P, Lopez-Belmonte J, DelaRosa O, Bueren JA, et al. Adipose-derived mesenchymal stromal cells modulate experimental autoimmune arthritis by inducing an early regulatory innate cell signature. Immunity, Inflamm Dis. 2016;4(2):213–24.

37. Le Blanc K, Frassoni F, Ball L, Locatelli F, Roelofs H, Lewis I, et al. Mesenchymal

stem cells for treatment of steroid-resistant, severe, acute graft-versus-host disease: a phase II study. Lancet. 2008;371(9624):1579–86.

38. Karamini A, Bakopoulou A, Andreadis D, Gkiouras K, Kritis A. Therapeutic Potential of Mesenchymal Stromal Stem Cells in Rheumatoid Arthritis: a Systematic Review of In Vivo Studies. Stem Cell Rev Rep. 2020;16(2):276-287

39. Lopez-Santalla M, Fernandez-Perez R, Garin MI. Mesenchymal Stem/Stromal Cells for Rheumatoid Arthritis Treatment: An Update on Clinical Applications. Cells. 2020;9(8):1852.

40. Medzhitov R. Origin and physiological roles of inflammation. Nature. 2008;454(7203):428-35.

41. Hannoodee S, Nasuruddin DN. Acute Inflammatory Response. In: StatPearls [Internet]. Treasure Island (FL): StatPearls Publishing; 2020. Available from: https://www.ncbi.nlm.nih.gov/books/NBK556083/

42. Joel MDM, Yuan J, Wang J, Yan Y, Qian H, Zhang X, et al. MSC: Immunoregulatory effects, roles on neutrophils and evolving clinical potentials. Am J Transl Res. 2019;11(6):3890–904.

43. Novak ML, Koh TJ. Macrophage phenotypes during tissue repair. J Leukoc Biol. 2013;93(6):875–81.

44. Murray PJ, Wynn TA. Protective and pathogenic functions of macrophage subsets. Nat Rev Immunol. 2011;11(11):723-37..

45. Atri C, Guerfali FZ, Laouini D. Role of Human Macrophage Polarization in Inflammation during Infectious Diseases. Int J Mol Sci. 2018;19(6):1801.

46. Tarique AA, Logan J, Thomas E, Holt PG, Sly PD, Fantino E. Phenotypic, Functional, and Plasticity Features of Classical and Alternatively Activated Human Macrophages. Am J Respir Cell Mol Biol. 2015;53(5):676–88.

47. Fleit HB. Chronic Inflammation. In: Pathobiology of Human Disease: A Dynamic Encyclopedia of Disease Mechanisms. Elsevier Inc.; 2014. p. 300–14.

48. Munir H, Ward LSC, McGettrick HM. Mesenchymal stem cells as endogenous regulators of inflammation. In: Advances in Experimental Medicine and Biology. Springer New York LLC; 2018. 1060:73-98.

49. Eseonu OI, De Bari C. Homing of mesenchymal stem cells: mechanistic or stochastic? Implications for targeted delivery in arthritis. Rheumatology (Oxford). 2015;54(2):210–8.

50. Ullah M, Liu DD, Thakor AS. Mesenchymal Stromal Cell Homing: Mechanisms and Strategies for Improvement. iScience. 2019;15:421-438.

51. Wang Y, Chen X, Cao W, Shi Y. Plasticity of mesenchymal stem cells in immunomodulation: pathological and therapeutic implications. Nat Immunol. 2014;15(11):1009-16.

52. Ren G, Zhang L, Zhao X, Xu G, Zhang Y, Roberts AI, et al. Mesenchymal Stem Cell-Mediated Immunosuppression Occurs via Concerted Action of Chemokines and Nitric Oxide. Cell Stem Cell. 2008;2(2):141–50.

53. Andreeva E, Bobyleva P, Gornostaeva A, Buravkova L. Interaction of multipotent mesenchymal stromal and immune cells: Bidirectional effects. Cytotherapy. 2017;19(10):1152–66.

54. Bernardo ME, Fibbe WE. Mesenchymal stromal cells: sensors and switchers of inflammation. Cell Stem Cell. 2013;13(4):392-402.

55. Monsel A, Zhu YG, Gennai S, Hao Q, Liu J, Lee JW. Cell-based therapy for acute organ injury: preclinical evidence and ongoing clinical trials using mesenchymal stem cells. Anesthesiology. 2014;121(5):1099-121.

56. Pandey AC, Lancaster JJ, Harris DT, Goldman S, Juneman E. Cellular Therapeutics for Heart Failure: Focus on Mesenchymal Stem Cells. Stem Cells Int. 2017;2017:9640108.

57. Lee RH, Pulin AA, Seo MJ, Kota DJ, Ylostalo J, Larson BL, et al. Intravenous hMSCs improve myocardial infarction in mice because cells embolized in lung are activated to secrete the anti-inflammatory protein TSG-6. Cell Stem Cell.

2009;5(1):54–63.

58. Jin SZ, Liu BR, Xu J, Gao FL, Hu ZJ, Wang XH, et al. Ex vivo-expanded bone marrow stem cells home to the liver and ameliorate functional recovery in a mouse model of acute hepatic injury. Hepatobiliary Pancreat Dis Int. 2012;11(1):66–73.

59. Tögel F, Hu Z, Weiss K, Isaac J, Lange C, Westenfelder C. Administered mesenchymal stem cells protect against ischemic acute renal failure through differentiation-independent mechanisms. Am J Physiol Renal Physiol. 2005;289(1):F31-42.

60. Premer C, Schulman IH, Jackson JS. The role of mesenchymal stem/stromal cells in the acute clinical setting. Am J Emerg Med. 2020;S0735-6757(20)31044-5.

61. Shen H, Kreisel D, Goldstein DR. Processes of Sterile Inflammation. J Immunol. 2013;191(6):2857–63.

62. Oliva J. Therapeutic Properties of Mesenchymal Stem Cell on Organ Ischemia-Reperfusion Injury. Int J Mol Sci. 2019;20(21):5511.

63. Zhang Z, Tian H, Yang C, Liu J, Zhang H, Wang J, et al. Mesenchymal Stem Cells Promote the Resolution of Cardiac Inflammation After Ischemia Reperfusion Via Enhancing Efferocytosis of Neutrophils. J Am Heart Assoc. 2020;9(5):e014397.

64. Bartolucci J, Verdugo FJ, González PL, Larrea RE, Abarzua E, Goset C, et al. Safety and efficacy of the intravenous infusion of umbilical cord mesenchymal stem cells in patients with heart failure: A phase 1/2 randomized controlled trial (RIMECARD trial [Randomized clinical trial of intravenous infusion umbilical cord mesenchymal stem cells on cardiopathy]). Circ Res. 2017;121(10):1192–204.

65. Galipeau J, Sensébé L. Mesenchymal Stromal Cells: Clinical Challenges and Therapeutic Opportunities. Cell Stem Cell. 2018;22(6):824–33.

66. Le Blanc K, Davies LC. Mesenchymal stromal cells and the innate immune response. Immunol Lett. 2015;168(2):140–6.

67. Carty F, Mahon BP, English K. The influence of macrophages on mesenchymal stromal cell therapy: passive or aggressive agents? Clin Exp Immunol. 2017;188(1):1–11.

68. Abumaree MH, Stone PR, Chamley LW. The effects of apoptotic, deported human placental trophoblast on macrophages: Possible consequences for pregnancy. J Reprod Immunol. 2006;72(1–2):33–45.

69. Maqbool M, Algraittee SJR, Boroojerdi MH, Sarmadi VH, John CM, Vidyadaran S, et al. Human mesenchymal stem cells inhibit the differentiation and effector functions of monocytes. Innate Immun. 2020;26(5):424–34.

70. Di G, Du X, Qi X, Zhao X, Duan H, Li S, et al. Mesenchymal Stem Cells Promote Diabetic Corneal Epithelial Wound Healing Through TSG-6-Dependent Stem Cell Activation and Macrophage Switch. Invest Ophthalmol Vis Sci. 2017;58(10):4344–4354.

71. He Z, Hua J, Qian D, Gong J, Lin S, Xu C, et al. Intravenous hMSCs Ameliorate Acute Pancreatitis in Mice via Secretion of Tumor Necrosis Factor-α Stimulated Gene/Protein 6. Sci Rep. 2016;6(1):1–17.

72. Liu L, Song H, Duan H, Chai J, Yang J, Li X, et al. TSG-6 secreted by human umbilical cord-MSCs attenuates severe burn-induced excessive inflammation via inhibiting activations of P38 and JNK signaling. Sci Rep. 2016;6(1):1–13.

73. Choi H, Lee RH, Bazhanov N, Oh JY, Prockop DJ. Anti-inflammatory protein TSG-6 secreted by activated MSCs attenuates zymosan-induced mouse peritonitis by decreasing TLR2/NF-κB signaling in resident macrophages. Blood. 2011;118(2):330–8.

74. Dalbeth N, Choi HK, Joosten LAB, Khanna PP, Matsuo H, Perez-Ruiz F, Stamp LK. Gout. Nat Rev Dis Primers. 2019;5(1):69.

75. Pascual E, Jovaní V. Synovial fluid analysis. Best Pract Res Clin Rheumatol. 2005;19(3):371-86.

76. Dalbeth N, Merriman TR, Stamp LK. Gout. Lancet. 2016;388(10055):2039–52.

77. Punzi L, Scanu A, Ramonda R, Oliviero F. Gout as autoinflammatory disease: new mechanisms for more appropriated treatment targets. Autoimmun Rev. 2012;12(1):66-71.

78. Raffaghello L, Bianchi G, Bertolotto M, Montecucco F, Busca A, Dallegri F, et al. Human Mesenchymal Stem Cells Inhibit Neutrophil Apoptosis: A Model for Neutrophil Preservation in the Bone Marrow Niche. Stem Cells. 2008;26(1):151–62.

79. Jiang D, Muschhammer J, Qi Y, Kügler A, de Vries JC, Saffarzadeh M, et al. Suppression of Neutrophil-Mediated Tissue Damage-A Novel Skill of Mesenchymal Stem Cells. Stem Cells. 2016;34(9):2393–406.

80. Mittal SK, Mashaghi A, Amouzegar A, Li M, Foulsham W, Sahu SK, et al. Mesenchymal stromal cells inhibit neutrophil effector functions in a murine model of ocular inflammation. Investig Ophthalmol Vis Sci. 2018;59(3):1191–8.

81. Selleri S, Bifsha P, Civini S, Pacelli C, Dieng MM, Lemieux W, et al. Human mesenchymal stromal cell-secreted lactate induces M2-macrophage differentiation by metabolic reprogramming. Oncotarget. 2016;7(21):30193–210.

82. Chiossone L, Conte R, Spaggiari GM, Serra M, Romei C, Bellora F, et al. Mesenchymal Stromal Cells Induce Peculiar Alternatively Activated Macrophages Capable of Dampening Both Innate and Adaptive Immune Responses. Stem Cells. 2016;34(7).

83. Németh K, Leelahavanichkul A, Yuen PST, Mayer B, Parmelee A, Doi K, et al. Bone marrow stromal cells attenuate sepsis via prostaglandin E 2-dependent reprogramming of host macrophages to increase their interleukin-10 production. Nat Med. 2009 Jan 21;15(1):42–9.

84. Park HJ, Kim J, Saima FT, Rhee K-J, Hwang S, Kim MY, et al. Adipose-derived stem cells ameliorate colitis by suppression of inflammasome formation and regulation of M1-macrophage population through prostaglandin E2. Biochem Biophys Res Commun. 2018;498(4):988–95.

85. Song W-J, Li Q, Ryu M-O, Ahn J-O, Ha Bhang D, Chan Jung Y, et al. TSG-6 Secreted by Human Adipose Tissue-derived Mesenchymal Stem Cells Ameliorates DSS-induced colitis by Inducing M2 Macrophage Polarization in Mice. Sci Rep. 2017;7(1):5187.

86. Lv H, Liu Q, Sun Y, Yi X, Wei X, Liu W, et al. Mesenchymal stromal cells ameliorate acute lung injury induced by LPS mainly through stanniocalcin-2 mediating macrophage polarization. Ann Transl Med. 2020;8(6):334–334.

87. Jackson M V., Morrison TJ, Doherty DF, McAuley DF, Matthay MA, Kissenpfennig A, et al. Mitochondrial Transfer via Tunneling Nanotubes is an Important Mechanism by Which Mesenchymal Stem Cells Enhance Macrophage Phagocytosis in the In Vitro and In Vivo Models of ARDS. Stem Cells. 2016;34(8):2210–23.

88. Lee KC, Lin HC, Huang YH, Hung SC. Allo-transplantation of mesenchymal stem cells attenuates hepatic injury through IL1Ra dependent macrophage switch in a mouse model of liver disease. J Hepatol. 2015;63(6):1405–12.

89. Galleu A, Riffo-Vasquez Y, Trento C, Lomas C, Dolcetti L, Cheung TS, et al. Apoptosis in mesenchymal stromal cells induces in vivo recipient-mediated immunomodulation. Sci Transl Med. 2017;9(416).

90. Luk F, de Witte SFH, Korevaar SS, Roemeling-van Rhijn M, Franquesa M, Strini T, et al. Inactivated Mesenchymal Stem Cells Maintain Immunomodulatory Capacity. Stem Cells Dev. 2016;25(18):1342–54.

91. Eggebeen AT. Gout: an update. Am Fam Physician. 2007;76(6):801-8.

92. Chhana A, Dalbeth N. The gouty tophus: a review. Curr Rheumatol Rep. 2015;17(3):19.

93. Mattiuzzi C, Lippi G. Recent updates on worldwide gout epidemiology. Clin Rheumatol. 2020;39(4):1061-1063.

94. Kuo C-F, Grainge MJ, Zhang W, Doherty M. Global epidemiology of gout: prevalence, incidence and risk factors. Nat Rev Rheumatol. 2015;11(11):649–62.

95. Rothschild B. Contributions of paleorheumatology to understanding contemporary disease. Reumatismo. 2002;54(3):272-84.

96. Desai J, Steiger S, Anders HJ. Molecular Pathophysiology of Gout. Trends Mol Med. 2017;23(8):756-768.

97. Martinon F, Pétrilli V, Mayor A, Tardivel A, Tschopp J. Gout-associated uric acid crystals activate the NALP3 inflammasome. Nature. 2006;440(7081):237–41.

98. Agostini L, Martinon F, Burns K, McDermott MF, Hawkins PN, Tschopp J. NALP3 forms an IL-1β-processing inflammasome with increased activity in Muckle-Wells autoinflammatory disorder. Immunity. 2004;20(3):319–25.

99. de Zoete MR, Palm NW, Zhu S, Flavell RA. Inflammasomes. Cold Spring Harb Perspect Biol. 2014;6(12):a016287–a016287.

100. Cai X, Chen J, Xu H, Liu S, Jiang QX, Halfmann R, et al. Prion-like polymerization underlies signal transduction in antiviral immune defense and inflammasome activation. Cell. 2014;156(6):1207–22.

101. Christgen S, Place DE, Kanneganti TD. Toward targeting inflammasomes: insights into their regulation and activation. Cell Res. 2020;30(4):315-327.

102. He WT, Wan H, Hu L, Chen P, Wang X, Huang Z, et al. Gasdermin D is an executor of pyroptosis and required for interleukin-1β secretion. Cell Res. 2015;25(12):1285–98.

103. Aglietti RA, Dueber EC. Recent Insights into the Molecular Mechanisms Underlying Pyroptosis and Gasdermin Family Functions. Trends Immunol. 2017;38(4):261-271.

104. So AK, Martinon F. Inflammation in gout: mechanisms and therapeutic targets. Nat Rev Rheumatol. 2017;13(11):639–47.

105. Liu-Bryan R, Scott P, Sydlaske A, Rose DM, Terkeltaub R. Innate immunity conferred by Toll-like receptors 2 and 4 and myeloid differentiation factor 88 expression is pivotal to monosodium urate monohydrate crystal-induced

inflammation. Arthritis Rheum. 2005;52(9):2936–46.

106. Cronstein BN, Sunkureddi P. Mechanistic Aspects of Inflammation and Clinical Management of Inflammation in Acute Gouty Arthritis. JCR J Clin Rheumatol. 2013;19(1):19–29.

107. Holzinger D, Nippe N, Vogl T, Marketon K, Mysore V, Weinhage T, et al. Myeloid-related proteins 8 and 14 contribute to monosodium urate monohydrate crystal-induced inflammation in gout. Arthritis Rheumatol. 2014;66(5):1327–39.

108. An L-L, Mehta P, Xu L, Turman S, Reimer T, Naiman B, et al. Complement C5a potentiates uric acid crystal-induced IL-1β production. Eur J Immunol. 2014;44(12):3669–79.

109. Gong T, Yang Y, Jin T, Jiang W, Zhou R. Orchestration of NLRP3 Inflammasome Activation by Ion Fluxes. Trends Immunol. 2018;39(5):393-406.

110. Zamudio-Cuevas Y, Hernández-Díaz C, Pineda C, Reginato AM, Cerna-Cortés JF, Ventura-Ríos L, et al. Molecular basis of oxidative stress in gouty arthropathy. Clin Rheumatol. 2015;34(10):1667–72.

111. He Y, Zeng MY, Yang D, Motro B, Núñez G. NEK7 is an essential mediator of NLRP3 activation downstream of potassium efflux. Nature. 2016;530(7590):354–7.

112. Chevriaux A, Pilot T, Derangère V, Simonin H, Martine P, Chalmin F, et al. Cathepsin B Is Required for NLRP3 Inflammasome Activation in Macrophages, Through NLRP3 Interaction. Front Cell Dev Biol. 2020;8:167.

113. Liu-Bryan R. Intracellular innate immunity in gouty arthritis: role of NALP3 inflammasome. Immunol Cell Biol. 2010;88(1):20–3.

114. Steiger S, Harper JL. Mechanisms of Spontaneous Resolution of Acute Gouty Inflammation. Curr Rheumatol Rep. 2014;16(1):392.

115. Neumann K, Castiñeiras-Vilariño M, Höckendorf U, Hannesschläger N, Lemeer S, Kupka D, et al. Clec12a is an inhibitory receptor for uric acid crystals that

regulates inflammation in response to cell death. Immunity. 2014;40(3):389–99.

116. Sancho D, Reis e Sousa C. Sensing of cell death by myeloid C-type lectin receptors. Curr Opin Immunol. 2013;25(1):46-52.

117. Lang T, Mansell A. The negative regulation of Toll-like receptor and associated pathways. Immunol Cell Biol. 2007;85(6):425–34.

118. Nakahira K, Haspel JA, Rathinam VAK, Lee SJ, Dolinay T, Lam HC, et al. Autophagy proteins regulate innate immune responses by inhibiting the release of mitochondrial DNA mediated by the NALP3 inflammasome. Nat Immunol. 2011;12(3):222–30.

119. Oliviero F, Scanu A. How Factors Involved in the Resolution of Crystal-Induced Inflammation Target IL-1β. Front Pharmacol. 2017;8(MAR):164.

120. Wahl SM, Costa GL, Corcoran M, Wahl LM, Berger AE. Transforming growth factor-beta mediates IL-1-dependent induction of IL-1 receptor antagonist. J Immunol. 1993;150(8).

121. Zeng M, Dang W, Chen B, Qing Y, Xie W, Zhao M, et al. IL-37 inhibits the production of pro-inflammatory cytokines in MSU crystal-induced inflammatory response. Clin Rheumatol. 2016;35(9):2251–8.

122. Chen YH, Hsieh SC, Chen WY, Li KJ, Wu CH, Wu PC, et al. Spontaneous resolution of acute gouty arthritis is associated with rapid induction of the anti-inflammatory factors TGFβ1, IL-10 and soluble TNF receptors and the intracellular cytokine negative regulators CIS and SOCS3. Ann Rheum Dis. 2011;70(9):1655–63.

123. Fadok VA, Bratton DL, Konowal A, Freed PW, Westcott JY, Henson PM. Macrophages that have ingested apoptotic cells in vitro inhibit proinflammatory cytokine production through autocrine/paracrine mechanisms involving TGF-β, PGE2, and PAF. J Clin Invest. 1998;101(4):890–8.

124. Schett G, Schauer C, Hoffmann M, Herrmann M. Why does the gout attack stop? A roadmap for the immune pathogenesis of gout. RMD Open. 2015;15(1(Suppl

1)):e000046.

125. Qaseem A, Harris RP, Forciea MA. Management of Acute and Recurrent Gout: A Clinical Practice Guideline From the American College of Physicians. Ann Intern Med. 2017;166(1):58.

126. Pascart T, Richette P. Current and future therapies for gout. Expert Opin Pharmacother. 2017;18(12):1201-1211.

127. Schlee S, Bollheimer LC, Bertsch T, Sieber CC, Härle P. Crystal arthritides - gout and calcium pyrophosphate arthritis : Part 3: Treatment. Z Gerontol Geriatr. 2018;51(6):703-710.

128. Gómez Reino J, Loza E, Andreu JL, Balsa A, Batlle E, Cañete JD, et al. Consensus Statement of the Spanish Society of Rheumatology on Risk Management of Biologic Therapy in Rheumatic Patients. Reumatol Clínica. 2011;7(5):284–98.

129. McGrath JC, Lilley E. Implementing guidelines on reporting research using animals (ARRIVE etc.): new requirements for publication in BJP. Br J Pharmacol. 2015;172(13):3189–93.

130. Pineda C, Fuentes-Gómez AJ, Hernández-Díaz C, Zamudio-Cuevas Y, Fernández-Torres J, López-Macay A, et al. Animal model of acute gout reproduces the inflammatory and ultrasonographic joint changes of human gout. Arthritis Res Ther. 2015;17(1):37.

131. Miguelez R, Palacios I, Navarro F, Gutierrez E, Sanchez-Pernaute O, Egido J, et al. Anti-inflammatory effect of a PAF receptor antagonist and a new molecule with antiproteinase activity in an experimental model of acute urate crystal arthritis. J Lipid Mediat Cell Signal. 1996;13(1):35–49.

132. Wakefield RJ, Balint P V, Szkudlarek M, Filippucci E, Backhaus M, D'Agostino M-A, et al. Musculoskeletal ultrasound including definitions for ultrasonographic pathology. J Rheumatol. 2005;32(12):2485–7.

133. Szkudlarek M, Court-Payen M, Jacobsen S, Klarlund M, Thomsen HS, Østergaard M. Interobserver agreement in ultrasonography of the finger and toe joints in

rheumatoid arthritis. Arthritis Rheum. 2003;48(4):955–62.

134. Grassi W, Meenagh G, Pascual E, Filippucci E. “Crystal clear”-sonographic assessment of gout and calcium pyrophosphate deposition disease. Semin Arthritis Rheum. 2006;36(3):197–202.

135. Valencia J, Blanco B, Yáñez R, Vázquez M, Herrero Sánchez C, Fernández-García M, et al. Comparative analysis of the immunomodulatory capacities of human bone marrow– and adipose tissue–derived mesenchymal stromal cells from the same donor. Cytotherapy. 2016;18(10):1297–311.

136. Krenn V, Morawietz L, Burmester G-R, Kinne RW, Mueller-Ladner U, Muller B, et al. Synovitis score: discrimination between chronic low-grade and high-grade synovitis. Histopathology. 2006;49(4):358–64.

137. Lis GJ, Litwin JA, Furgal-Borzych A, Zarzecka J, Cichocki T. Macrophage-specific RAM11 monoclonal antibody cross-reacts with basal cells of stratified squamous epithelia. Folia Histochem Cytobiol. 2007;45(3):229–32.

138. Lau SK, Chu PG, Weiss LM. CD163: A specific marker of macrophages in paraffin-embedded tissue samples. Am J Clin Pathol. 2004;122(5):794–801.

139. Fishman JM, Lowdell MW, Urbani L, Ansari T, Burns AJ, Turmaine M, et al. Immunomodulatory effect of a decellularized skeletal muscle scaffold in a discordant xenotransplantation model. Proc Natl Acad Sci U S A. 2013;110(35):14360–5.

140. Martínez-Calatrava MJ, Prieto-Potín I, Roman-Blas JA, Tardio L, Largo R, Herrero-Beaumont G. RANKL synthesized by articular chondrocytes contributes to juxta-articular bone loss in chronic arthritis. Arthritis Res Ther. 2012;14(3):R149.

141. Larrañaga-Vera A, Lamuedra A, Pérez-Baos S, Prieto-Potin I, Peña L, Herrero-Beaumont G, et al. Increased synovial lipodystrophy induced by high fat diet aggravates synovitis in experimental osteoarthritis. Arthritis Res Ther. 2017;19(1):264.

142. Ono K, Satoh M, Yoshida T, Ozawa Y, Kohara A, Takeuchi M, et al. Species

identification of animal cells by nested PCR targeted to mitochondrial DNA. Vitr Cell Dev Biol - Anim. 2007;43(5–6):168–75.

143. Pérez-Baos S, Barrasa JI, Gratal P, Larrañaga-Vera A, Prieto-Potin I, Herrero-Beaumont G, et al. Tofacitinib restores the inhibition of reverse cholesterol transport induced by inflammation: understanding the lipid paradox associated with rheumatoid arthritis. Br J Pharmacol. 2017;174(18):3018–31.

144. Buechler C, Ritter M, Orsó E, Langmann T, Klucken J, Schmitz G. Regulation of scavenger receptor CD163 expression in human monocytes and macrophages by pro- and antiinflammatory stimuli. J Leukoc Biol. 2000;67(1):97–103.

145. Nakada H, Yamashita A, Kuroki M, Furukoji E, Uchino N, Asanuma T, et al. A synthetic tryptophan metabolite reduces hemorrhagic area and inflammation after pulmonary radiofrequency ablation in rabbit nonneoplastic lungs. Jpn J Radiol. 2014;32(3):145–54.

146. Hannemann N, Cao S, Eriksson D, Schnelzer A, Jordan J, Eberhardt M, et al. Transcription factor Fra-1 targets arginase-1 to enhance macrophage-mediated inflammation in arthritis. J Clin Invest. 2019;129(7):2669–84.

147. Geng Y, Zhang L, Fu B, Zhang J, Hong Q, Hu J, et al. Mesenchymal stem cells ameliorate rhabdomyolysis-induced acute kidney injury via the activation of M2 macrophages. Stem Cell Res Ther. 2014;5(3):80.

148. Roddy GW, Oh JY, Lee RH, Bartosh TJ, Ylostalo J, Coble K, et al. Action at a distance: systemically administered adult stem/progenitor cells (MSCs) reduce inflammatory damage to the cornea without engraftment and primarily by secretion of TNF-α stimulated gene/protein 6. Stem Cells. 2011;29(10):1572–9.

149. Vieira AT, Galvão I, Macia LM, Sernaglia ÉM, Vinolo MA, Garcia CC, Tavares LP, Amaral FA, Sousa LP, Martins FS, Mackay CR, Teixeira MM. Dietary fiber and the short-chain fatty acid acetate promote resolution of neutrophilic inflammation in a model of gout in mice. J Leukoc Biol. 2017;101(1):275-284.

150. Dhanasekar C, Rasool M. Morin, a dietary bioflavonol suppresses monosodium urate crystal-induced inflammation in an animal model of acute gouty arthritis

with reference to NLRP3 inflammasome, hypo-xanthine phospho-ribosyl transferase, and inflammatory mediators. Eur J Pharmacol. 2016;786:116–27.

151. Li L, Wang D, Wang X, Bai R, Wang C, Gao Y, et al. N-Butyrylated hyaluronic acid ameliorates gout and hyperuricemia in animal models. Pharm Biol. 2019;57(1):717–28.

152. Rossato MF, Hoffmeister C, Trevisan G, Bezerra F, Cunha TM, Ferreira J, et al. Monosodium urate crystal interleukin-1β release is dependent on Toll-like receptor 4 and transient receptor potential V1 activation. Rheumatol (United Kingdom). 2020;59(1):233–42.

153. Li L, Teng M, Liu Y, Qu Y, Zhang Y, Lin F, Wang D. Anti-Gouty Arthritis and Antihyperuricemia Effects of Sunflower *(Helianthus annuus)* Head Extract in Gouty and Hyperuricemia Animal Models. Biomed Res Int. 2017;2017:5852076.

154. Peng Y, Lu J, Liu F, Lee C, Lee H, Ho Y, et al. Astaxanthin attenuates joint inflammation induced by monosodium urate crystals. FASEB J. 2020;34(8):11215–26.

155. Powers NE, Swartzwelter B, Marchetti C, De Graaf DM, Lerchner A, Schlapschy M, et al. PASylation of IL-1 receptor antagonist (IL-1Ra) retains IL-1 blockade and extends its duration in mouse urate crystalinduced peritonitis. J Biol Chem. 2020;295(3):868–82.

156. Yang G, Lee HE, Moon SJ, Ko KM, Koh JH, Seok JK, et al. Direct Binding to NLRP3 Pyrin Domain as a Novel Strategy to Prevent NLRP3-Driven Inflammation and Gouty Arthritis. Arthritis Rheumatol. 2020;72(7):1192–202.

157. Martin WJ, Walton M, Harper J. Resident macrophages initiating and driving inflammation in a monosodium urate monohydrate crystal-induced murine peritoneal model of acute gout. Arthritis Rheum. 2009;60(1):281–9.

158. Mariotte A, de Cauwer A, Po C, Abou-Faycal C, Pichot A, Paul N, et al. A mouse model of MSU-induced acute inflammation in vivo suggests imiquimod-dependent targeting of Il-1β as relevant therapy for gout patients. Theranostics. 2020;10(5):2158–71.

159. Yang G, Yeon SH, Lee HE, Kang HC, Cho YY, Lee HS, et al. Suppression of NLRP3 inflammasome by oral treatment with sulforaphane alleviates acute gouty inflammation. Rheumatol (United Kingdom). 2018;57(4):727–36.

160. Martin WJ, Shaw O, Liu X, Steiger S, Harper JL. Monosodium urate monohydrate crystal-recruited noninflammatory monocytes differentiate into M1-like proinflammatory macrophages in a peritoneal murine model of gout. Arthritis Rheum. 2011;63(5):1322–32.

161. Romano M, Faggioni R, Sironi M, Sacco S, Echtenacher B, Di Santo E, et al. Carrageenan-induced acute inflammation in the mouse air pouch synovial model. Role of tumour necrosis factor. Mediators Inflamm. 1997;6(1):32–8.

162. Ryckman C, McColl SR, Vandal K, De Médicis R, Lussier A, Poubelle PE, et al. Role of S100A8 and S100A9 in neutrophil recruitment in response to monosodium urate monohydrate crystals in the air-pouch model of acute gouty arthritis. Arthritis Rheum. 2003;48(8):2310–20.

163. Lu J, Dalbeth N, Yin H, Li C, Merriman TR, Wei WH. Mouse models for human hyperuricaemia: a critical review. Nat Rev Rheumatol. 2019;15(7):413-426.

164. Yao R, Geng Z, Mao X, Bao Y, Guo S, Bao L, Sun J, Gao Y, Xu Y, Guo B, Meng F, Cui X. *Tu-Teng-Cao* Extract Alleviates Monosodium Urate-Induced Acute Gouty Arthritis in Rats by Inhibiting Uric Acid and Inflammation. Evid Based Complement Alternat Med. 2020;2020:3095624.

165. Stavric B, Nera EA. Use of the uricase-inhibited rat as an animal model in toxicology. Clin Toxicol. 1978;13(1):47–74.

166. Nishimura A, Akahoshi T, Takahashi M, Takagishi K, Itoman M, Kondo H, et al. Attenuation of monosodium urate crystal-induced arthritis in rabbits by a neutralizing antibody against interleukin-8. J Leukoc Biol. 1997;62(4):444–9.

167. Tramontini N, Huber C, Liu-Bryan R, Terkeltaub RA, Kilgore KS. Central role of complement membrane attack complex in monosodium urate crystal-induced neutrophilic rabbit knee synovitis. Arthritis Rheum. 2004;50(8):2633–9.

168. Naredo E, Uson J, Jiménez-Palop M, Martínez A, Vicente E, Brito E, et al. Ultrasound-detected musculoskeletal urate crystal deposition: which joints and what findings should be assessed for diagnosing gout? Ann Rheum Dis. 2014;73(8):1522–8.

169. Ogdie A, Taylor WJ, Neogi T, Fransen J, Jansen TL, Schumacher HR, et al. Performance of Ultrasound in the Diagnosis of Gout in a Multicenter Study: Comparison With Monosodium Urate Monohydrate Crystal Analysis as the Gold Standard. Arthritis Rheumatol. 2017;69(2):429–38.

170. Terkeltaub R. Gout. Novel therapies for treatment of gout and hyperuricemia. Arthritis Res Ther. 2009;11(4):236.

171. Krenn V, Morawietz L, Häupl T, Neidel J, Petersen I, König A. Grading of chronic synovitis--a histopathological grading system for molecular and diagnostic pathology. Pathol Res Pract. 2002;198(5):317–25.

172. Chen S, Zheng Q, Liu H, Zeng J, Ye Z, Su Y, et al. Sonography Is Superior to Serum-Based Biomarkers for Measuring Disease Status in Experimental Rheumatoid Arthritis. J Ultrasound Med. 2016;35:2223–30.

173. Clavel G, Marchiol-Fournigault C, Renault G, Boissier M-C, Fradelizi D, Bessis N. Ultrasound and Doppler micro-imaging in a model of rheumatoid arthritis in mice. Ann Rheum Dis. 2008;67(12):1765–72.

174. Szade A, Grochot-Przeczek A, Florczyk U, Jozkowicz A, Dulak J. Cellular and molecular mechanisms of inflammation-induced angiogenesis. IUBMB Life. 2015;67(3):145–59.

175. Scalia R, Lefer AM. In vivo regulation of PECAM-1 activity during acute endothelial dysfunction in the rat mesenteric microvasculature. J Leukoc Biol. 1998;64(2):163–9.

176. Bogen S, Pak J, Garifallou M, Deng X, Muller WA. Monoclonal antibody to murine PECAM-1 (CD31) blocks acute inflammation in vivo. J Exp Med. 1994;179(3):1059–64.

177. Solowiej A, Biswas P, Graesser D, Madri JA. Lack of platelet endothelial cell adhesion molecule-1 attenuates foreign body inflammation because of decreased angiogenesis. Am J Pathol. 2003;162(3):953–62.

178. Woodfin A, Voisin MB, Nourshargh S. PECAM-1: a multi-functional molecule in inflammation and vascular biology. Arterioscler Thromb Vasc Biol. 2007;27(12):2514-23.

179. Kelly S, Bombardieri M, Humby F, Ng N, Marrelli A, Riahi S, et al. Angiogenic gene expression and vascular density are reflected in ultrasonographic features of synovitis in early Rheumatoid Arthritis: an observational study. Arthritis Res Ther. 2015;17(1):58.

180. Schett G, Dayer JM, Manger B. Interleukin-1 function and role in rheumatic disease. Nat Rev Rheumatol. 2016;12(1):14-24.

181. Eastgate JA, Wood NC, Di Giovine FS, Symons JA, Grinlinton FM, Duff GW. Correlation of plasma interleukin 1 levels with disease activity in rheumatoid arthritis. Lancet. 1988;332(8613):706–9.

182. Prockop DJ, Oh JY, Lee RH. Data against a Common Assumption: Xenogeneic Mouse Models Can Be Used to Assay Suppression of Immunity by Human MSCs. Mol Ther. 2017;25(8):1748-1756.

183. Gutierrez-Fernandez M, Rodríguez-Frutos B, Ramos-Cejudo J, Otero-Ortega L, Fuentes B, Vallejo-Cremades TT, et al. Comparison between xenogeneic and allogeneic adipose mesenchymal stem cells in the treatment of acute cerebral infarct: Proof of concept in rats. J Transl Med. 2015;13(1):46.

184. Ankrum JA, Ong JF, Karp JM. Mesenchymal stem cells: immune evasive, not immune privileged. Nat Biotechnol. 2014;32(3):252-60.

185. Le Blanc K, Tammik C, Rosendahl K, Zetterberg E, Ringdén O. HLA expression and immunologic properties of differentiated and undifferentiated mesenchymal stem cells. Exp Hematol. 2003;31(10):890–6.

186. Melief SM, Zwaginga JJ, Fibbe WE, Roelofs H. Adipose Tissue-Derived

Multipotent Stromal Cells Have a Higher Immunomodulatory Capacity Than Their Bone Marrow-Derived Counterparts. Stem Cells Transl Med. 2013;2(6):455–63.

187. Li CY, Wu XY, Tong JB, Yang XX, Zhao JL, Zheng QF, et al. Comparative analysis of human mesenchymal stem cells from bone marrow and adipose tissue under xeno-free conditions for cell therapy. Stem Cell Res Ther. 2015;6(1).

188. Tyndall A. Mesenchymal stromal cells and rheumatic disorders. Immunol Lett. 2015;168(2):201–7.

189. Franceschetti T, De Bari C. The potential role of adult stem cells in the management of the rheumatic diseases. Ther Adv Musculoskelet Dis. 2017;9(7):165–79.

190. Sala E, Genua M, Petti L, Anselmo A, Arena V, Cibella J, et al. Mesenchymal Stem Cells Reduce Colitis in Mice via Release of TSG6, Independently of Their Localization to the Intestine. Gastroenterology. 2015;149(1):163–176.e20.

191. Kabat M, Bobkov I, Kumar S, Grumet M. Trends in mesenchymal stem cell clinical trials 2004-2018: Is efficacy optimal in a narrow dose range? Stem Cells Transl Med. 2020;9(1):17–27.

192. Li X, Lu X, Sun D, Wang X, Yang L, Zhao S, et al. Adipose-derived mesenchymal stem cells reduce lymphocytic infiltration in a rabbit model of induced autoimmune dacryoadenitis. Investig Ophthalmol Vis Sci. 2016;57(13):5161–70.

193. Ueda S, Shimasaki M, Ichiseki T, Ueda Y, Tsuchiya M, Kaneuji A, et al. Prevention of glucocorticoid-associated osteonecrosis by intravenous administration of mesenchymal stem cells in a rabbit model. BMC Musculoskelet Disord. 2017;18(1):480.

194. Wang SS, Hu SW, Zhang QH, Xia AX, Jiang ZX, Chen XM. Mesenchymal stem cells stabilize atherosclerotic vulnerable plaque by anti-inflammatory properties. PLoS One. 2015;10(8):1–17.

195. Alberts A, Klingberg A, Wessig AK, Combes C, Witte T, Brand K, et al. C-reactive

protein (CRP) recognizes uric acid crystals and recruits proteases C1 and MASP1. Sci Rep. 2020;10(1):1–13.

196. Fuentes-Julián S, Arnalich-Montiel F, Jaumandreu L, Leal M, Casado A, García-Tuñon I, et al. Adipose-Derived Mesenchymal Stem Cell Administration Does Not Improve Corneal Graft Survival Outcome. Beltrami AP, editor. PLoS One. 2015;10(3):e0117945.

197. Sensebé L, Fleury-Cappellesso S. Biodistribution of mesenchymal stem/stromal cells in a preclinical setting. Stem Cells Int. 2013;2013:678063.

198. Leibacher J, Henschler R. Biodistribution, migration and homing of systemically applied mesenchymal stem/stromal cells. Stem Cell Res Ther. 2016;7(1):7.

199. Arnberg F, Lundberg J, Olsson A, Samén E, Jaff N, Jussing E, et al. Intra-arterial Administration of Placenta-Derived Decidual Stromal Cells to the Superior Mesenteric Artery in the Rabbit: Distribution of Cells, Feasibility, and Safety. Cell Transplant. 2016;25(2):401–10.

200. Brooks A, Futrega K, Liang X, Hu X, Liu X, Crawford DHG, et al. Concise Review: Quantitative Detection and Modeling the In Vivo Kinetics of Therapeutic Mesenchymal Stem/Stromal Cells. Stem Cells Transl Med. 2018;7(1):78–86.

201. Toupet K, Maumus M, Peyrafitte JA, Bourin P, Van Lent PLEM, Ferreira R, et al. Long-term detection of human adipose-derived mesenchymal stem cells after intraarticular injection in SCID mice. Arthritis Rheum. 2013;65(7):1786–94.

202. Toupet K, Maumus M, Luz-Crawford P, Lombardo E, Lopez-Belmonte J, van Lent P, et al. Survival and biodistribution of xenogenic adipose mesenchymal stem cells is not affected by the degree of inflammation in arthritis. PLoS One. 2015;10(1):e0114962.

203. Wang Y, Luo C, Yang G, Wei X, Liu D, Zhou S. A Luteolin-Loaded Electrospun Fibrous Implantable Device for Potential Therapy of Gout Attacks. Macromol Biosci. 2016;16(11):1598–609.

204. Newson J, Stables M, Karra E, Arce-Vargas F, Quezada S, Motwani M, et al.

Resolution of acute inflammation bridges the gap between innate and adaptive immunity. Blood. 2014;124(11):1748–64.

205. Prieto-Potín I, Roman-Blas J, Martínez-Calatrava M, Gómez R, Largo R, Herrero-Beaumont G. Hypercholesterolemia boosts joint destruction in chronic arthritis. An experimental model aggravated by foam macrophage infiltration. Arthritis Res Ther. 2013;15(4):R81.

206. Liu Y, Tang H, Liu X, Chen H, Feng N, Zhang J, et al. Frontline Science: Reprogramming COX-2, 5-LOX, and CYP4A-mediated arachidonic acid metabolism in macrophages by salidroside alleviates gouty arthritis. J Leukoc Biol. 2019;105(1):11–24.

207. Torres R, Macdonald L, Croll SD, Reinhardt J, Dore A, Stevens S, et al. Hyperalgesia, synovitis and multiple biomarkers of inflammation are suppressed by interleukin 1 inhibition in a novel animal model of gouty arthritis. Ann Rheum Dis. 2009;68(10):1602–8.

208. Bauernfeind FG, Horvath G, Stutz A, Alnemri ES, MacDonald K, Speert D, et al. Cutting Edge: NF-κB Activating Pattern Recognition and Cytokine Receptors License NLRP3 Inflammasome Activation by Regulating NLRP3 Expression. J Immunol. 2009;183(2):787–91.

209. Lee DJ, Du F, Chen SW, Nakasaki M, Rana I, Shih VFS, et al. Regulation and Function of the Caspase-1 in an Inflammatory Microenvironment. J Invest Dermatol. 2015;135(8):2012–20.

210. Liu T, Zhang L, Joo D, Sun SC. NF-κB signaling in inflammation. Signal Transduct Target Ther. 2017;2:17023.

211. Yan X, Cen Y, Wang Q. Mesenchymal stem cells alleviate experimental rheumatoid arthritis through microRNA-regulated IκB expression. Sci Rep. 2016;6:28915.

212. Kim J, Kim WJ, Ha KS, Han ET, Park WS, Yang SR, et al. Perivascular stem cells suppress inflammasome activation during inflammatory responses in macrophages. Int J Stem Cells. 2019;12(3):419–29.

213. Inokuchi T, Moriwaki Y, Tsutsui H, Yamamoto A, Takahashi S, Tsutsumi Z, et al. Plasma interleukin (IL)-18 (interferon-γ-inducing factor) and other inflammatory cytokines in patients with gouty arthritis and monosodium urate monohydrate crystal-induced secretion of IL-18. Cytokine. 2006;33(1):21–7.

214. Cavalcanti NG, Marques CDL, Lins E Lins TU, Pereira MC, Rêgo MJB de M, Duarte ALBP, et al. Cytokine Profile in Gout: Inflammation Driven by IL-6 and IL-18? Immunol Invest. 2016;45(5):383–95.

215. Wang G, Cao K, Liu K, Xue Y, Roberts AI, Li F, et al. Kynurenic acid, an IDO metabolite, controls TSG-6-mediated immunosuppression of human mesenchymal stem cells. Cell Death Differ. 2018;25(7):1209–23.

216. Um S, Kim HY, Lee JH, Song IS, Seo BM. TSG-6 secreted by mesenchymal stem cells suppresses immune reactions influenced by BMP-2 through p38 and MEK mitogen-activated protein kinase pathway. Cell Tissue Res. 2017;368(3):551–61.

217. Oh JY, Ko JH, Lee HJ, Yu JM, Choi H, Kim MK, et al. Mesenchymal stem/stromal cells inhibit the NLRP3 inflammasome by decreasing mitochondrial reactive oxygen species. Stem Cells. 2014;32(6):1553–63.

218. Naji A, Muzembo BA, Yagyu K-I, Baba N, Deschaseaux F, Sensebé L, et al. Endocytosis of indium-tin-oxide nanoparticles by macrophages provokes pyroptosis requiring NLRP3-ASC-Caspase1 axis that can be prevented by mesenchymal stem cells. Sci Rep. 2016;6:26162.

219. Mosser DM, Edwards JP. Exploring the full spectrum of macrophage activation. Nat Rev Immunol. 2008;8(12):958-69.

220. Awad F, Assrawi E, Jumeau C, Georgin-Lavialle S, Cobret L, Duquesnoy P, et al. Impact of human monocyte and macrophage polarization on NLR expression and NLRP3 inflammasome activation. Lai H-C, editor. PLoS One. 2017;12(4):e0175336.

221. Rőszer T. Understanding the Mysterious M2 Macrophage through Activation Markers and Effector Mechanisms. Mediators Inflamm. 2015;2015:816460.

222. Jeong JH, Hong S, Kwon OC, Ghang B, Hwang I, Kim YG, et al. CD14+ cells with the phenotype of infiltrated monocytes consist of distinct populations characterized by anti-inflammatory as well as pro-inflammatory activity in gouty arthritis. Front Immunol. 2017;8(OCT):1260.

223. Xie Z, Hao H, Tong C, Cheng Y, Liu J, Pang Y, et al. Human umbilical cord-derived mesenchymal stem cells elicit macrophages into an anti-inflammatory phenotype to alleviate insulin resistance in type 2 diabetic rats. Stem Cells. 2016;34(3):627–39.

224. Zhang X-L, Guo Y-F, Song Z-X, Zhou M. Vitamin D Prevents Podocyte Injury via Regulation of Macrophage M1/M2 Phenotype in Diabetic Nephropathy Rats. Endocrinology. 2014;155(12):4939–50.

225. Desando G, Bartolotti I, Cavallo C, Schiavinato A, Secchieri C, Kon E, et al. Short-Term Homing of Hyaluronan-Primed Cells: Therapeutic Implications for Osteoarthritis Treatment. Tissue Eng Part C Methods. 2018;24(2):121–33.

226. Yamane K, Leung KP. Rabbit M1 and M2 macrophages can be induced by human recombinant GM-CSF and M-CSF. FEBS Open Bio. 2016;6(9):945-53.

227. Lu X, Li N, zhao L, Guo D, Yi H, Yang L, et al. Human umbilical cord mesenchymal stem cells alleviate ongoing autoimmune dacryoadenitis in rabbits via polarizing macrophages into an anti-inflammatory phenotype. Exp Eye Res. 2020;191:107905.

228. Braza F, Dirou S, Forest V, Sauzeau V, Hassoun D, Chesné J, et al. Mesenchymal Stem Cells Induce Suppressive Macrophages Through Phagocytosis in a Mouse Model of Asthma. Stem Cells. 2016;34(7):1836–45.

229. Mao F, Wu Y, Tang X, Wang J, Pan Z, Zhang P, et al. Human umbilical cord mesenchymal stem cells alleviate inflammatory bowel disease through the regulation of 15-LOX-1 in macrophages. Biotechnol Lett. 2017;39(6).

230. Wang Y, Viollet B, Terkeltaub R, Liu-Bryan R. AMP-activated protein kinase suppresses urate crystal-induced inflammation and transduces colchicine effects in macrophages. Ann Rheum Dis. 2016;75(1):286–94.

231. Dalbeth N, Lauterio TJ, Wolfe HR. Mechanism of action of colchicine in the treatment of gout. Clin Ther. 2014;36(10):1465-79.

232. Eggenhofer E, Luk F, Dahlke MH, Hoogduijn MJ. The life and fate of mesenchymal stem cells. Front Immunol. 2014;5:148.

233. Porta C, Rimoldi M, Raes G, Brys L, Ghezzi P, Di Liberto D, et al. Tolerance and M2 (alternative) macrophage polarization are related processes orchestrated by p50 nuclear factor κB. Proc Natl Acad Sci U S A. 2009;106(35):14978–83.

234. Miteva K, Pappritz K, Sosnowski M, El-Shafeey M, Müller I, Dong F, et al. Mesenchymal stromal cells inhibit NLRP3 inflammasome activation in a model of Coxsackievirus B3-induced inflammatory cardiomyopathy. Sci Rep. 2018;8(1).

235. Shin T-H, Kim H-S, Kang T-W, Lee B-C, Lee H-Y, Kim Y-J, et al. Human umbilical cord blood-stem cells direct macrophage polarization and block inflammasome activation to alleviate rheumatoid arthritis. Cell Death Dis. 2016;7(12):e2524.

236. Sokolowska M, Chen L-Y, Liu Y, Martinez-Anton A, Qi H-Y, Logun C, et al. Prostaglandin E2 Inhibits NLRP3 Inflammasome Activation through EP4 Receptor and Intracellular Cyclic AMP in Human Macrophages. J Immunol. 2015;194(11):5472–87.

237. Vasandan AB, Jahnavi S, Shashank C, Prasad P, Kumar A, Jyothi Prasanna S. Human Mesenchymal stem cells program macrophage plasticity by altering their metabolic status via a PGE 2 -dependent mechanism. Sci Rep. 2016; 6:38308.

APPENDIX

APPENDIX

LIST OF PUBLICATIONS ARISING FROM THIS THESIS

- Naredo Esperanza, **Medina Juan Pablo**, Pérez-Baos Sandra, Mediero Aranzazu, Herrero-Beaumont Gabriel, Largo Raquel. *Validation of Musculoskeletal Ultrasound in the Assessment of Experimental Gout Synovitis*. Ultrasound Med Biol. 2018 Jul;44(7):1516–24.

- **Medina Juan Pablo,** Pérez-Baos Sandra, Bermejo-Álvarez Ismael, Yáñez Rosa, Fernández-García María, García-Olmo Damián, Bueren Juan, Herrero-Beaumont Gabriel, Largo Raquel. *Parenteral Injection Of Human Adipose-Derived Mesenchymal stromal cells Shortens An Experimental Acute Gouty Arthritis Inactivating NLRP3 Inflamasome.* Arthritis & Rheumatology (in preparation).

OTHER PUBLICATIONS

- Gratal Paula, Lamuedra Ana, **Medina Juan Pablo**, Bermejo-Álvarez Ismael, Largo Raquel, Herrero-Beaumont Gabriel, Mediero Aranzazu. *Purinergic System Signaling in Metainflammation-Associated Osteoarthritis*. Front Med (Lausanne). 2020 Aug 28;7:506

Ultrasound in Med. & Biol., Vol. ■■, No. ■■, pp. ■■–■■, 2018

0301-5629/$ - see front matter

https://doi.org/10.1016/j.ultrasmedbio.2018.03.018

● *Original Contribution*

VALIDATION OF MUSCULOSKELETAL ULTRASOUND IN THE ASSESSMENT OF EXPERIMENTAL GOUT SYNOVITIS

Esperanza Naredo, Juan Pablo Medina, Sandra Pérez-Baos, Aranzazu Mediero, Gabriel Herrero-Beaumont, and Raquel Largo

Bone and Joint Research Unit, Department of Rheumatology, Hospital Universitario Fundación Jiménez Díaz, IIS-Fundación Jiménez Díaz UAM, Madrid, Spain

(*Received* 11 *January* 2018; *revised* 20 *March* 2018; *in final form* 21 *March* 2018)

Abstract—The objective of this study was to validate musculoskeletal ultrasound (US) in a rabbit model of acute gout. Acute gout was induced by intra-articular injection of monosodium urate (MSU) crystals in 10 rabbits; the 3 controls received vehicle. Rabbit knees were assessed by B-mode and power Doppler (PD) US 24 and 72 h after injections. After 72 h, all rabbits were euthanized. US discriminated between the MSU-injected and control groups with respect to the different inflammatory findings at both at 24 and 72 h and for MSU crystal-related findings after 24 h of injection. US synovial thickening, intra-synovial power Doppler signal and global joint distension significantly correlated with the synovial global histopathological score ($r = 0.47$, $p = 0.0188$), tissue vascularization measured by CD31 immunohistochemical-positive staining ($r = 0.46$, $p = 0.0172$) and tissue levels of interleukin-1β ($r = 0.53$, $p = 0.0078$), respectively. US is a valid method for assessment of synovial inflammation in experimental gouty arthritis in rabbits. (E-mail: gherrero@fjd.es)

Key Words: **Musculoskeletal ultrasound, Animal model, Experimental gout, Gout, Synovial inflammation, Synovial vascularization, Monosodium urate crystals.**

INTRODUCTION

Musculoskeletal ultrasound (MSKUS) has become an accurate imaging tool in rheumatic diseases (Keen et al. 2014). In gout, MSKUS is increasingly used as a diagnostic tool (Filippucci et al. 2009; Grassi et al. 2006; Naredo et al. 2014; Neogi et al. 2015; Ogdie et al. 2017; Ottaviani et al. 2012; Thiele and Schlesinger 2007; Wright et al. 2007), based on its proven capability to detect monosodium urate (MSU) crystal deposits in joints (*i.e.,* double-contour sign in the articular cartilage or intra- and periarticular tophi) compared with microscopic identification of MSU crystal in aspirated synovial fluid or tophi (Naredo et al. 2014; Perez-Ruiz et al. 2007). In addition, the presence of MSKUS-detected joint inflammation (*i.e.,* joint effusion, synovial thickening and synovial Doppler signal) has been widely described in human gout, both in chronic arthritis and in acute episodes of arthritis (Grassi et al. 2006; Stewart et al. 2017; Thiele and Schlesinger 2007).

Animal models provide essential information on the pathogenesis of joint diseases, as well as a research setting for testing potential therapeutic agents. Animal models of gout are induced mainly by MSU injection because of the difficulty of inducing chronic hyperuricemia associated with increased synthesis (Schett et al. 2015). Acute gout models have a rapid resolution, within days, hampering the analysis of gout pathophysiology and therapeutic response (Schett et al. 2015). A non-invasive technique such as MSKUS would more easily allow *in vivo* sequential analysis. Despite its potential for assessing synovial inflammation, the validity of MSKUS has been only scarcely investigated in animal models of joint inflammation, including gout (Bouta et al. 2015; Chen et al. 2016; Clavel et al. 2008; Pineda et al. 2015).

The objective of this experimental study was to determine whether MSKUS features can be used as an outcome measure in rabbit gouty arthritis for the evaluation of synovial inflammation. MSKUS features were compared with clinical, histologic and molecular standard measurements of tissue inflammation.

Address correspondence to: Gabriel Herrero-Beaumont, Bone and Joint Research Unit, IIS-Fundacion Jimenez Diaz UAM, Av. Reyes Católicos, 2, 28040 Madrid, Spain. E-mail: gherrero@fjd.es

Conflicts of Interest: All authors declare no competing interests with the topic.

METHODS

Experimental model

Thirteen white adult male New Zealand rabbits weighing 3 to 3.5 kg (Granja San Bernardo, Navarra, Spain) were used for the experimental procedures. Animal handling and experimentation were performed in accordance with national regulations and the *Guidelines for the Care and Use of Laboratory Animals* drawn up by the National Institutes of Health (Bethesda, MD, USA). The experimental protocol was approved by the institutional ethics committee.

The experimental model was induced as previously described with minor modifications (Miguélez et al. 1996). In brief, after 1 wk of adaptation to our facilities, 10 rabbits received an intra-articular injections of 1 mL of MSU crystals (50 mg/mL) into both knees (MSU group), and 3 rabbits received 1 mL of phosphate-buffered saline (as vehicle, control group). Ten rabbits (20 knees) were included in the MSU group, to diminish possible differences in the crystal injection response among different knees, based on recently published data in which ultrasound was found to have a great capacity to discriminate between MSU-injected and control knees with respect to features of MSU crystal deposition and synovial inflammation (Pineda et al. 2015). To minimize the number of animals employed, 3 rabbits (6 knees) were included to assess healthy rabbits, because of the more homogeneous features observed in these rabbits than in the MSU-injected rabbits. The degree of joint swelling was determined 24 and 72 h after injections by measuring knee perimeter with a digital caliper. All animals were euthanized 72 h after intra-articular injections with an overdose of pentobarbital (Braun Medical SA, Barcelona, Spain). Rabbit knees were dissected, and infrapatellar synovial membranes were cut into two pieces: one was fixed in 4% buffered paraformaldehyde, dehydrated and embedded in paraffin for histologic evaluation; the other was immediately frozen and employed for protein extraction studies (López-Armada et al. 2002).

MSKUS assessment

Rabbits underwent B-mode and power Doppler (PD) US assessment of both knees at two times, 24 and 72 h after injections, by a rheumatologist highly experienced in MSKUS who was blinded to the injection type and clinical data. All US examinations were carried out with a commercially available real-time scanner (LOGIQ e R7, GE Medical Systems, Jiangsu, China) equipped with a 22-MHz linear transducer.

B-Mode and PD machine settings were optimized before the study and standardized for the whole study as follows: B-mode gain of 47 dB, dynamic range of 72 dB, Doppler frequency of 14.3 MHz, Doppler gain of 28 dB, low-wall filters and pulse repetition frequency of 700 Hz.

After being anesthetized, rabbits were placed in the supine position with their knees flexed 10° to 20°. The US assessment consisted of systematic longitudinal and transverse B-mode and PD examination of the suprapatellar, lateral and medial recesses of the knee joint. Given its more superficial anatomic location, we selected the lateral recess for scoring MSKUS findings.

The MSKUS inflammatory findings investigated were B-mode recess global distension (GD), synovial fluid (SF) and synovial thickening (STh) and intra-synovial PD signal (PD). We used the Outcome Measures in Rheumatology (OMERACT) US definition for synovitis components in inflammatory arthritis (Wakefield et al. 2005) modified as follows. SF was defined as hypo-echoic or anechoic material within the synovial recess that was displaceable by compression with the US probe. STh was defined as abnormal hypo-echoic thickening of the tissue located between the outer recess boundary and the synovial space that was not displaceable and poorly compressible by compression with the US probe. GD, SF, STh and PD were scored semi-quantitatively on a scale of 0–3 (*i.e.,* 0 = absence, 1 = mild, 2 = moderate; 3 = marked) as described elsewhere (D'Agostino et al. 2017; Szkudlarek et al. 2003). A score ≥2 was considered pathologic for GD and SF, and a score ≥1 was considered pathologic for STh and PD. STh and PD scores were correlated with synovial histopathological damage and synovial tissue vascularization.

The following MSKUS findings previously described in acute gout (Grassi et al. 2006) were also investigated as features of MSU crystal deposition within the lateral recess of the rabbit knees: (i) iso-echoic sand-like material (SM) floating in the synovial fluid and displaceable when compressed with the US probe; (ii) hyper-echoic aggregates (AG) within the sand-like material; and (iii) bright foci (BF) within the sand-like material.

Intra-observer reliability of the MSKUS assessment was evaluated by recording representative images from the examinations of all rabbit knees at 24 and 72 h. The stored images were scored for inflammatory and MSU crystal findings under blinded conditions by the same ultrasonographer investigator a minimum of 3 mo later.

Histologic assessment

Synovial histopathology was evaluated in hematoxylin and eosin (HE)-stained sections by two blinded observers, according to the Krenn scale, as previously described (Alvarez-Soria et al. 2006; Krenn et al. 2002; Prieto-Potín et al. 2013). Briefly, lining hyperplasia, fibrovascular alterations at the interstitium and tissue cell infiltration were independently evaluated using 0- to 3-point subscales, where 0 = absent, 1 = mild, 2 = intermediate and 3 = strong. The total score was the sum of partial grades with a maximum total score of 9 (Krenn et al. 2002).

Immunohistochemistry

In the synovial membrane, we identified vascular endothelial cells using a monoclonal anti-CD31 antibody (Abcam, Cambridge, UK), according to protocol (Prieto-Potín et al. 2013). The antibody was detected with a biotinylated goat anti-mouse IgG (1:200; Amersham, Arlington Heights, IL, USA) visualized with a horseradish peroxidase/avidin–biotin (AB) complex using 3,3-diaminobenzidine tetrahydrochloride as the chromogen (Dako, Camarillo, CA, USA). The tissues were counterstained with hematoxylin and mounted in DPX medium (VWR International, Leuven, Belgium). Synovium sample slides were scanned in the Coreo Iscan Au scanner (Ventana Medical Systems, Tucson, AZ, USA), and then total cells, CD31- positive cells and the entire sample area were assessed with Virtuoso Image management software (Ventana Medical Systems, Tucson, AZ, USA). The results were expressed as the ratio of CD31 positive cells to area in square millimeters (Prieto-Potín et al. 2013).

Western blot analysis

Synovial membranes were homogenized in liquid nitrogen, and total proteins were extracted employing an extraction buffer containing 15 mM HEPES ((4-(2-hydroxyethyl)-1-piperazineethanesulfonic acid), 10% glycerol, 0.5% Nonidet P-40, 250 mM NaCl, 1 mM ethylenediaminetetraacetic acid, 1:1000 phenylmethanesulfonyl fluoride and a protease inhibitor cocktail (Sigma-Aldrich, St. Louis, MO, USA). Protein concentration was determined as previously described (Alvarez-Soria et al. 2006; Prieto-Potín et al. 2013), and subsequently, 20 µg of total protein from each tissue was resolved on 15% acrylamide–sodium dodecyl sulfate gels. After transfer to polyvinylidene difluoride membranes (Millipore, Molsheim, France), membranes were blocked in 5% skimmed milk in phosphate-buffered saline–Tween 20 for 1 h at room temperature and incubated overnight at 4 °C with an anti-rabbit interleukin-1β (IL-1β) antibody (Cloud-Clone Corp, Houston TX, USA). Antibody binding was detected by enhanced chemoluminescence using peroxidase-labeled secondary antibodies, and the results were expressed as arbitrary densitometric units (AU). A loading control was performed on 15% acrylamide–sodium dodecyl sulfate gels by employing EZBlue gel staining reagent (Sigma-Aldrich).

Statistical analysis

Statistical analysis was performed using the GraphPad Prism package (Version 5.0 for Windows) and the SPSS package (Version 11.0 for Windows). Quantitative variables are presented as the mean ± standard deviation. Categorical variables are presented as absolute frequencies and percentages. To assess differences between healthy and injured knees, categorical variables were analyzed using Fisher's exact test**.** Differences in quantitative variables between healthy and injured knees were assessed with the Mann–Whitney *U*-test. Correlation between MSKUS and histopathological scores and clinical variables was analyzed with Spearman's correlation coefficient. p Values < 0.05 were considered to indicate significance.

Intra-observer reliability of MSKUS assessment was evaluated with weighted Cohen's κ for inflammatory findings and unweighted Cohen's κ for MSU crystal deposit features. κ values of 0–0.20 were considered poor, >0.20–0.40 fair, >0.40–0.60 moderate, >0.60–0.80 good and >0.80–1 excellent.

RESULTS

Joint perimeter measurement

Monosodium urate injection induced a significant increase in joint swelling. Knee perimeter was significantly greater in the MSU group than in controls at the two times studied: 24 h: 1.04 ± 0.71 vs. 0.35 ± 0.48 mm, $p = 0.011$; 72 h: 1.02 ± 0.60 vs. 0.44 ± 0.34, $p = 0.048$).

MSKUS features

Table 1 outlines the prevalence of each MSKUS pathologic finding defined as described under Methods at 24 and 72 h after intra-articular injections. MSKUS was able to discriminate between MSU and control groups with respect to the different inflammatory findings at both 24 and 72 h (Table 1). Representative images of MSKUS inflammatory and MSU crystal-related findings, as well as

Table 1. Prevalence and scores of MSKUS pathologic findings in MSU crystal-injected knees and control knees 24 and 72 hours after MSU injection

MSKUS feature	MSU frequency	Control frequency	MSU	Control
At 24 h				
GD	19 (95)*	0 (0)	2.5 ± 0.6*	1 ± 0
SF	19 (95)*	0 (0)	2.4 ± 0.6*	1 ± 0
STh	14 (70)*	0 (0)	1 ± 0.8*	0 ± 0
PD	11 (55)*	0 (0)	1.2 ± 1.3*	0 ± 0
SM	11 (55)*	0 (0)		
AG	7 (35)*	0 (0)		
BF	11 (55)*	0 (0)		
SM or AG or BF	15 (75)*	0 (0)		
At 72 h				
GD	19 (95)*	1 (16.67)	2.0 ± 0.7*	1.2 ± 0.4
SF	15 (75)*	1 (16.67)	2.0 ± 0.7*	1.2 ± 0.4
STh	12 (60)*	0 (0)	1.1 ± 0.8*	0 ± 0
PD	9 (45)*	0 (0)	1.0 ± 1.1	0 ± 0
SM	8 (40)	0 (0)		
AG	1 (5)	0 (0)		
BF	2 (10)	0 (0)		
SM or AG or BF	8 (40)	0 (0)		

MSKUS = musculoskeletal ultrasound; MSU = monosodium urate; GD = global distension; SF = synovial fluid; STh = synovial thickening; PD = synovial power Doppler signal; SM = sand-like material; AG = hyperechoic aggregates; BF = bright foci.

* $p < 0.05$ versus control group.

Values are expressed as the number (%) or mean ± standard deviation. n = 20 for MSU-injected knees. n = 6 for control knees.

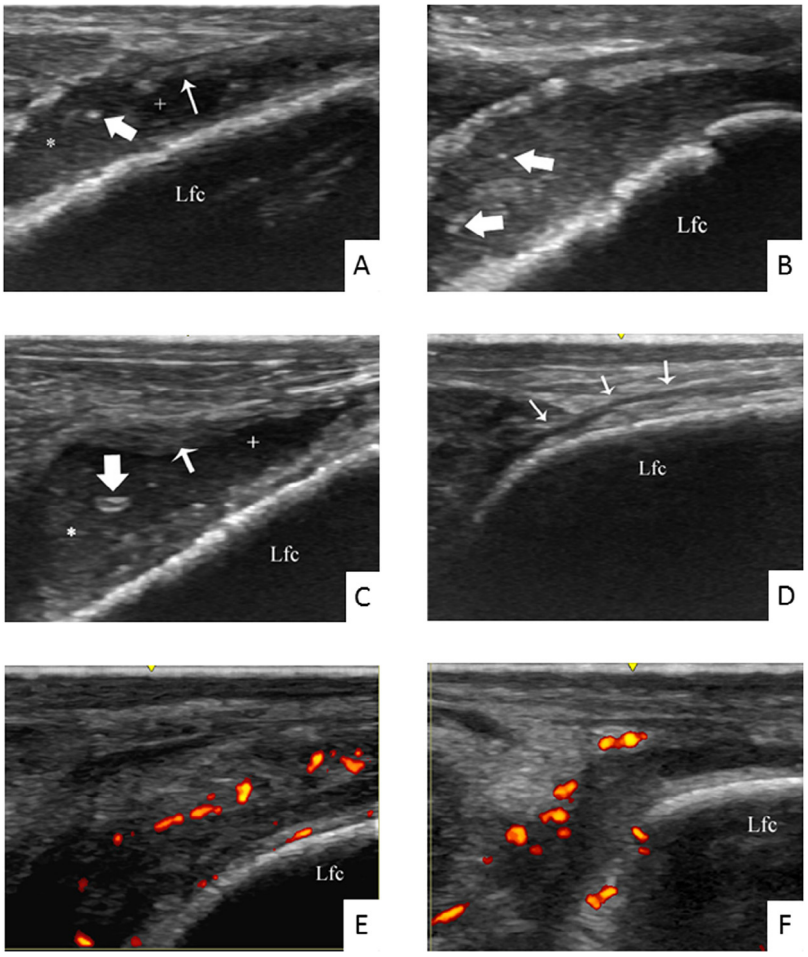

Fig. 1. Ultrasound images of the lateral recess of a monosodium urate crystal-injected rabbit knee (a) Increased synovial fluid (+), synovial thickening (*thin arrow*), sand-like material (*) and a bright focus (*thick arrow*). (b) Bright foci (*thick arrows*) inside sand-like material. (c) Increased synovial fluid (+), synovial thickening (*thin arrow*), sand-like material (*) and a hyperechoic aggregate (*thick arrow*). (d) Normal ultrasound image of the lateral recess of the rabbit knee (*arrows*). (e, f) Power Doppler-detected pathologic flow in the synovial tissue. Lfc = lateral femoral condyle.

a normal US image of the lateral recess of the rabbit knee, are provided in Figure 1a–1f. STh and PD signal were detected only in MSU-injected knees (Table 1), mostly in the outer boundary of the synovial cavity (Fig. 1e, 1f). MSU crystal-related findings were detected both 24 and 72 h after MSU injection (Fig. 1a–c). However, MSKUS discriminated MSU crystal-related findings only at 24 h after intraarticular injections (Table 1). Nineteen of 20 MSU knees exhibited inflammatory features at both time points, whereas 15 of these 20 knees exhibited any MSU crystal-related finding at 24 h. MSKUS assessment was able to detect a clear decrease in the presence of MSU crystal-related findings between 24 and 72 h in the MSU group.

Table 1 also lists MSKUS scores of the inflammatory findings for the MSU and control groups at 24 and 72 h. MSKUS was able to indicate significant differences in the inflammatory scores between both groups at both time points.

Table 2 outlines the ability of MSKUS to discriminate between inflammatory feature scores at 24 and 72 h for each experimental group. MSKUS was able to detect a significant improvement in GD and SF scores between 24 and 72 h in the MSU group, reflecting the expected auto-limited inflammatory reaction described in this experimental model. However, STh and PD did not significantly change between 24 and 72 h.

Intra-observer concordance was excellent for most of the MSKUS findings and good for some of these findings. κ values for the MSKUS assessment at 24 were 0.82 for GD, 0.81 for SF, 0.82 for STh, 0.84 for PD, 0.92 for SM, 1 for AG and 0.92 for BF. κ values for the MSKUS assessment at 72 h were 0.62 for GD, 0.62 for SF, 1 for STh, 0.96 for PD, 1 for SM and 1 for AG. The κ value for BF at 72 h was not obtained because this finding was not detected in any rabbit knee in the two readings.

Table 2. Comparison of MSKUS scores of the inflammation findings between 24 and 72 h in the MSU crystal-injected and control groups

	MSKUS score (mean ± standard deviation)	
MSKUS feature	24 h	72 h
MSU-injected (n = 20)		
GD	2.5 ± 0.6*	2.0 ± 0.7
SF	2.4 ± 0.6*	2.0 ± 0.7
STh	1.0 ± 0.8	1.0 ± 0.8
PD	1.2 ± 1.3	1.0 ± 1.1
Control (n = 6)		
GD	1 ± 0	1.2 ± 0.4
SF	1 ± 0	1.2 ± 0.4
STh	0 ± 0	0 ± 0
PD	0 ± 0	0 ± 0

MSKUS = musculoskeletal ultrasound; MSU = monosodium urate; GD = global distension; SF = synovial fluid; STh = synovial thickening; PD = synovial power Doppler signal.

* $p < 0.05$ versus 72 h.

Correlation between joint swelling and MSKUS features

The increase in knee perimeter significantly correlated with the GD score measured 24 h after intra-articular injections (Spearman's correlation coefficient $r = 0.60$, $p = 0.0019$) (Fig. 2a). However, this correlation was not statistically significant 72 h after the injections (Spearman's correlation coefficient $r = 0.03$, $p = 0.9005$) (Fig. 2b).

Synovial histopathology and its correlation with MSKUS features

The synovial membrane of MSU rabbits exhibited increased lining hyperplasia, stromal alterations and a greater presence of infiltrating cells, in comparison to control samples (Fig. 3a, 3b). Thus, the synovitis score was significantly increased in the MSU group in comparison to control (Fig. 3c). The MSKUS STh score was statistically significantly correlated with the synovitis histopathological score, with a Spearman's correlation coefficient $r = 0.47$ ($p = 0.0188$) (Fig. 3d).

Tissue vascularization and its correlation with PD signal

The presence of vessels in the synovial tissue was studied by immunohistochemical studies employing CD31 staining. As expected, in the MSU group, synovial membranes exhibited an increased presence of vessels in the lining and in the sublining, in comparison to controls (Fig. 4a, 4b). Quantification of CD31-positive staining revealed a significant increase in this marker in the MSU group (Fig. 4c). Furthermore, there was a significant correlation between intra-synovial PD signal after 72 h of MSU injection and CD31-positive staining ($r = 0.46$, $p = 0.0172$) (Fig. 4d).

Synovial IL-1β concentration and its correlation with MSKUS features

As expected, the presence of the pro-inflammatory cytokine IL-1β was significantly greater in MSU samples than in control samples (Fig. 5a). Interestingly, IL-1β synthesis significantly correlated with MSKUS GD score (Fig. 5b).

DISCUSSION AND CONCLUSIONS

Musculoskeletal US was able to identify and quantify inflammatory findings and monosodium urate crystal features in the knee of a rabbit model of gout. MSKUS measurements correlated with histologic inflammation and vascularization of the synovium and molecular markers of inflammation in an experimental model of gout in rabbits. Our results encourage the use of MSKUS as a potential endpoint in pre-clinical studies on the efficacy of systemic and local interventions for the treatment of gout.

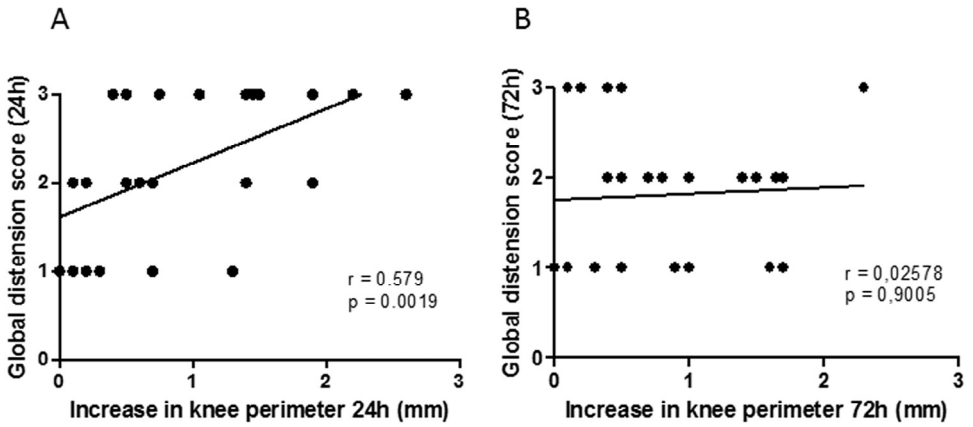

Fig. 2. Correlation of global distension measured by musculoskeletal ultrasound with the increase in knee perimeter, 24 h (a) and 72 h (b) after monosodium urate injections. Global distension was measured as described under Methods.

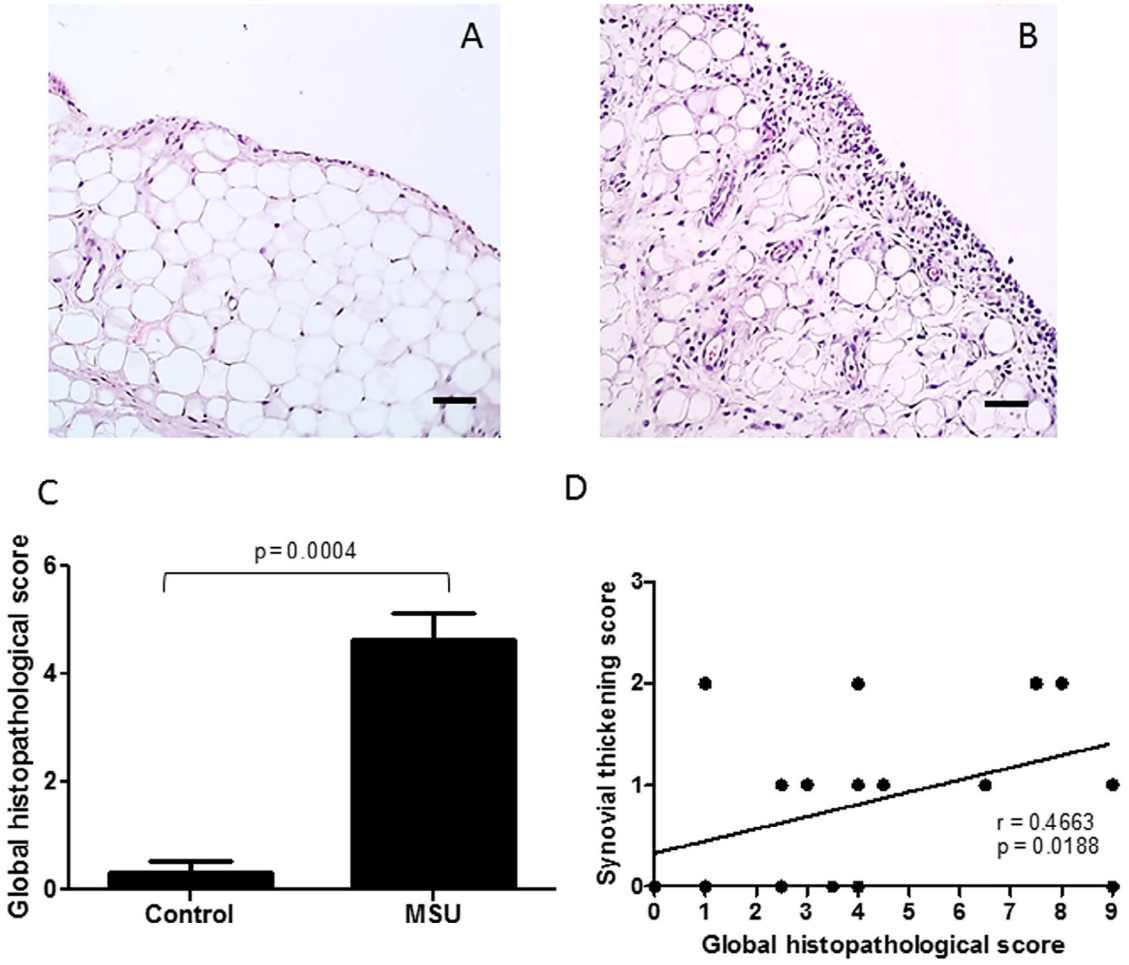

Fig. 3. Histopathological features of the synovial membranes. (a, b) Representative sections of synovial membranes stained with hematoxylin and eosin from control rabbit (A) and MSU-injected rabbit (B) 72 h after the intra-articular injection. Bars = 50 μm. In (b), note the proliferation of the lining layer, accumulation of infiltrating cells and alterations in synovial stroma. (c) Bars indicate synovium histopathological scores measured as described under Methods for control and MSU-injected knees and expressed as the mean and standard error of the mean. (d) Correlation between musculoskeletal synovial thickening and the global histopathological score measured as described under Methods. n = 19–20 for MSU. n = 6 for controls. MSU = monosodium urate.

Experimental gout models are widely used in pre-clinical studies (Miguélez et al. 1996). Although experimental gout is essentially different from human gout, primary pathologic features such as intra-articular MSU crystal deposition and synovial inflammation are present in both. Our study determined the performance and reproducibility of a commercially available portable US device in discriminating MSU crystal-injected knees from control knees with respect to inflammatory findings and MSU crystal features in a rabbit model of gout. In addition, MSKUS detected an improvement in MSU crystal-related findings between the time points, which supports its sensitivity to change in experimental gout.

Above all, our study found that MSKUS imaging measurements correlate with joint swelling, histologic inflammation and vascularization of the synovium in an experimental model of gout in rabbits. Furthermore, GD measured by MSKUS correlated with the level of IL-1β, a pro-inflammatory cytokine involved in the pathogenesis of gout.

Although MSKUS has been reported to detect different pathologic findings in human and experimental gout (Filippucci et al. 2009; Grassi et al. 2006; Naredo et al. 2014; Neogi et al. 2015; Ogdie et al. 2017; Ottaviani et al. 2012; Pineda et al. 2015; Stewart et al. 2017; Thiele and Schlesinger 2007; Wright et al. 2007), the correlation between the semi-quantitative B-mode and PD evaluation of synovial histologic alterations and markers of tissue inflammation has not been studied.

In this study, we found that GD correlated with joint perimeter increase measured 24 h after intra-articular injection, a measurement of joint swelling similar to that

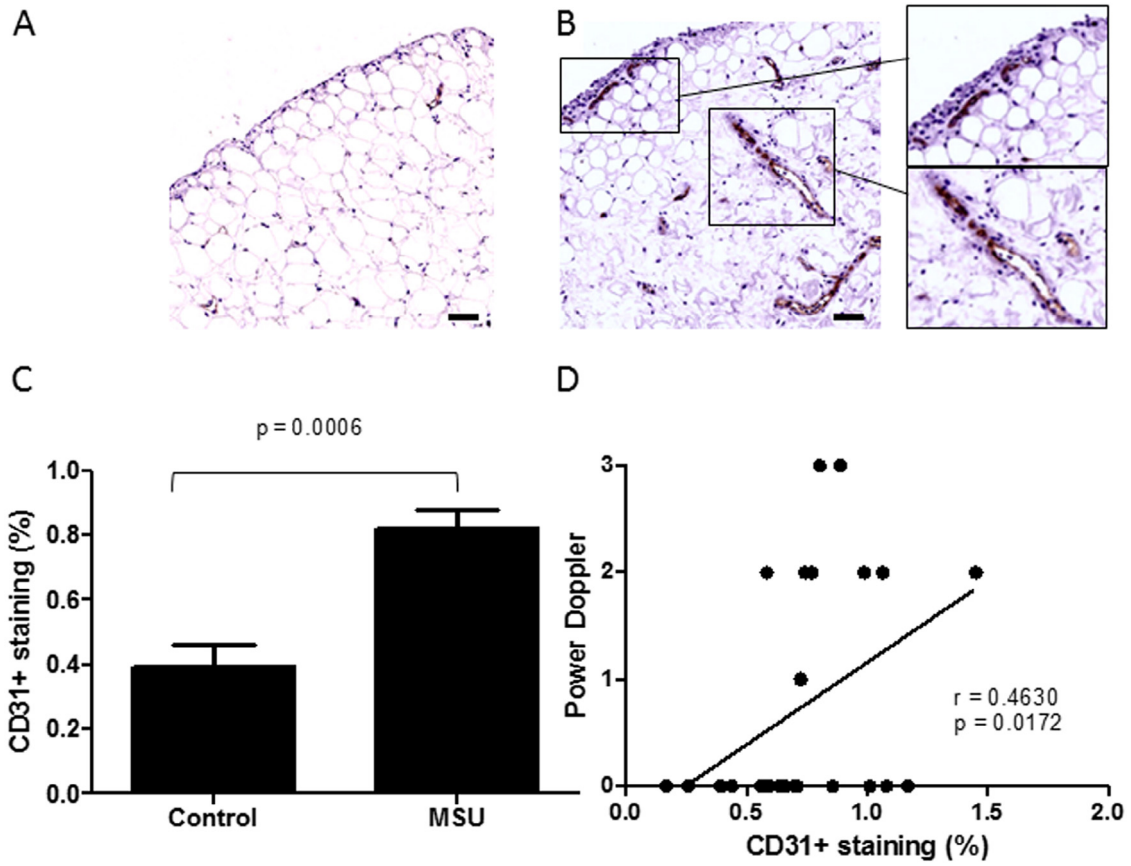

Fig. 4. (a, b) Representative sections of immunohistochemical staining of CD31 in the synovial membrane of control (a) and monosodium urate-injected (b) knees. Bar = 100 µm. (c) Semi-quantification of CD31-positive vascularization in the synovium of each group of animals. Bars represent the mean and standard error of the mean (n = 7 to 9 rabbits per group). (d) Correlation between the percentage of CD31-positive staining and power Doppler signal in the synovial membrane of rabbits 72 h after the intra-articular injections. n = 19 or 20 for MSU. n = 6 for controls.

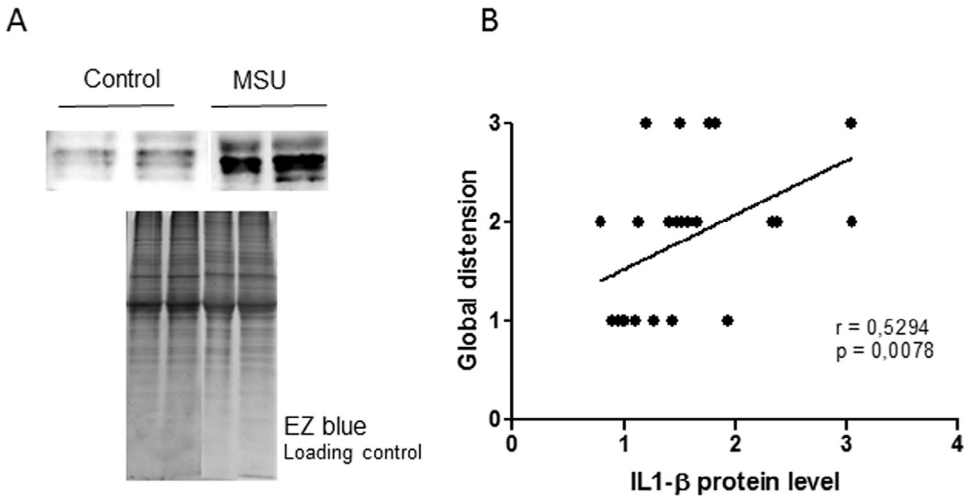

Fig. 5. (a) Representative Western blot of IL-1β protein levels expressed in the synovial membrane of the rabbits in each group. EZ blue staining was used as the protein loading control. (b) Correlation between global distension measured by musculoskeletal ultrasound and IL-1β protein synthesis in the synovial membrane measured by Western blot studies. n = 20 for monosodium urate and n = 6 for controls.

observed in gouty patients, which allows the study of disease progression and response to treatment. However, this correlation was lost 72 h after injections, by which time joint swelling was partially diminished in this model of spontaneous resolution. Joint perimeter measurement reflects not only intra-articular but also peri-articular inflammation, both expected in acute gout, whereas we measured only joint recess distension (*i.e.,* intra-articular inflammation) with US. Is it possible that peri-articular swelling improves earlier than intra-articular inflammation. The use of a semi-quantitative score for GD versus a continuous variable for the knee perimeter can also explain that the sensitivity to change was apparently greater for the perimeter measurement.

We also found that STh score evaluated by MSKUS exhibited a good correlation with the global synovitis score, which was evaluated after 72 h of MSU injection. Therefore, MSKUS evaluation was sensitive enough to detect inflammatory changes compared with a simple physical examination of joint swelling. The correlation between MSKUS score and the corresponding histopathological scores was consistent with those reported in animal models of rheumatoid arthritis (Chen et al. 2016; Clavel et al. 2008).

Synovial thickening assessed by US comprises a number of synovial tissue elements, such as synovial lining cells, infiltrating cells, interstitial fluid, subintimal connective and fibrotic tissue and vascular tissue. All these elements are evaluated in the histopathological Krenn score that was employed for synovitis scoring (Krenn et al. 2002). Synovial cell proliferation, subintimal architecture destruction and circulating cell infiltration are key events in inflammatory arthritis. Matrix metalloproteinases synthesized by these cells are responsible for cartilage degradation and bone erosions (Villalvilla et al. 2014). Therefore, MSKUS evaluation of inflammatory tissue could be an important element in the assessment of disease activity in experimental gouty arthritis. However, a different synovial localization was evaluated in MSKUS imaging and histopathological studies, as described under Methods. Therefore, our results indicate that synovial inflammation would have similar characteristics in both localizations explored in this experimental model of gout.

Furthermore, our data indicated that synovial vascular density can be accurately evaluated by PD US in this model of gout, allowing *in vivo* follow-up in this design. CD31 is an endothelial cell marker, and thus an indicator of tissue vascularization, in relation to synovial inflammation. Synovial PD quantification has been also reported to correlate with pro-angiogenic gene expression profile in this tissue in early patients with early rheumatoid arthritis (Kelly et al. 2015).

The main weaknesses of our study are the relatively small number of rabbit knees and the failure to perform histopathological evaluation at 24 h because of the limited sample size. However, this was a pilot study on the applicability of MSKUS in an experimental model of gout. In addition, our results cannot be directly extrapolated to clinical studies as the time courses of US and histologic synovial inflammation could differ; that is, clinical gout exhibits greater variability than experimental models. In this sense, further research is warranted. Nevertheless, our main purpose was to validate MSKUS for pre-clinical intervention studies.

Acknowledgments—This study was supported by research grants from the Instituto de Salud Carlos III (PIE15/00048; PI15/00770; PI15/00340; PI16/00065, PI16/00991; CP15/00053), co-funded by Fondo Europeo de Desarrollo Regional (FEDER).

REFERENCES

Alvarez-Soria MA, Largo R, Santillana J, Sánchez-Pernaute O, Calvo E, Hernández M, Egido J, Herrero-Beaumont G. Long term NSAID treatment inhibits COX-2 synthesis in the knee synovial membrane of patients with osteoarthritis: Differential proinflammatory cytokine profile between celecoxib and aceclofenac. Ann Rheum Dis 2006; 65:998–1005.

Bouta EM, Banik PD, Wood RW, Rahimi H, Ritchlin CT, Thiele RG, Schwarz EM. Validation of power Doppler versus contrast enhanced magnetic resonance imaging quantification of joint inflammation in murine inflammatory arthritis. J Bone Min Res 2015; 30:690–694.

Chen S, Zheng Q, Liu H, Zeng J, Ye Z, Su Y, Lv G. Sonography is superior to serum-based biomarkers for measuring disease status in experimental rheumatoid arthritis. J Ultrasound Med 2016;35:2223–2230.

Clavel G, Marchiol-Fournigault C, Renault G, Boissier MC, Fradelizi D, Bessis N. Ultrasound and Doppler micro-imaging in a model of rheumatoid arthritis in mice. Ann Rheum Dis 2008;67:1765–1772.

D'Agostino MA, Terslev L, Aegerter P, Backhaus M, Balint P, Bruyn GA, Filippucci E, Grassi W, Iagnocco A, Jousse-Joulin S, Kane D, Naredo E, Schmidt W, Szkudlarek M, Conaghan PG, Wakefield RJ. Scoring ultrasound synovitis in rheumatoid arthritis: A EULAR-OMERACT Ultrasound Taskforce: Part 1. Definition and development of a standardized, consensus-based scoring system. RMD Open 2017; 3:e000428.

Filippucci E, Riveros MG, Georgescu D, Salaffi F, Grassi W. Hyaline cartilage involvement in patients with gout and calcium pyrophosphate deposition disease: An ultrasound study. Osteoarthritis Cartilage 2009;17:178–181.

Grassi W, Meenagh G, Pascual E, Filippucci E. Crystal clear"-sonographic assessment of gout and calcium pyrophosphate deposition disease. Semin Arthritis Rheum 2006;36:197–202.

Keen HI, Wakefield R, Conaghan PG. Optimising ultrasonography in rheumatology. Clin Exp Rheumatol 2014;32(5, Suppl 85):S13–S16.

Kelly S, Bombardieri M, Humby F, Ng N, Marrelli A, Riahi S, DiCicco M, Mahto A, Zou L, Pyne D, Hands RE, Pitzalis C. Angiogenic gene expression and vascular density are reflected in ultrasonographic features of synovitis in early rheumatoid arthritis: An observational study. Arthritis Res Ther 2015;17:58.

Krenn V, Morawietz L, Häupl T, Neidel J, Petersen I, König A. Grading of chronic synovitis—A histopathological grading system for molecular and diagnostic pathology. Pathol Res Pract 2002;198:317–325.

López-Armada MJ, Sánchez-Pernaute O, Largo R, Diez-Ortego I, Palacios I, Egido J, Herrero-Beaumont G. Modulation of cell recruitment by anti-inflammatory agents in antigen-induced arthritis. Ann Rheum Dis 2002;61:1027–1030.

Miguélez R, Palacios I, Navarro F, Gutierrez S, Sanchez-Pernaute O, Egido J, González E, Herrero-Beaumont G. Anti-inflammatory effect of a PAF receptor antagonist and a new molecule with antiproteinase activity in an experimental model of acute urate crystal arthritis. J Lipid Mediat Cell Signal 1996;13:35–49.

Naredo E, Uson J, Jiménez-Palop M, Martínez A, Vicente E, Brito E, Rodríguez A, Cornejo FJ, Castañeda S, Martínez MJ, Sanz J, Möller I, Batlle-Gualda E, Garrido J, Pascual E. Ultrasound-detected musculoskeletal urate crystal deposition: Which joints and what findings should be assessed for diagnosing gout? Ann Rheum Dis 2014;73:1522–1528.

Neogi T, Jansen TL, Dalbeth N, Fransen J, Schumacher HR, Berendsen D, Brown M, Choi H, Edwards NL, Janssens HJ, Lioté F, Naden RP, Nuki G, Ogdie A, Perez-Ruiz F, Saag K, Singh JA, Sundy JS, Tausche AK, Vazquez-Mellado J, Yarows SA, Taylor WJ. 2015 Gout classification criteria: An American College of Rheumatology/European League Against Rheumatism collaborative initiative. Ann Rheum Dis 2015;74:1789–1798.

Ogdie A, Taylor WJ, Neogi T, Fransen J, Jansen TL, Schumacher HR, Louthrenoo W, Vazquez-Mellado J, Eliseev M, McCarthy G, Stamp LK, Perez-Ruiz F, Sivera F, Ea HK, Gerritsen M, Cagnotto G, Cavagna L, Lin C, Chou YY, Tausche AK, Lima Gomes Ochtrop M, Janssen M, Chen JH, Slot O, Lazovskis J, White D, Cimmino MA, Uhlig T, Dalbeth N. Performance of ultrasound in the diagnosis of gout in a multicenter study: Comparison with monosodium urate monohydrate crystal analysis as the gold standard. Arthritis Rheumatol 2017;69:429–438.

Ottaviani S, Richette P, Allard A, Ora J, Bardin T. Ultrasonography in gout: A case–control study. Clin Exp Rheumatol 2012;30:499–504.

Perez-Ruiz F, Martin I, Canteli B. Ultrasonographic measurement of tophi as an outcome measure for chronic gout. J Rheumatol 2007;34:1888–1893.

Pineda C, Fuentes-Gómez AJ, Hernández-Díaz C, Zamudio-Cuevas Y, Fernández-Torres J, López-Macay A, Alba-Sánchez I, Camacho-Galindo J, Ventura L, Gómez-Quiróz LE, Gutiérrez-Ruíz MC, García-Vázquez F, Reginato AM, Gutiérrez M, López-Reyes A. Animal model of acute gout reproduces the inflammatory and ultrasonographic joint changes of human gout. Arthritis Res Ther 2015;17:37.

Prieto-Potín I, Roman-Blas J, Martínez-Calatrava M, Gómez R, Largo R, Herrero-Beaumont G. Hypercholesterolemia boosts joint destruction in chronic arthritis: An experimental model aggravated by foam macrophage infiltration. Arthritis Res Ther 2013;15:R81.

Schett G, Schauer C, Hoffmann M, Herrmann M. Why does the gout attack stop? A roadmap for the immune pathogenesis of gout. RMD Open 2015;1(Suppl 1):e000046.

Stewart S, Dalbeth N, Vandal AC, Allen B, Miranda R, Rome K. Ultrasound features of the first metatarsophalangeal joint in gout and asymptomatic hyperuricemia: Comparison with normouricemic individuals. Arthritis Care Res (Hoboken) 2017;69:875–883.

Szkudlarek M, Court-Payen M, Jacobsen S, Klarlund M, Thomsen HS, Østergaard M. Interobserver agreement in ultrasonography of the finger and toe joints in rheumatoid arthritis. Arthritis Rheum 2003;48:955–962.

Thiele RG, Schlesinger N. Diagnosis of gout by ultrasound. Rheumatology 2007;46:1116–1121.

Villalvilla A, Gomez R, Roman-Blas JA, Largo R, Herrero-Beaumont G. SDF-1 signaling: A promising target in rheumatic diseases. Expert Opin Ther Targets 2014;18:1077–1087.

Wakefield RJ, Balint PV, Szkudlarek M, Filippucci E, Backhaus M, D'Agostino MA, Sanchez EN, Iagnocco A, Schmidt WA, Bruyn GA, Kane D, O'Connor PJ, Manger B, Joshua F, Koski J, Grassi W, Lassere MN, Swen N, Kainberger F, Klauser A, Ostergaard M, Brown AK, Machold KP, Conaghan PG. OMERACT 7 Special Interest Group. Musculoskeletal ultrasound including definitions for ultrasonographic pathology. J Rheumatol 2005;32:2485–2487.

Wright SA, Filippucci E, McVeigh C, Grey A, McCarron M, Grassi W, Wright GD, Taggart AJ. High-resolution ultrasonography of the first metatarsal phalangeal joint in gout: A controlled study. Ann Rheum Dis 2007;66:859–864.

Parenteral Injection Of Human Adipose-Derived Mesenchymal Stem Cells Shortens An Experimental Acute Gouty Arthritis Inactivating NLRP3 Inflammasome.

Medina Juan Pablo [1], Pérez-Baos Sandra [1,2,5], Bermejo-Álvarez Ismael [1,5], Yáñez Rosa [3], Fernández-García María [3], García-Olmo Damián [4], Bueren Juan [3], Herrero-Beaumont Gabriel [1], Largo Raquel [1]

[1] Bone and Joint Research Unit, Rheumatology Dept, IIS-Fundación Jiménez Díaz UAM, Madrid, Spain
[2] Present Address: Department of Microbiology, NYU School of Medicine, New York, NY 10016, USA
[3] Hematopoietic Innovative Therapies Division. Centro de Investigaciones Energéticas, Medioambientales y Tecnológicas (CIEMAT) and Centro de Investigación Biomédica en Red de Enfermedades Raras (CIBER-ER), Madrid, Spain.
IIS- Fundación Jiménez Díaz UAM, Madrid, Spain
[4] New Therapies Laboratory, IIS-Fundación Jiménez Díaz UAM, Avda. Reyes Católicos, 2, 28040, Madrid, Spain.
Department of Surgery, Fundación Jiménez Díaz University Hospital, Avda. Reyes Católicos, 2, 28040, Madrid, Spain.
Department of Surgery, School of Medicine UAM, C/Arzobispo Morcillo s/n, 28034, Madrid, Spain.
[5] These authors contributed equally to this work

Correspondence to:

Prof. Gabriel Herrero-Beaumont,
Bone and Joint Research Unit,
IIS-Fundacion Jimenez Diaz UAM,
Reyes Católicos, 2, 28040 Madrid, Spain.
E-mail: gherrero@fjd.es
Phone +34 915 504 978
Conflicts of Interest: All authors declare no competing interests with the topic.

Juan Pablo Medina, MSc, jpablo.medina@quironsalud.es
Sandra Pérez-Baos, PhD, sandra.perezbaos@nyulangone.org
Ismael Bermejo Álvarez, MSc, ismael.bermejo@quironsalud.es
Rosa María Yáñez, PhD, rosamaria.yanez@ciemat.es
María Fernández García, PhD, maria.fernandez@ciemat.es
Juan Antonio Bueren, PhD, juan.bueren@ciemat.es
Damián García-Olmo, MD, PhD, damian.garcia@uam.es
Gabriel Herrero-Beaumont, MD, PhD, gherrero@fjd.es
Raquel Largo, PhD, rlargo@fjd.es

Acknowledgments—This study was supported by research grants from the Instituto de Salud Carlos III (PIE15/00048; PI15/00770; PI16/00065; PI18/00261), co-funded by Fondo Europeo de Desarrollo Regional (FEDER).

ABSTRACT

Objective. The specific effect of Adipose-Derived Mesenchymal Stem Cells (Ad-MSCs) on acute joint inflammation, where the response mostly depends on innate immunity activation, remains elusive. The pathogenesis of gouty arthritis, characterized by the deposition of monosodium urate (MSU) crystals in the joints, associated to acute flares, has been associated to NLRP3 inflammasome activation and subsequent amplification of the inflammatory response. Our aim was to study the effect of human Ad-MSCs administration in the clinical inflammatory response, and the molecular mechanisms involved.

Methods. Ad-MSCs were administered by intraarterial route shortly after intraarticular MSU crystal injections. Joint and systemic inflammation was sequentially studied, and the mechanisms involved in NLRP3 inflammasome activation, and the synthesis of inflammatory mediators were assessed in the synovial membranes 72h after insult. Ad-MSCd and THP-1-derived macrophages stimulated with MSU were co-cultured in Transwell and direct contact experiment.

Results. A single systemic dose of Ad-MSCs accelerated the resolution of local and systemic inflammatory response. In the synovial membrane, Ad-MSC promoted alternatively activated macrophage presence, inhibiting NLRP3 inflammasome and inducing the production of anti-inflammatory cytokines, such as IL-10 or TGF-β, and decreasing nuclear factor-κB activity. Ad-MSC blocked the inflammatory activity of THP-1 cells stimulated with MSU.

Conclusion. Ad-MSCs are able to accelerate the auto-limited acute inflammatory response resolution by inhibiting NLRP3 inflammasome activation in an acute gouty arthritis model mainly mediated by the activation of innate immune response. Therefore, this therapeutic approach could be considered as a pharmacological alternative in patients with comorbidities that preclude conventional treatment.

INTRODUCTION

During the last decades, cell therapy has achieved little success in translating promising results from pre-clinical models into clinical practice in a wide range of diseases, including chronic joint, immune and inflammatory disorders (1). First studies employing MSCs arose from their regenerative potential, with the hypothesis that they could replace damaged cells in pathologies characterized by tissue destruction. However, further studies suggested that improvement of tissue injuries could be rather based on MSC immune-regulatory properties. Most studies have mainly focused on the ability of MSCs to regulate the adaptive immune response, inhibiting the survival and activity of T-regulatory and T-effector cells, as well as the activation, proliferation and differentiation of B lymphocytes (2,3). These effects are explained by the synthesis of regulating factors in an inflammatory mileu, such as nitric oxide (NO), indoleamine 2,3 dioxygenase (IDO), prostaglandin E2 (PGE2), or IL-10 and transforming growth factor (TGF)-β, well-known anti-inflammatory mediators secreted by MSCs (4). Additionally, MSCs actively interact with various types of innate immune cells, such as dendritic cells, natural killers and macrophages (5). MSCs activated by inflamed tissue macrophages induce the synthesis of different mediators, such as PGE2 or TNF-stimulated gene (TSG)-6 (6). Through direct and indirect mechanisms, both MSC mediators would then inhibit macrophage activity, induce the M2 anti-inflammatory polarization, or attenuate NF-κB activation (6–8). Recent *in vitro* data have revealed that MSCs inhibit the NOD-like receptor family, pyrin domain containing 3 (NLRP3) inflammasome (9,10), although their effect on NLRP3 or macrophage polarization *in vivo* during acute joint inflammation remain poorly described. Both adaptive and innate immune mechanisms are integrated during chronic inflammation, coexisting at the same time the processes of induction and resolution of the phenomena associated with the chronicity of the process. This complex network of interactions makes difficult to dissect, in an *in vivo* scenario, the mechanisms purely associated to innate immune system activation and regulation by MSCs. Undoubtedly, to describe how MSCs

act in the modulation of innate immune response, we should use models of acute inflammation, self-limited, in which these mechanisms can be adequately assessed.

Acute gout is a prototype of innate immune response mediated joint disease. It is characterized by recurrent flares of articular and periarticular swelling, redness, stiffness and produce great pain, although it usually resolves spontaneously within a few days leaving minimal residual lesions, even without intervention. Gout is caused by deposition of monosodium urate (MSU) crystals into the joints, which induces a massive infiltration of neutrophils and monocytes (11). This early inflammatory phase is characterized by IL-1β production, that induces the release of different chemokines, cytokines, adhesion molecules which, in turn, increments cell infiltration. The release of IL-1β is driven by NRLP3 inflammasome activation induced by MSU crystals in myeloid cells (12,13). Upon sensing a priming signal, there is a robust increase in the gene transcription of NLRP3, pro-caspase-1, pro-IL-1β and pro-IL-18 via NF-κB activation, thus providing an abundance of protein for downstream processing. A second signal delivered by different ligand detected by NLRP3 unchains the assembly of the inflammasome complex (e.g. NLRP3, Apoptosis-associated Speck-like protein (ASC) and Caspase-1), which subsequently triggers the cleavage of pro-interleukin 1 and 18 and the release of the active cytokines. NLRP3 inflammasome is present in monocyte cells lineage responsible of the innate immune response in metabolic, autoimmune and auto-inflammatory diseases, and therefore targeting its activity could be an effective approach of reducing inflammatory response (14,15). Our previous work points out that MSU induced arthritis in rabbit knees show a pronounced inflammation in the joint, being more than a suitable animal model to reproduce an arthritic flare and to study inflamed synovial membranes (16).

Therefore, the main goal of this work was to study the effect of human MSC in an *in vivo* model of a self-limited acute gouty arthritis in rabbits. Furthermore, we aim to study the effect of MSC administration on NLRP3 activation and macrophage polarization *in vivo* and *in vitro*.

MATERIALS AND METHODS

MSCs generation and characterization.

Adipose tissue derived human MSC (Ad-MSCs) were isolated from lipoaspirates from healthy donors, as previously described (17). In all cases, informed consent was previously obtained according to institutional guidelines. MSC were isolated, expanded and characterized as already described (18). Briefly, for immunophenotype analysis, Mesenchymal cell Kit (Immunostep, Spain) was used following manufacturer´s instructions. The flow cytometry analysis included CD29, CD44, CD73, CD90, CD105, CD166, CD14, CD19, CD34, CD45 and HLA-DR expression. Results were analyzed with FlowJo Analysis (Tree Star, USA). The osteogenic and adipogenic Ad-MSCs differentiation capacity was demonstrated using NH-OsteoDiff Medium and NH-AdipoDiff Medium (Miltenyi Biotec GmbH, Germany) respectively, according to the manufacturer's instructions. Ad-MSCs clonogeneic capacity was assessed seeding 200 cells/well in 6 well-plate, and cells were cultured with complete fresh medium for 10 days at 37ºC, 5% CO_2. Then, fibroblast colony forming units (CFU-F) were fixed and stained with hematoxylin (Thermo Fisher Scientific, USA).

To obtain Ad-MSCs for rabbit injections, Ad-MSCs were cultured for a week in α-MEM supplemented with GlutaMAX™ (Thermo Fisher Scientific) and 5% human platelet lysate (Cook Regentec, USA) at a density of $4x10^3$ cells/cm^2. Then, cells at passage 3 were harvested, counted and resuspended in cooled PBS for injection.

Animal model

For the *in vivo* study we employed three-month old New Zealand White male rabbits (2.5-3.0 kg body weight, Granja San Bernardo, Spain) that were housed in individual cages (0.50 m height, 0.6 m^2 floor space) and exposed to a 12-hour light/dark cycle. After 2 weeks of adaptation to our facilities, an acute gout flare was induced in 24 anesthetized rabbits by intraarticular injections of 50 mg MSU crystals resuspended in

1ml of PBS into both knees, as previously described (16,19). Immediately after MSU injection, right femoral artery was dissected and cannulated with a 24G gauge needle (Abbocath, Venisystems, Spain). One hour after MSU injection, 12 of these rabbits received a single dose of $2x10^6$ Ad-MSCs/Kg, resuspended in 2ml of cooled PBS through the right femoral artery (MSU+MSC group), while the other 12 rabbits received PBS through the same procedure (MSU group). We simultaneously followed 4 sex- and age-matched rabbits, which received intraarticular injections of 1ml PBS in both knees, and were employed as controls. All procedures were performed under aseptic conditions and general anesthesia (16,20). One rabbit from MSU+MSC died during the surgical procedure.

Eight rabbits were euthanized 24 hours after MSU injections by intra-cardiac injection of pentobarbital (50 mg/kg, Braun Medical SA, Spain), and were employed for the differential cell count study. Synovial fluid (SF) from these animals was collected after knee joint lavage with 1 ml of PBS injected into each joint cavity. All the remaining animals were euthanized 72h after MSU administration. Then, the SF, and synovial membranes (SM) were collected, and processed for further studies. A piece of SM was fixed in 4% buffered formalin (Sigma) for 24h and then embedded in paraffin. Another SM piece from each knee was immediately frozen in liquid nitrogen (21).

Knee joint swelling was measured using a digital caliper at different time points: just before intraarticular injection and 6, 18, 24, 48 and 72 h after MSU administration. Blood samples were collected from the auricular artery 24 and 72 h after MSU administration.

All the experiments were performed in accordance with the Animal Research Reporting of *In vivo* Experiments (ARRIVE) guidelines and with the National regulation and the Guidelines for the Care and Use of Laboratory Animals, drawn up by the National Institutes of Health (Bethesda, MS, USA) (22). These procedures were approved by the Institutional Ethics and Animal Welfare Committee of IIS-FJD.

Synovial fluid cell count.

Total leukocyte number was calculated in each synovial fluid sample staining with Türk's solution (Sigma-Aldrich, St Louis, Missouri, USA) and counting by LUNA-II™ Automated Cell Counter (Logos Biosystems, Gyeonggi-do, South Korea). Haemorrhagic synovial fluid samples were discarded (MSU n=1 paw and MSU-MSC n=2 paws). Leukocyte differential count was performed for synovial fluid (SF) from each knee joint cavity. SF smears were fixed in methanol and subsequently stained with May-Grünwald Giemsa (Sigma-Aldrich, St Louis, Missouri, USA) staining. Ten different pictures in each sample were obtained with a Leica DM 6000 LED instrument (Leica, Microsystems, Inc. Buffalo Grove, IL, USA) in order to calculate the percentage of polymorphonuclear (PMN) and mononuclear (MN) cells present in each sample.

Serum C-Reactive Protein (C-RP)

Serum C-RP levels at 24 and 72h after MSU administration were determined with a commercial ELISA kit (ab157726, Abcam, Cambridge, UK) (23).

Histological evaluation.

SM inflammation was evaluated in hematoxylin-eosin stained sections by three blinded observers, according to the Krenn score (16,24). Briefly, lining hyperplasia, tissue cell infiltration and stromal activation were independently evaluated using a subscale graded from 0 to 3 points. The total synovitis score was calculated summing partial grades, with a maximum of 9 points.

Immunohistochemistry

Vascularisation in the SM was evaluated using a monoclonal anti-CD31 antibody (Abcam, Cambridge, UK; clone JC/70A; 1/20 dilution). SM macrophages were stained employing amonoclonal anti-rabbit macrophage RAM11 antibody (Dako, Glostrup, Denmark; 1/100 dilution) and the monoclonal anti-human CD163 antibody (Serotec,

Raleigh, NC, USA; clone EDhu-1, 1/500 dilution), as described (23,25). Arginase-1 presence was examined using a goat polyclonal anti-Liver Arginase (Abcam, Cambridge, UK; 1/500 dilution) antibody (26). In brief, 3μm paraffin sections were rehydrated and incubated with blocking solution (PBS 6% sheep serum, 4% BSA). Sections were incubated with the primary antibodies in blocking solution, overnight at 4ºC. A biotinylated goat anti-mouse IgG (Amersham, Arlington Heights, IL, USA; 1/800 dilution) was employed as secondary antibody, which was visualized employing ABComplex (Dako, Camarillo, CA, USA). Tissue sections were counterstained with haematoxylin and mounted in DPX medium (VWR International, Leuven, Belgium). For CD31+ and Arginase-1+ analysis, 10 microphotographs were randomly taken in each tissue sample (20X magnification), while 5 random pictures along lining area were obtained at 40X magnification for macrophage analysis, using a Leica DM 6000 LED instrument (Leica, Microsystems, Inc. Buffalo Grove, IL, USA). Each image was analysed using the Color Deconvolution plugin of ImageJ software (NIH, Bethesda, MD, USA) to calculate the percentage of positive staining relative to the total tissue area. The means of positive area corresponding to each sample was then calculated for each group (21,27).

Western-blotting.

Total proteins were extracted from SM, resolved on SDS-PAGE gels and transferred to nitrocellulose membranes in a semi-dry Trans-Blot device (Bio-Rad, Madrid, Spain) as described (21,25). The following primary antibodies were applied overnight at 4°C: anti-human COX-2 (Santa Cruz Biotechnology, Dallas TX, USA), anti-rabbit IL-6, anti-rabbit TNF, anti-rabbit IL-10, anti-rabbit TGF-β (all from Cloud-Clone Corp; 1/250 dilution); anti-human NLRP3 (AdipoGen, Liestal, Switzerland; 1/1000 dilution); anti-human Caspase-1 (Thermo Fisher Scientific, IL, USA; 1/500 dilution), anti-rabbit IL-18 and IL-1β antibodies (Cloud-Clone Corp, Houston TX, USA; 1/250 dilution). Protein loading control was performed employing EZBlue gel staining reagent (Sigma-Aldrich) (16,21).

Nuclear factor-κB (NF-κB) activation assay

NF-κB activation was assessed using an ELISA-based TransAM NF-κB p65 kit (Active Motif, CA, USA) in accordance to manufacturer's protocol. Briefly, nuclear proteins were isolated from total protein extracts and incubated with NF-κB consensus sequences. Then, hybridization was detected by a colorimetric reaction, and quantified by absorbance measurement(28).

***In vitro* experiments**

THP-1 monocyte cells (passage 6 to 11) (American Type Culture Collection, Manassas, Virginia, USA) were grown at 37°C and 5% CO2 in RPMI 1640 (Gibco BRL, Grand Island, NY) supplemented with 10% heat-inactivated FBS, 50 units/ml penicillin-streptomycin and 2 mM L-Glutamine (Gibco BRL). THP-1 monocytes were differentiated to macrophages in the presence of 0.5 μM Phorbol 12-myristate 13-acetate (PMA, Sigma-Aldrich) for 3 hours. Approximately, $1x10^5$ Thp-1/cm^2 were seeded in 6 well plates. Cells were incubated O/N at 37°C and 5% CO2 in RPMI 1640, 2% FBS, 50 units/ml penicillin-streptomycin and 2 mM L-Glutamine. Ad-MSC (passage 3-4) were incubated O/N in RPMI 1640, 2% FBS, 50 units/ml penicillin-streptomycin and 2 mM L-Glutamine. For Transwell experiments, $2.5x10^5$ Ad-MSC were seeded into polycarbonate Transwell inserts of 24 mm and 0.4 μm membrane pore size (Corning, New York, USA) before being used in experiments.

PMA-differentiated THP-1 macrophages were stimulated with 300 μg MSU crystals (Invivogen, San Diego, USA) or vehicle (PBS). One hour after the addition of the stimuli, MSC were harvested and $2.5x10^5$ cells were seeded over THP-1 cells for direct co-culture experiments. One hour after the addition of the crystals, Transwell inserts were placed over THP-1 macrophages. Cells were co-cultured for 24 h after the addition of the stimuli.

RNA isolation and RT-PCR

RNA was isolated from cell culture experiments using TRIzol reagent (Roche Diagnostics, Barcelona, Spain), suspended in nuclease-free water and quantified with a NanoDrop ND1000 spectrophotometer (Thermo Fisher Scientific, Waltham, Massachusetts, USA). A High Capacity cDNA Reverse Transcription Kit (Applied Biosystems, San Francisco, California, USA) was used to reverse-transcript 0.8 μg RNA following manufacter's instructions. Step One Plus Detection system (Applied Biosystems, Foster City, CA) was employed to analyze RNA expression by single-reporter real-time PCR. Specific commercial TaqMan® probes were purchased from Applied Biosystems to assess the expression of human IL-1β, NLRP3, Caspase-1, Caspase-1, TNF-α, COX-2, TGF-β, IL-10. RNA expression levels were quantified using the ΔΔCt method, and hypoxanthine-guanine phosphoribosyltransferase (HPRT) expression as endogenous control.

Statistical analysis

GraphPad Prism package (5.0 for Windows) was used for statistical analysis. Sample size for each experimental group was calculated based on reported recommendations (22). To compare the evolution of joint edema between the different groups, two-way analysis of variance ANOVA was employed followed by Bonferroni correction. Mann-Whitney U-test was used for pairwise comparisons between two groups. Quantitative data was expressed as means ± SEM. P values less than 0.05 were considered significant.

RESULTS

Characterization Ad-MSC

Cultured Ad-MSCs showed a fibroblast-like morphology and their inmunophenotype analysis confirmed that they fulfilled all the International Society of Cell Therapy criteria (29) (Figure Suppl. 1A) (supplementary data). Ad-MSCs differentiation capacity was also

confirmed for their osteogenic and adipogenic differentiation (Figure Suppl. 1B) as well as their clonogenic capacity (Fig Suppl. 1C) through CFU-F assays (supplementary data).

Effect of intraarterial administration of Ad-MSCs in joint and systemic inflammation

We first analyzed whether Ad-MSC administration has any effect on joint swelling and SM inflammation in MSU crystal-induced arthritic rabbits. Our data showed that MSU induced a clear increase in knee perimeter, with a maximum after 48 h of injections (Fig. 1A). In the MSU group, SM inflammation was evident 72 h after MSU injection (Fig. 1B), and characterized by hyperplasia of lining layer, stromal activation with increased cellularity, irregular adipocytes and increased fibrotic component in the synovial stroma, and a boost of infiltrating cells, in comparison to control SM (Fig. 1D, 1E). We then specifically assessed synovial neo-angiogenesis by the analysis of %$CD31^+$ by immunostaining in SM samples. In line with the synovitis score, we observed an increased presence of newly formed vessels in the SM of MSU rabbits, in comparison to controls (Fig. 1C, 1G, 1H). Furthermore, intraarticular MSU injection induced a time-dependent increase in serum CRP concentration, as a measurement of systemic inflammation (Fig. 1J). A single dose of Ad-MSC evoked a significant decrease in knee perimeter both after 48 and 74 h of MSU injection, in comparison to untreated knees (Fig. 1A). A clear decrease in SM inflammation was also observed, with amelioration of synovial hypertrophy and in the accumulation of inflammatory cells (Fig 1B, 1E, 1F), while a significant reduction of vascularization was induced by Ad-MSC treatment (Fig. 1C, 1H, 1I). Furthermore, Ad-MSCs had an appreciable effect on the systemic inflammation evoked 24h after MSU injection, but not so evident 72 h post injury (Fig. 1J).

Effect of intraarterial administration of Ad-MSCs on leukocyte population in the synovial fluid of rabbit knees

There was an increased presence of leukocytes in the synovial fluid of MSU injected rabbits 24 and 72 h after injury (Fig. 2A). Ad-MSC infusion decreased the number

of inflammatory cells in the MSU-rabbit synovial fluid at 72 h, in comparison with the untreated animals (Fig. 1). Differential cell count revealed that, 24 h after MSU crystal injection, SF was mainly infiltrated by PMN cells, comprising almost the 90 % of total leukocytes present in both treated and non-treated knees. However, 72 h after injury, the percentage of PMN dropped under the 50% in the MSU and MSU+MSC groups (Fig 2B, 2C).

Effect of Ad-MSC treatment in the synovial presence of infiltrated M1 and M2 macrophages in arthritic rabbits

Gouty arthritis is characterized by extensive macrophage infiltration. So, we then analyzed the presence of macrophages in different phenotypes in the rabbit SM employing RAM11 antibody, that recognizes rabbit macrophages in all different phenotypes; and anti-CD-163, a monocyte and macrophage marker which has been reported to be overexpressed in M2a macrophages (30,31). RAM 11 positive cells were mainly located in the SM lining layer of MSU rabbits, but also some accumulations were observed surrounding adipocytes forming “crown-like” structures close to the sublining vessels. Thus, macrophage presence was quantified in the SM lining layer. RAM11 positive staining was significantly incremented in MSU rabbits when compared to controls (Fig. 3B, 3G). Although a trend to a lesser presence of RAM11 positive cells was observed in the MSU-MSC group when compared to the MSU group, no statistically significant effect was observed (Fig. 3C, 3G).However, both MSU and MSU+MSC samples showed an increased presence of CD163 positive cells in the lining layer, in comparison to control rabbits (Fig. 3E, 3F, 3H), and no statistically significant differences were observed between these arthritic groups (Fig. 3H). In order to simultaneously evaluate the presence of these macrophage markers, we analyzed the ratio between CD163 and RAM11 staining as a marker of M2 to total macrophage presence in the SM of the rabbits. Figure 3I shows an increased ratio CD163/RAM11 in the MSU+MSC group in comparison to MSU animals, indicating an increased presence of M2a macrophages in the Ad-MSC treated animals (32).

Additionally, it is considered that arginase-1 expression is induced in rabbit M2 macrophages(33). Thus, we studied the presence of this marker in SM and observed that arthritic animals overexpressed this protein along the lining layer of SM, where a higher number of macrophages were found. Our results indicate that treated animals' trend to an increased expression of arginase-1 compared to vehicles.

Modulation of the synthesis of different pro- and anti-inflammatory mediators by Ad-MSC in the SM of arthritic rabbits.

As expected, MSU rabbits showed an increased synthesis of pro-inflammatory cytokines in the SM at the time of sacrifice. COX-2 and TNF presence was increased in MSU rabbits, while no differences were observed in IL-6 presence, in comparison to control rabbits (Fig. 4A). Regarding some mediators that have been associated to inflammation inhibition in acute processes, such as IL-10 and TGF-β, no differences with control rabbits were observed in the SM of MSU group. The administration of Ad-MSC induced a statistically significant decrease in the presence of COX-2 and TNF in the SM of the rabbits, while a clear increase in the anti-inflammatory mediators IL-10 and TGF-β was observed in the SM of the treated rabbits (Figure 4B).

Protein expression of NLRP3 inflammasome components in the SM of arthritic rabbits after Ad-MSC infusion.

In order to determine whether Ad-MSC were able to decrease inflammasome activation in gouty arthritic rabbits, we assessed the presence of different mediators associated to the activation of this system in the SM. Our results indicate that NALP-3, pro-Caspase-1 and pro-IL-1β protein presence was increased in the SM of MSU rabbits, while no differences were observed in the local synthesis of the mature form of IL-1β (data not shown) or in IL-18 synthesis, in comparison to control animals (Fig. 5). The administration of Ad-MSC induced a significant decrease in the presence of these components if the NLRP3 inflammasome in comparison to untreated MSU group (Fig.5).

The activation of the downstream nuclear factor of the inflammasome pathway, NF-κB was also increased in the SM of MSU arthritic rabbits, while a significant decrease was observed in these animals when treated with Ad-MSC (Figure 6).

Ad-MSC effect on THP-1 cells stimulated with MSU crystals

We next investigated whether Ad-MSC were able to modulate the inflammatory status of macrophages stimulated by MSU crystals through different *in vitro* approaches. On the one hand, we tested Ad-MSC paracrine capacity to regulate expression of inflammasome components and pro-inflammatory cytokines through Transwell co-culture system. THP-1 differentiated macrophages were stimulated with MSU crystals, triggering a robust inflammatory response, as observed in NLRP3, Caspase-1, IL-1β, TNF-α and COX-2 compared to vehicle expression 24 hours post-stimuli. IL-10 and TGF-β were also over-expressed at this time point. In order to reproduce *in vivo* settings, Ad-MSC were transferred into THP-1 wells 1 hour after stimuli. Interestingly, as observed in Fig. 8A, although the levels of cytokines expressed by MSU crystals-activated THP-1 cells slightly increased in presence of Ad-MSC, the difference of THP-1 cell expression levels between MSU and MSU+MSC groups was evident. Notably, NLRP3 but not Caspase-1 expression was also inhibited in Ad-MSC-treated macrophages (Figure 7A). On the other hand, direct co-culture system allowed us the study of the direct interaction between Ad-MSC and THP-1-derived macrophages, both being in contact with MSU crystals. Surprisingly, Ad-MSC prevented macrophage activity in the same fashion to that observed previously (Fig. 7B). Regarding inflammasome components, NLRP3 and Caspase-1 expression was attenuated after Ad-MSC addition (Figure 7B).

DISCUSSION

We demonstrated that a single dose of xenogeneic Ad-MSC was able to shorten the intensity and duration of acute arthritis induced by MSU crystals injection in rabbit knee. Molecular studies showed that Ad-MSC inhibited the synthesis of the NLRP3

inflammasome components, reduced NF-κB activation and pro-IL-1β secretion in synovial tissue. In addition, we observed that MSC treatment induced a change in synovial macrophage polarization towards M2 phenotype in the synovium, along with a high expression of anti-inflammatory cytokines.

Despite initial promising results of MSC application as an efficacious therapy in different preclinical studies of inflammatory and autoimmune diseases, and in the early phases of clinical trials in different human diseases, its success has not been further confirmed in most high-standard, large scale clinical trials. This could indicate that preclinical models could not accurately reproduce human diseases. Furthermore, it is plausible that the beneficial effect of MSC could be a consequence of the inhibition of pathways not quite well identified in these models and, therefore, not successfully translated to human pathology. Up to date, most studies have focused on chronic diseases, in which the adaptive and the innate immune responses are integrated, coexisting a continuum of induction and resolution processes. This complex network of interactions makes difficult to clearly dissect the mechanisms responsible for the improvement in the progression of these chronic conditions. Therefore, in order to find out whether MSCs can specifically modulate acute inflammatory response, where the activation of the innate immune response is the only mechanism responsible for the inflammatory flare, it is necessary to resort to experimental models of acute, self-limited inflammation. Although currently there is no data describing the effect of MSC in acute models of sterile inflammation in joint diseases, MSCs have been employed in models reproducing acute conditions, such as acute kidney disease, corneal injury, severe skin burning, or acute pancreatitis, where tissue damage clearly decreased after treatment (34–37). However, some of the etiologic agents

inducing tissue damage in these models do not entirely reproduce human clinical processes. Besides, these models reproduce infrequent acute conditions in general population. This complexity hinders the study of MSC effect in specific acute conditions and its translation into the clinic.

We developed an acute auto-limited gouty arthritis model, which is the paradigm of an acute joint disease mediated by innate immune response, without any contribution of adaptive immunity. This experimental model accurately reproduce the pathophysiology of an acute gout flare in humans (16,19,38,39). Human gout is a microcrystal-induced arthritis, a prevalent joint disease with unmet therapeutic needs (5). In Western countries, prevalence of gout varies from 2% to 6%, increasing up to 9% in adults older than 60 years of age in USA. Many gout patients are unresponsive to, intolerant, or have contraindications to conventional treatments, especially elderly patients with comorbidities (40) IL-1β inhibitors such as anakinra and canakinumab are a high cost therapy and their use is not recommended for patients with high infection risk (41). Therefore, the development of alternative therapies is urgently required. Our previous work points out that exogenous administration of MSU crystals produce a pronounced inflammation in the rabbit joint (16,19). Not only this model accurately reproduce the pathophysiology of human knee response to an acute arthritic flare, but also, compared to other pure inflammation models, the knee joint size and the amount of exudate produced facilitates its follow up through a direct observational measurement of joint swelling (19,38,39). What is more, our model can be easily reproduced, displaying a homogeneous clinical outcome. Therefore, MSU crystal-induced acute arthritis in rabbit is a reliable model to study *in vivo* the

pathophysiology in acute inflammatory processes as well as the efficacy and mechanisms of action of novel therapeutic options.

Our results show that a single dose of MSCs substantially improved a self-limited urate induced acute arthritis, and normalized serum C-RP in a short interval of time after their systemic administration. Histologic studies confirmed that synovial membranes from treated animals showed less pathological features compared to non-treated MSU group, with a 40% reduction of histologic score. Synovium showed a thinner lining layer and less altered stromal structure, including a maintenance of the adipocyte structure, reduced fibrosis, and diminished synovial neovascularization (21,25). Synovial fluid examination indicated that 24 h after injury, PMN covered nearly 90% of total leukocyte population, as described in the very early phase in gout patients (42). However, 72 h after MSU injection, the relative amount of mononuclear phagocytes increases, as described in human gout. In our study, mononuclear cells were the predominant WBC population 72 hours after MSU administration, comprising almost 60% of total leukocytes in MSU rabbits. The administration of MSC to arthritic rabbits did not alter total cell infiltration 24 hours after MSU administration, while it induced a relevant decrease in the total amount of WBC in the joint exudate without a significant change in the relative distribution of monocytes and neutrophils in the synovial fluid. In line with previous data, 65 % of total WBC presence was reduced in synovial fluid of treated animals at the latter time point. Thus, MSC promoted total cell clearance from 24 h to 72 h. The modification of the ratio PMN/Total cells during the evolution of the inflammatory response agrees with other acute inflammation models. For example, in a mouse peritonitis model, total number of infiltrated cells decreased few hours after human MSC peritoneal application. In

this model, monocyte number rise followed by PMNs clearance (8). Additionally, this fact coincides with the cellular events occurring in a rat MSU air-pouch model (43). In our model, MSC reduced about 65% of joint swelling 72 h after injury. Remarkably, although cautious shall be taken when comparing efficacy of other treatment modalities assessed in different experimental models and animal species, the size effect achieved by MSC treatment is similar to that observed when using COX-2 inhibitors. Both salidroside and celecoxib halved ankle swelling, cell count and histologic scores 24 h after MSU induced injury in rat and rabbit models(44). A IL-1 trap slightly limited ankle swelling for 4 days in a MSU induced ankle arthritis in mice(45). Six hour after MSU injection, resveratrol reduce 20% foot thickness in a murine arthritis model, while 50% of total infiltrated cells were decreased in a MSU peritonitis model (46). In a randomized, double-blind clinical trial using anakinra, joint swelling score diminished about 50% in three days. Additionally, the short half-life (46 h) of this drug requires daily administration, in contrast to the single dose of MSC treatment.

In our model, at 72 h post crystals injection, NF-κB, which is responsible of the up-regulation of the synthesis of inflammasome components and other pro-inflammatory proteins (47–49), was active in arthritic animals. In line with previously published findings, MSC diminished the activity of NF-κB (8,37,50); and as expected, NLRP3, Caspase-1 and Il-1β levels were decreased in treated arthritic synovial membranes. Inhibition of NLRP3 inflammasome by MSC in sterile acute inflammatory disease models has been scarcely investigated *in vivo*. In a Na-T induced severe acute pancreatitis in mice (51), NLRP3 inflammasome activity and NF-κB signaling synthesis and activity was down-regulated in acinar cells after MSC treatment. Secretome from perivascular SC was also capable of attenuating

MSU crystal-induced peritonitis in mice, inhibiting expression of NLRP3 inflammasome proteins in macrophages (52). On the other side, IL-18 and IL-6 remained invariable among healthy and arthritic groups. Evolution of inflammatory profile in a peritoneal model of MSU-arthritis indicated that over time, some cytokines may be overexpressed while others could have returned to normal levels, given the self-limiting nature of gouty arthritis(53). In line with previous data, COX-2 and TNF-α levels, which were increased in arthritic synovial membranes, were reduced in synoviums of MSC treated groups.

It has been established that the spontaneous shutdown of the gouty inflammation process is curtailed by several mechanisms, which includes clearance of apoptotic cells and induction of anti-inflammatory cytokines, such as TGF-β and IL-10, by M2 macrophages (53–55). In effect, there was an increased number of M2 macrophage with an increase of TGF-β and IL-10 proteins in MSC treated synovium. It has been previously described that MSC can favor its polarization toward alternative M2 macrophage phenotype. MSC tested in an asthma model in mice induced the expression of TGF-β and IL-10 in lung macrophages (56). It has been also depicted that MSC could diminish frequency of total infiltrated macrophages and induce their anti-inflammatory phenotype (57–59). On the other side, MSC can enhance its accumulation into damaged tissue, favoring their differentiation into M2 subsets (34).

One limitation of our study is that we have not revealed the specific molecular pathway through which MSC attenuate acute gouty flare. However, it has been extensively reported in different acute inflammation models that MSC are able to interact with immune cells in an inflammatory milieu producing a broad spectrum

of different anti-inflammatory molecules (60). In our model, most MSC were accumulated in peripheral organs, implying that leukocyte modulation could be produced from distant sites by the release of soluble factors, as previously reported. Nevertheless, we cannot exclude that the small fraction of MSC localized at damaged synovium could take part in the therapeutic process. In our model, MSC could be directly promoting monocyte polarization towards M2 subset, favoring their accumulation in arthritic synovial membranes. Some studies specify that during the polarization of macrophages towards M2 phenotype, NLRP3 expression is suppressed, and so IL-1b secretion(61). This process could be mediated through a diminished NF-kB activity(62). On the other hand, several MSC derived soluble factors have been described to inhibit NLRP3 activity (9,59,63). Hence, suppression of NLRP3 activity could alter macrophage phenotype into M2 subset, limiting the inflammatory response. Lastly, it has been also reported that MSC derived TSG-6 inhibited TLR2-mediated nuclear translocation of the NF-kB, suppressing the transcription of pro-inflammatory cytokines(8). Additionally,TSG-6 was proposed to inhibit NF-kB activity and synthesis of NLRP3 inflammasome components(37). Thus, MSC targeting NF-kB activity could lead to inhibition of pro-inflammatory cytokines and NLRP3 inflammasome components, favoring M2 macrophage phenotype.

CONCLUSION

In conclusion, treatment with a single systemic dose of MSCs is able to attenuate the inflammatory response in an acute gouty arthritis model in rabbits, suppressing NF-kB activity, inhibiting synthesis of NLRP3 inflammasome components, and promoting the presence of alternative activated macrophages.

Therefore, this therapeutic approach could be an alternative to conventional pharmacological treatments for patients in whom the possibility of a standard treatment is very limited, as in polymorbid, elderly patients, and patients with renal pathology or with adverse reaction to NSAIDs.

REFERENCES

1. Squillaro T, Peluso G, Galderisi U. Clinical Trials with Mesenchymal Stem Cells: An Update. Cell Transplant. 2016 May;25(5):829–48.

2. Qi K, Li N, Zhang Z, Melino G. Tissue regeneration: The crosstalk between mesenchymal stem cells and immune response. Cell Immunol. 2018;326:86–93.

3. Uccelli A, Moretta L, Pistoia V. Mesenchymal stem cells in health and disease. Nat Rev Immunol. 2008;8(9):726–36.

4. Voswinkel J, Francois S, Simon J-M, Benderitter M, Gorin N-C, Mohty M, et al. Use of Mesenchymal Stem Cells (MSC) in Chronic Inflammatory Fistulizing and Fibrotic Diseases: a Comprehensive Review. Clin Rev Allergy Immunol. 2013 Oct;45(2):180–92.

5. Le Blanc K, Davies LC. Mesenchymal stromal cells and the innate immune response. Immunol Lett. 2015 Dec 1;168(2):140–6.

6. Prockop DJ. Concise review: Two negative feedback loops place mesenchymal stem/stromal cells at the center of early regulators of inflammation. Stem Cells. 2013;31(10):2042–6.

7. Ylöstalo JH, Bartosh TJ, Coble K, Prockop DJ. Human mesenchymal stem/stromal cells cultured as spheroids are self-activated to produce prostaglandin E2 that directs stimulated macrophages into an anti-inflammatory phenotype. Stem Cells. 2012;30(10):2283–96.

8. Choi H, Lee RH, Bazhanov N, Oh JY, Prockop DJ. Anti-inflammatory protein TSG-6 secreted by activated MSCs attenuates zymosan-induced mouse peritonitis by decreasing TLR2/NF-κB signaling in resident macrophages. Blood. 2011 Jul 14;118(2):330–8.

9. Oh JY, Ko JH, Lee HJ, Yu JM, Choi H, Kim MK, et al. Mesenchymal stem/stromal cells inhibit the NLRP3 inflammasome by decreasing mitochondrial reactive oxygen species. Stem Cells. 2014 Jun;32(6):1553–63.

10. Shin T-H, Kim H-S, Kang T-W, Lee B-C, Lee H-Y, Kim Y-J, et al. Human umbilical cord blood-stem cells direct macrophage polarization and block inflammasome activation to alleviate rheumatoid arthritis. Cell Death Dis. 2016 Dec 22;7(12):e2524.

11. Dalbeth N, Merriman TR, Stamp LK. Gout. Lancet. 2016 Oct 22;388(10055):2039–52.

12. Martinon F, Pétrilli V, Mayor A, Tardivel A, Tschopp J. Gout-associated uric acid crystals activate the NALP3 inflammasome. Nature. 2006 Mar 11;440(7081):237–41.

13. So AK, Martinon F. Inflammation in gout: mechanisms and therapeutic targets. Nat Rev Rheumatol. 2017 Sep 28;13(11):639–47.

14. Barbé F, Douglas T, Saleh M. Advances in Nod-like receptors (NLR) biology. Cytokine Growth Factor Rev. 2014 Dec;25(6):681–97.

15. Herrero-Beaumont G, Pérez-Baos S, Sánchez-Pernaute O, Roman-Blas JA, Lamuedra A, Largo R. Targeting chronic innate inflammatory pathways, the main road to prevention of osteoarthritis progression. Biochem Pharmacol. 2019;(February):0–1.

16. Naredo E, Medina JP, Pérez-Baos S, Mediero A, Herrero-Beaumont G, Largo R. Validation of Musculoskeletal Ultrasound in the Assessment of Experimental Gout Synovitis. Ultrasound Med Biol. 2018 Jul;44(7):1516–24.

17. Lopez-Santalla M, Mancheño-Corvo P, Menta R, Lopez-Belmonte J, DelaRosa O, Bueren JA, et al. Human Adipose-Derived Mesenchymal Stem Cells Modulate Experimental Autoimmune Arthritis by Modifying Early Adaptive T Cell Responses. Stem Cells. 2015 Dec;33(12):3493–503.

18. Valencia J, Blanco B, Yáñez R, Vázquez M, Herrero Sánchez C, Fernández-García M, et al. Comparative analysis of the immunomodulatory capacities of human bone marrow– and adipose tissue–derived mesenchymal stromal cells from the same

donor. Cytotherapy. 2016 Oct 1;18(10):1297–311.

19. Miguelez R, Palacios I, Navarro F, Gutierrez E, Sanchez-Pernaute O, Egido J, et al. Anti-inflammatory effect of a PAF receptor antagonist and a new molecule with antiproteinase activity in an experimental model of acute urate crystal arthritis. J Lipid Mediat Cell Signal. 1996;13(1):35–49.

20. Largo R, S??nchez-Pernaute O, Marcos ME, Moreno-Rubio J, Aparicio C, Granado R, et al. Chronic arthritis aggravates vascular lesions in rabbits with atherosclerosis: A novel model of atherosclerosis associated with chronic inflammation. Arthritis Rheum. 2008;58(9):2723–34.

21. Larrañaga-Vera A, Lamuedra A, Pérez-Baos S, Prieto-Potin I, Peña L, Herrero-Beaumont G, et al. Increased synovial lipodystrophy induced by high fat diet aggravates synovitis in experimental osteoarthritis. Arthritis Res Ther. 2017 Dec 1;19(1):264.

22. McGrath JC, Lilley E. Implementing guidelines on reporting research using animals (ARRIVE etc.): new requirements for publication in BJP. Br J Pharmacol. 2015 Jul;172(13):3189–93.

23. Pérez-Baos S, Barrasa JI, Gratal P, Larrañaga-Vera A, Prieto-Potin I, Herrero-Beaumont G, et al. Tofacitinib restores the inhibition of reverse cholesterol transport induced by inflammation: understanding the lipid paradox associated with rheumatoid arthritis. Br J Pharmacol. 2017 Sep;174(18):3018–31.

24. Krenn V, Morawietz L, Burmester G-R, Kinne RW, Mueller-Ladner U, Muller B, et al. Synovitis score: discrimination between chronic low-grade and high-grade synovitis. Histopathology. 2006 Oct;49(4):358–64.

25. Prieto-Potín I, Roman-Blas J, Martínez-Calatrava M, Gómez R, Largo R, Herrero-Beaumont G. Hypercholesterolemia boosts joint destruction in chronic arthritis. An experimental model aggravated by foam macrophage infiltration. Arthritis Res Ther. 2013 Aug 13;15(4):R81.

26. Fishman JM, Lowdell MW, Urbani L, Ansari T, Burns AJ, Turmaine M, et al. Immunomodulatory effect of a decellularized skeletal muscle scaffold in a discordant xenotransplantation model. Proc Natl Acad Sci U S A. 2013 Aug 27;110(35):14360–5.

27. Martínez-Calatrava MJ, Prieto-Potín I, Roman-Blas JA, Tardio L, Largo R, Herrero-Beaumont G. RANKL synthesized by articular chondrocytes contributes to juxta-articular bone loss in chronic arthritis. Arthritis Res Ther. 2012;14(3):R149.

28. Pérez-Baos S, Gratal P, Barrasa JI, Lamuedra A, Sánchez-Pernaute O, Herrero-Beaumont G, et al. Inhibition of pSTAT1 by tofacitinib accounts for the early improvement of experimental chronic synovitis. J Inflamm. 2019 Dec;16(1):2.

29. Dominici M, Le Blanc K, Mueller I, Slaper-Cortenbach I, Marini F, Krause D, et al. Minimal criteria for defining multipotent mesenchymal stromal cells. The International Society for Cellular Therapy position statement. Cytotherapy. 2006;8(4):315–7.

30. Buechler C, Ritter M, Orsó E, Langmann T, Klucken J, Schmitz G. Regulation of scavenger receptor CD163 expression in human monocytes and macrophages by pro- and antiinflammatory stimuli. J Leukoc Biol. 2000 Jan 1;67(1):97–103.

31. Tarique AA, Logan J, Thomas E, Holt PG, Sly PD, Fantino E. Phenotypic, Functional, and Plasticity Features of Classical and Alternatively Activated Human Macrophages. Am J Respir Cell Mol Biol. 2015 Nov 30;53(5):676–88.

32. Nakada H, Yamashita A, Kuroki M, Furukoji E, Uchino N, Asanuma T, et al. A synthetic tryptophan metabolite reduces hemorrhagic area and inflammation after pulmonary radiofrequency ablation in rabbit nonneoplastic lungs. Jpn J Radiol. 2014 Mar;32(3):145–54.

33. Yamane K, Leung K-P. Rabbit M1 and M2 macrophages can be induced by human recombinant GM-CSF and M-CSF.

34. Geng Y, Zhang L, Fu B, Zhang J, Hong Q, Hu J, et al. Mesenchymal stem cells ameliorate rhabdomyolysis-induced acute kidney injury via the activation of M2 macrophages. Stem Cell Res Ther. 2014 Jun 24;5(3):80.

35. Roddy GW, Oh JY, Lee RH, Bartosh TJ, Ylostalo J, Coble K, et al. Action at a distance: systemically administered adult stem/progenitor cells (MSCs) reduce inflammatory damage to the cornea without engraftment and primarily by secretion of TNF-α stimulated gene/protein 6. Stem Cells. 2011 Oct;29(10):1572–9.

36. Liu L, Song H, Duan H, Chai J, Yang J, Li X, et al. TSG-6 secreted by human umbilical

cord-MSCs attenuates severe burn-induced excessive inflammation via inhibiting activations of P38 and JNK signaling. Sci Rep. 2016 Jul 22;6(1):1–13.

37. He Z, Hua J, Qian D, Gong J, Lin S, Xu C, et al. Intravenous hMSCs Ameliorate Acute Pancreatitis in Mice via Secretion of Tumor Necrosis Factor-α Stimulated Gene/Protein 6. Sci Rep. 2016 Dec 5;6(1):1–17.

38. Nishimura A, Akahoshi T, Takahashi M, Takagishi K, Itoman M, Kondo H, et al. Attenuation of monosodium urate crystal-induced arthritis in rabbits by a neutralizing antibody against interleukin-8. J Leukoc Biol. 1997 Oct;62(4):444–9.

39. Pineda C, Fuentes-Gómez AJ, Hernández-Díaz C, Zamudio-Cuevas Y, Fernández-Torres J, López-Macay A, et al. Animal model of acute gout reproduces the inflammatory and ultrasonographic joint changes of human gout. Arthritis Res Ther. 2015;17(1):37.

40. Schlesinger N. Anti-interleukin-1 therapy in the management of gout. Curr Rheumatol Rep. 2014 Feb;16(2):1–6.

41. Gómez Reino J, Loza E, Andreu JL, Balsa A, Batlle E, Cañete JD, et al. Consensus Statement of the Spanish Society of Rheumatology on Risk Management of Biologic Therapy in Rheumatic Patients. Reumatol Clínica (English Ed. 2011 Sep 1;7(5):284–98.

42. Scanu A, Oliviero F, Ramonda R, Frallonardo P, Dayer JM, Punzi L. Cytokine levels in human synovial fluid during the different stages of acute gout: Role of transforming growth factor β1 in the resolution phase. Ann Rheum Dis. 2012;71(4):621–4.

43. Schiltz C, Lioté F, Prudhommeaux F, Meunier A, Champy R, Callebert J, et al. Monosodium urate monohydrate crystal-induced inflammation in vivo: Quantitative histomorphometric analysis of cellular events. Arthritis Rheum. 2002 Jun 1;46(6):1643–50.

44. Liu Y, Tang H, Liu X, Chen H, Feng N, Zhang J, et al. Frontline Science: Reprogramming COX-2, 5-LOX, and CYP4A-mediated arachidonic acid metabolism in macrophages by salidroside alleviates gouty arthritis. J Leukoc Biol. 2019 Jan 28;105(1):11–24.

45. Torres R, Macdonald L, Croll SD, Reinhardt J, Dore A, Stevens S, et al. Hyperalgesia,

synovitis and multiple biomarkers of inflammation are suppressed by interleukin 1 inhibition in a novel animal model of gouty arthritis. Ann Rheum Dis. 2009 Oct 1;68(10):1602–8.

46. Li H, Ou G, He Y, Ren L, Yang X, Zeng M. Resveratrol attenuates the MSU crystal-induced inflammatory response through the inhibition of TAK1 activity. Int Immunopharmacol. 2019 Feb 1;67:62–8.

47. Bauernfeind FG, Horvath G, Stutz A, Alnemri ES, MacDonald K, Speert D, et al. Cutting Edge: NF-κB Activating Pattern Recognition and Cytokine Receptors License NLRP3 Inflammasome Activation by Regulating NLRP3 Expression. J Immunol. 2009 Jul 15;183(2):787–91.

48. Lee DJ, Du F, Chen SW, Nakasaki M, Rana I, Shih VFS, et al. Regulation and Function of the Caspase-1 in an Inflammatory Microenvironment. J Invest Dermatol. 2015 Aug 21;135(8):2012–20.

49. Liu T, Zhang L, Joo D, Sun SC. NF-κB signaling in inflammation [Internet]. Vol. 2, Signal Transduction and Targeted Therapy. Springer Nature; 2017. p. 1–9.

50. Yan X, Cen Y, Wang Q. Mesenchymal stem cells alleviate experimental rheumatoid arthritis through microRNA-regulated IκB expression. Sci Rep. 2016;6:28915.

51. Sun X, Hao H, Han Q, Song X, Liu J, Dong L, et al. Human umbilical cord-derived mesenchymal stem cells ameliorate insulin resistance by suppressing NLRP3 inflammasome-mediated inflammation in type 2 diabetes rats. Stem Cell Res Ther. 2017 Nov 2;8(1):241.

52. Kim J, Kim WJ, Ha KS, Han ET, Park WS, Yang SR, et al. Perivascular stem cells suppress inflammasome activation during inflammatory responses in macrophages. Int J Stem Cells. 2019 Nov 30;12(3):419–29.

53. Martin WJ, Walton M, Harper J. Resident macrophages initiating and driving inflammation in a monosodium urate monohydrate crystal-induced murine peritoneal model of acute gout. Arthritis Rheum. 2009 Jan;60(1):281–9.

54. Martin WJ, Shaw O, Liu X, Steiger S, Harper JL. Monosodium urate monohydrate crystal-recruited noninflammatory monocytes differentiate into M1-like proinflammatory macrophages in a peritoneal murine model of gout. Arthritis

Rheum. 2011 May 1;63(5):1322–32.

55. Chen YH, Hsieh SC, Chen WY, Li KJ, Wu CH, Wu PC, et al. Spontaneous resolution of acute gouty arthritis is associated with rapid induction of the anti-inflammatory factors TGFβ1, IL-10 and soluble TNF receptors and the intracellular cytokine negative regulators CIS and SOCS3. Ann Rheum Dis. 2011 Sep 1;70(9):1655–63.

56. Braza F, Dirou S, Forest V, Sauzeau V, Hassoun D, Chesné J, et al. Mesenchymal Stem Cells Induce Suppressive Macrophages Through Phagocytosis in a Mouse Model of Asthma. Stem Cells. 2016 Jul 1;34(7):1836–45.

57. Song W-J, Li Q, Ryu M-O, Ahn J-O, Ha Bhang D, Chan Jung Y, et al. TSG-6 Secreted by Human Adipose Tissue-derived Mesenchymal Stem Cells Ameliorates DSS-induced colitis by Inducing M2 Macrophage Polarization in Mice. Sci Rep. 2017 Jul 12;7(1):5187.

58. Mao F, Wu Y, Tang X, Wang J, Pan Z, Zhang P, et al. Human umbilical cord mesenchymal stem cells alleviate inflammatory bowel disease through the regulation of 15-LOX-1 in macrophages. Biotechnol Lett. 2017;39(6).

59. Park HJ, Kim J, Saima FT, Rhee K-J, Hwang S, Kim MY, et al. Adipose-derived stem cells ameliorate colitis by suppression of inflammasome formation and regulation of M1-macrophage population through prostaglandin E2. Biochem Biophys Res Commun. 2018 Apr 15;498(4):988–95.

60. Shi Y, Wang Y, Li Q, Liu K, Hou J, Shao C, et al. Immunoregulatory mechanisms of mesenchymal stem and stromal cells in inflammatory diseases. Nat Rev Nephrol. 2018 Aug 12;14(8):493–507.

61. Awad F, Assrawi E, Jumeau C, Georgin-Lavialle S, Cobret L, Duquesnoy P, et al. Impact of human monocyte and macrophage polarization on NLR expression and NLRP3 inflammasome activation. Lai H-C, editor. PLoS One. 2017 Apr 12;12(4):e0175336.

62. Porta C, Rimoldi M, Raes G, Brys L, Ghezzi P, Di Liberto D, et al. Tolerance and M2 (alternative) macrophage polarization are related processes orchestrated by p50 nuclear factor κB. Proc Natl Acad Sci U S A. 2009 Sep 1;106(35):14978–83.

63. Miteva K, Pappritz K, Sosnowski M, El-Shafeey M, Müller I, Dong F, et al.

Mesenchymal stromal cells inhibit NLRP3 inflammasome activation in a model of Coxsackievirus B3-induced inflammatory cardiomyopathy. Sci Rep. 2018;8(1).

FIGURE LEGENDS

Figure 1. Systemic administration of MSCs through the right femoral artery attenuates synovitis in rabbit knees injected with MSU crystals. A, joint swelling evolution of each paw during 72h after MSU crystal injection. Bars show the mean and SEM (n=7 paws for controls, n=16 paws for MSU and n=14 paws for MSU+MSC group). Two-way ANOVA for the comparison between groups for each time point, *p<0.05 vs. Control, #p<0.05 vs. MSU. **B,** global histopathology score according to Krenn scale. Bars show the mean and SEM (n=7 paws for controls, n=16 paws for MSU and n=14 paws for MSU+MSC group). **D-F**, Representative sections of synovium hematoxylin and eosin staining. Control (D), MSU (E), MSU+MSC (F). **C,** shows densitometric analysis of CD31 staining percentage in the SM of each group of animals. Bars show the mean and SEM (n=7 for controls, n=16 for MSU and n=14 for MSU+MSC group). Mann-Whitney test, *p<0.05 vs. Control, #p<0.05 vs. MSU. **(G-I)** Representative sections of immunohistochemical staining of CD31 in the synovium of control (G), MSU and (H) and MSU+MSC (I) groups at 72h. Scale bars=50μm. **J,** serum C-Reactive protein concentration levels at 24h and 72h of study. Bars show the mean and SEM (n=4 rabbits for controls, n=8 rabbits for MSU and n=7 rabbits for MSU+MSC group). Mann-Whitney test, *p<0.05 vs. Control, #p<0.05 vs. MSU. MSC: mesenchymal stromal cells; MSU: monosodium urate.

Figure 2. Systemic administration of MSC reduces total leukocyte population at 72 h but do not alter percentage of PMN-MN cells. A, leukocyte count in synovial fluid at 24 h and 72 h. Mann-Whitney test, * p<0.05 vs. Control, # p<0.05 vs. MSU at their respective time. **B,** differential leukocyte count at 24 h and 72 h. Mann-Whitney test, * p<0.05 vs. PMN at 24 h, # p<0.05 vs. PMN at 24 h, $ p<0.05 vs. MN at 24 h. Bars show the mean and SEM (n = 7 for controls, n = 8 for MSU and n = 8 for MSU+MSC FEM group at 24 h; n = 15 for MSU and n = 12 for MSU+MSC group at 72 h). **C,** representative images of synovial fluid samples of MSU and MSU+MSC groups stained with May-Grünwald Giemsa at 24 h and 72 h. Scale bar = 50 μm. MSC: mesenchymal stromal cells; MSU: monosodium urate.

Figure 3. Immunohistochemical analysis of macrophage population within synovial membranes at 72h after insult. (A-C) RAM11 antigen staining in the synovium of control (A), MSU and (B) and MSU+MSC (C) groups. **(D-F),** Representative sections of CD-163

staining in control (D), MSU and (E) and MSU+MSC (F) groups. **(G-I),**arginase-1 staining in SM in control (G), MSU and (H) and MSU+MSC (I) groups scale bar=50μm. J, shows densitometric analysis of RAM11 staining percentage, and K of CD163 staining percentage in the SM of each group of animals. L, ratio of CD163 to RAM11 positive staining. M, percentage of arginase-1 staining in lining layer. Bars show the mean and SEM (n=7 for controls, n=16 for MSU and n=14 for MSU+MSC group). Mann-Whitney test, *p<0.05 vs. Control, #p<0.05 vs. MSU. MSC: mesenchymal stromal cells; MSU: monosodium urate.

Figure 5. MSCs modulates pro- and anti-inflammatory cytokine profile in synovial membranes of arthritic rabbits. Representative western blot of protein levels of IL-6, Cox-2, TNF-α, TGF-β and IL-10. EZ blue staining was used as protein loading control and to normalize the results, which are expressed as a fold-change of the healthy group. Bars show the mean and SEM (n=7 for controls, n=16 for MSU and n=14 for MSU+MSC group). Mann-Whitney test, *p<0.05 vs. Control, #p<0.05 vs. MSU. MSC: mesenchymal stromal cells; MSU: monosodium urate.

Figure 6. Protein expression of inflammasome components is modulated in arthritic rabbits treated with MSCs. Activated NALP3, pro-caspase-1, IL-1β, and IL-18 were assessed by western blot. EZ blue staining was used as protein loading control. Results are normalized by EZ blue staining and expressed as a fold-change of the healthy group.Bars show the mean and SEM (n=7 for controls, n=16 for MSU and n=14 for MSU+MSC group). Mann-Whitney test, *p<0.05 vs. Control, #p<0.05 vs. MSU. MSC: mesenchymal stromal cells; MSU: monosodium urate.

Figure 7. NF-kB p65 was analyzed by TransAM kit assay. Results are expressed inoptical density (OD) units. Bars show the mean and SEM (n=7 for controls, n=16 for MSU and n=14 for MSU+MSC group). Mann-Whitney test, *p<0.05 vs. Control, #p<0.05 vs. MSU. MSC: mesenchymal stromal cells; MSU: monosodium urate.

Figure 8. **MSC inhibit MSU crystals-stimulated THP-1 cells inflammatory activity *in vitro*.** A, Gene expression levels of different cytokines produced by THP-1 cells 24 h after stimuli in Transwell co-culture system. B, Gene expression levels of different cytokines produced by THP-1 cells 24 h after stimuli in direct co-culture system. Bars show the mean and SEM (n=4 independent experiments). Mann-Whitney test, a: p<0.05 vs. V, b: p<0.05 vs. V+MSC, c: p<0.05 vs. MSU. MSC: mesenchymal stem cells; COX-2: Ciclooxygenase-2; IL: interleukin; NLRP3: NLR Family Pyrin Domain Containing 3; TGF-β: tumor growth factor-β, TNF-α: tumor necrosis factor α; V: vehicle; MSU: monosodium urate.

Supplementary 1. Ad-MSCs characterization. **A,** Ad-MSCs immunophenotype, negative for hematopoietic markers CD34 and CD45, positive for CD29, CD44, CD73, CD90, CD105 and CD166 expression. **B**, Adipogenic and Osteogenic differentiation. **C,** Ad-MSCs clonogenic capacity.

FIGURE 1

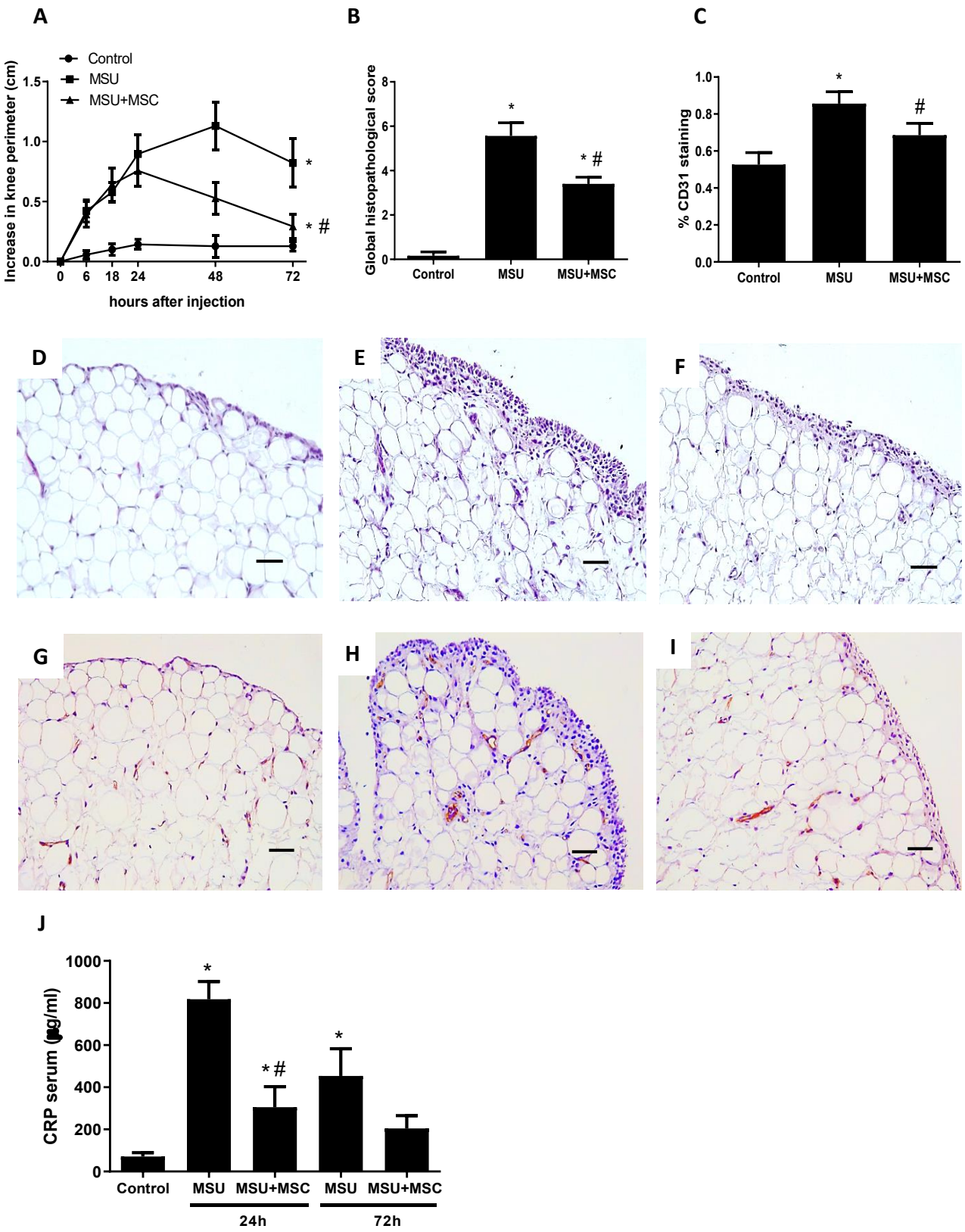
A
Control
MSU
MSU+MSC
Increase in knee perimeter (cm)
1.5
1.0
0.5
0.0
0
6
18
24
48
72
hours after injection
*
* #
B
Global histopathological score
8
6
4
2
0
*
* #
Control
MSU
MSU+MSC
C
% CD31 staining
1.0
0.8
0.6
0.4
0.2
0.0
*
#
Control
MSU
MSU+MSC
D
E
F
G
H
I
J
CRP serum (μg/ml)
1000
800
600
400
200
0
*
* #
*
Control
MSU
MSU+MSC
MSU
MSU+MSC
24h
72h

FIGURE 2

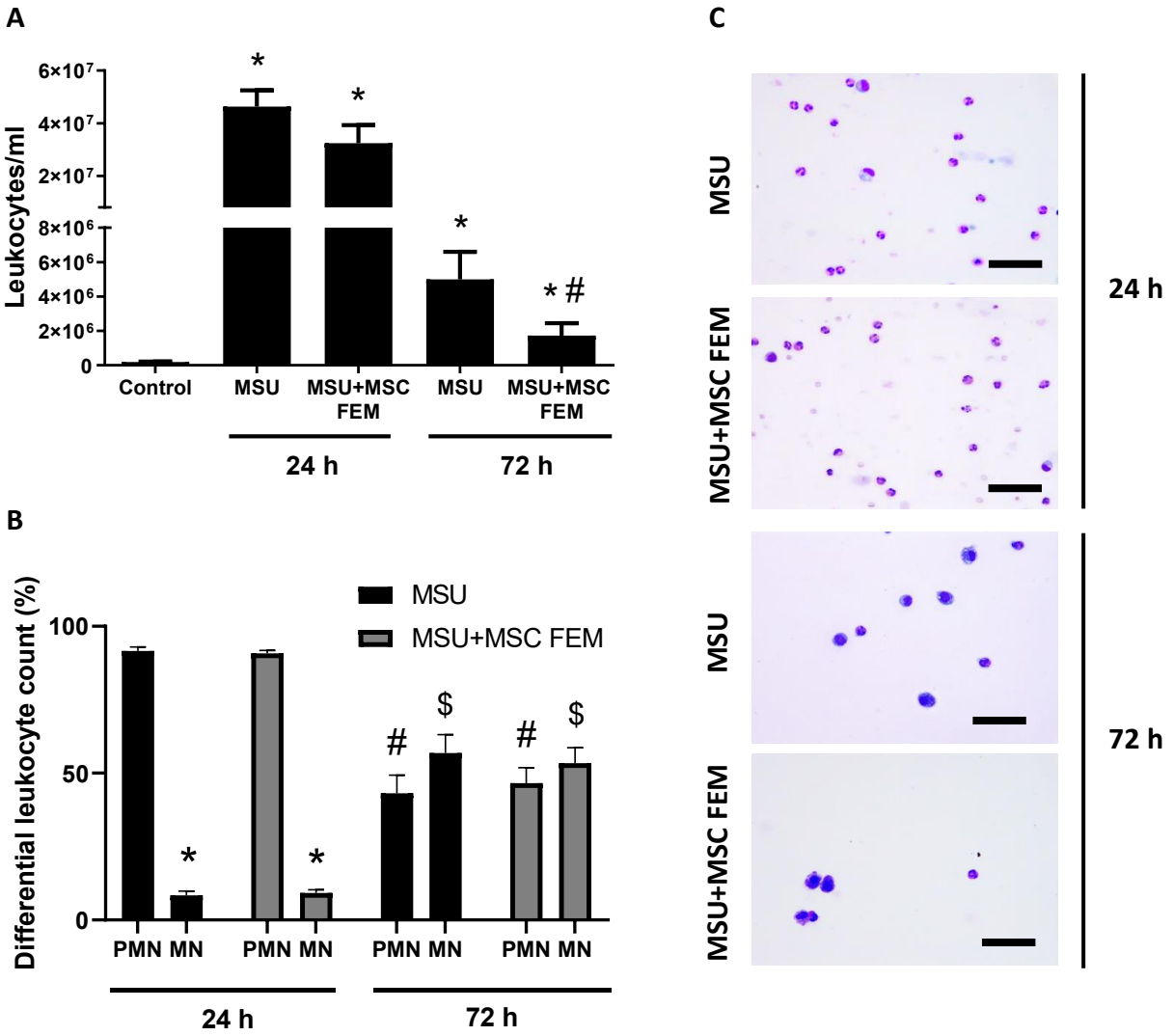
A
Leukocytes/ml
6×10⁷
4×10⁷
2×10⁷
8×10⁶
6×10⁶
4×10⁶
2×10⁶
0
Control
MSU
MSU+MSC FEM
MSU
MSU+MSC FEM
24 h
72 h
B
Differential leukocyte count (%)
100
50
0
MSU
MSU+MSC FEM
PMN MN PMN MN PMN MN PMN MN
24 h
72 h
C
MSU
MSU+MSC FEM
24 h
MSU
MSU+MSC FEM
72 h

FIGURE 3

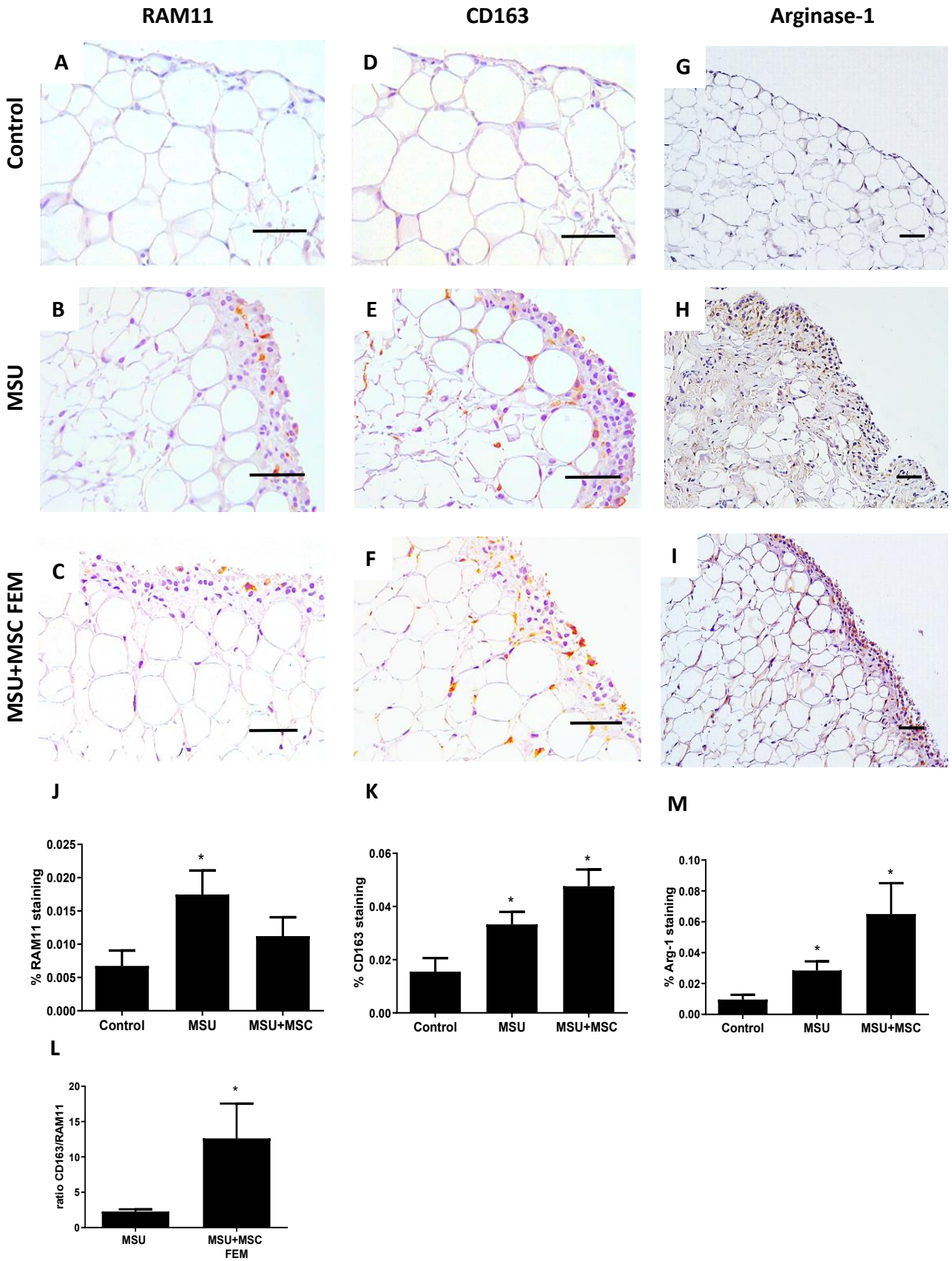
RAM11
CD163
Arginase-1
Control
MSU
MSU+MSC FEM
A
B
C
D
E
F
G
H
I
J
K
M
L
% RAM11 staining
0.025
0.020
0.015
0.010
0.005
0.000
Control
MSU
MSU+MSC
% CD163 staining
0.06
0.04
0.02
0.00
% Arg-1 staining
0.10
0.08
0.06
0.04
0.02
0.00
ratio CD163/RAM11
20
15
10
5
0
MSU
MSU+MSC FEM
*

FIGURE 4

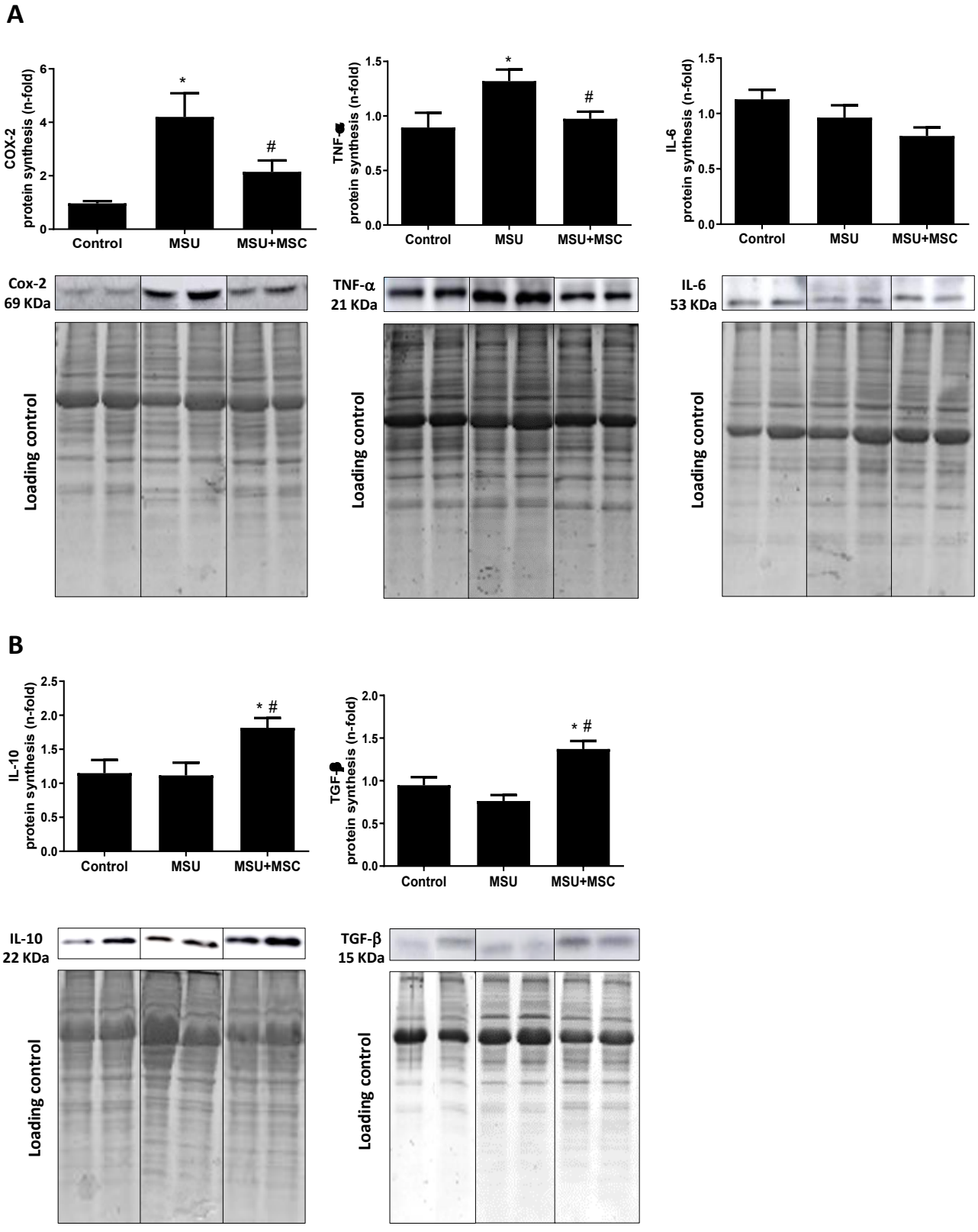
A
COX-2 protein synthesis (n-fold)
TNF-α protein synthesis (n-fold)
IL-6 protein synthesis (n-fold)
Control
MSU
MSU+MSC
Cox-2 69 KDa
TNF-α 21 KDa
IL-6 53 KDa
Loading control
B
IL-10 protein synthesis (n-fold)
TGF-β protein synthesis (n-fold)
IL-10 22 KDa
TGF-β 15 KDa

FIGURE 5

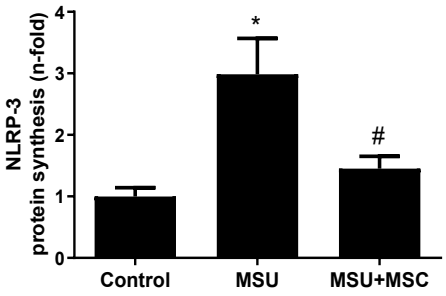
NLRP-3
protein synthesis (n-fold)
0
1
2
3
4
*
#
Control
MSU
MSU+MSC

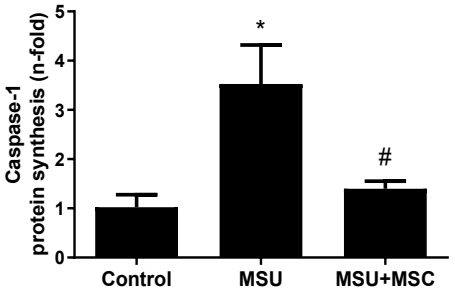
Caspase-1
protein synthesis (n-fold)
0
1
2
3
4
5
*
#
Control
MSU
MSU+MSC

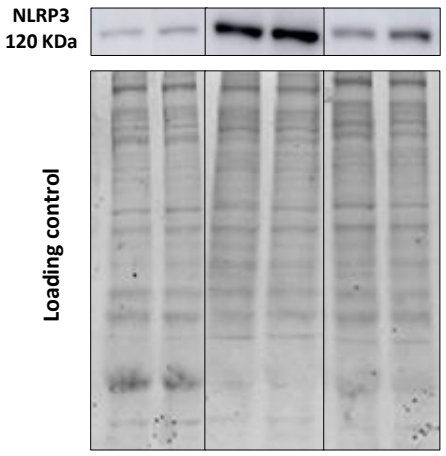
NLRP3
120 KDa
Loading control

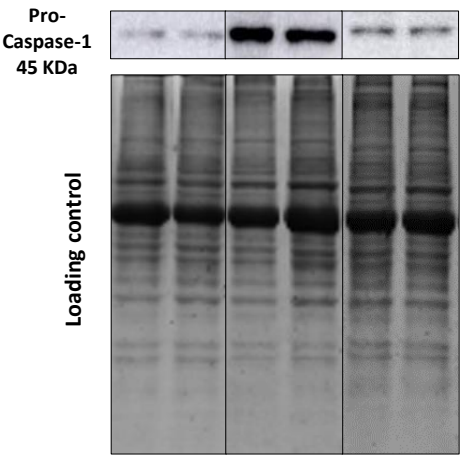
Pro-
Caspase-1
45 KDa
Loading control

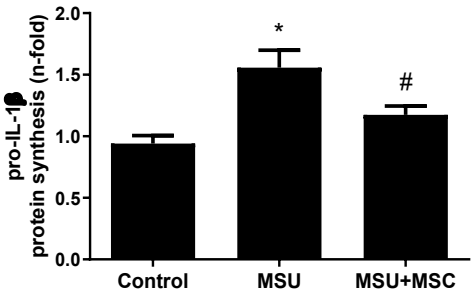
pro-IL-1β
protein synthesis (n-fold)
0.0
0.5
1.0
1.5
2.0
*
#
Control
MSU
MSU+MSC

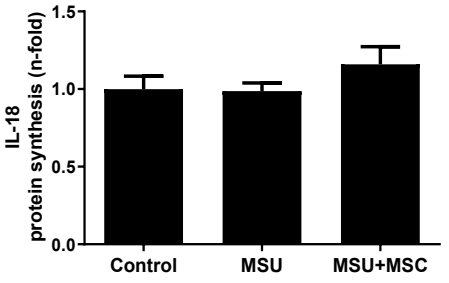
IL-18
protein synthesis (n-fold)
0.0
0.5
1.0
1.5
Control
MSU
MSU+MSC

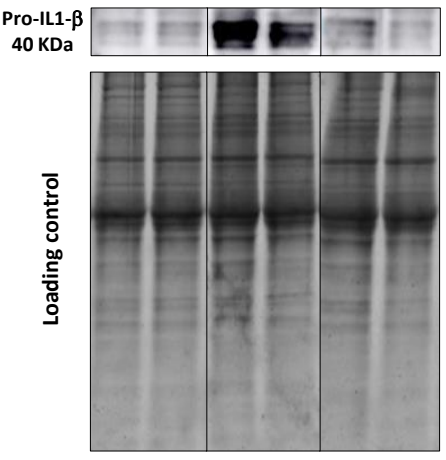
Pro-IL1-β
40 KDa
Loading control

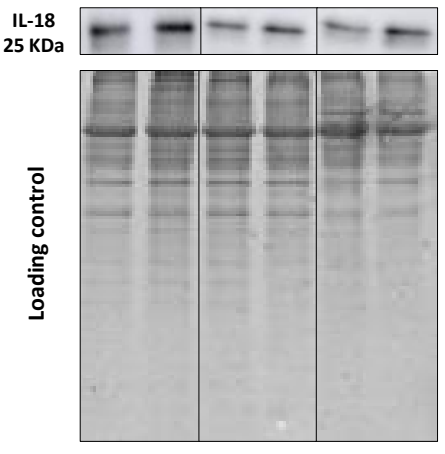
IL-18
25 KDa
Loading control

FIGURE 6

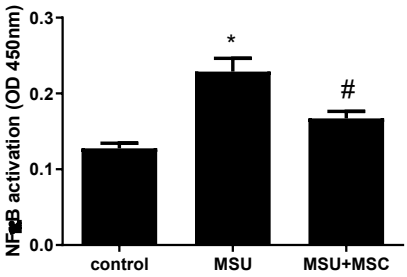

FIGURE 7

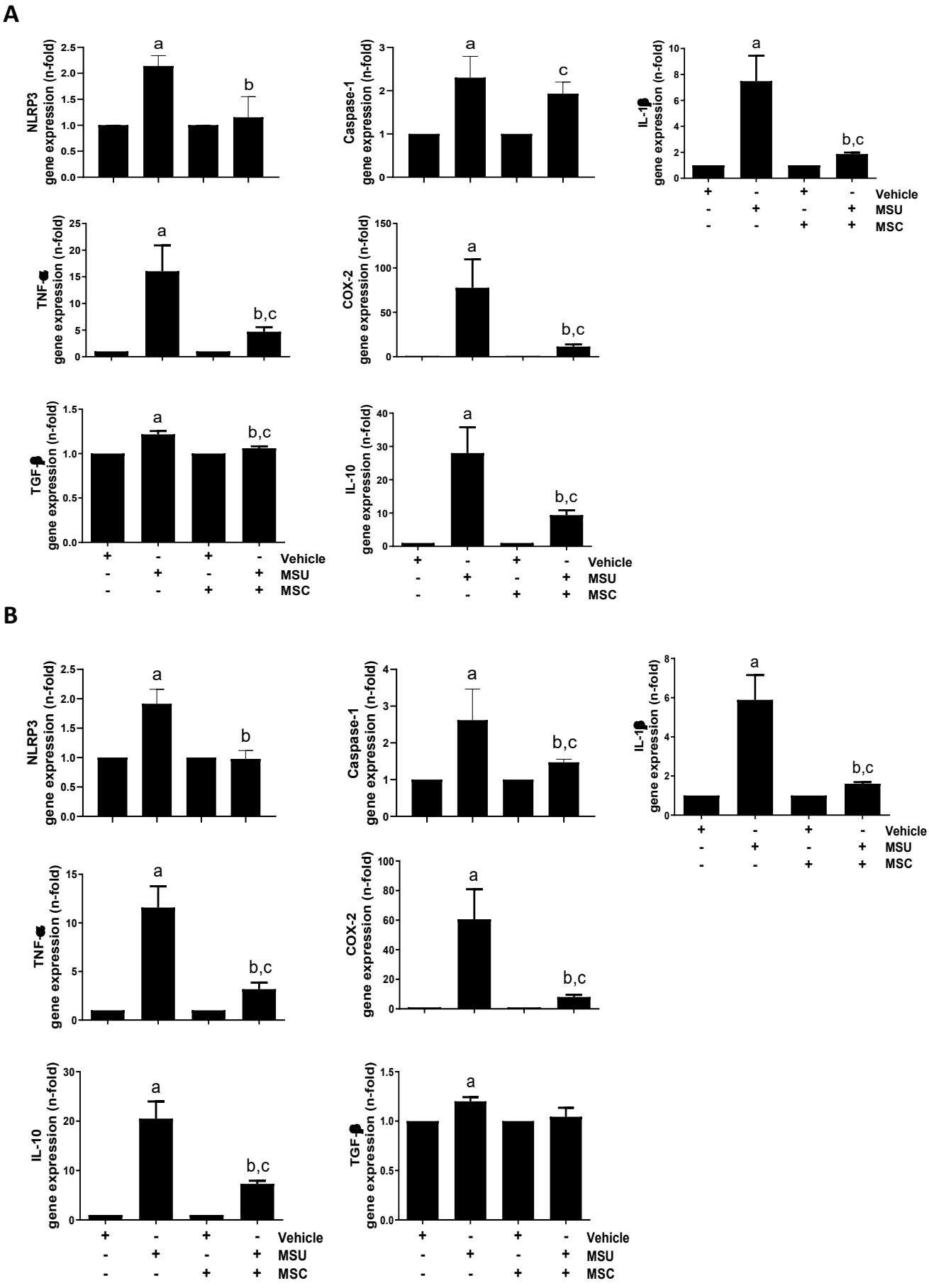
A
NLRP3 gene expression (n-fold)
Caspase-1 gene expression (n-fold)
IL-1β gene expression (n-fold)
TNF-α gene expression (n-fold)
COX-2 gene expression (n-fold)
TGF-β gene expression (n-fold)
IL-10 gene expression (n-fold)
a
b
c
b,c
Vehicle
MSU
MSC
B
NLRP3 gene expression (n-fold)
Caspase-1 gene expression (n-fold)
IL-1β gene expression (n-fold)
TNF-α gene expression (n-fold)
COX-2 gene expression (n-fold)
IL-10 gene expression (n-fold)
TGF-β gene expression (n-fold)
a
b
b,c
Vehicle
MSU
MSC

SUPPLEMENTARY 1

A

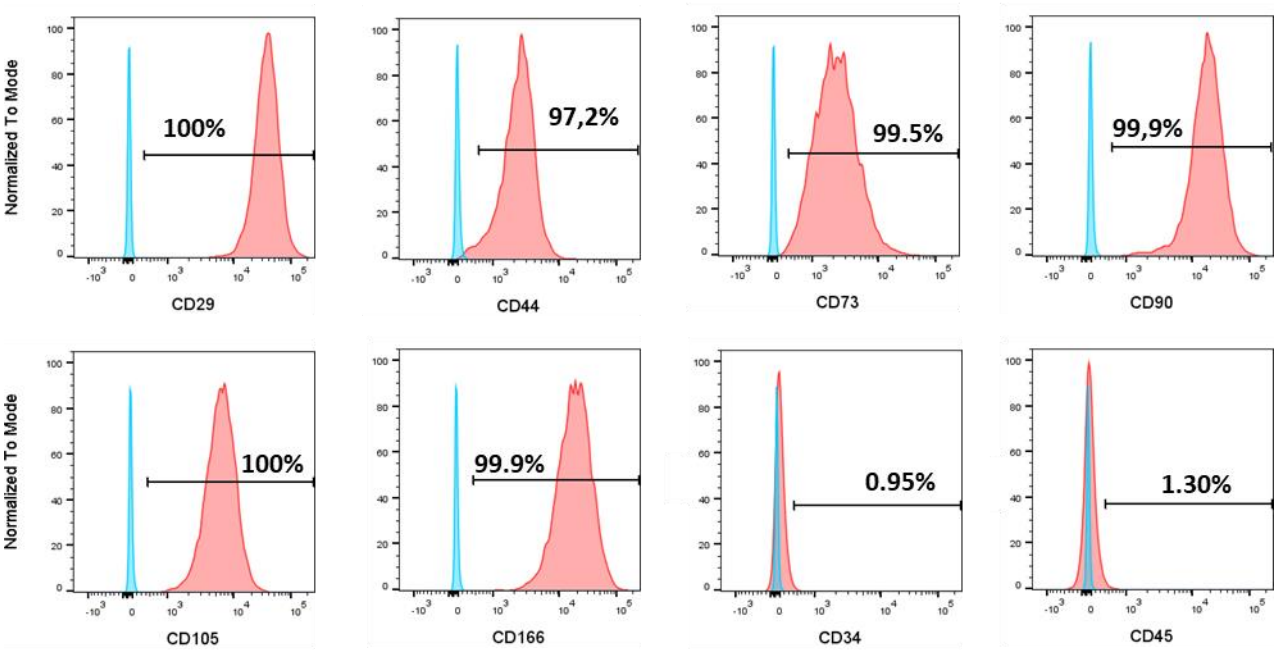

B

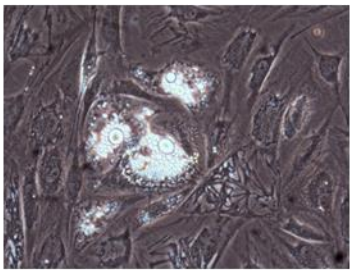

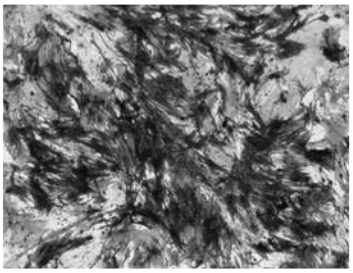

C